



PhD-FSTC-2018-47
The Faculty of Sciences, Technology and Communication

DISSERTATION

Defence held on 11/06/2018 in Luxembourg

to obtain the degree of

DOCTEUR DE L'UNIVERSITÉ DU LUXEMBOURG
EN SCIENCES DE L'INGÉNIEUR

by

Matthias BRAUN

Born on 8th November 1971 in Kusel (Germany)

INVESTIGATION OF THE LOAD-BEARING
BEHAVIOUR OF CoSFB-DOWELS

Dissertation defence committee

Prof. Dr.-Ing. Christoph Odenbreit, dissertation supervisor
Professor, Université du Luxembourg

Prof. Dr.-Ing. Markus Schäfer, Chairman
Professor, Université du Luxembourg

Dr.-Ing. Ferdinand Reif
Geschäftsführer Spannverbund Luxembourg S.A.

Dr. Olivier Vassart
Head of ArcelorMittal Global R&D Construction, Infrastructures & Long Products

Prof. Dr.-Ing. Ulrike Kuhlmann
Professor, Institut für Konstruktion und Entwurf, Universität Stuttgart

Abstract

This Thesis is the first PhD thesis written about CoSFB-Dowels. Therefore, focus of the scientific work presented here, was on the identification of parameters influencing the load-bearing behaviour in general and on parameters contributing to the load-bearing capacity of CoSFB-Dowels in detail. A CoSFB-Dowel is an innovative shear connector for steel-concrete composite slim-floor beams. It consists of circular openings drilled in the web of the steel section with reinforcement bars passing through and filled with normal concrete in-situ.

Push-out tests have been performed already in an earlier research project initiated by the author. In this Thesis, detailed analysis of the test results was done and a finite element model developed simulating the push-out tests, which led to an improved understanding of the overall load-bearing behaviour. Further, the numerical model was used to identify and to evaluate components contributing to the stiffness, to the linear-elastic load and to the maximum load. The findings of this research led to the formulation of a mechanical model and an analytical method to evaluate the load-bearing capacity of a CoSFB-Dowel. The analytical method was validated with the test results. This Thesis is concluded by a proposal allowing for a conservative determination of the design resistance of CoSFB-Dowels.

Acknowledgment

How to acknowledge all the people who helped me with this Thesis and not forgetting anybody? I have to admit, that this seems to be much too challenging for me. So many people have crossed my way in the recent years and they all influenced my work. Therefore, my apologies in case I have forgotten to name anybody and I would like to thank all the people who helped me.

It was almost a decade ago when I was searching for a new type of shear connector for composite slim-floor beams. Working at that time for ArcelorMittal, it was a big luck that Oliver Hechler had the office next door. He came up with the idea to use concrete dowels, which quickly led to a research project on this subject. I would like to give my sincere thanks to Oliver for his help and scientific contribution during this project.

I would like to extend my heartfelt thanks to Renata Obiala. She coordinated the research work between ArcelorMittal and our project partner, the University of Stuttgart. This brings me to thank Matthias Konrad (at that time University of Stuttgart), who once asked me, why am I not doing a PhD? Looking back it was exactly this moment, which was the initiation for me to do a PhD-Thesis (it must have been in the late 2009 already). In addition, I deeply acknowledge the highly professional work from Gunter Hauf and Florian Eggert. Together with Matthias and the people from the MPA at the University of Stuttgart, they made it work! Without their commitment to the project, scientific input and excellent performance on the execution of the tests, this Thesis would not have been possible.

I gratefully acknowledge Prof. Ulrike Kuhlmann (University of Stuttgart) for her support and kind advice. She was responsible for the work performed at the University of Stuttgart and a member of my defence committee. From the beginning of the project in 2009 until the defence of this Thesis in 2018 we walked down a long road together. Thank you very much!

I want to thank Prof. Markus Schäfer, Ferdinand Reif and Olivier Vassart warmly for all the helpful advice and explanations during my Thesis. They helped me through a tough time.

Also sincere thanks for the opportunity to do my PhD at the University of Luxembourg to my PhD supervisor Prof. Christoph Odenbreit.

Further, I wish to thank Jules Mathieu and Matti Leskelä. The exchange we had over years was more influencing my work than they might imagine.

A special and very big "Thank you" to Jesper Harrild Sørensen from the Technical University of Denmark for the open exchange about his work and all his kind explanations. I really hope I understood everything correctly.

Special thanks to Job Duarte for his encouraging words in difficult times. It was a great pleasure and very motivating sharing the office with you! Thank you!

Finally, I would like to express my warmest thanks again to Renata Obiala. Whenever I needed to exchange about my work or any feedback, she was available. I would like to thank her also for her support and advice with the numerical simulation. Especially for her patience explaining me again and again how to use Abaqus.

List of Content

List of Figures	VIII
List of Tables	XI
1 Introduction	1
1.1 Motivation.....	1
1.2 Scope	2
1.3 Slim-Floor Construction	3
2. Literature Review	5
2.1 Introduction	5
2.2 Dowel Action	5
2.3 Concrete Dowels as shear connector in composite beams.....	25
2.4 Shear Connection by Transversal Bars.....	38
3 Testing of CoSFB-Dowels	39
3.1 Introduction	39
3.2 Push-Out Tests	39
3.2.1 Overview	39
3.2.2 Test specimen, testing procedure and measurement.....	39
3.2.3 Material properties	43
3.2.3.1 Concrete.....	43
3.2.3.2 Reinforcement	44
3.2.3.3 Structural Steel	45
3.2.4 Opening of the specimens	45
3.2.5 Test results	48
3.3 Additional Tests on Dowel Reinforcement	48
4 Evaluation of Push-out Tests	51
4.1 Test Overview and Results.....	51
4.2 Test Analysis.....	55
4.3 Conclusions from Test Analysis.....	62
5 Numerical Simulation of Push-Out Tests	63
5.1 Introduction	63
5.2 Numerical Model	63
5.2.1 Geometry, Boundary Conditions	63
5.2.2 Finite Element Mesh	64
5.2.3 Load.....	65

5.2.4 Interactions, Contact Definition.....	65
5.3 Material Models.....	66
5.3.1 Introduction	66
5.3.2 Structural Steel	66
5.3.3 Reinforcement Mesh, Q257.....	66
5.3.4 Dowel Reinforcement	66
5.3.5 Concrete.....	71
5.3.5.1 Introduction	71
5.3.5.2 Uniaxial behaviour of concrete in compression	71
5.3.5.3 Uniaxial behaviour of concrete in tension.....	73
5.3.5.4 Multiaxial behaviour - Concrete Damage Plasticity.....	74
5.3.5.5 Concrete confinement	79
5.4 Development of a Numerical Model for Series 1a	81
5.4.1 Introduction	81
5.4.2 Influence of various parameters.....	81
5.5 Simulation of Test Series 1b.....	90
5.6 Simulation of Test Series 2-1a and 2-1b	94
5.7 Simulation of Test Series 2-2a.....	96
5.8 Simulation of Test Series 2-2b	97
5.9 Simulation of Test Series 2-3	98
5.10 Conclusions from Numerical Simulation	99
6 Formulation of the Load-Bearing Capacity, P_{max}	105
6.1 Introduction	105
6.2 Concrete Component, P_{lin}	106
6.3 Dowel Action, P_{Dowel}	108
6.4 Limit Condition for a CoSFB-Dowel.....	115
6.5 Evaluation of the Analytical Method to determine P_{Dowel}	116
7 Design Proposal	121
7.1 Introduction	121
7.2 Design Resistance of the Concrete Component, P_{lin}	122
7.3 Design Resistance of the Dowel Action, P_{Dowel}	126
7.4 Design Resistance of a CoSFB-Dowel.....	127
8 Conclusions.....	129
Outlook	131
References.....	133

Annex A – Drawings of Push-Out Tests143

Annex B – Test Results155

 B1 – Load-Slip Curves.....156

 B2 – Load-Slip Curves, Initial Stiffness S_{ini} and P_{linear}160

 B3 – Strain Measurements.....163

 B4 – Tensile Tests of Dowel Reinforcement Uni LU (2018)178

Annex C – Input for Numerical Simulation (Abaqus)181

Annex D – Analytics185

List of Figures

- Fig. 1.1: CoSFB-Dowel [ES2014]
- Fig. 1.3.1: Historical slim-floor construction [Pe1922]
- Fig. 1.3.2: Prussian cap floor [Stk2018]
- Fig. 1.3.3: Types of slim-floor beams [Sch2007]
- Fig. 1.3.4: Slim-floor beam with shear studs [SC2015]
- Fig. 2.2.1: Load and Deflection of an elastic structure embedded in an elastic mass, Friberg [Fri1938]
- Fig. 2.2.2: Deflection of a dowel across a pavement joint, Friberg [Fri1938]
- Fig. 2.2.3: Deformed dowel bar and distribution of forces, Johansen [Jo1949]
- Fig. 2.2.4: Test arrangement and results, Rasmussen [Ra1963]
- Fig. 2.2.5: Dowel deformation and loading at failure, Rasmussen [Ra1963]
- Fig. 2.2.6: Deflection, soil reaction and bending moment for a long restrained pile, Broms [Br1964]
- Fig. 2.2.7a: Test set-up, Dulacska [Du1972]
- Fig. 2.2.7b: Assumed system of forces, Dulacska [Du1972]
- Fig. 2.2.8: Test set-up and results, Paulay [Pau1974]
- Fig. 2.2.9: Mechanism of dowel action, Paulay [Pau1974]
- Fig. 2.2.10: Test set-up, Sourashian [Sou1986]
- Fig. 2.2.11a: Inclined dowel bar, Sourashian [Sou1986]
- Fig. 2.2.11b: Failure condition, Sourashian [Sou1986]
- Fig. 2.2.12: Tests on concrete foundation modulus, Sourashian [Sou1986]
- Fig. 2.2.13: Failure mechanism, Vintzeleou [Vin1986]
- Fig. 2.2.14: Plastic displacement of a dowel at failure, Vintzeleou [Vin1986]
- Fig. 2.2.15: Test set-up, Vintzeleou [Vin1987]
- Fig. 2.2.16: Theoretical dowel resistance and test results, Vintzeleou [Vin1986]
- Fig. 2.2.17: Test set-up, Pruijssers [Pru1988]
- Fig. 2.2.18: Failure mechanism due to plastification, Pruijssers [Pru1988]
- Fig. 2.2.19: Equilibrium condition for the plastic hinge, Pruijssers [Pru1988]
- Fig. 2.2.20: Parameters in study of dowel action, Dei Poli [Dei1992]
- Fig. 2.2.21: Limit analysis of dowel, Dei Poli [Dei1992]
- Fig. 2.2.22: Test specimen with concrete-embedded ducts, Dei Poli [Dei1992]
- Fig. 2.2.23: Load displacement curves, Dei Poli [Dei1992]
- Fig. 2.2.24: Test specimen, Tanaka [Ta2011]
- Fig. 2.2.25: Relationship of $(K \cdot d)$ and $(f_c' \cdot d^2)$ based on experiments, Tanaka [Ta2011]
- Fig. 2.2.26: Load at first yielding and spalling in relation to dowel index $d^2 \cdot (f_c' \cdot f_y)^{0.5}$, Tanaka [Ta2011]
- Fig. 2.2.27: Schematics of the failure mechanism of dowel bar, Tanaka [Ta2011]
- Fig. 2.2.28: Two sided joint, Sørensen [Sor2017]
- Fig. 2.2.29: Test set-up, Sørensen [Sor2017]
- Fig. 2.2.30: Test results, Sørensen [Sor2017]
- Fig. 2.3.1: Test set-up, Andrä [An1985]
- Fig. 2.3.2: Load-slip curves, Andrä [An1985]
- Fig. 2.3.3: Tests on metal strip with circular openings, Andrä [An1985]
- Fig. 2.3.4: Metal strip after testing, Andrä [An1985]

- Fig. 2.3.5: Perfobond connector, Leonhardt [Leo1987]
Fig. 2.3.6: Local situation at opening, Leonhardt [Leo1987]
Fig. 2.3.7: Trajectories in compression and tension, Leonhardt [Leo1987]
Fig. 2.3.8: Push-out specimen, Leonhardt [Leo1987]
Fig. 2.3.9: Geometries of tested Perfobond, Leonhardt [Leo1987]
Fig. 2.3.10: Load-displacement of static push-out tests after cycles, Leonhardt [Leo1987]
Fig. 2.3.11: Shear resistance of Perfobond strip (PBL) in comparison to shear studs (KBD), Leonhardt [Leo1987]
Fig. 2.3.12: Kombi-Verdübelung, Brendel [Z-26.4-39]
Fig. 2.3.13: Loading of concrete dowel, Kraus [Kr1997b]
Fig. 2.3.14: Spring model concrete dowel, Kraus [Kr1997b]
Fig. 2.3.15: Push-out test and geometries of concrete dowels, Kraus [Kr1997b]
Fig. 2.3.16: Typical load-slip curve, Kraus [Kr1997b]
Fig. 2.3.17: Relation between P_{max} and concrete compression strength, Kraus [Kr1997b]
Fig. 2.3.18: Failure criteria according to Zapfe, with $\gamma_v = 1.25$ [Za2001]
Fig. 2.3.19: Geometry according to Reitz [Re2003]
Fig. 2.3.20: Comparison of numerical simulation and test, Zheng [Ze2016]
Fig. 2.3.21a: Mechanism with rebar, Zheng [Ze2016]
Fig. 2.3.21b: Mechanism according to Kraus [Kr1997b]
Fig. 2.4.1: Transversal bar as connector, Leskelä [Les2008]
Fig. 2.4.2: Tests performed by Leskelä [Les2008]
Fig. 3.2.2.1: Push-out Test Specimen [Stu2011]
Fig. 3.2.2.2: Schematic Drawing of Push-out Tests [CC2013]
Fig. 3.2.2.3: Position of Extensometers [Stu2011]
Fig. 3.2.4.1: Cutting of Push-out Specimen
Fig. 3.2.4.2: Extracted Dowel Reinforcement Bars
Fig. 3.2.4.3: Concrete in the web-opening
Fig. 3.2.4.4: Opening of Specimens by hand
Fig. 3.2.5: Load-slip curves for Series 1a
Fig. 3.3.1: Stress-strain curves from tensile tests, Uni LU 2018
Fig. 3.3.2: Tensile Test Specimen 1a, Uni LU 2018
Fig. 4.1.1: Push-out test Series 1a, definition of S_{ini} and $P_{e,lin}$
Fig. 4.1.2: Series 1a and 1b
Fig. 4.1.3: Series 2-1a and 2-1b
Fig. 4.1.4: Series 1a and 2-1a
Fig. 4.1.5: Series 1b and 2-1b
Fig. 4.1.6: Series 1a and 2-2b
Fig. 4.1.7: Series 1b and 2-2b
Fig. 4.1.8: Series 1a and 2-2a
Fig. 4.1.9: Series 1b and 2-2a
Fig. 4.2.1a: $P_{e,max}$ versus f_{cm}
Fig. 4.2.1b: $P_{e,lin}$ versus f_{cm}
Fig. 4.2.2: η versus $f_{cm} \cdot t_w \cdot \varnothing_0$
Fig. 4.2.3: Test 1a – P1
Fig. 4.2.4: Test 1b – P2

List of Figures and Tables

- Fig. 4.2.5: S_{ini} versus f_{cm}
- Fig. 4.2.6: ΔP_e versus $f_{cm} \cdot t_w$
- Fig. 4.2.7: ΔP_e versus f_{cm}
- Fig. 4.2.8: ΔP_e per dowel versus f_{cm} – Tension and Shear dominated Failure
- Fig. 4.2.9: Load-slip curves Series 2-3
- Fig. 4.2.10: Test 2-1b-P1, Friction
- Fig. 4.2.11: Hooked bar, test 2-2a-P3
- Fig. 5.2.1: Geometry of numerical model
- Fig. 5.2.2: Finite element mesh
- Fig. 5.2.4: Areas of contact definition of the dowel reinforcement
- Fig. 5.3.4.1: Typical stress-strain behaviour [Abaqus]
- Fig. 5.3.4.2: Progressive damage degradation [Abaqus]
- Fig. 5.3.4.3: Exponential evolution of damage [Abaqus]
- Fig. 5.3.5.2: Stress-strain relationship of concrete in uniaxial compression [EN 1992]
- Fig. 5.3.5.3: Postfailure stress-displacement curve [Abaqus]
- Fig. 5.3.5.4.1: Concrete in uniaxial loading in tension [Abaqus]
- Fig. 5.3.5.3.2: Concrete in uniaxial loading in compression [Abaqus]
- Fig. 5.3.5.4.3: Definition of the compressive inelastic strain $\tilde{\epsilon}_c^{in}$ [Abaqus]
- Fig. 5.3.5.4.4: Yield surfaces in the deviatoric plane, corresponding to different values of K_c [Abaqus]
- Fig. 5.3.5.4.5: Yield surface in plane stress [Abaqus]
- Fig. 5.3.5.5.1: Zones of concrete confinement
- Fig. 5.3.5.5.2: Concrete confinement [Elb2011]
- Fig. 5.4.2.1: Influence of displacement at failure for shear damage, u_f
- Fig. 5.4.2.2: Influence of plastic displacement for ductile damage, u_{pl}
- Fig. 5.4.2.3: Influence of concrete tension strength, f_{ctm}
- Fig. 5.4.2.4: Variation of fracture energy, G_F
- Fig. 5.4.2.5: Influence of fracture energy, G_F
- Fig. 5.4.2.6: Influence of friction between foundation and specimen
- Fig. 5.4.2.7: Influence of friction between steel section and concrete
- Fig. 5.4.2.8: Influence of dilation angle
- Fig. 5.4.2.9: Reinforcement mesh [Stu2011]
- Fig. 5.4.2.10: Concrete tension damage, longitudinal crack
- Fig. 5.4.2.11: Influence of reinforcement mesh above the upper flange
- Fig. 5.4.2.12: Variation of contact between dowel bar and concrete
- Fig. 5.4.2.13: Influence of contact definition for dowel reinforcement
- Fig. 5.5.1: Simulation of Series 1b, Variation of global friction
- Fig. 5.5.2: Stress-strain relationship for concrete confinement
- Fig. 5.5.3: Influence of concrete confinement, Series 1b,
- Fig. 5.5.4: Concrete compression model with extended plateau
- Fig. 5.5.5: Influence of extended plateau, Series 1b
- Fig. 5.6.1: Simulation of Series 2-1a
- Fig. 5.6.2: Simulation of Series 2-1b
- Fig. 5.7: Simulation of Series 2-2a
- Fig. 5.8: Simulation of Series 2-2b
- Fig. 5.9: Simulation of Series 2-3
- Fig. 5.10.1: Simulation of Series 1a, Conclusion

- Fig. 5.10.2a: Forces Dowel Reinforcement, Shear Force
Fig. 5.10.2b: Forces Dowel Reinforcement, Bending Moment
Fig. 5.10.3: Tension Forces Dowel Reinforcement
Fig. 5.10.4a: Evolution of forces in the dowel bar, Shear Force
Fig. 5.10.4b: Evolution of forces in the dowel bar, Bending Moment
Fig. 5.10.5a: Position of dowel reinforcement bar
Fig. 5.10.5b: Cut for illustration of concrete damage
Fig. 6.2.1: Correlation of experimental values of $P_{e,lin}$ versus $f_{cm} \cdot t_w \cdot \varnothing_0$
Fig. 6.2.2: Comparison of P_e and P_t according to Equation 6.2
Fig. 6.3.1: Development of a mechanism in the dowel reinforcement
Fig. 6.3.2: Undeformed state and distribution of moment and shear
Fig. 6.3.3: Deformed state with distribution of contact pressure
Fig. 6.5.1: Evaluation of $P_{Dowel}(u)$
Fig. 6.5.2: Development of tension in the dowel reinforcement
Fig. 6.5.3: Influence of enhancement factor
Fig. 6.5.4: Influence of friction on $P_{t,Dowel}$ and comparison to Series 1a
Fig. 7.1: Components of a CoSFB-Dowel
Fig. 7.2: Comparison of P_e and P_t according to Equation 7.2 and 7.3
Fig. 8.1: Load-bearing behaviour of a CoSFB-Dowel
Fig. 8.2: Dowel action by a mechanism of plastic hinges

List of Tables

- Table 2.2: Specifications and material properties, Sørensen [Sor2017]
Table 3.2.1: Overview – CoSFB Push-out Tests 2009 + 2011 [Stu2009], [Stu2011]
Table 3.2.3.1: Test Results – Concrete
Table 3.2.3.2: Test Results – Reinforcement
Table 3.2.3.3: Test Results – Structural Steel
Table 3.3: Tensile Tests Uni LU 2018 – Test Results (Engineering stresses)
Table 4.1.1: Push-out test Series 2011, investigated parameters
Table 4.1.2: Results push-out test Series 2011
Table 4.2: Results push-out test Series 2011, ΔP_e
Table 5.4.1: Geometry of push-out Series 1a
Table 5.5: Geometry of push-out Series 1b
Table 5.6: Geometry of push-out Series 2-1a and 2-1b
Table 5.7: Geometry of push-out Series 2-2a
Table 5.8: Geometry of push-out Series 2-2b
Table 5.9: Geometry of push-out Series 2-3
Table 5.10.1: Stress development in dowel reinforcement
Table 5.10.2: Evolution of concrete compression and concrete tension damage
Table 6.5.1: Determination of $P_{t,Dowel}$ and comparison with ΔP_e
Table 7.2: Statistical evaluation of Equation 7.2
Table 7.3: Partial differentiation of Equation 7.2
Table 7.4: Validity range of Equation 7.5

1 Introduction

1.1 Motivation

A research on the potential use of concrete dowels as shear connectors for slim-floor beams was initiated in 2009 by ArcelorMittal. As employee of ArcelorMittal, the author investigated a possible influence of this kind of shear connector on the beam design. The outcome of this theoretical work led to expectation of a significant potential of concrete dowels for an economic optimisation of slim-floor beams and resulted in a subsequent test campaign comprising of 6 push-out and 4 beam tests, financed by ArcelorMittal. The tests were carried out at the Chair of Prof. U. Kuhlmann at the University of Stuttgart, Germany. Results are given in [Stu2009]. The general outcome of these tests was supporting the findings of the initial study. However, the results of a push-out test with a higher concrete compressive strength showed a lower maximum load. This initially surprising result required further investigation.

Aiming for a Technical Approval for Germany of concrete dowels as shear connector for slim-floor beams, further referred to as “CoSFB-Dowel”, a second test campaign was initiated. The author initiated this research project at ArcelorMittal and was responsible to define the test campaign, to design the test set-up and to follow the project to a successful outcome [Z-26.4-59]. The tests of the second campaign were also performed at the University of Stuttgart. Test results can be found in [Stu2011]. The Technical Approval was based on the statistical evaluation of the results.

The in depth understanding of the mechanical behaviour of the CoSFB-Dowel, as originated from the tests results, was the main motivation of the research presented hereafter.

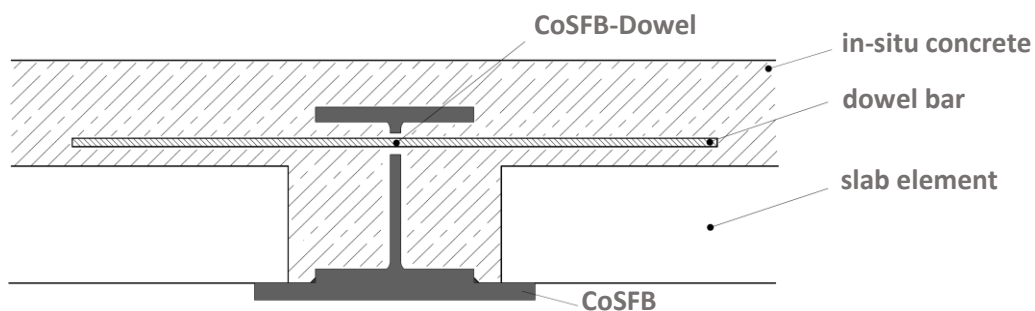


Figure 1.1: CoSFB-Dowel [ES2014]

This Thesis presents fundamental investigations of the load-bearing behaviour of CoSFB-Dowels. The CoSFB-Dowel is composed of openings drilled in the web of a hot-rolled steel section, Figure 1.1. These web-openings are equidistantly positioned along the beam. In transversal direction to the beam span, standard reinforcement bars are placed through the web-openings. On-site the chamber of the beam is filled with concrete. CoSFB-Dowels connect the steel section to a concrete slab by activating a composite action.

1.2 Scope

This Thesis is the first research work investigating the load-bearing behaviour of CoSFB-Dowels. Focus was given on the detailed analysis of the mechanical behaviour based on the available results of push-out tests. Components contributing to the stiffness, to the linear-elastic load and to the maximum load are identified and evaluated. Detailed analyses of the push-out and numerical simulations were completed. Based on the findings of this analysis, a mechanical model and an analytical equation to calculate the maximum load of CoSFB-Dowels were derived and its applicability assessed towards the test results. The Thesis is concluded by a proposal allowing to determine conservatively the design resistance of CoSFB-Dowels.

The literature review presents most relevant research about dowel action – the transfer of shear forces by a steel bar – and about the use of concrete dowels as shear connector, as e.g. Perfobond.

The research starts from detailed investigation of the performed tests. Test set-up and the results of push-out tests on CoSFB-Dowels are given in Chapter 3. Understanding the important influence of the ductility of the dowel reinforcement on the load-bearing capacity, additional tensile tests to determine the fracture strain of the dowel reinforcement bars were performed at the University of Luxembourg in February 2018, Chapter 3. The diameter of the dowel reinforcement was 12mm. In one push-out test a diameter of the dowel reinforcement of 25mm was used. However, in this test the concrete at the abutment failed and therefore no information about the resistance of the load-bearing capacity of the CoSFB-Dowels could be obtained. The investigated diameters of the web-opening are 25mm and 40mm, other diameters were not tested. No tests were carried-out under cyclic loading. Therefore, the results and findings of this Thesis are valid for monotonic loading only. The analysis of beams with CoSFB-Dowels are not part of this research work. Parametric studies, as e.g. varying the diameter of the dowel reinforcement were not performed.

Based on the test results the load-bearing behaviour of CoSFB-Dowels was analysed in detail, Chapter 4. Comparison of the measured load-slip curves with varying parameters is discussed. The observation is completed by the analysis of damage as the specimen has been cut after testing and deformed reinforcement bars were taken out. This allowed to observe also the character of damage.

The push-out tests have been further modelled using FE software Abaqus. More than 500 numerical simulations using 3-dimensional non-linear material properties and interactions were performed to develop numerical models allowing for the simulation of the load-bearing behaviour and the failure modes observed in the push-out tests. Findings of this extensive research work on numerical modelling are presented in Chapter 5. The numerical simulations well represented the tests results and allow for further investigation of the parameters, which have influence on the behaviour of the connector and obtained maximum load. The modelling confirmed the influence of the concrete compression class on the failure mode and provided further information about the local behaviour of concrete in this structural system.

Based on the experimental and numerical study qualitative contribution of various components on the load bearing of CoSFB-Dowels are derived, an analytical method describing dowel action and the overall load-bearing behaviour was developed. Analytical formulations are proposed to calculate linear-elastic load, P_{lin} , before activating the concrete dowel and predict the maximum load, P_{max} , based on the evaluation of the test results and the outcome of the numerical simulations. Special attention was given to the influence of the concrete compression class, Chapter 6.

Finally, a proposal allowing for a conservative determination of the design value of the load-bearing capacity of CoSFB-Dowels is given in Chapter 7.

Conclusions and outlook are closing the Thesis.

1.3 Slim-Floor Construction

Slim-Floor construction is characterized by the integration of a steel beam into a slab. Developed in the 19th century with the aim to increase the span of the floor by using hot-rolled steel sections – at that time a new and modern product – and improving the fire resistance of the steel sections by their integration into the slab, this construction method was commonly used, Figures 1.3.1 and 1.3.2.

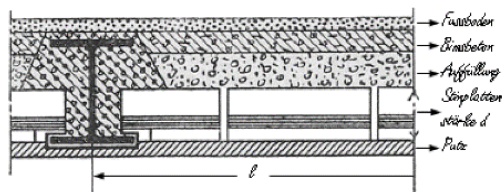


Figure 1.3.1: Historical slim-floor construction [Pe1922]

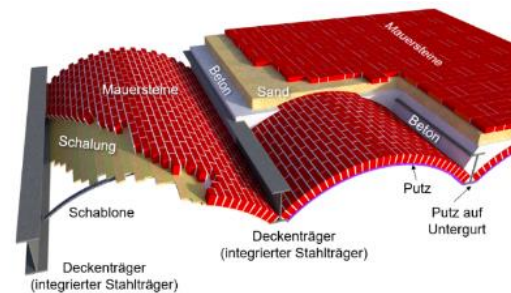


Figure 1.3.2: Prussian cap floor [StK2018]

But, a relatively small load-bearing capacity of the slab elements resulted in a small distance of the beams and a high steel consumption. And due to a high demand for steel in the 1st and 2nd world war, slim-floor construction was used less.

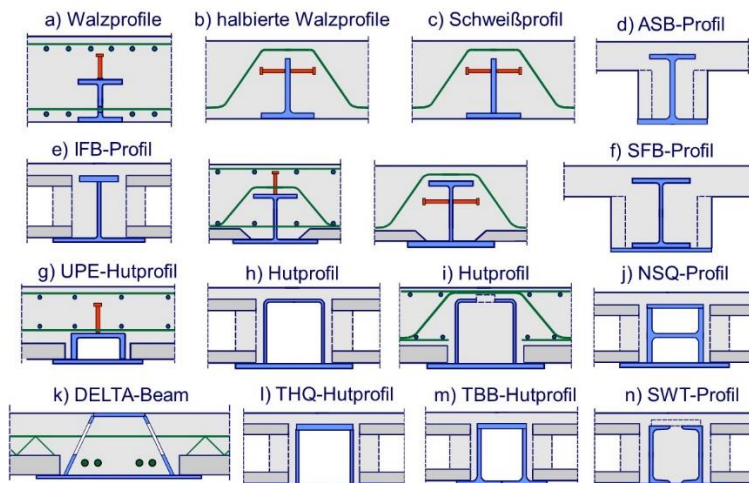


Figure 1.3.3: Types of slim-floor beams [Sch2007]

The development of prefabricated slab elements, allowing for a larger beam distance optimising the overall steel consumption in combination with a short construction time, led to a revival of slim-floor construction in the years of 1980s [ECCS74]. Searching for further optimisations, different forms of slim-floor beams have been developed, Figure 1.3.3.

Usually the beams were designed as non-composite beams, because an activation of a composite action between the steel section and in-situ concrete by means of shear studs, welded onto the upper flange of the beam, would require either a reduction of the beam height or an increase of the slab thickness, Figure 1.3.4.

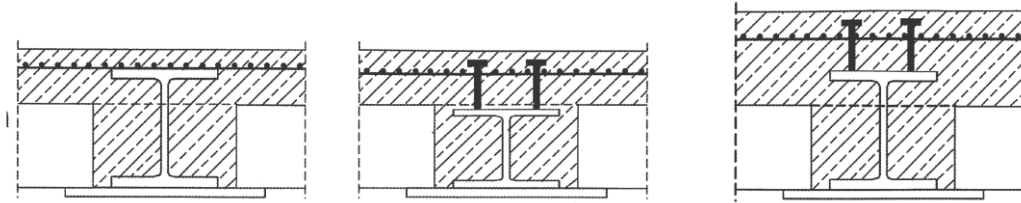


Figure 1.3.4: Slim-floor beam with shear studs [SC2015]

These considerations led to the development of the CoSFB-Dowel, Figure 1.1. Positioned in the web of a hot-rolled section, a maximum of the slab thickness can be used by the beam, leading to an optimization of the load-bearing capacity of the beam and the consumption of steel.

As already stated in Section 1.1, simple values of the design resistance for CoSFB-Dowels are given in a Technical Approval [Z-26.4-59]. The development of CoSFB-Dowels - from the idea to a Technical Approval - was awarded in 2015 by the German Steel Construction Industry [bfs 2015].

An excellent overview about the historical development of composite construction is given in [Pel2016].

2. Literature Review

2.1 Introduction

Even concrete dowels as shear connectors in steel-concrete composite construction and the transfer of shear forces in reinforced concrete structures by dowel action are established and well analysed construction forms, little is known about reinforced concrete dowels as shear connector, positioned in the web of a hot-rolled steel section, referred to as CoSFB-Dowel. Therefore, no direct state-of-the-art for CoSFB-Dowels available. Consequently, this Chapter is divided into two main parts: First, an overview about research on dowel action is given, Section 2.2. Section 2.3 presents most relevant research about the application of concrete dowels as shear connector in composite beams.

The load-bearing behaviour of dowel action is divided further into linear-elastic models, such as the beam-on-elastic-foundation model (BEF) and non-linear models, based on the theory of plasticity. Obviously, a linear-elastic model is limited to small deformations, when plastic limit analysis is appropriate to describe the load-bearing capacity, Section 2.2.

The description of concrete dowels as shear connector for composite beams focus on metal strips (Perfobond). Chapter 2.3 presents most relevant research about Perfobond shear connector for composite beams.

The research work is presented hereafter in a chronological order, allowing for a better understanding of the historical development.

2.2 Dowel Action

Friberg 1938 – Dowel Action in Concrete Pavements

An analytical formulation of dowel action has been published by Friberg already in 1938 [Fri1938]. Using the beam-on-elastic-foundation model (BEF), as mathematically described by Timoshenko [Ti1925], Friberg focus on the design of dowels in transverse joints of concrete pavements. As the limitation of the vertical deformation is of main interest for this type of joints, Friberg is limiting the dowel resistance to its elastic strength. The dowel is considered as an elastic structure embedded into an elastic mass, Figure 2.2.1.

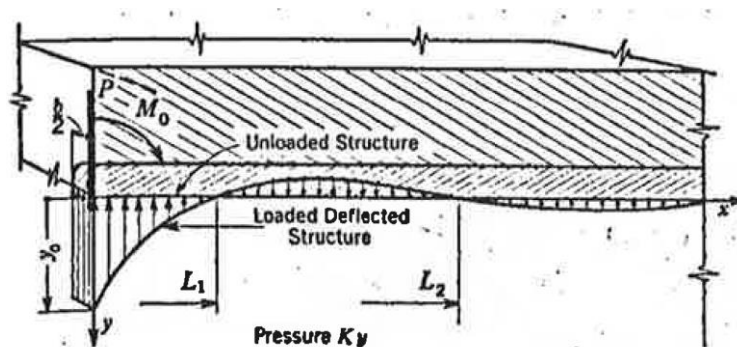


Figure 2.2.1: Load and Deflection of an elastic structure embedded in an elastic mass, Friberg [Fri1938]

With the assumption that the dowels are not bonded to the concrete and that they fit snugly into the concrete, Friberg derived the following Equations. The deflection y_0 at the joint, the bending moment M and the shear force V is given as a function of the position x along the bar:

$$y_0 = \frac{P - \beta \cdot M_0}{2 \cdot \beta^3 \cdot E_a \cdot I} \quad (2.1)$$

$$-E_a \cdot I \cdot \frac{d^2 y}{dx^2} = M = -\frac{e^{-\beta \cdot x}}{\beta} \cdot [P \cdot \sin(\beta \cdot x) - \beta \cdot M_0 \cdot (\sin(\beta \cdot x) + \cos(\beta \cdot x))]$$

$$\frac{dM}{dx} = V = -e^{-\beta \cdot x} \cdot [(2 \cdot \beta \cdot M_0 - P) \cdot \sin(\beta \cdot x) - P \cdot \cos(\beta \cdot x)]$$

with:

P concentrated load, acting downwards at the joint interface

M_0 bending moment, acting at the face of the joint interface, clockwise positive

β stiffness coefficient, with $\beta = \sqrt[4]{\frac{K \cdot b}{4 \cdot E_a \cdot I}}$,

where K = modulus of support; b = width (diameter) of the bar; E_a = modulus of elasticity of the bar; I = moment of Inertia of the bar.

By assuming that a point of contraflexure exists in the dowel at the center of the joint with a joint width a , he derives $M_0 = -P \cdot \frac{a}{2}$. And finally for the maximum moment in the dowel:

$$M_{max} = -\frac{P \cdot e^{-\beta \cdot x_m}}{2 \cdot \beta} \cdot \sqrt{1 + (1 + \beta \cdot a)^2} \quad (2.2)$$

with the position x_m , where the maximum moment occurs in the dowel x_m , determined with $\frac{dM}{dx} = V = 0$ from the Equation above.

It can be directly taken, that the location of the maximum moment is independent from the magnitude of P . Further, the value of the modulus of the supporting concrete K , which may depend on the local pressure at the dowel, has only a minor influence on the stress distribution along the dowel, because β is proportional to $K^{1/4}$.

Friberg derives the total deflection Δ of the joint of concrete pavements as the sum of the deflection at each joint face y_0 , the deflection due to the dowel slope over one-half of the joint $\frac{a}{2} \cdot \frac{dy_0}{dx}$ and, the deflection of the dowel steel over one-half of the joint $\frac{P}{3 \cdot E_a \cdot I} \cdot \left(\frac{a}{2}\right)^3$, Figure 2.2.2. Hence the deflection Δ is obtained with:

$$\Delta = \frac{P}{2 \cdot E_a \cdot I} \cdot \left(\frac{1 + (1 + \beta \cdot a)^2}{\beta^2} + \frac{a^3}{6} \right) \quad (2.3)$$

The deflection is direct proportional to the acting load P .

He points out, for the application of dowels in transverse joints of concrete pavements the bearing stress in the concrete is the critical one. Further, that the steels in the dowels should have a sufficiently high yielding point, so that it is not reached before the bearing stress of the concrete has exceeded any possible value.

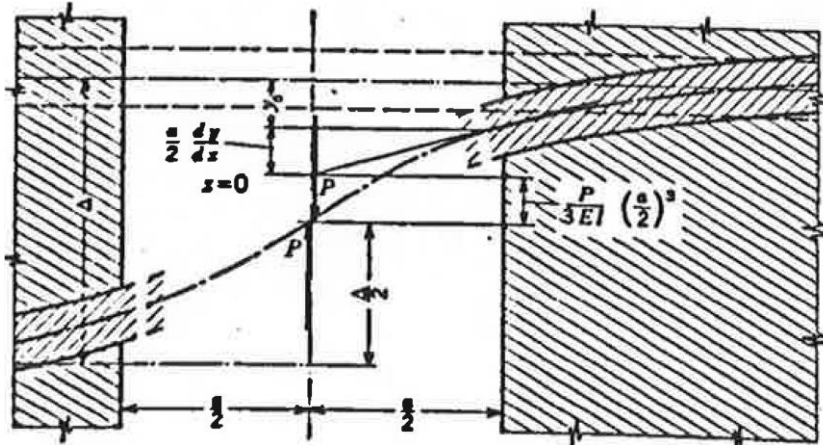


Figure 2.2.2: Deflection of a dowel across a pavement joint, Friberg [Fri1938]

Johansen 1949 – Dowel Action in Timber Joints

A fundamental theory about connections in timber structures was published by Johansen [Jo1949]. He performed shear tests on timber joints with a dowel and a toothed dog to prevent horizontal slipping of the timber elements. According to Johansen the dowel action depends on its resistance to bending and the resistance of the supporting wood to crushing. In addition, tensional effect of the dowel, which depends on its resistance and to friction between the abutting surfaces, was analysed. Therefore, Johansen formulates the load capacity of a dowel on the basis of plastic material behaviour of the dowel and plastic behaviour of the embedding wood. The bending resistance of the dowel is reached and it bends in the balk and the straps, Figure 2.2.3. Johansen assumes a plastic pressure on the wood between the bends and the pressure against the dowel must be $s_H \cdot d$. As the shear force V is equal to zero at the position of the extremal bending moments, M_{max} and M_{min} , these must lie at the same distance z from the joint, as the transverse force in the joint must be $\frac{1}{2} \cdot P = s_H \cdot d \cdot z$. Further, with the equation of moments between the bends, an equation for the load bearing capacity P can be formulated.

$$\begin{aligned}
 M_{max} + M_{min} &= 2 \cdot \frac{\pi}{32} \cdot s_B \cdot d^3 = \frac{1}{2} \cdot P \cdot z = s_H \cdot d \cdot z^2 \\
 z &= \sqrt{\frac{\pi}{16} \cdot \frac{s_B}{s_H} \cdot d^2} = 0.442 \cdot d \cdot \sqrt{\frac{s_B}{s_H}} \\
 P &= 0.885 \cdot d^2 \cdot \sqrt{s_B \cdot s_H}
 \end{aligned} \tag{2.4}$$

With:

- d the diameter of the dowel
- s_B yield strenght of the dowel material
- s_H the pressure on the bearing surface, $s_H = p/d$.
- p the load per unit length of the dowel

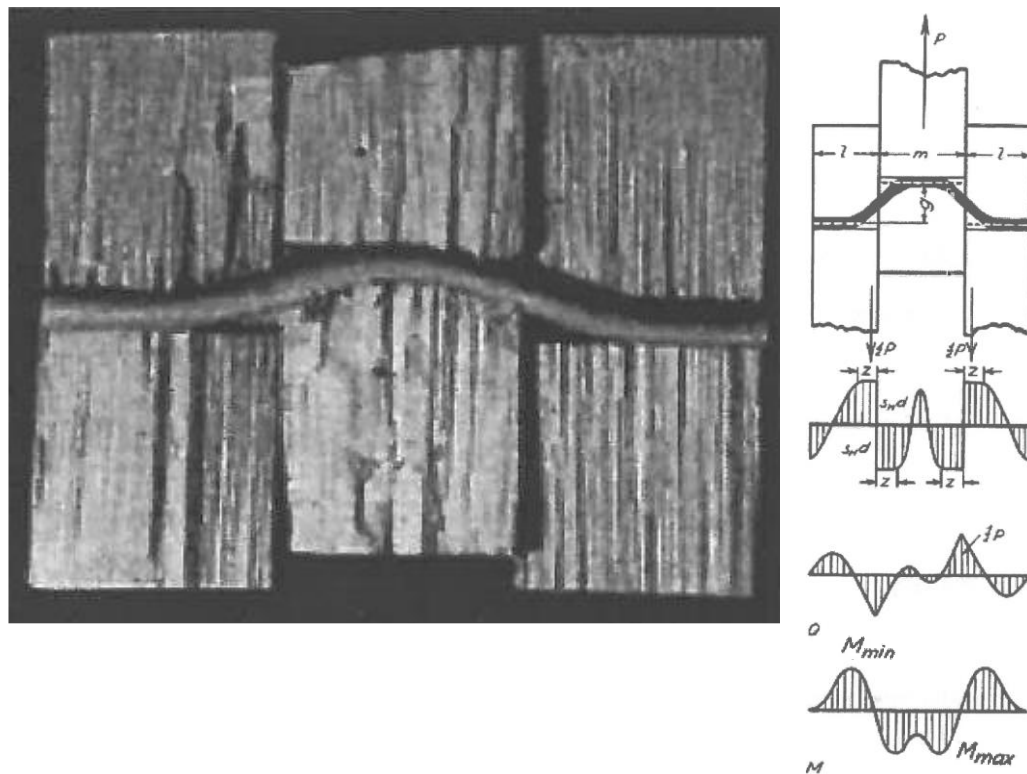


Figure 2.2.3: Deformed dowel bar and distribution of forces, Johansen [Jo1949]

Johansen limited the bending resistance of the dowel to its elastic bending resistance. Further, the equations given by Johansen are not taking into account any interaction of bending and tension forces and no verification of the dowel for shear and tension is performed.

Rasmussen 1963 – Dowel Action in Concrete Construction

Rasmussen performed shear tests on steel bars embedded into a concrete block and protruding at the face of the specimen [Ra1963]. At the free edge the bar was loaded transversely to the longitudinal direction of the bar, acting as shear. His test set-up is given in Figure 2.2.4.

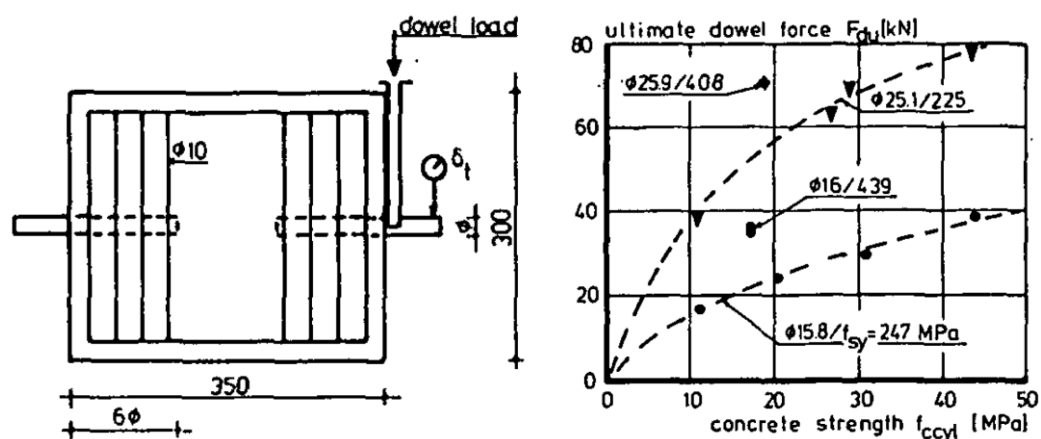


Figure 2.2.4: Test arrangement and results, Rasmussen [Ra1963]

According to Rasmussen plastic hinges develop in the bar accompanied by considerable crushing of the concrete under the bar. He determines the bearing capacity of a shear loaded dowel based on the assumption of a constant resistance of the concrete compression strenght under the dowel and using the plastic bending resistance of the dowel cross section. Similar to the approach of Johansen presented before [Jo1949], Rasmussen determines the maximum load P_{\max} by formulating the equilibrium of the dowel resistance in bending and the maximum concrete pressure, Figure 2.2.5.

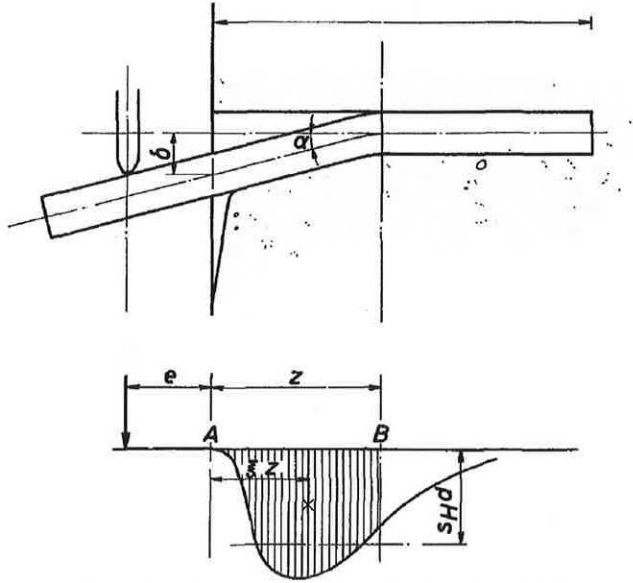


Figure 2.2.5: Dowel deformation and loading at failure, Rasmussen [Ra1963]

The maximum support pressure of the concrete is calibrated on test results. Therefore, his final solution requires a constant c , which was determined empirically. For dowel forces applied at a distance e from the concrete face, the dowel resistance can be predicted by:

$$P = c \cdot \left(\sqrt{1 - (\varepsilon \cdot c)^2} - \varepsilon \cdot c \right) \cdot d^2 \cdot \sqrt{\sigma_C \cdot \sigma_F} \quad (2.5)$$

$$\varepsilon = 3 \cdot \frac{e}{d} \cdot \sqrt{\frac{\sigma_C}{\sigma_F}}$$

With:

- d the diameter of the dowel
- e distance between concrete surface and point where P acts on dowel
- σ_C cylinder strenght of concrete
- σ_F yield stress for dowel determined by tensile tests
- c constant determined empirically, $c = 1.30$.

The failure mode according to Rasmussen is spalling of the concrete at the free edge, Point A in Figure 2.2.5. Hence, a concrete pressure at Point A equal to zero is assumed.

Broms 1964, 1965 – Dowel Action in Pile Foundation

A method to predict the failure load of piles driven in cohesive soils is presented by Broms [Br1964, Br1965]. Broms derived an analytical formulation of the failure load by assuming that the ultimate strength of the pile section or the ultimate strength of the supporting soil has been reached. Further, failure is defined by transforming the pile into a mechanism through the formation of plastic hinges. According to Broms failure takes place for piles, which are restrained (piles with rotational restraint at their top) and having a large penetration depth, when two plastic hinges form at the locations of the maximum positive and negative bending moments, Figure 2.2.6.

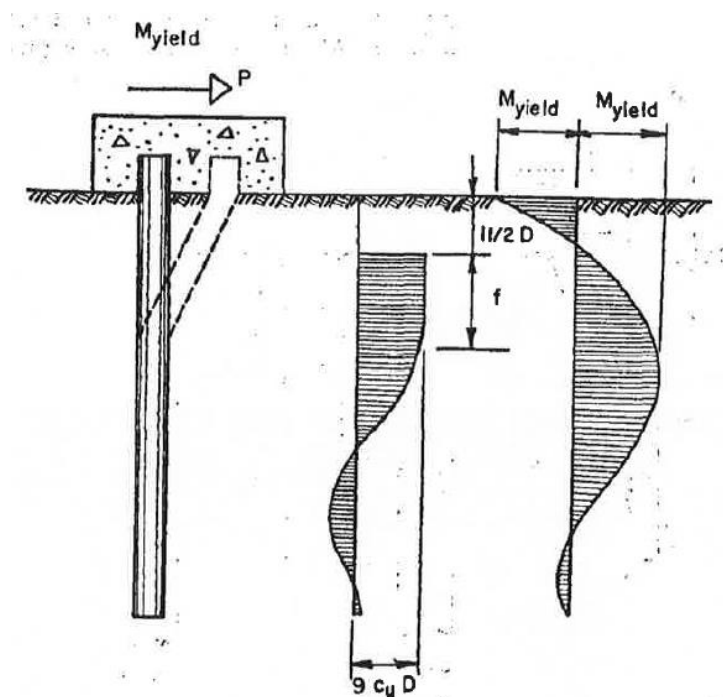


Figure 2.2.6: Deflection, soil reaction and bending moment for a long restrained pile, Broms [Br1964]

He pointed out, that for truly fixed-headed conditions the maximum negative bending moment is larger than the maximum positive bending moment. Hence, the yield strength of the pile section is generally exceeded first at the top of the pile. After formation of the first plastic hinge the pile is still able to resist additional lateral loads until a second plastic hinge forms at the point of the maximum positive bending moment. The lateral earth pressure acting at failure on a laterally loaded pile in a saturated cohesive soil is approximately $2 \cdot c_u$ at the ground surface. It is increasing with depth and reaches a maximum of eight to twelve times c_u at approximately three times the pile diameter below the ground surface. As a simplification, Broms assumed the lateral soil reactions equal to zero up to a depth of 1.5 times the pile diameter and equal to $9 \cdot c_u \cdot D$ below this depth. The maximum moment occurs at the level where the total shear force in the pile is equal to zero at a depth below the ground surface of $1.5 \cdot D + f$.

The distance f can be calculated from

$$f = \frac{P}{9 \cdot c_u \cdot D} \quad (2.6)$$

and the ultimate lateral resistance can be determined by

$$P_{ult} = \frac{2 \cdot M_{yield}}{(1.5 \cdot D + 0.5 \cdot f)} \quad (2.7)$$

with

M_{yield} is the resistance of the pile section to bending,

D is the diameter of the pile and

c_u is the cohesive strength of the soil.

For the formulation of maximum working loads, maximum loads for different failure modes and maximum loads for non-restrained, free-headed piles it is referred to [Br1964, Br1965].

Dulacska 1972 – Dowel Action in Concrete Construction

Helen Dulacska formulated failure forces for dowel action of steel crossing artificial cracks in reinforced concrete [Du1972]. She performed shear tests with reinforcement, crossing cracks at different angles to explore the influence of the inclination. The cracks were simulated by a 0.2mm thick sheet brass separating the specimen in two concrete blocks. Figure 2.2.7a. The assumed forces and concrete pressure on the reinforcement is given in Figure 2.2.7b.

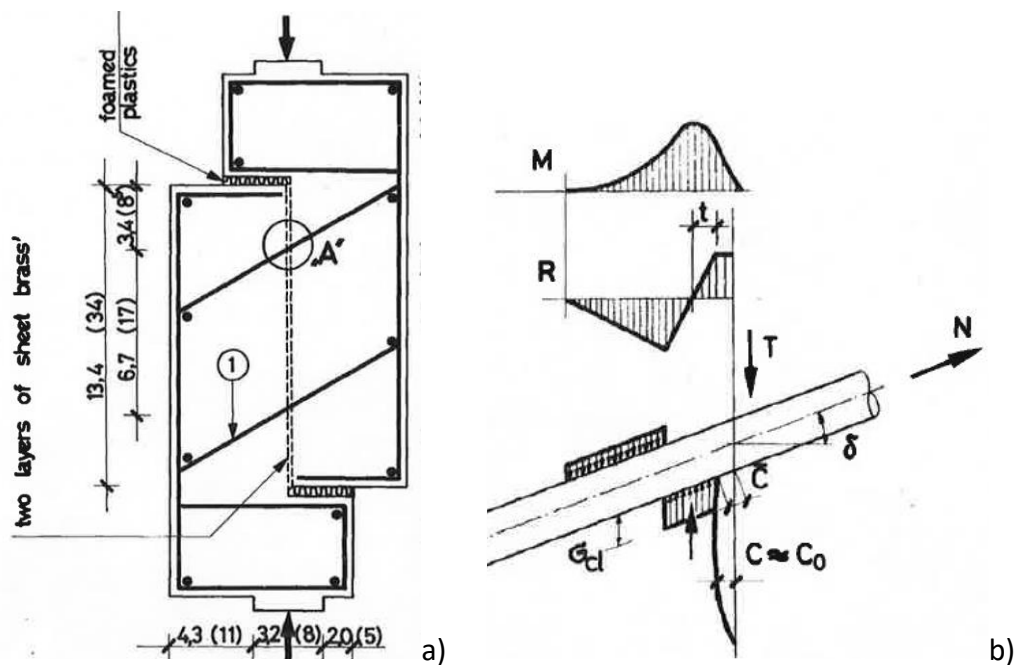


Figure 2.2.7: a) Test set-up, b) Assumed system of forces; Dulacska [Du1972]

Due to the inclination of the reinforcement at the beginning of the test, the bar was subjected to shear and tension directly when the load was applied. With the assumption of an increase of the local compression of the concrete compared to its cube strength by the factor 4 and a constant, determined by comparison with test results set to 0.05, Dulacska derived the following empirical equation to determine the failure force T_f :

$$T_f = 0.2 \cdot \phi^2 \cdot \sigma_y \cdot \sin(\delta) \cdot \left[\sqrt{1 + \frac{\sigma_c}{0.03 \cdot \sigma_y \cdot \sin^2(\delta)}} - 1 \right] \quad (2.8)$$

with

- ϕ bar size
- δ angle of reinforcement crossing the crack
- σ_y yield stress of steel
- σ_c cube strength of concrete

Paulay 1974 – Dowel Action in Concrete Construction

Paulay used the term of “interface shear transfer” to denote the tangential shear force transmitted along a plane, such as a construction joint [Pau1974]. According to Paulay shear is transmitted by bond, dowel action and interface friction. He stated, that the attempt to separate the dowel action from the other mechanisms of interface shear transfer is seldom successful. His test set-up and results are presented in Figure 2.2.8.

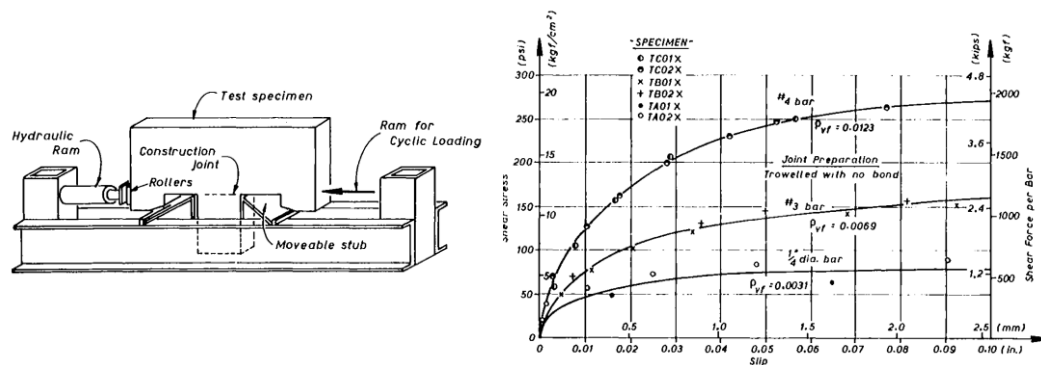


Figure 2.2.8: Test set-up and results, Paulay [Pau1974]

Based on 30 push-off tests, he derived the dowel strength from three basic mechanisms: the flexure of the dowel reinforcement, the shear across the bars and the kinking of the reinforcement.

If flexure of the reinforcement predominates, the transferred shear force can be expected to be proportional to the cube of the bar diameter. For shear across the bar and kinking, the transferred shear force would be proportional to the square of the bar diameter. When the dowels are large, the strength of the surrounding concrete in bearing, rather than the yield strength of the reinforcement, limits the shear capacity of a dowel.

According to his test results the dowel force is proportional to the total area of the reinforcement. Paulay identified shear and kinking as the principal mechanisms of dowel action, Figure 2.2.9.

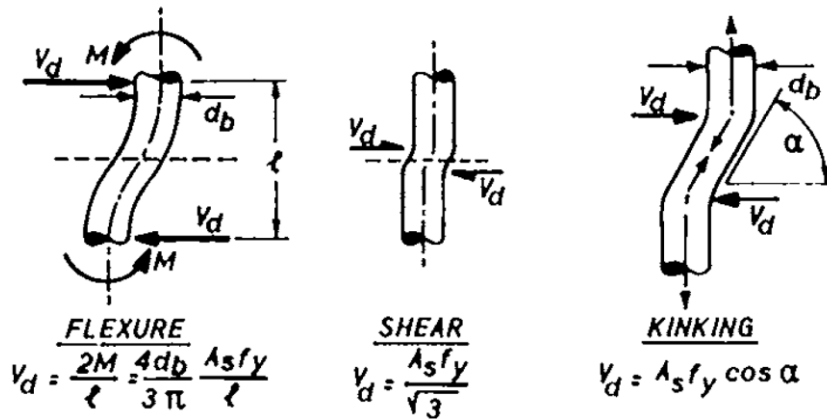


Figure 2.2.9: Mechanism of dowel action, Paulay [Pau1974]

Sourashian 1986, 1987 – Dowel Action in Concrete Construction

Paviz Sourashian performed tests on dowel action aiming for an application in earthquake design [Sou1986]. The test set-up used was similar to the one from H. Dulacska [Du1972], but with increased bar diameters, Figure 2.2.10. After the appearance of split crack, a drop in the dowel load was reported. The dowel strength is formulated for a dowel bar, inclined to the shear interface and therefore subjected also to tension forces, Figure 2.2.11.

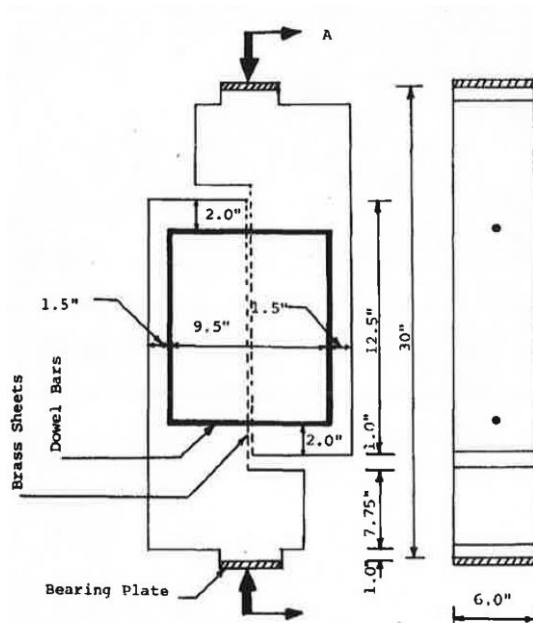


Figure 2.2.10 : Test set-up [Sou1986]

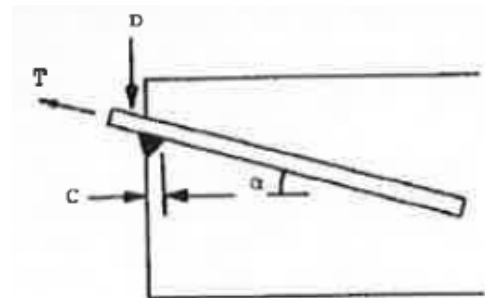


Figure 2.2.11a: Inclined dowel bar [Sou1986]

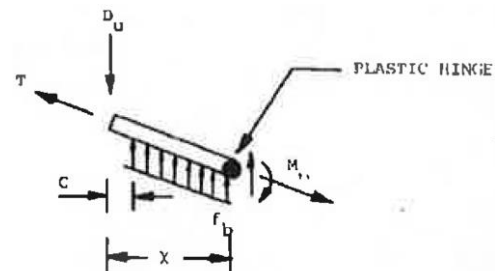


Figure 2.2.11b: Failure condition [Sou1986]

To predict the position of the maximum bending moment in the bar the BEF model was used. The maximum bending moment at a distance x from the dowel load is given by

$$x = \frac{\pi}{4 \cdot \sqrt[4]{k_f \cdot d / E_a \cdot I}} \quad (2.9)$$

with

k_f modulus of support

d diameter of the bar

E_a modulus of elasticity of the bar

I moment of Inertia of the bar.

Failure in the dowel bar is assumed to occur, when a plastic hinge with moment M_p is developed at the position x . Further, it is assumed that the concrete underneath the bar is crushed on a length c , measured from the crack surface. Beyond c up to the distance x , the bearing stress applied to the dowel bar is taken as equal to the value of the concrete strength f_b , Figure 2.2.11b.

The dowel strength is formulated by equilibrium of moments around the plastic hinge for the assumed failure condition. The ultimate dowel strength D_u is given by:

$$D_u = 0.5 \cdot f_b \cdot (0.37 \cdot \gamma \cdot d - c)^2 + 0.45 \cdot f_y \cdot d^2 \cdot \frac{(1 - T^2 / T_y^2)}{\gamma} \quad (2.10)$$

where

$$\gamma = \sqrt[4]{E_a / k_f \cdot d}$$

f_y dowel bar yield stress

c length of the crushed concrete zone with $c = \frac{0.05 \cdot f_y \cdot d}{f'_c} \sin(\alpha)$, where f'_c is the concrete compressive strength

f_b concrete bearing strength under the bar, with $f_b = 37.6 \cdot \sqrt{f'_c} / \sqrt[3]{d}$

T axial force in the dowel bar

T_y plastic tensile force of the dowel bar with $T_y = \pi \cdot d^2 \cdot f_y / 4$

The ultimate resistance and the stiffness of dowel bars bearing on concrete depend on the bearing strength and the bearing stiffness (foundation modulus) of the concrete under the action of the dowel bars. In order to obtain more information about this foundation modulus, additional test were performed and presented by Sourashian et al. [Sou1987], Figure 2.2.12.

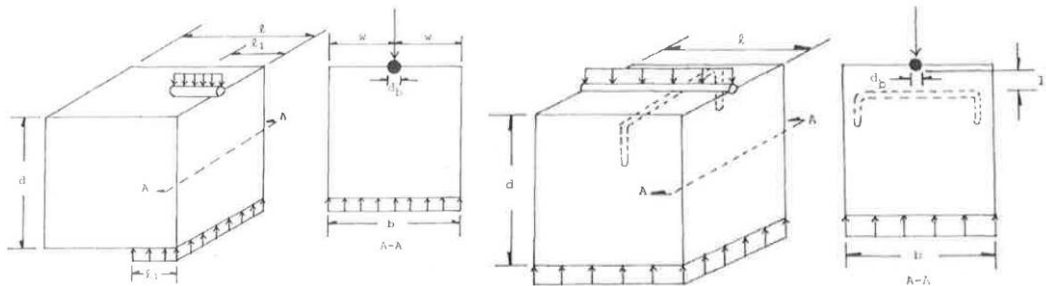


Figure 2.2.12: Tests on concrete foundation modulus, Sourashian [Sou1987]

A ductile failure in the specimen with transversal reinforcement (confined specimen) was observed. Sourashian concluded, that the ductility of dowel bar behaviour can be improved by providing confining reinforcement, but did not considerably influence the bearing strenght of stiffness of the concrete. According to Sourashian the bearing strenght, f_b , can be estimated by:

$$f_b = 8 \cdot \sqrt{f'_c \cdot l/l_1} \cdot (w/d_b)^{1/2} \quad (2.11)$$

with

f'_c	concrete compressive strenght [MPa]
l	length of concrete block
l_1	embedment length of dowel bar
w	distance from edge of block to center line of dowel bar
d_b	bar diameter

And for the determination fo the concrete bearing stiffness, K_f , he gives:

$$K_f = 127 \cdot c_1 \cdot \sqrt{f'_c} \cdot (1/d_b)^{1/2} \quad (2.12)$$

with

c_1	coefficient depending upon bar spacing
f'_c	concrete compressive strenght [MPa]

Vintzeleou 1986, 1987 – Monotonic and Cylcic Tests

E.N. Vintzeleou developped analytical formulation to describe the behaviour of dowels embedded in concrete with the aim to predict the dowel strenght and the transverse displacements [Vin1986]. In addition, she analyzed the load-bearing behaviour of dowels under cyclic loading, which is not of interest for this Thesis, reference is made to [Vin1987].

She indentified two failure modes for dowel mechanism: Failure mode I is based on the yield of the bar and concrete crushing under the dowel and Failure mode II is concrete splitting in case of small concrete cover [Vin1986]. Focus is given here to Failure mode I, which is based on plastic limit analysis. Assuming that the bar behaves as a free-headed pile in cohesive soil as given in Figure 2.2.13.

Failure occurs, when a plastic hinge forms at a distance a , measured from the surface to the position of maximum bending moment [Br1964]. With the knowledge that in case a concentrated load is imposed on an infinitely extended homogenous and isotropic body, the bearing capacity of the loaded body is several times as high than its uniaxial value [Pra1920], she formulated the following quadratic equation for the dowel resistance D_u .

$$D_u^2 + (10 \cdot f_{cc} \cdot e \cdot d) \cdot D_u - 1.7 \cdot d^4 \cdot f_{cc} \cdot f_y = 0 \quad (2.13)$$

with

f_y	dowel bar yield stress
f_{cc}	concrete compressive strength
e	eccentricity of dowel force
d	dowel bar diameter

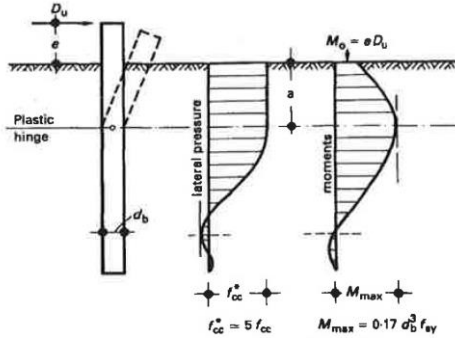


Figure 2.2.13: Failure mechanism Vintzeleou [Vin1986]

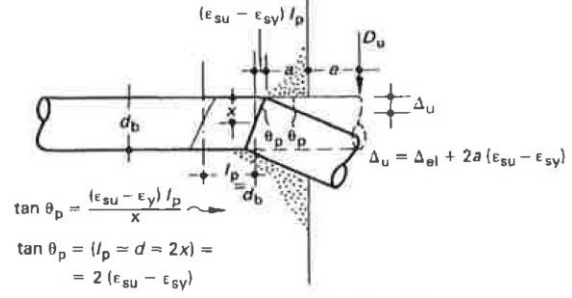


Figure 2.2.14: Plastic displacement of a dowel at failure [Vin1986]

In addition Vintzeleou derived an analytical formulation of the transverse displacement of the dowel at failure Δ_u by summing up the elastic displacement Δ_{el} and the plastic Δ_{pl} . For the calculation of the plastic deflection she assumed that the length of the concrete influenced by the dowel shear force is approximately equal to $2 \cdot d$, the plastic rotation θ_p of the plastic hinge is given by the expression $\tan(\theta_p) = 2 \cdot (\epsilon_{su} - \epsilon_{sy})$ and the depth of the plastic hinge a , is given by $a = d \cdot \left(1 - \sqrt[3]{0.22 \cdot \frac{e}{d}}\right) / \sqrt{\frac{f_{cc}}{20}}$, see Figure 2.2.14. And the displacement of the dowel at failure is given by:

$$\Delta_u = \Delta_{el} + \Delta_{pl}$$

$$\Delta_u = \frac{2 \cdot D_u \cdot \beta \cdot (e \cdot \beta + 1)}{E_{cc}} + 2 \cdot (\epsilon_{su} - \epsilon_{sy}) \cdot d \cdot \left(1 - \sqrt[3]{0.22 \cdot \frac{e}{d}}\right) / \sqrt{\frac{f_{cc}}{20}} \quad [\text{N/mm}^2] \quad (2.14)$$

where

ϵ_{su} rupture strain of the dowel bar

ϵ_{sy} yield strain of the dowel bar

E_{cc} Young's modulus of elasticity of concrete

β Foundation modulus $\beta = \left(\frac{k_f \cdot d}{4 \cdot E_a \cdot I}\right)^{1/4}$

The test set-up is given in Figure 2.2.15 and her comparison of the theoretical values for the dowel strenght D_u and experimental results is given in Figure 2.2.16.

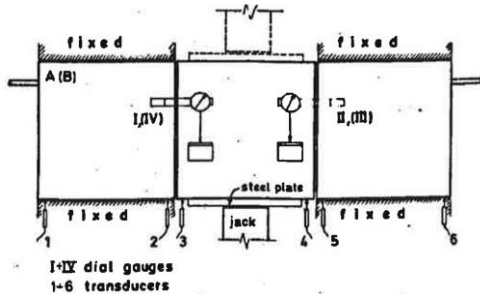


Figure 2.2.15: Test set-up [Vin1987]

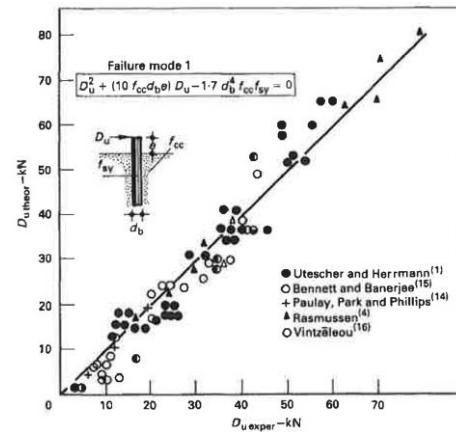


Figure 2.2.16: Theoretical dowel resistance and test results [Vin1986]

Pruijssers 1988 – Offshore Structures

The aim of the research work of Pruijssers was to determine the relationship between stresses and displacements occurring in the crack plane of foundations for offshore structures in the arctic sea [Pru1988]. He performed shearing tests with “low-intensity high-cycling”, Figure 2.2.17.

According to Pruijssers, with increasing dowel force the concrete stresses at the vicinity of the bar exceed the uniaxial concrete compressive strength. Because the surrounding concrete provides a considerable confining pressure, thus a triaxial compressive zone under the bar forms. Therefore, the concrete strength can be several times as high as the uniaxial strength and the bar becomes the weakest link. Pruijssers postulates that the ultimate force is reached when the bar yields and a plastic hinge forms, Figure 2.2.18. Formulating the equilibrium in the plastic hinge he considers the bond between the bar and the supporting concrete, resulting in a bond force, situated at a distance z_n from the centreline of the bar, Figure 2.2.19. The bond force results in an increase of the plastic bending resistance of the bar of 34%, where the presence of an acting tensile force the shift z_n is decreasing which leads to a reduction of the dowel strength.

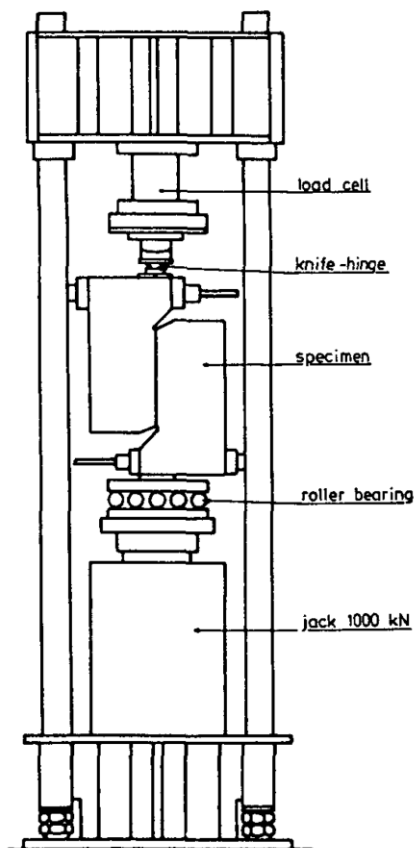


Figure 2.2.17: Test set-up [Pru1988]

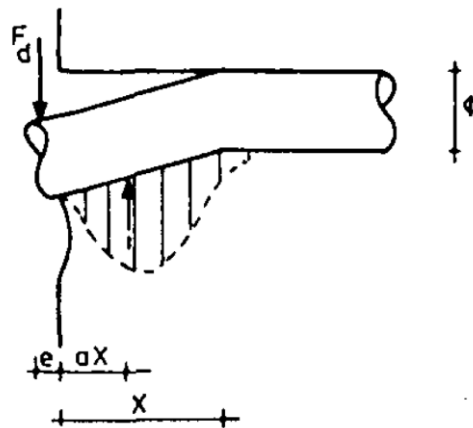


Figure 2.2.18: Failure mechanism due to plastification [Pru1988]

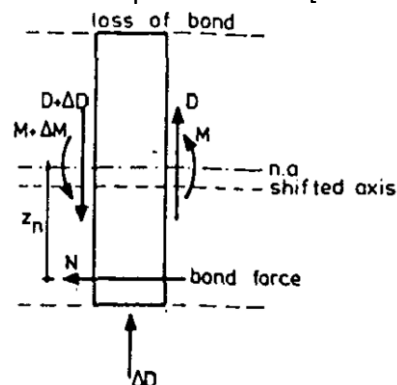


Figure 2.2.19: Equilibrium condition for the plastic hinge [Pru1988]

Dei Poli 1992 – Shear Joints in Reinforced Concrete

Dei Poli pointed out, that the analogy of a beam on elastic and cohesionless foundation (BEF analogy) is less applicable to describe the maximum load. At ultimate load situation concrete and steel exhibit nonlinear behaviour, the concrete is cohesive, and the embedment efficiency is affected by the geometry [Dei1992]. The most relevant parameter is the subgrade stiffness of the concrete embedment k , Figure 2.2.20. With reference to ultimate load situation, both concrete and steel nonlinearities have to be considered, as well as the localized damage within the concrete, Figure 2.2.21.

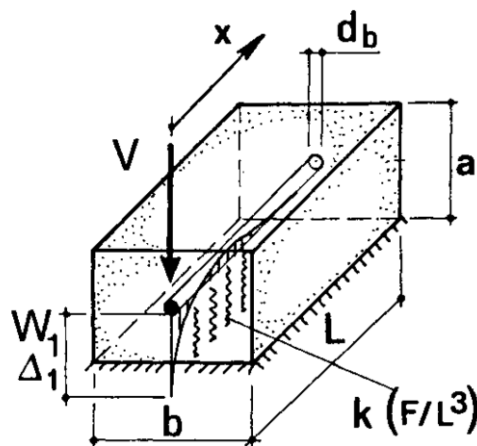


Figure 2.2.20: Parameters in study of dowel action [Dei1992]

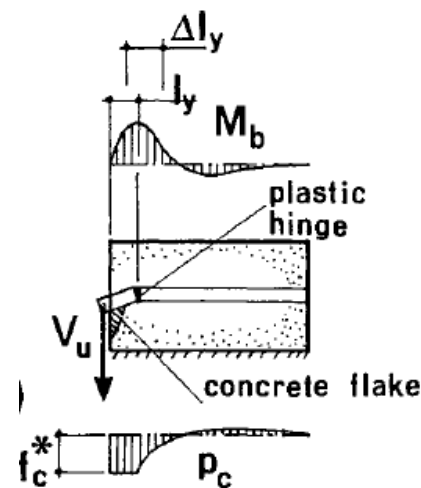


Figure 2.2.21: Limit analysis of dowel [Dei1992]

Further, the collapse of the dowel action may be triggered either by the local crushing of the concrete under the dowel or by the yielding of the dowel. But, eventually both phenomena are activated, because both are characterized by a ductile behaviour. Many researchers have evaluated the load-carrying capacity of the dowel strength within a limit-analysis approach, based on the simultaneous formation of a plastic hinge in the bar and a crushed zone in the concrete.

Dei Poli proposed, that a constant value could be given to the subgrade stiffness k in the linear, elastic phase (BEF model). While in the nonlinear phase k should be formulated as a function of the displacement at the interface with the dowel bar to introduce the “damage” due to load build-up. The damage may be represented also by parameters other than the displacement, such as the “load level” V/V_u , where V_u is the ultimate capacity of the dowel and V is the actual load applied to the dowel.

To analyse the transverse displacement of a long dowel embedded in concrete subjected to a shear load at the free edge, Dei Poli performed a set of 27 block-type reinforced concrete specimens. The tests were performed displacement controlled and the displacement of the reinforcement bar was directly measured using ducts, Figure 2.2.22.

The tests were stopped at a displacement of the loaded section to a value of $1/5$ to $1/3$ of the bar diameter. He observed, that at 80% of the maximum load the concrete under the dowel close to the forefront of the specimen started to deteriorate, which eventually led to the detachment of a flake. At load levels below 40% of the maximum load, the bars did not show any plasticization.

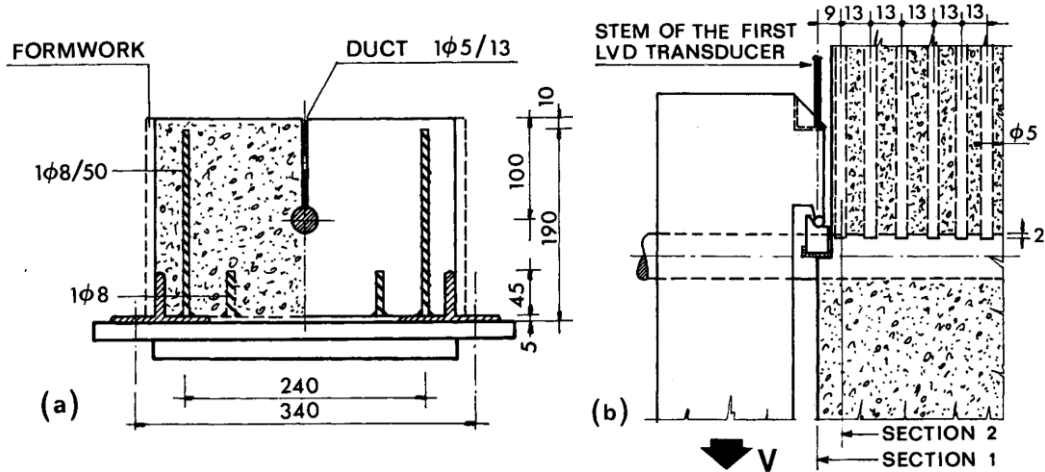


Figure 2.2.22: Test specimen with concrete-embedded ducts [Dei1992]

The load displacement curves for bar diameters 14mm, 18mm and 24mm are given in Figure 2.2.23. The displacement is given at two positions, section 1 (Figure b) and section 2 (Figure a).

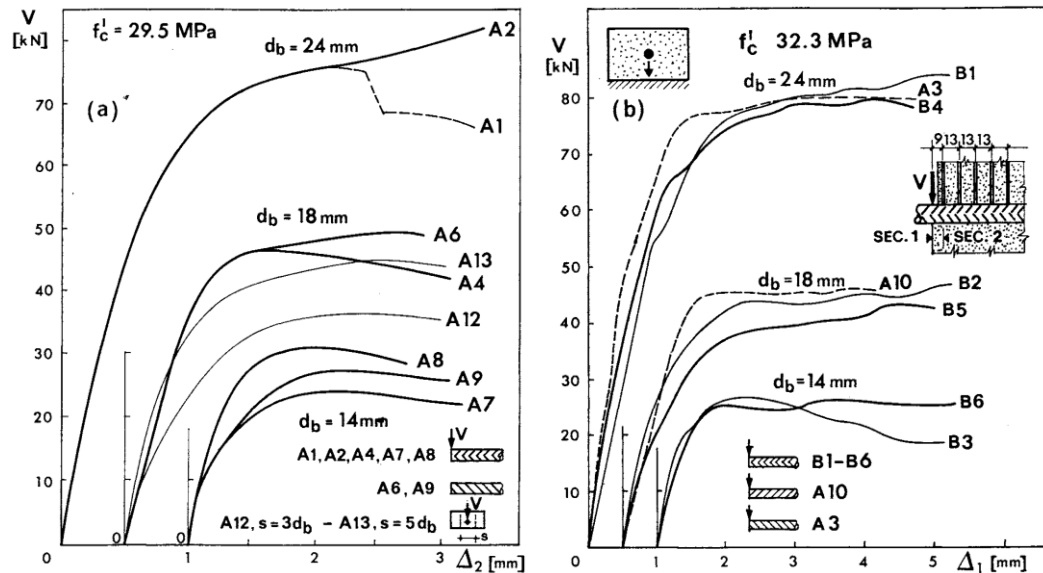


Figure 2.2.23: Load displacement curves, Dei Poli [Dei1992]

Dei Poli pointed out, that for a bar at right angles to the shear plane, the ultimate capacity of a dowel formulated by simple limit-analysis models as proposed by Dulacska [Du1972] and Sourashian [Sou1986] gives reliable values. But, a possible inclination of the bar affects the dowel capacity due to the acting tension force in the dowel.

Tanaka 2011 – Dowel Action in Concrete Construction

To investigate the load bearing behaviour of steel bars embedded in concrete (dowel bars) and transversely loaded, Tanaka performed 14 tests [Ta2011], Figure 2.2.24.

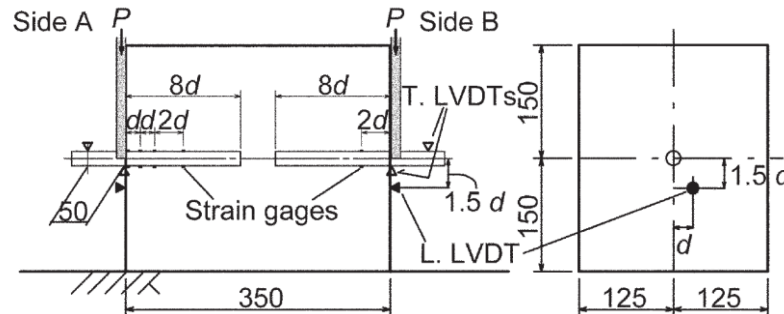


Figure 2.2.24: Test specimen, Tanaka [Ta2011]

Tanaka investigated the applicability of the traditional BEF analogy for the elastic behaviour of dowel bars, but also a possible extension of this analogy to post yielding of the bars. Aim of the performed test series was to examine the dowel behaviour and to determine values for the foundation modulus K . After yielding of the dowel bar, failure occurred in the tests by spalling of the concrete under the dowel bar at the surface of the concrete. According to Tanaka, the measured K -values (= foundation modulus) are likely to increase with the increase of the bar diameter, Figure 2.2.25.

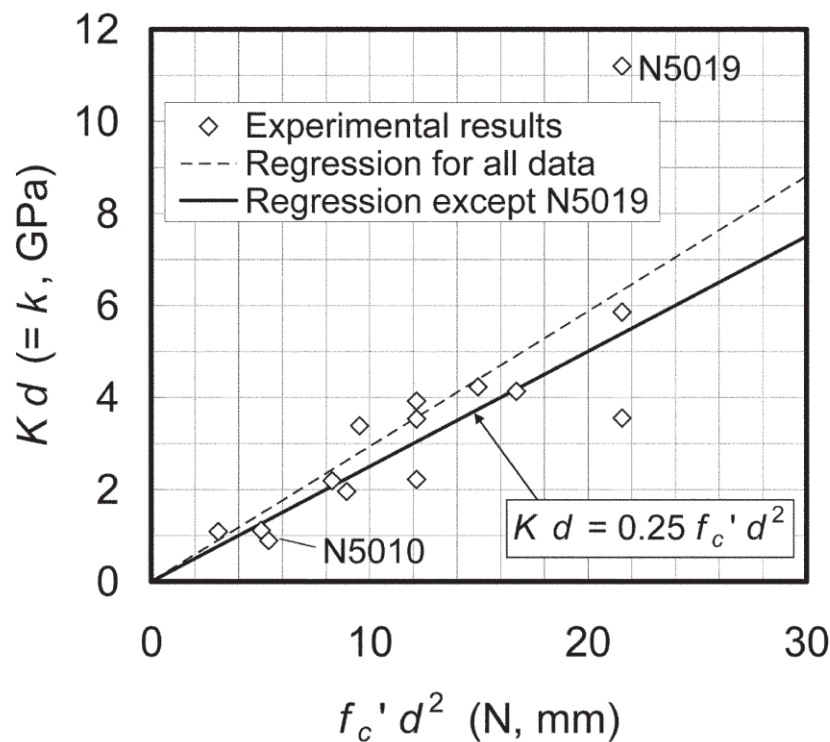


Figure 2.2.25: Relationship of ($K \cdot d$) and ($f_c' \cdot d^2$) based on experiments [Ta2011]

Tanaka proposed the following equations for the load at first yielding P_y , at spalling P_{sp} and for the ultimate load P_u .

$$P_y = \frac{\pi \cdot d^3 \cdot f_y}{32} \cdot \frac{\beta \cdot e^{\beta \cdot L_m}}{[(1 - \beta \cdot g) \cdot \sin(\beta \cdot L_m) - \beta \cdot g \cdot \cos(\beta \cdot L_m)]} \quad (2.15)$$

$$P_{sp} = 0.84 \cdot d^2 \cdot \sqrt{f'_c \cdot f_y} \quad (2.16)$$

$$P_u = 1.0 \cdot d^2 \cdot \sqrt{f'_c \cdot f_y} \quad (2.17)$$

with

$$L_m = \frac{1}{\beta \cdot \tan\left(\frac{1}{1 - 2 \cdot \beta \cdot g}\right)}$$

$$\beta = \sqrt[4]{\frac{K \cdot d}{4 \cdot E_a \cdot I}}$$

d Diameter of dowel bar

K foundation modulus of concrete under the dowel bar, $K = 0.25 \cdot d \cdot f'_c$

E_a Young modulus of dowel material

I Inertia of dowel bar

g excentricity of the applied load to surface of specimen.

Loads at at first yielding and spalling in relation to the dowel index $d^2 \cdot (f'_c \cdot f_y)^{0.5}$ are shown in Figure 2.2.26.

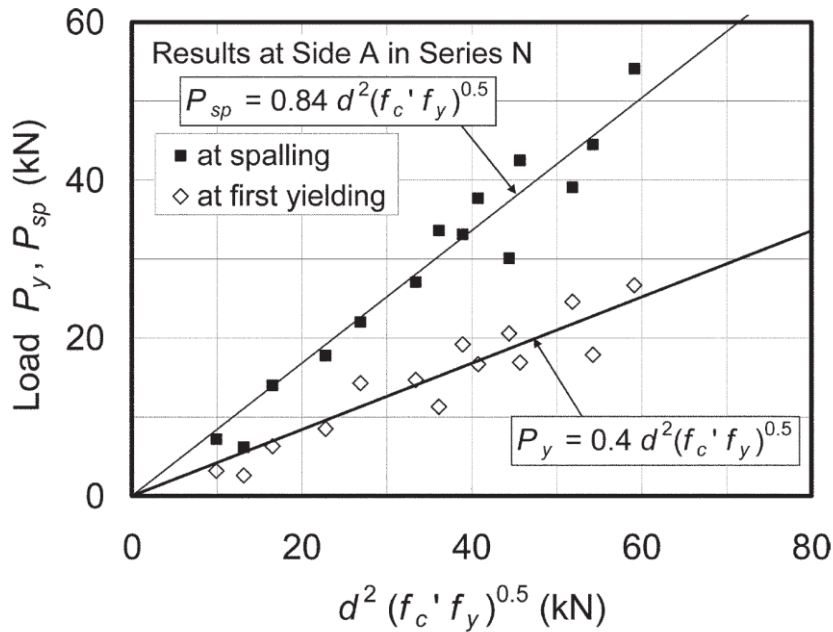
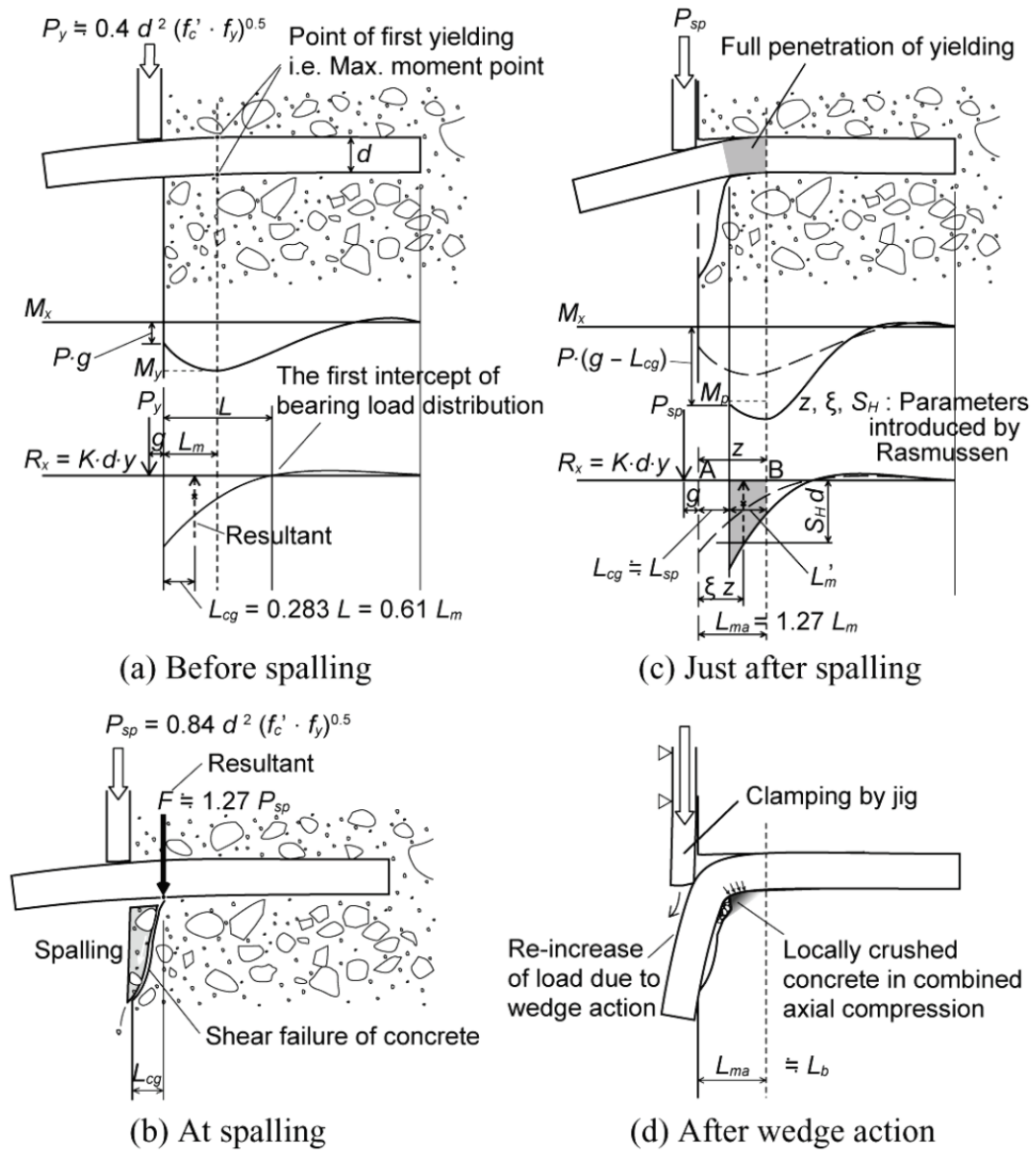


Figure 2.2.26: Load at first yielding and spalling in relation to dowel index $d^2 \cdot (f'_c \cdot f_y)^{0.5}$, Tanaka [Ta2011]

Tanaka described, that a plastic hinges forms in the dowel at distance L_m from the edge of the specimen. The depth L_m can be defined by elastic BEF analogy, defining L_m as the point of first yielding. Further, assuming that the BEF analogy would be still applicable to the dowel bars in the remaining concrete after spalling, the origin for another axis (x' -axis) is positioned at the delaminated surface of the concrete. The process up to failure of the dowel is schematically given in Figure 2.2.27.



note: Additional notation, introduced by Rasmussen

S_H = ratio of the average of bearing stress distribution to f'_c

z = assumed depth to plastic hinge of bar, mm (in.)

ξ = assumed ratio of depth to the resultant of bearing stress to z

Figure 2.2.27: Schematics of the failure mechanism of dowel bar [Ta2011]

Sørensen 2017 – Limit Analysis by Second Order Plasticity Model

Sørensen developed a model to describe the shear behaviour of two-sided dowel joints at large shear displacements in the non-linear regime [Sor2016], [Sor2017]. He used a second order rigid-plastic approach to establish a link between the shear displacement u and combinations of moment and tension that develop in the rebar crossing the joint by utilizing kinematic relations and the normality condition of plastic theory. Sørensen assumes a mechanism of two plastic hinges, and further, that the plastic deformations, an elongation Δ and a rotation θ , are acting in the plastic hinges only, Figure 2.2.28.

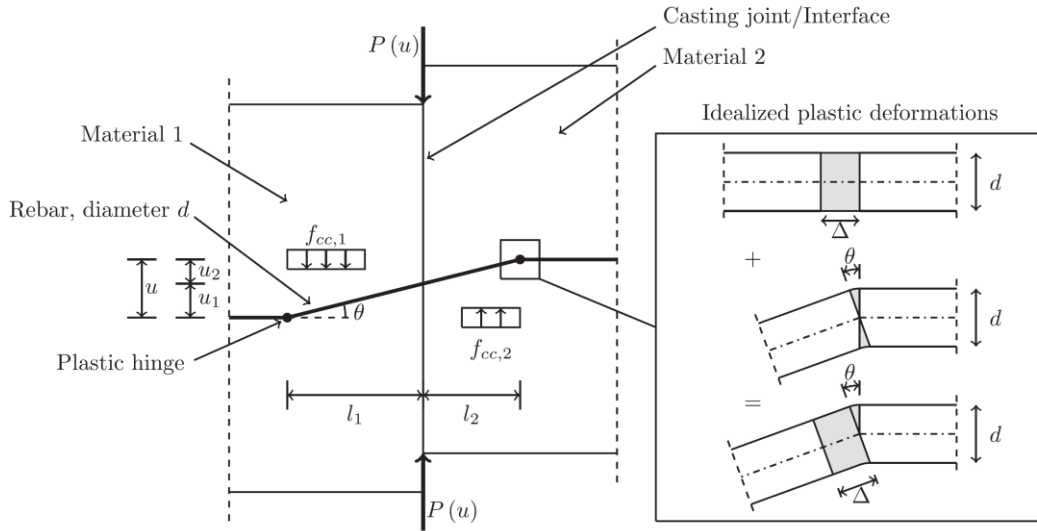


Figure 2.2.28: Two sided joint, Sørensen [Sor2017]

By establishing the kinematic relationship for the assumed mechanism he determined the rates of plastic deformations. Then, by imposing the normality condition of plastic theory and by applying the work Equation for increments of displacement, he derived an Equation for the maximum shear load of a smooth, frictionless joint P_s as a function of the displacement u . The total work is composed of work causing the elongation and the rotation in the plastic hinges and of the rebar crushing the concrete underneath. In addition, Sørensen included the possible contribution of friction P_f , caused by compressive stresses normal to the shear interface. The shear load P as a function of the displacement u is given by:

$$P_{total}(u) = P_s(u) + P_f(u) \quad (2.18)$$

with

$$P_s(u) = \begin{cases} \frac{1}{2} \cdot f_{cc,1} \cdot d \cdot \frac{l_{1,ef}^2}{l_1 + l_2} + \frac{1}{2} \cdot f_{cc,2} \cdot d \cdot \frac{l_{2,ef}^2}{l_1 + l_2} + 2 \cdot N(u) \cdot \dot{\Delta} + 2 \cdot M(u) \cdot \dot{\theta}; & \text{for } N(u) < N_{pl} \\ 2 \cdot N_{pl} \cdot \dot{\Delta}; & \text{for } N(u) = N_{pl} \end{cases}$$

$$P_f(u) = \mu \cdot N(u) \cdot \cos(\theta)$$

It should be noted, that this approach only predicts the non-linear behaviour.

Sørensen validated his model by comparison with test results. His test set-up is given in Figure 2.2.29. He performed 25 push-off tests, varied the quantity of bars crossing the shear joint and the surface conditions (Concrete or Mortar). The diameter of the dowel reinforcement was constant with $d = 8\text{mm}$. Detailed specification of his tests and material properties are given in Table 2.2. , results are given in Figure 2.2.30. For more information it is referred to [Sor2017].

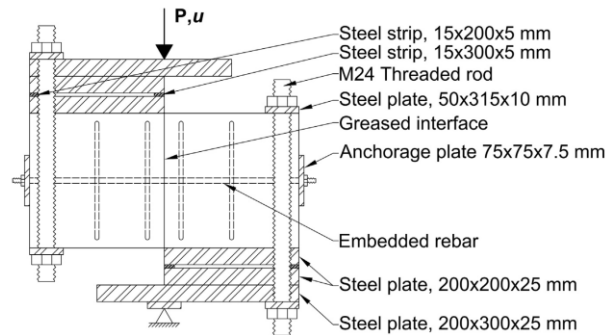


Figure 2.2.29: Test set-up, Sørensen [Sor2017]

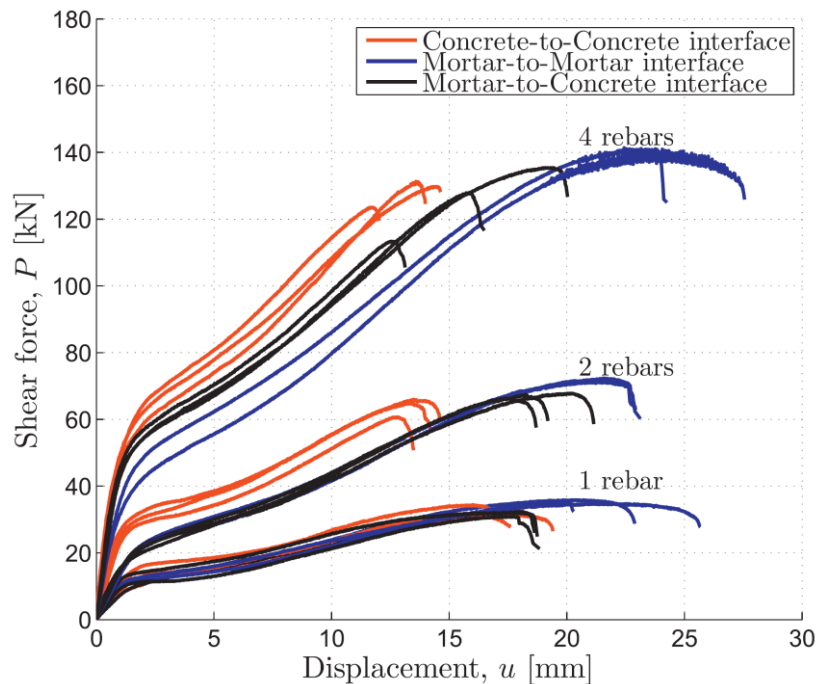


Figure 2.2.30: Test results, Sørensen [Sor2017]

Table 2.2: Specifications and material properties, Sørensen [Sor2017]

n	Interface combination	d [mm]	f_y [Mpa]	f_u [MPa]	f_{c1} [MPa]	f_{c2} [MPa]	No. of rep.
1	C/C	8	614	729	48.0	48.0	3
1	M/M	8	614	729	33.1	33.1	3
1	M/C	8	614	729	33.3	47.7	3
2	C/C	8	614	729	46.5	46.5	3
2	M/M	8	614	729	34.1	34.1	2
2	M/C	8	614	729	30.3	35.3	3
4	C/C	8	551	708	43.0	43.0	3
4	M/M	8	614	729	34.5	34.5	2
4	M/C	8	551	708	37.2	45.4	3

2.3 Concrete Dowels as shear connector in composite beams

Steels strips can be used as shear connector in composite structures. The development of this type of connector is basically described in this Section, based on thorough literature review. Focus is given on the basic load transfer and mechanical principles of metal strips as shear connector. Puzzle-shaped shear connectors see e.g. [P621, P804, Se2009], are less of interest for this Thesis.

Leonhardt, Andrä (1985, 1987, 1990) – Development of Perfobond strip, Germany

Searching for a continuous shear connector with improved fatigue behaviour compared to shear studs, H.-P. Andrä described pull-out tests done at the University of Stuttgart, Germany, using a steel strip, which can be welded on the upper flange of a steel beam [An1985]. Aim of this research was the economical improvement of another type of a continuous shear connector used by Leonhardt [Leo1951]. Andrä performed pull-out tests on metal strips with punched rectangular openings of different size. The test set-up and load-slip curves are shown in Figure 2.3.1 and Figure 2.3.2.

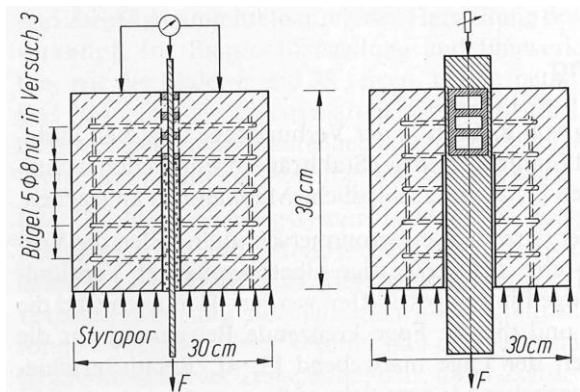


Figure 2.3.1: Test set-up, Andrä [An1985]

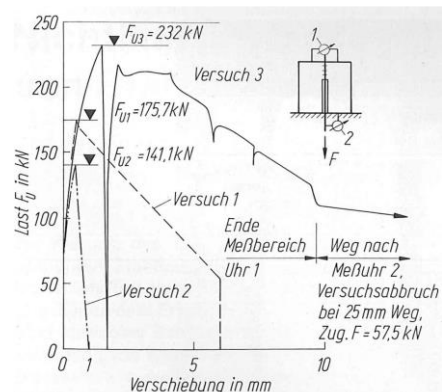


Figure 2.3.2: Load-slip curves, Andrä [An1985]

Test number 3 (= “Versuch 3”) was performed with additional stirrup reinforcement (“Bügel”), which demonstrated a higher load-bearing capacity and an increase of the ductility of specimen 3. Failure of tests number 1 and 2 (“Versuch 1” and “Versuch 2”) occurred due to splitting of the concrete specimen. In test 3 failure of the webs of the steel strip due to shear was observed. The additional reinforcement led to concrete confinement, acting as a restraint and consequently increasing the concrete compressive strength at the openings of the metal strip.

In addition, Andrä reported about a pull-out test of a metal strip with circular openings, which could act as shear connector for composite beams, welded on the upper flange of a steel beam. Probably this was the first test of the future “Perfobond” shear connector. The dimensions of the metal strip, load-displacement curve and the metal-strip after testing are given in Figure 2.3.3 and 2.3.4.

To avoid splitting of the concrete perpendicular to the metal strip, Andrä added in total 8 transversal reinforcement bars with a diameter of 8mm outside of the circular openings. This type of shear connector showed a high stiffness up to 80% of the total load and at larger displacements a very ductile behaviour. Andrä reports further, that the test was stopped at a displacement of 30mm, when still no failure could be observed. It is remarkable that, this metal strip achieved a shear resistance of 2015 kN/m, which represented the resistance of 20 traditional shear studs with a diameter of 22mm, according to Andrä. He pointed out, that the cost of the metal strip is only 1/5 of the cost of 20 shear studs, which underlined the economical potential of metals strips as shear connector for composite beams. Finally, the high stiffness at serviceability state and the ductile behaviour after reaching the ultimate load before failure of this type of shear connector convinced Andrä and Leonhardt to continue their research.

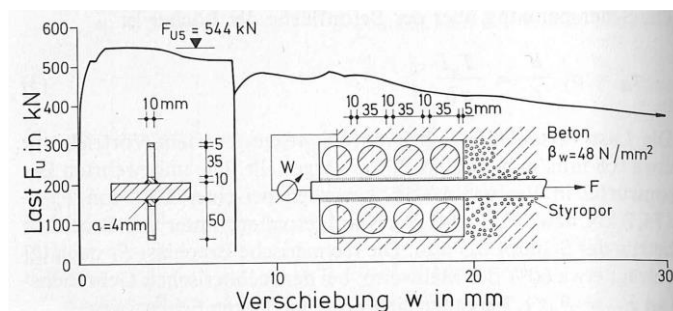


Figure 2.3.3: Tests on metal strip with circular openings, Andrä [An1985]

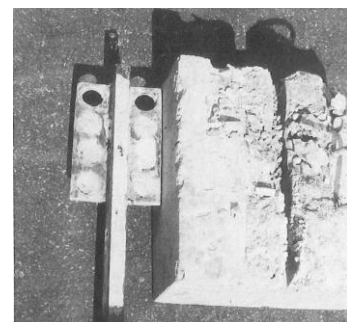


Figure 2.3.4: Metal strip after testing [An1985]

Consequently, Leonhardt and Andrä performed further tests on metal strips with circular openings. Results of a series of three push-out tests on the shear connector tested by Andrä were published in 1987 [Leo1987]. The tests were done at the University of Stuttgart, Germany. In this publication they refer to the flat steel strip with large, punched holes at close intervals as “Perfobond” strip, Figure 2.3.5.

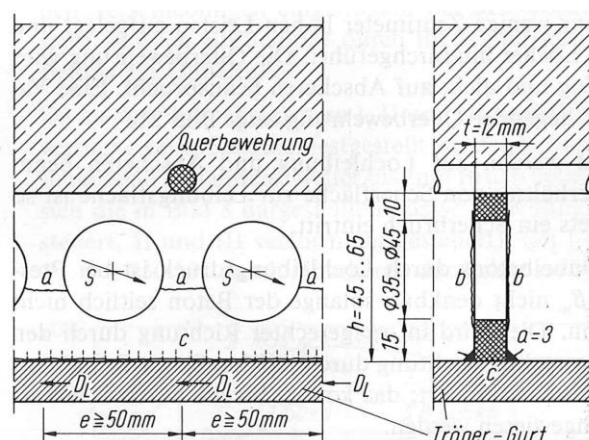


Figure 2.3.5: Perfobond connector [Leo1987]

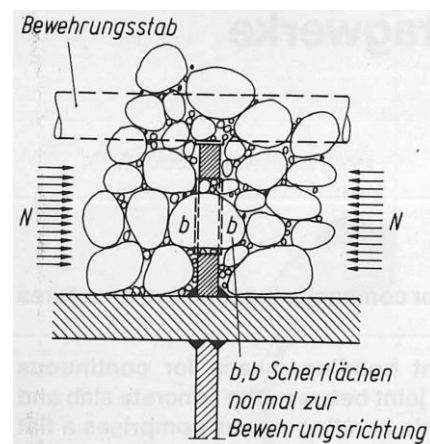


Figure 2.3.6 Local situation at opening [Leo1987]

According to Leonhardt, the concrete going placed in the circular openings transfers the shear forces by aggregate interlock, acting as a concrete dowel. Two shear surfaces occur, one at each edge of the steel strip, Figure 2.3.6. The uplift of the concrete slab is prevented by the circular openings in the steel strip. Tensile forces, resulting from the widening of the compression stresses, are first counterbalanced by the concrete in the opening and at further load increase, by the transversal reinforcement. The trajectories in compression and tension are given in Figure 2.3.7.

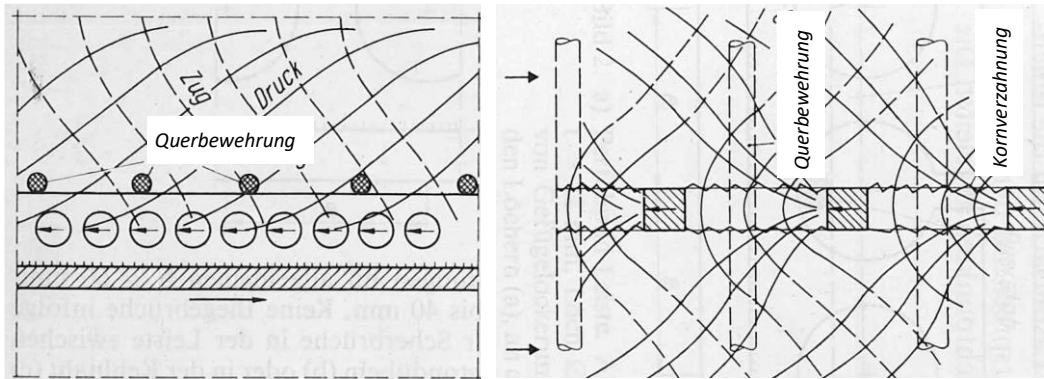


Figure 2.3.7: Trajectories in compression and tension, Leonhardt [Leo1987]

Leonhardt provided the following general explanations of the load transfer: A transversal reinforcement placed above the metal strip is subjected to tensile actions only. In case it is put through the holes, it is also subjected to shear. Failure of the concrete directly in the circular opening cannot occur, as long as the concrete is kept in place, is restraint. The horizontal shear force is divided into local pressure of the concrete in the openings on the web of the steel strip between the holes. From the web the force is transferred via the fillet welds continuously to the steel flange. Failure modes are the shearing of the concrete dowels or of the metal strip at the holes. Due to the vertical and horizontal restraint of the concrete in the circular openings, the concrete in the holes is confined and practically cannot fail. It has a resistance of at least 8 times the uniaxial compressive strength. After reaching the load bearing resistance significant transfer of the shear force remains, plastic design is applicable.

To investigate the behaviour of the Perfobond connector, Leonhardt performed dynamic tests with $N \geq 2,5 \cdot 10^6$ load cycles, applied at a frequency of 2.75 Hz. Geometry of the push-out specimen and the Perfobond strips is given in Figure 2.3.8 and 2.3.9. Before the start of the load cycles, a static load of 800 kN was applied, the estimated load for the use phase. The displacement measured at the cycling tests remained at very low level, around 0.12mm and no damage was observed after the load cycles. Therefore, static testing till failure of the 3 specimens was done. The resulting load-slip curves are given in Figure 2.3.10. Test 1 failed due to shearing of the metals strip (steel failure). Due to a defect on the loadpress for test 2, the load was applied as impact load. Consequently, the corresponding displacements could not be recorded. Failure occurred due to shearing of the concrete dowels. Test 3 was performed displacement controlled and an ultimate load of 1830 kN was reached.

Failure occurred due to shearing of the steel strip and of the concrete dowels simultaneously. Leonhardt pointed out, that the Perfobond shear connector showed a much better behaviour (no slip increase with increasing load cycles) than headed shear studs. For further reference see also [An1990].

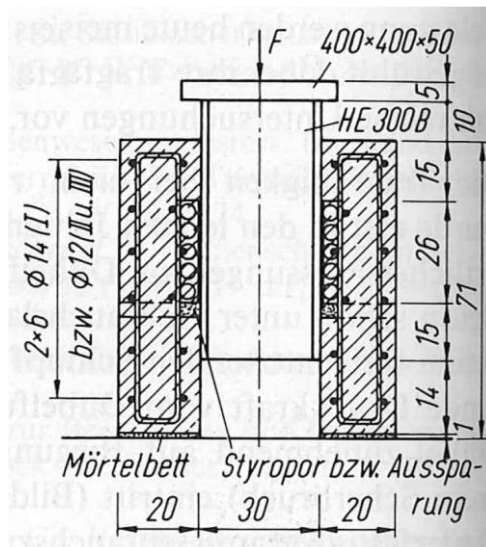


Figure 2.3.8: Push-out specimen [Leo1987]

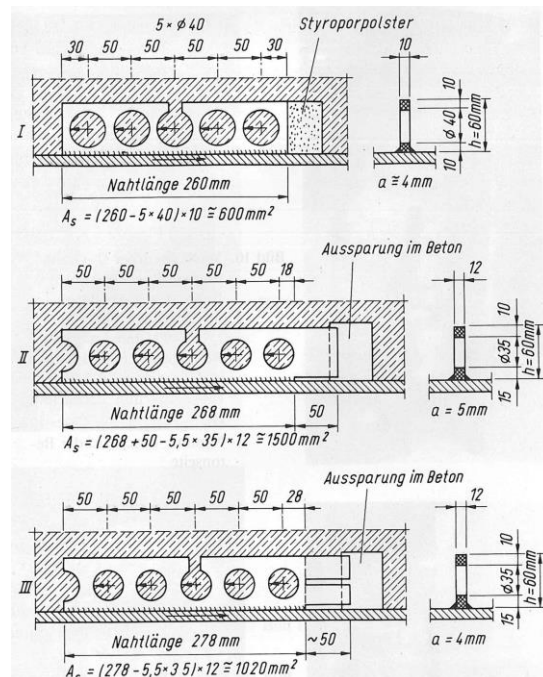


Figure 2.3.9: Geometries of tested Perfobond [Leo1987]

Based on his test observations Leonhardt pointed out, that at low load levels the shear connection behaves rigid, while at increasing load the stiffness of the shear connection is reducing. Further, after the shear resistance is reached, load is still transferred by friction, curve III in Figure 2.3.10. The splitting of the concrete specimen at the shear surfaces is prevented either by transversal reinforcement or by external pressure (e.g. transversal bending of the slab or by prestressing). Even at huge displacements of several millimeters the friction coefficient is nearly not reducing.

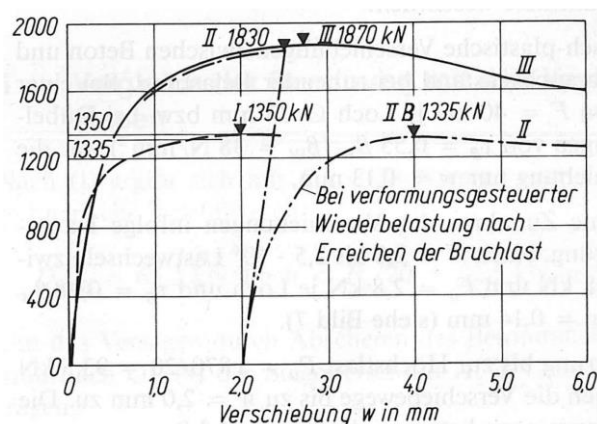


Figure 2.3.10: Load-displacement of static push-out tests after cycles [Leo1987]

According to Leonhardt shear failure of the concrete dowels happened for test III at a concrete shear stress of around $\tau_u \sim 1.3 \cdot \beta_w$. Based on this observation and assuming the steel strip is designed as such, that no shear failure can occur in the strip, he proposes to use as design resistance for the concrete dowel the following equation, where index c indicates possible concrete failure and index s steel failure:

$$D_{PBL,c} = 1.4 \cdot d^2 \cdot \beta_{WN} \leq D_{PBL,s} = 1.44 \cdot A_s \cdot \beta_s \quad (2.19)$$

with

PBL Perfobond steel strip

d diameter of web opening

β_{WN} concrete cube strenght

A_s smallest surface of the steel web

β_s yield strenght of steel strip

To limit the concrete pressure in the opening, the thickness of the steel strip t should be chosen that the following equation is fulfilled:

$$D_{PBL,c,d}/(d \cdot t) \leq 6 \cdot \beta_{WN} \quad (2.20)$$

Further, to prevent splitting of the concrete, transversal reinforcement has to be added. By assuming an angle of $\tan v = 0.4$ of the compression strut and by reducing the stresses to 50% of the yield stress, Leonhardt proposed a minimum surface of the transversal reinforcement $A_{s,q}$ of:

$$A_{s,q} > 0.8 \cdot D_{PBL,c}/\beta_{sq} \quad (2.21)$$

with

β_{sq} yield strenght of reinforcement

A comparison of shear resistance of Perfobond strip (PBL) with shear studs (KBD) is given in Figure 2.3.11. Reading the diagram it has to be considered, that the resistance of shear studs was calculated according to [DIN1981].

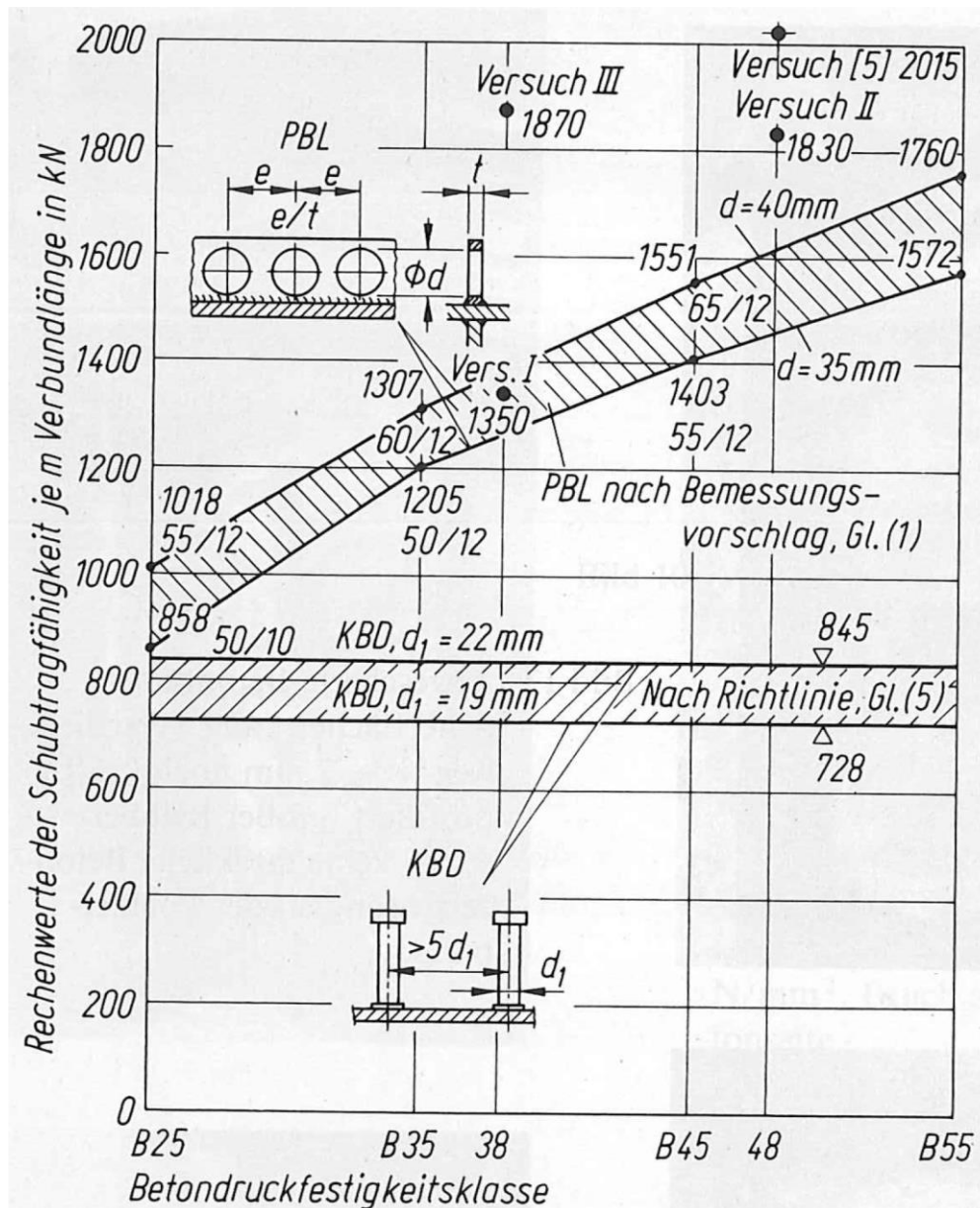


Figure 2.3.11: Shear resistance of Perforbond strip (PBL) in comparison to shear studs (KBD), Leonhardt [Leo1987]

In a following publication [An1990] the design of the dowel resistance was slightly modified to a value of $D_{PBL,c} = 1.0 \cdot d^2 \cdot \beta_{WN}$, when the transverse (splitting) reinforcement remained at a value of $A_{s,q} = 0.8 \cdot 1.4 \cdot d^2 \cdot \beta_{WN} / \beta_{sq}$.

The research from Leonhardt and Andrä concluded in an technical approval for the "Perforbondleiste" [Z-26.4-38]. The design method given in [Z-26.4-38] is based on a the partial safety factor method, while in the research presented in [An1985], [Leo1987], [An1990], still a global safety factor is used to derive design values.

Patent and technical Approval from Brendel 1987 - Kombi-Verdübelung

At the time Andrä and Leonhardt investigated the load-bearing behaviour of Perfobond, Brendel performed research on a puzzle shaped shear connector. In 1987 he applied for a Patent for the so called “Kombi-Verdübelung”. Rules for the application of Kombi-Verdübelung were defined in a technical approval [Z-26.4-39], Figure 2.3.12.

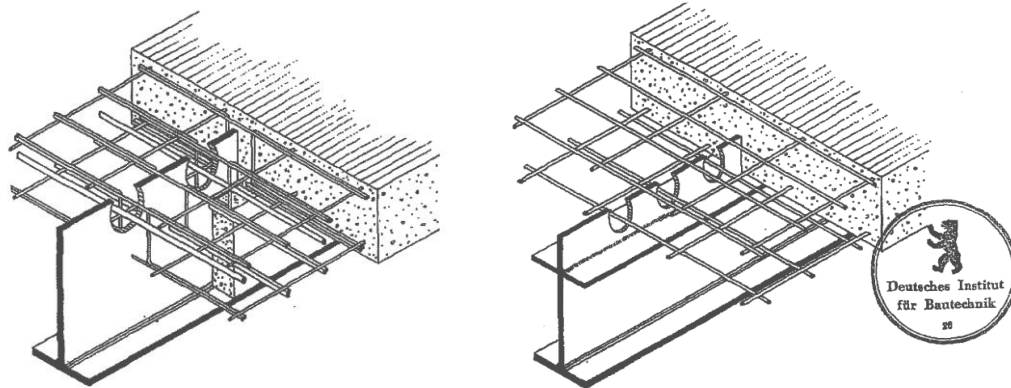


Figure 2.3.12: Kombi-Verdübelung, Brendel [Z-26.4-39]

Later this Technical Approval was extended to different Geometries [Z-26.4-56].

University of Armed Forces, Munich, Germany - Research on Concrete Dowels

A mechanical model to describe the load-bearing behaviour of concrete dowels was developed by Otto Wurzer [Kr1997a]. Based on test observations and results obtained with nonlinear finite-element modelling of concrete dowels, he describes the load transfer by a concrete dowel as follows: The composite force is transmitted from the steel strip to the concrete slab by extreme local compression (effect of partial area loading), which acts at the contact surfaces of the hole. The area, where the load spread is taking place in the concrete dowel, may be separated in two main parts named zone A and zone B, Figure 2.3.13. In the load transmission zone A, concrete is confined causing triaxial compression. There the bearing and deformation behaviour of the concrete depends mainly on the pore structure of the cement stone. Above a critical load step, crushing of pore sides occurs caused by the triaxial compression. Afterwards damaged concrete fills up the pores. In the load distribution zone B compression acts longitudinal and tension transverse to the direction of the load spread. Cracking parallel to the composite force occurs, when the transverse stresses exceed the tensile strength of the concrete. After cracking the splitting reinforcement of the concrete dowel takes the transverse tensile forces. Nominal transverse reinforcement close to the concrete dowel participates as well.

A limit state is reached, when the pores in zone A are completely filled with damaged concrete material and no further volume reduction is possible there. The pulverized material causes a quasi-hydrostatic pressure on the confining concrete, which may lead to splitting of the concrete slab and finally to local wedging-off of parts of the slab surface close to the dowels, [Kr1997b].

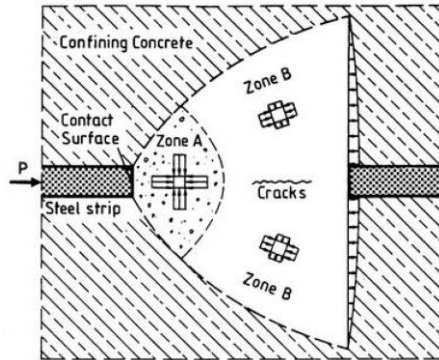


Figure 2.3.13: Loading of concrete dowel, Kraus [Kr1997b]

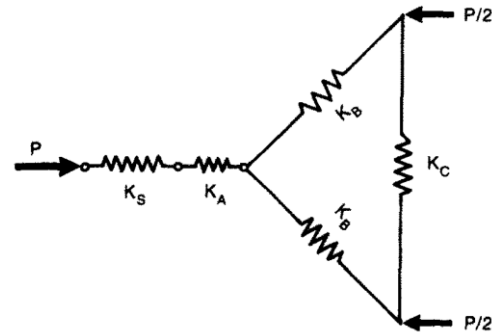


Figure 2.3.14: Spring model concrete dowel [Kr1997b]

To evaluate the slip corresponding to the shear load P , Wurzer derived a spring model with the following components (Figure 2.3.14):

$$S(P) = S_S + S_A + S_B + S_C \quad (2.22)$$

with

s_S local deformation of the steel stems, remaining between the holes

s_A crushing of the pore structure in cement stone of zone A

s_B the deformations of the compression filed in zone B

s_C lateral strain, cracking and crack opening in zone B.

Wurzer performed overall 42 push-put tests on concrete dowels, investigating the influence of different geometries of the stem opening, the concrete compression class, transverse reinforcement and loading of the concrete slab. Test set-up and geometry is given in Figure 2.3.15.

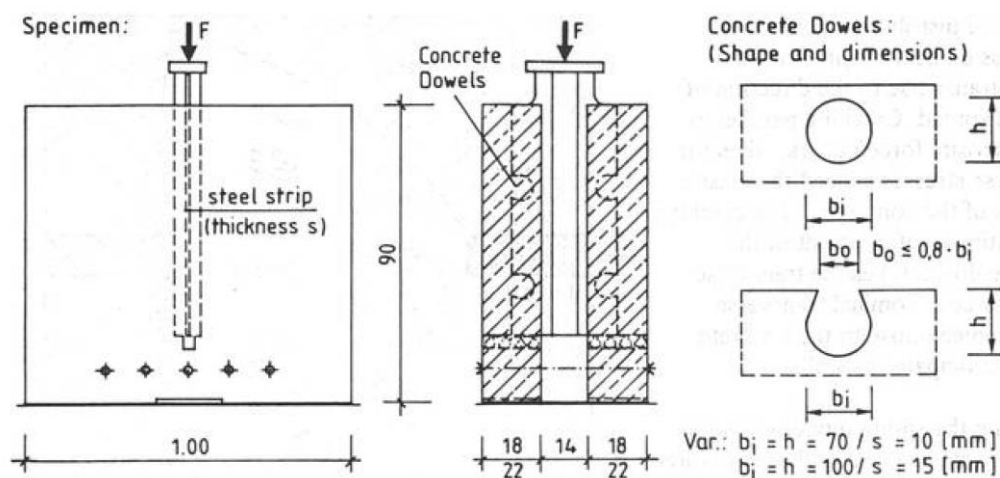


Figure 2.3.15: Push-out test and geometries of concrete dowels [Kr1997b]

A typical load-slip curve is given in Figure 2.3.16. Wurzer divided the load-slip curve into three parts: - Part I, at lower load steps only small deformations occur. To remove adhesion between the steel strip and the concrete, 25 load cycles have been introduced in at the beginning of the test. In Part II, longitudinal splitting cracks occur in the concrete slab at a load level $P_{crack} \approx 0.75 \cdot P_{max}$, which cause a sharp increase in deformation with further load increase. The maximum shear load P_{max} is reached, when the local parts of the slab surface are wedging-off close to the concrete dowels. After reaching P_{max} the load is decreasing slowly at further slip increase. Some of test results are given in Figure 2.3.17. He found a nearly linear relationship of the maximum load P_{max} and the uniaxial concrete compression strenght f_{cm} . An increase of the surface of the transversal reinforcement A_{sq} was also leading to an increase of P_{max} . In addition he pointed out, that increasing dimensions of the opening is also leading to an increase of P_{max} , which he explained with an increase of the contact surface between steel strip and concrete, Figure 2.3.13. However, he observed a reduction of the local compressive stresses in the contact surface with an increase of the dimensions of the opening. For further information it is referred to [Wu1998].

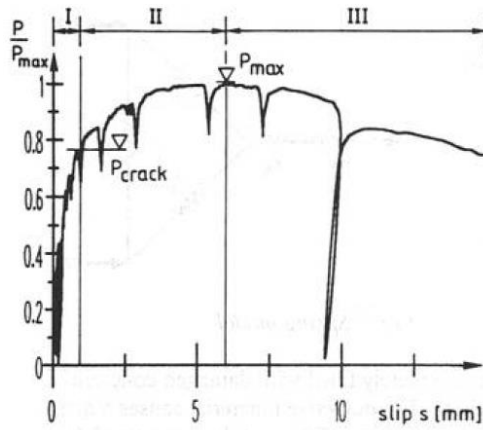


Figure 2.3.16: Typical load-slip curve, Kraus [Kr1997b]

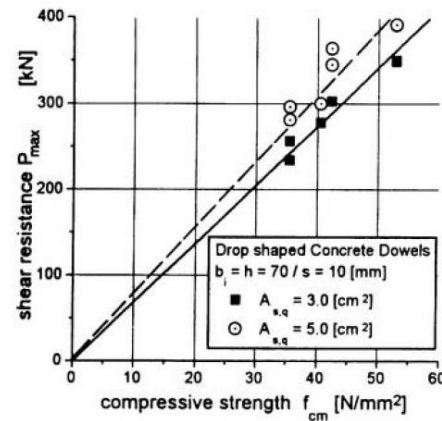


Figure 2.3.17: Relation between P_{max} and concrete compression strenght [Kr1997b]

Based on the above described mechanical model, Wurzer proposes the following design concept for the determination of the design shear resistance P_{Rd} of concrete dowels at the ultimate limit state. The factor η depends on the dimensions and the shape of concrete dowels. To avoid splitting of the concrete a minimum transversal reinforcement has to be added, which should be designed for 50% of P_{Rd} :

$$P_{Rd} = \eta \cdot f_{ck} \cdot h \cdot s \cdot \frac{1}{\gamma_v} \quad (2.23)$$

where

η factor, found by statistical evaluation of test results

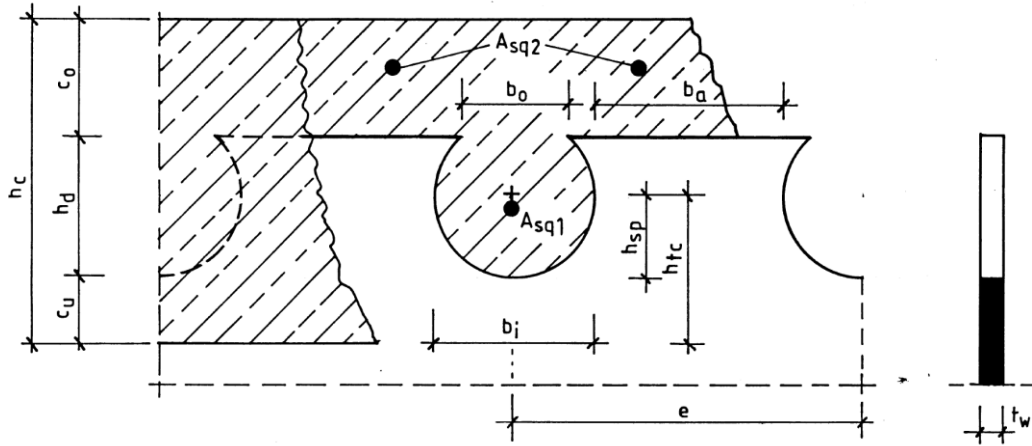
f_{ck} characteristic cylinder strenght of the concrete

h height of holes of concrete dowels

s thickness of steel strip

γ_v partial safety factor $\gamma_v = 1.25$

Cedrik Zapfe refined and extended the above described mechanical model from Wurzer [Za2001]. He investigated the behaviour of concrete dowels under cyclic loading and performed push-out and beam tests. Main parameter in his push-out tests was the geometry of the concrete dowels (opening geometry) and the concrete compression strength. In all tests performed by Zapfe transversal reinforcement with varying surface was present. He defined three failure criteria for static loading: local pressure failure, punching failure and dowel shearing off failure. The different failure modes and the corresponding design equations as proposed by Zapfe are given in Figure 2.3.18.



Local pressure failure:

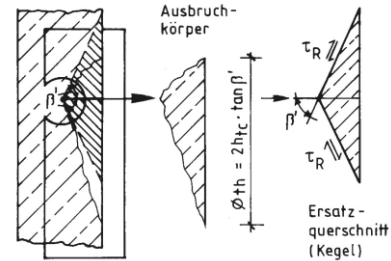
$$P_{Rd1} = 72.7 \cdot \sqrt{f_{ck}} \cdot h_d \cdot t_w \cdot \frac{1}{\gamma_v} \quad (2.24)$$

Punching failure:

$$P_{Rd2} = 25.6 \cdot h_{tc}^2 \cdot f_{ctk} \cdot \rho_i \cdot \frac{1}{\gamma_v} \quad (2.25)$$

with

$$\rho_i = 1 + (E_a/E_{cm} - 1) \cdot A_d$$



Shearing off failure:

$$P_{Rd3} = 23.4 \cdot A_d \cdot f_{ctk} \cdot \rho_i \cdot f_h \cdot \frac{1}{\gamma_v} \quad (2.26)$$

with

$$f_h = (1.2 - h_d/180) \leq 1$$

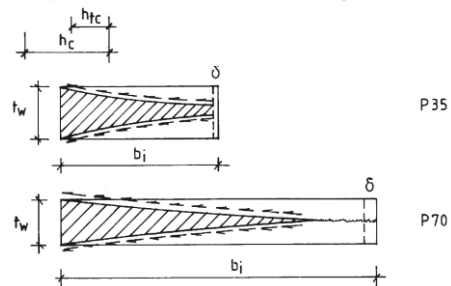


Figure 2.3.18: Failure criteria according to Zapfe, with $\gamma_v = 1.25$ [Za2001]

For further information it is referred to [Za2001].

For the Thesis presented here, the local concrete pressure failure as described by Wurzer [Wu1998] and Zapfe [Za2001] is of special interest. In [Za2003] Zapfe pointed-out: Based on dismantled concrete dowels after push-out test execution the existence of a highly stressed zone in the contact areas between steel faces and concrete dowels could be proved, where load influences effected an approximate hydrostatic stress state depending on the concrete dowel shape and the grade of cording effectiveness of the surrounding concrete material.

For concrete dowels close to the edge of the slab he observed a punch cone failure, similar to a failure observed for shear stud placed in the ribs of metal decking. He defines this failure by applying shear stresses along the coating surface of a regular cone. Shearing off failure is defined by a double cut shearing off within the concrete material at the edges of the steel web perforation, with a modified shear area for large openings, which is considered by an empirical form factor. According to Zapfe this failure criterion is limited to deeply in the concrete slab placed concrete dowels. His research work was continued by [Bu2011], [Wa2011].

Reitz 2003 – Investigations on Perfobond as Ductile Shear Connector

Dieter Reitz performed push-out tests on Perfobond with diameters of the openings from 40mm to 54mm. The concrete compression strength, measured on cubes, varied from 36 MPa to 60 MPa [Re2003]. He confirmed the findings of other researchers of a ductile load-bearing behaviour of Perfobond. Based on his test observations he proposed design Equations considering shear failure of the steel strip and concrete failure. He defined the design load for concrete by:

$$P_{Rd} = 1.45 \cdot K_c \cdot d^2 \cdot f_{ck} \cdot \frac{1}{\gamma_v} \quad (2.27)$$

where

$$K_c = 2 \cdot \frac{l_3}{l_1} - 0.15 \leq 1$$

l_3 shortest distance of the openings, Figure 2.3.19

l_1 shortest distance of the opening to the edge, Figure 2.3.19

d Diameter of the opening, Figure 2.3.19

f_{ck} characteristic cylinder strength of the concrete

γ_v partial safety factor $\gamma_v = 1.25$

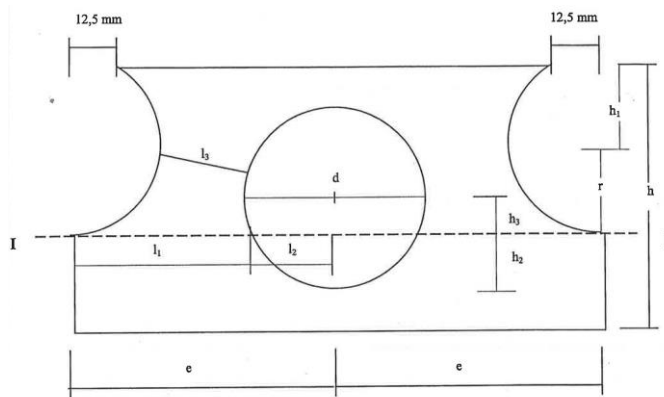


Figure 2.3.19: Geometry according to Reitz [Re2003]

Zheng 2016 – Parametric Study on Perfobond

ShuangJie Zheng performed a parametric study on the shear capacity of circular-hole and long-hole Perfobond shear connectors [Ze2016]. By analysing in detail the obtained failure modes, she derived numerical models simulating the failure modes observed in the experiments, Figure 2.3.20. Further, she refined the shear mechanism of Perfobond as given in [Kr1997b], by introducing a rebar in the opening, Figure 2.3.21. For more information it is referred to [Ze2016].

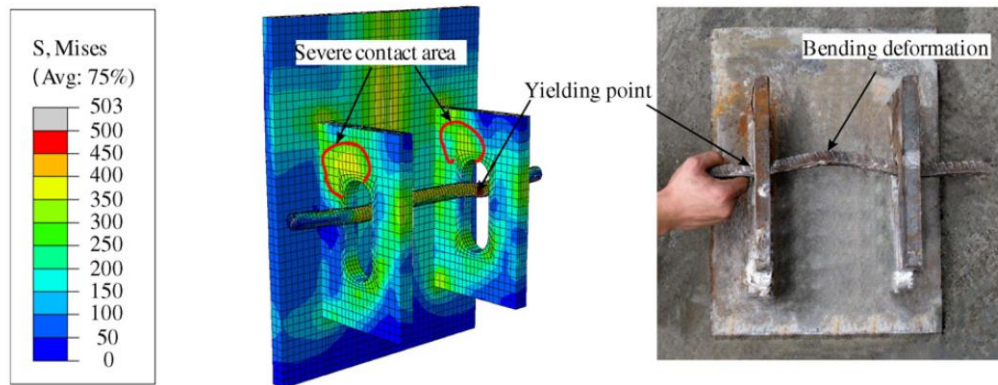


Figure 2.3.20: Comparison of numerical simulation and test, Zheng [Ze2016]

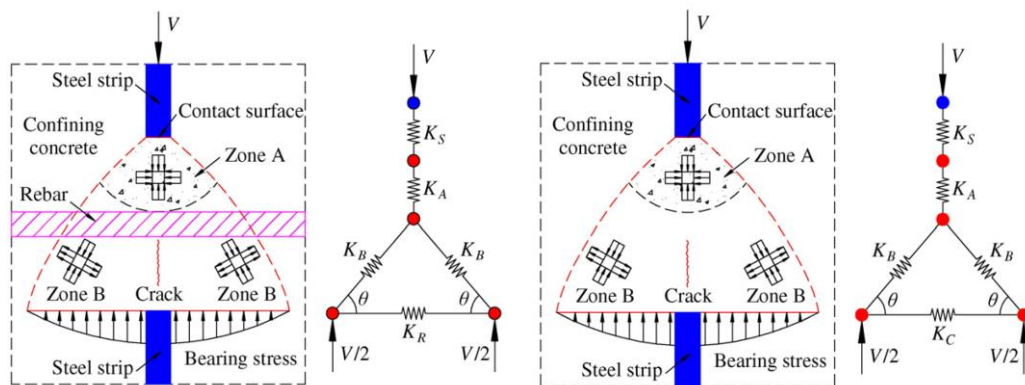


Figure 2.3.21a: Mechanism with rebar, Figure 2.3.21b: Mechanism according to Kraus [Kr1997b]
Zheng [Ze2016]

Perfobond – additional Research

The research on Perfobond is still a subject of interest and ongoing research. The author of this Thesis reviewed many other publications than given here before and analysed its relevance for CoSFB-Dowels. A short list of analysed publications is given hereafter.

Josef Fink published a design model for a continuous shear connector called “Kronendübel” (crowndowel) [Fi2007], which has a slightly different shape compared to the Kombi-Verdübelung from Brendel [Z-26.4-39].

More research about perfobond shear connector and concrete dowels as shear connector for composite beams was done in Canada by Oguejiofort, see e.g. [Ogu1997] and at the University of Coimbra, Portugal. Isabel Valente investigated the load-bearing behaviour using lightweight concrete [Val2004], [Val2009]. General research about the load-bearing behaviour of Perfobond shear connectors was performed and published e.g. by [Via2008], [Via2009], [Ca2010], [Ro2011], [Via2013] just to name a few.

Numerous investigations on Perfobond on various geometries and parameters was performed in Asia, e.g. [Je2009], [Ah2010], [Ki2013], [Ma2014], [Su2014], [Ch2016], even to using Perfobond as connector in steel-concrete joints [He 2016]. More recent research is dealing with the application of high-strength material [Hau2005], [P621], [Fel2007], [P804], [Gu2009], [Hei2012] and about the investigation of the influence of transversal bending on the load-bearing behaviour of concrete dowels [CI2016].

An excellent overview about research on concrete dowels can be found in [Hei2011] and [Wi2013].

2.4 Shear Connection by Transversal Bars

In 2008 Matti V. Leskelä published a design proposal for a shear connection composed of uniformly distributed web-openings along the beam and transverse rebars [Les2008]. According to Leskelä the shear connection for composite slim-floor beams can reside in any location of the interfaces between the components (steel section and concrete slab) [ECCS138]. Thus, the vertical position of the transverse reinforcing bars – acting as shear connector – can be specified in such way that the assembly is most easy, Figure 2.4.1.

Leskelä performed push-out tests where a single transversal bar connects two blocks of concrete on sides of a steel web plate with circular holes. The holes have a diameter of 75mm or 150mm, the transversal reinforcement bar diameters of 16mm, 20mm and 25mm. The holes are filled with in-situ concrete. In addition, he varied the position of the bar in relation to the edge of the hole, Figure 2.4.2.

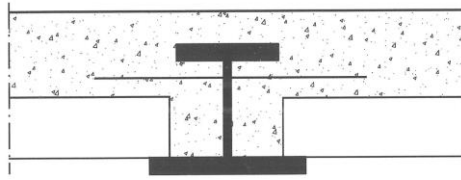


Figure 2.4.1: Transversal bar as connector [Les2008]

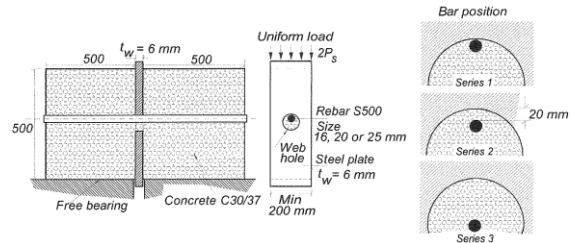


Figure 2.4.2: Tests performed by Leskelä [Les2008]

His proposal to assess the load-bearing capacity is based on an Equation derived by Rasmussen for shear connections using bolts cast in concrete [Ra1963], when Leskelä adapted some factors in accordance with his test results. He defines the shear resistance of one leg as:

$$P_{Rd,1} = \min\{\alpha_R \cdot d^2 \cdot \sqrt{f_{ck} \cdot f_{sk}}; k_{Ry} \cdot A_{sc} \cdot f_{sk}\} / \gamma_v \quad (2.28)$$

where

$$\alpha_R = 2.5 - 0.065 \cdot (d - 16) \leq 2.5$$

$$k_{Ry} = 0.8 - 0.025 \cdot (d - 16) \leq 0.8$$

d Diameter of the transversal reinforcement bar

f_{ck} characteristic cylinder strength of the concrete

f_{sk} characteristic strength of the bar

A_{sc} cross sectional area of the bar

γ_v safety factor, with $\gamma_v = 1.25$

Thus for two legs the design value is obtained with $P_{Rd} = 2 \cdot P_{Rd,1}$. Leskelä describes, that the resistance of his tests was defined for a slip of 6mm. But, slips of 10mm and more were obtained even without any fracture of the bar. Equation (2.28) is valid for nominal diameters of the transversal reinforcement bar from $16\text{mm} \leq d \leq 25\text{mm}$. Further reference is made to [Les2005] and [Les2006].

3 Testing of CoSFB-Dowels

3.1 Introduction

A first test series of CoSFB-Dowels was performed in 2009. This series consist of standard push-out tests to analyse the load bearing behaviour of the shear connection and shear beam and long span beam tests to verify its load bearing behaviour applied on beams. The push-out tests in 2009 were done using Cofradal 200 decking [Co200]. The analysis of the load-bearing behaviour of this decking is not part of this Thesis, consequently results of test series from 2009 are not taken into account for the research work presented here. The results of the push-out tests performed in 2009 showed, that an increase of the concrete compression class is not always leading to an increase of the load bearing capacity of the shear connection [Stu2009].

Therefore, another campaign of push-out tests with varying parameters was performed in 2011. The aim of this campaign was to evaluate in detail the influence of the concrete compression class, the web thickness and the diameter of the web opening on the load bearing behaviour of CoSFB-Dowels. In addition, one series of push-out tests was done with a varied diameter of the dowel reinforcement, Series 2-2b, which could not be evaluated together with the other series because of a different failure mode. Results of this test campaign were already published, as e.g. [CC2013], [Stb2014a], [Stb2014b], [ES2014], [Stu2011].

3.2 Push-Out Tests

3.2.1 Overview

From the campaigns of push-out tests with CoSFB-Dowels, only the tests from 2011 are considered in this research work, because a solid concrete slab was used. For completion reasons, also the 2009 parameters and results are briefly given in Table 3.2.1. The shop drawing of Series 2011 are given in Annex A.

3.2.2 Test specimen, testing procedure and measurement

The test procedure and measurements are performed in accordance with EN 1994-1-1 [EN1994]. A push-out specimen consists of two concrete slabs and two hot rolled sections with CoSFB-Dowels. To allow for a concreting of the slabs in horizontal position - the CoSFB-Dowel should be applied for composite slim-floor beams - each slab of the specimen had to be concreted separately. Special care was given to a simultaneous concreting of all three specimens for each series. Before testing, the steel sections were welded together to obtain a symmetrical specimen. Due to the excellent planeity of the lower edge of the concrete slabs, no mortar bed was put under the specimen, Figure 3.2.2.1.

The dimension of the specimens, the load introduction and the positioning of the dowel reinforcement can be found in Figure 3.2.2.2. Each slab was connected with 5 CoSFB-Dowels to the steel section. The axe-to-axe distance of the web openings was for all tests fixed to 125mm. The dowel reinforcement bars had a length of 180cm with an additional 90 degree end-hook to assure perfect anchorage.

All steel surfaces were treated with oil before concreting to reduce possible friction action between concrete and steel section to a minimum. The load introduction was done at the upper edge of the steel sections with the help of a load introduction plate, assuring an even load introduction to each steel section.

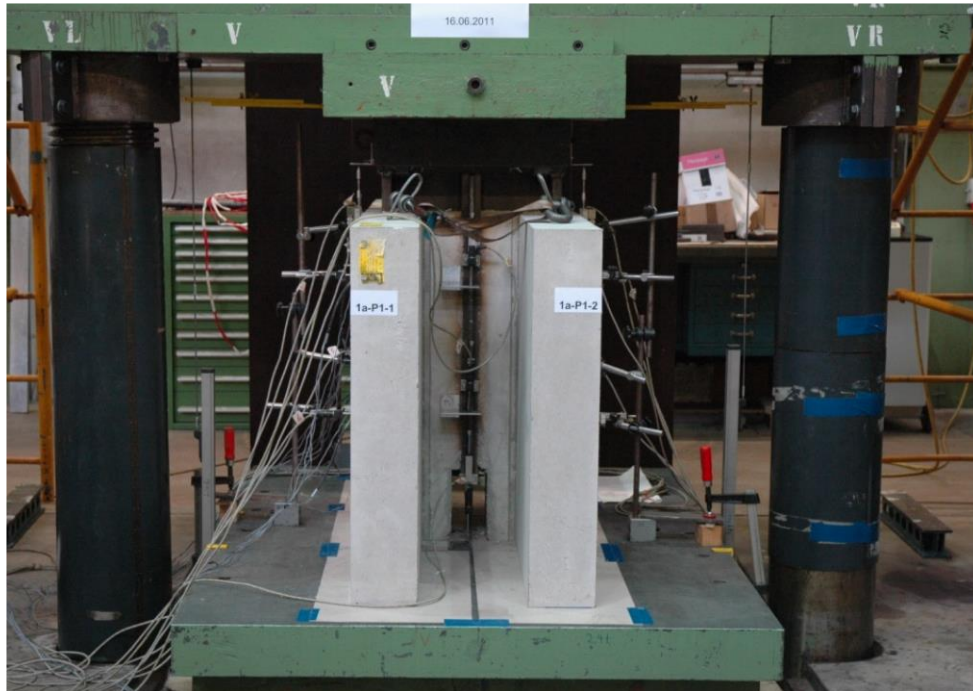


Figure 3.2.2.1: Push-out Test Specimen [Stu2011]

To allow for the evaluation of the development of strains in the dowel reinforcement and the overall load-bearing behaviour, strain gauges were placed at the dowel bars and extensometers to measure the relative slip between discrete points of the specimen and the steel plate, the specimen was placed onto.

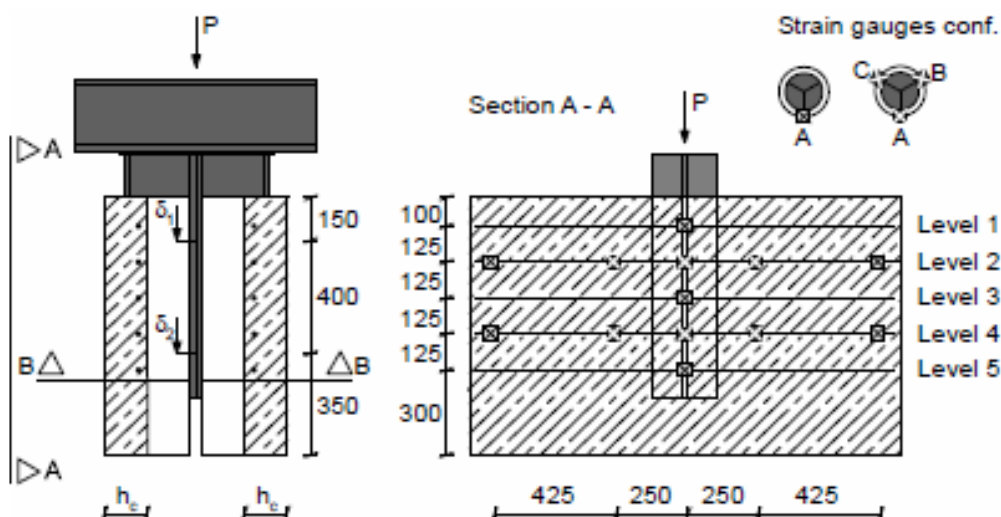


Figure 3.2.2.2: Schematic Drawing of Push-out Tests [CC2013]

Table 3.2.1: Overview - CoSFB Push-out Tests 2009 + 2011 [Stu2009], [Stu2011]

Year	Series	Test	Section	t_{web} [mm]	web opening [mm]	dowel reinf. [mm]	Concrete Class [MPa]	max. Load [kN]
2009	P1	1	HE220M	15.5	40	12	31.8	2141
		2					34.9	2292
		3					35.3	2070
	P2	1	HE220M	15.5	40	12	45.6	2249
		2					36.4	2343
		3					36.3	2254
2011	1a	1	HE220M	15.5	40	12	26.8	1895.5
		2					26.6	1930.5
		3					26.8	2065
	1b	1	HE220M	15.5	40	12	54.4	1668
		2					54.7	1612.5
		3					56.1	1684
	2-1a	1	HE240A	7.5	40	12	29.2	1579.5
		2					29.6	1841
		3					29.6	1764.5
	2-1b	1	HE240A	7.5	40	12	56.9	1536
		2					60.0	1582.5
		3					57.6	1655.5
	2-2a	1	HE220M	15.5	25	12	32.2	2033
		2					32.6	2022
		3					33.3	2034
	2-2b	1	HE220M	15.5	40	25	38.6	4143
		2					41.1	3993
		3					40.4	3798.5
	2-3	1	HE220M	15.5	25	12	37.7	1377.5
		2					38.4	1486
		3					38.7	1386

The position of the strain gauges is shown in Figure, 3.2.2.2. For the reinforcement bars in layer 1, 3 and 5 only one strain gauges was put at the centerline of the specimen. Gauges on bars in layer 3 and 5 were placed at the lower edge of the bar, when the bar in layer 1 had to be turned by 180 degrees before concreting, to avoid that the end hook sticks-out at the upper edge of the specimen after concreting. Therefore, the strain gauge on the reinforcement bar on level 1 was finally positioned at the upper edge of the bar. The dowel reinforcement in layer 2 and 4 had strain gauges at 5 positions: - at each end one strain gauge and three strain gauges at the centre and at a distance of 250mm of the centre towards each end. The three strain gauges were put at an angle of 120degrees to allow for measuring possible bending of the reinforcement bar. Because the strain gauges have to be placed on a flat surface to measure correctly, the diameter of the reinforcement had to be reduced slightly.

Extensometers were used to measure the relative slip between the concrete slabs and the steel sections and the steel plate the specimens were placed onto at specific points. The position of the extensometers are given in Figure 3.2.2.3. In detail:

- Extensometers 1 and 1-1 are placed at the centreline of the specimens,
- Extensometers 2 and 2-2 between the horizontal load introduction beam and the upper edge of the concrete slabs to allow for the determination of a possible inclination of the load introduction beam,
- Extensometers 4 and 4-4 and 6 and 6-6 allowed to identify a possible separation of the concrete slabs from the steel section (requirement of EN 1994-1-1, Annex B.2.4(4) [EN1994]),
- in combination with 3 and 3-3 and 5 and 5-5 a possible inclination of the concrete slabs can be determined.
- The relative displacement between the steel sections and the concrete slabs is measured with the extensometers " S_{oben} " and " S_{unten} ". With the values of 3 and 3-3 and 5 and 5-5 the slip between the steel sections and the concrete slabs was calculated.

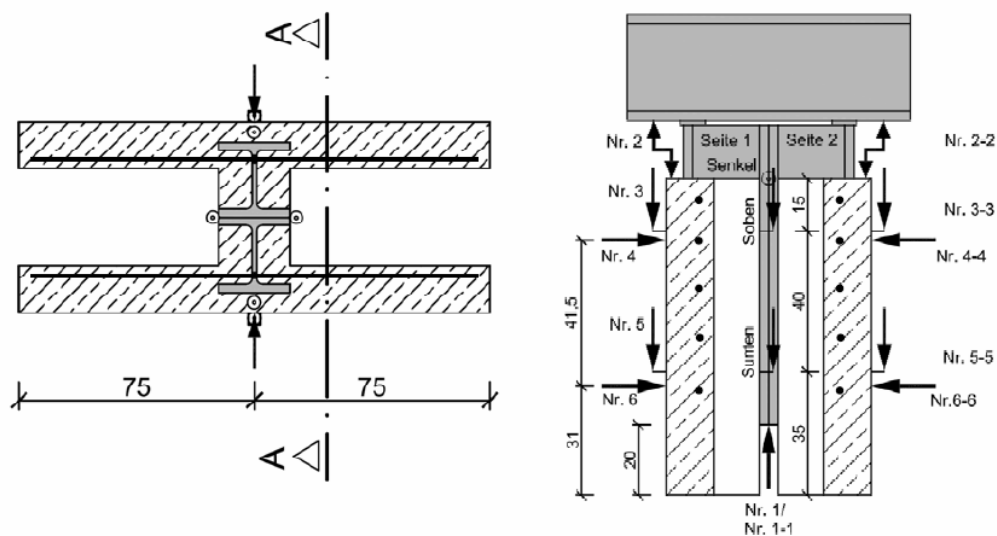


Figure 3.2.2.3: Position of Extensometers [Stu2011]

3.2.3 Material properties

3.2.3.1 Concrete

Together with the concreting of the push-out specimens, cubes with dimensions 15cm x 15cm x 15cm and rectangular prisms with dimensions 53cm x 10cm x 10cm were concreted [DIN12390-1], [DIN12390-2]. Per push-out series ten cubes and nine prisms were produced and stored next to the push-out specimens. Three cubes per series were stored under water. At the day of the push-out test, the corresponding material properties were determined with the cube tests (concrete compression strength, [DIN12390-3]) and the prisms (bending tensile strength, [DIN12390-4]). An overview of the cube and prism test results, given as mean values, and the time of testing is given in Table 3.2.3.1. The compression strength is given as cylinder value, calculated from the cube tests. The given results were performed by testing at the University of Stuttgart, Germany.

Table 3.2.3.1: Test Results - Concrete

Series	Concreting Date	Cube and Prism Tests	Concrete compression strength		Concrete Tensile Strength f_{ctm} [MPa]
			$f_{c,cube}$ [MPa]	$f_{c,cyl}^*$ [MPa]	
1a	29.04.2011	16.06.2011	33.1	26.8	4.1
		17.06.2011	32.8	26.6	
		27.06.2011	33.1	26.8	
1b	06.05.2011	28.06.2011	67.2	54.4	5.1
		29.06.2011	67.5	54.7	
2-1a	12.05.2011	30.06.2011	69.3	56.1	4.0
		04.07.2011	36.0	29.2	
		05.07.2011	36.6	29.6	
2-1b	18.05.2011	06.07.2011	36.5	29.6	5.3
		07.07.2011	70.2	56.9	
2-2a	26.05.2011	11.07.2011	74.1	60.0	4.4
		12.07.2011	71.1	57.6	
2-2b	10.06.2011	20.07.2011	39.7	32.2	4.7
		21.07.2011	40.2	32.6	
2-3	01.06.2011	13.07.2011	41.1	33.3	4.7
		20.07.2011	47.7	38.6	

* Converted from cube test to cylindrical compression strength, $f_{c,cyl} = 0.81 \times f_{c,cube}$

3.2.3.2 Reinforcement

Two different diameters had been used as dowel reinforcement, diameter 12mm and 25mm. Only three tensile tests were performed per diameter, because the dowel reinforcement bars were delivered from the same production series. The tensile strength was determined by a standard tension test according to [DIN50125] and [DIN10002], at the University of Stuttgart, Germany. The results of the tensile tests are given in Table 3.2.3.2.

Table 3.2.3.2: Test Results - Reinforcement

Diameter [mm]	Test	Cross-sectional area [mm ²]	R _{p0,2} [MPa]	R _m [MPa]	Yield strain [-]
12	1	111.4	529.9	583.6	2.65 x 10 ⁻³
	2	111.2	527.7	580.6	2.64 x 10 ⁻³
	3	111.2	534.6	583.4	2.67 x 10 ⁻³
Mean value:		111.3	530.6	582.5	2.65 x 10 ⁻³
25	1	495.2	524.5	633.2	2.62 x 10 ⁻³
	2	496.2	526.3	632.1	2.63 x 10 ⁻³
	3	497.0	537.2	645.3	2.69 x 10 ⁻³
Mean value:		496.1	529.3	636.9	2.65 x 10 ⁻³

3.2.3.3 Structural Steel

The testing of the material properties of the hot-rolled steel sections was performed in the laboratories of ArcelorMittal. The test specimens were taken from the top flange right “FR”, left “FL” and at the centre of the web, indicated with “W”, in accordance with [EN6892]. Results are given in Table 3.2.3.3.

Table 3.2.3.3: Test Results - Structural Steel

Specimen	Position	R _{eH} [MPa]	R _{eL} [MPa]	R _m [MPa]	Strain [-]
ROA1 (HE240A)	FR	439	431	523	2.195 x 10 ⁻³
	FL	443	440	523	2.215 x 10 ⁻³
	W	503	476	578	2.515 x 10 ⁻³
Mean value:		462	449	541	2.308 x 10⁻³
ROM1 (HE220M)	FR	364	356	496	1.820 x 10 ⁻³
	FL	373	365	506	1.865 x 10 ⁻³
	W	396	393	506	1.980 x 10 ⁻³
Mean value:		378	371	503	1.888 x 10⁻³
ROM2 (HE220M)	FR	392	379	505	1.960 x 10 ⁻³
	FL	364	360	500	1.820 x 10 ⁻³
	W	395	392	505	1.975 x 10 ⁻³
Mean value:		384	377	503	1.918 x 10⁻³
ROM3 (HE220M)	FR	367	363	506	1.835 x 10 ⁻³
	FL	387	377	514	1.935 x 10 ⁻³
	W	399	391	518	1.995 x 10 ⁻³
Mean value:		384	377	513	1.921 x 10⁻³
ROM4 (HE220M)	FR	362	359	500	1.810 x 10 ⁻³
	FL	380	377	509	1.900 x 10 ⁻³
	W	397	392	512	1.985 x 10 ⁻³
Mean value:		380	376	507	1.898 x 10⁻³

3.2.4 Opening of the specimens

After testing, selected push-out specimens were opened by cutting to obtain information about the deformation of the dowel reinforcement and the concrete damage near to the web opening, Figure 3.2.4.1. The cut was done at the edge of the web, through the concrete slab and the upper flange.

The deformation of the some dowel reinforcement bars is shown in Figure 3.2.4.2. From the deformed shape after testing the assumption of a shear dominated failure with two shear surfaces at the edge of the web of the reinforcement seems to be reasonable.



Figure 3.2.4.1: Cutting of Push-out Specimen



Figure 3.2.4.2: Extracted Dowel Reinforcement Bars

Directly in the web opening, the concrete matrix was totally destroyed. The concrete stone was crushed to sand and could be scratched out of the web opening very easily. Outside of the web opening the concrete was locally, under the dowel reinforcement damaged, where the concrete matrix next to the reinforcement bar seemed to remain undamaged, Figure 3.2.4.3.



Figure 3.2.4.3: Concrete in the web-opening

Opening of Test specimens in 2012

In addition, the author opened one specimen per push-out Series by hand, some results are given in Figure 3.2.4.4.

Push-out Test 1a:



Push-out Test 1b:



Push-out test 1b:



Push-out Test 2-2b:



Figure 3.2.4.4: Opening of Specimens by hand

3.2.5 Test results

The load-slip curves for the 2011 push-out test series are given in Annex B1 and B2. Hereafter only the curve for tests 1a is given, Figure 3.2.5. The relative displacement between the steel sections and the concrete slabs is calculated by the measurement of the extensometers “S_{oben}” and “S_{unten}” in combination with the values of 3 and 3-3 and 5 and 5-5.

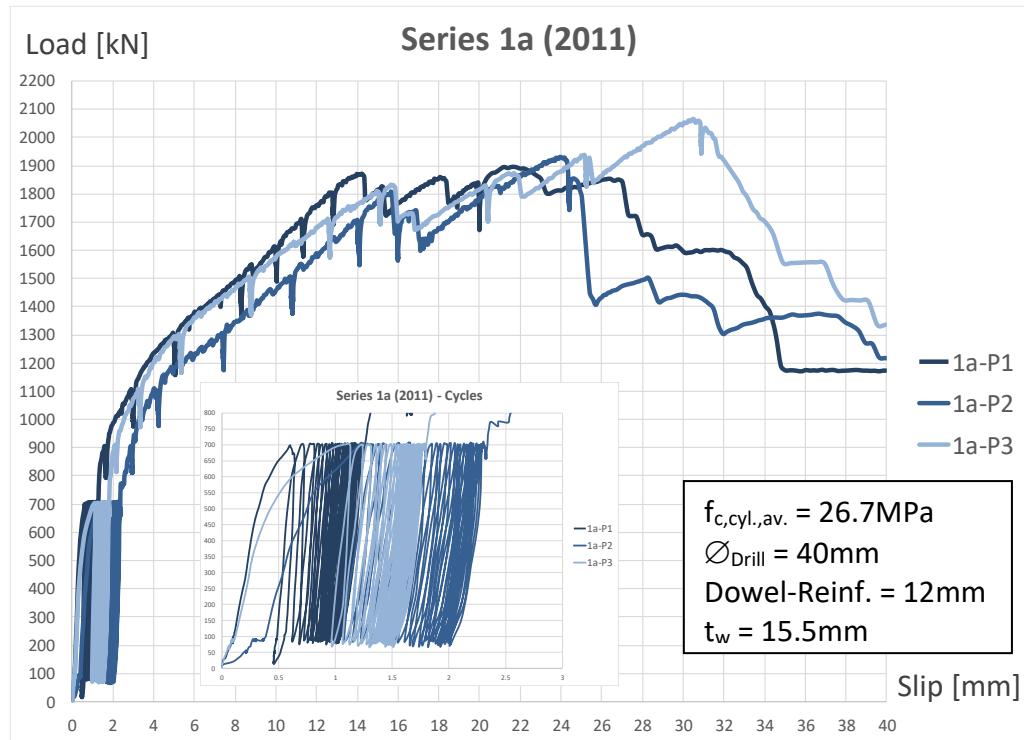


Figure 3.2.5: Load-Slip curves for Series 1a

The measurements of the strain gauges are given in Annex B3.

3.3 Additional Tests on Dowel Reinforcement

Additional tensile tests on dowel reinforcement bars extracted by the author from push-out specimens (cf. Section 3.2.4) were done at the University of Luxembourg. Aiming to measure the rupture strain ϵ_r and the cross sectional area at rupture A_r , the tests were performed displacement controlled, with a maximum test speed of 2.25mm/min. With the obtained data a true stress-logarithmic strain curve of the dowel reinforcement could be derived, which is required as input in Abaqus [Abaqus] for the simulation of ductile damage of metals and shear damage it is referred to Chapter 5.

Figure 3.3.1. presents the engineering stress-strain curve calculated from the measured load-displacement curve. As reference length l_0 (length before testing) the length between the fixation points, the clamps was taken. Additionally, two marks were fixed on the bar using red tape and the distance between the marks measured before and after testing. Figure 3.3.2 shows the dowel reinforcement for test 1a, pictures for the other tensile test specimens after rupture are given in Annex B4.

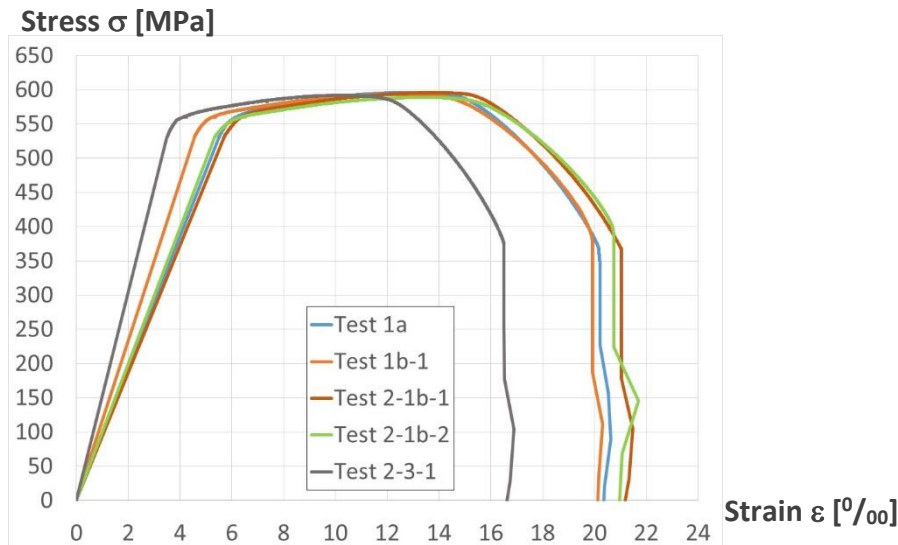


Figure 3.3.1: Stress-strain curves from tensile tests, Uni LU 2018

After testing also the circumference at rupture U_r was measured. To improve the precision for the measured values, the double circumference was measured, Table 3.3. This value was used to calculate the average diameter at rupture d_r and the corresponding cross sectional area at rupture A_r .

$$U_r = \pi \cdot d_r \Rightarrow d_r = \frac{U_r}{\pi} = \frac{25.9\text{mm}}{\pi} = 8.24\text{mm}$$

$$A_r = \pi \cdot \left(\frac{d_r}{2}\right)^2 \Rightarrow A_r = \pi \cdot \left(\frac{8.24}{2}\right)^2 = 53.4\text{mm}^2$$

Compared to the nominal cross sectional area before testing ($A_0 = 113.1\text{mm}^2$), the reduction of area was 53%. Using the assumption of a linear relationship of true stress versus logarithmic strain, a true-stress logarithmic strain curve was determined [Ar2011]. It is further assumed, that the onset of necking is starting at the ultimate stress and a reduction of the cross sectional area starts at this point. The true stress at rupture are now calculated with:

$$\sigma_{r,true} = \frac{\sigma_r \cdot A_0}{A_r} = \frac{379.7 \cdot 113.1}{53.4} = 804.5 \text{ N/mm}^2$$

Table 3.3: Tensile Tests Uni LU 2018 – Test Results (Engineering stresses)

Specimen	Length		Onset of Necking		Rupture		Circumference after testing
	l_0^a [mm]	l_1^b [mm]	Strain [‰]	Stress [N/mm ²]	Strain [‰]	Stress [N/mm ²]	2 x U_r [mm]
1a	93	111.9	12.804	596.45	20.147	370.12	51.0
1b – 1	93	111.7	12.642	593.68	19.892	385.96	52.5
2 - 1b – 1	91	110.3	13.824	596.06	21.020	368.24	51.0
2 - 1b – 2	91	110.1	13.226	589.09	20.726	394.31	53.0
2 – 3 – 1	110	128.3	10.366	592.41	16.483	377.46	51.5
Average^c:			13.12	593.8	20.45	379.7	$U_r = 25.9\text{mm}$

^a l_0 = Length between the clamps before testing

^b l_1 = Length between the clamps after testing

^c Test 2-3-1 not considered in calculation of average values

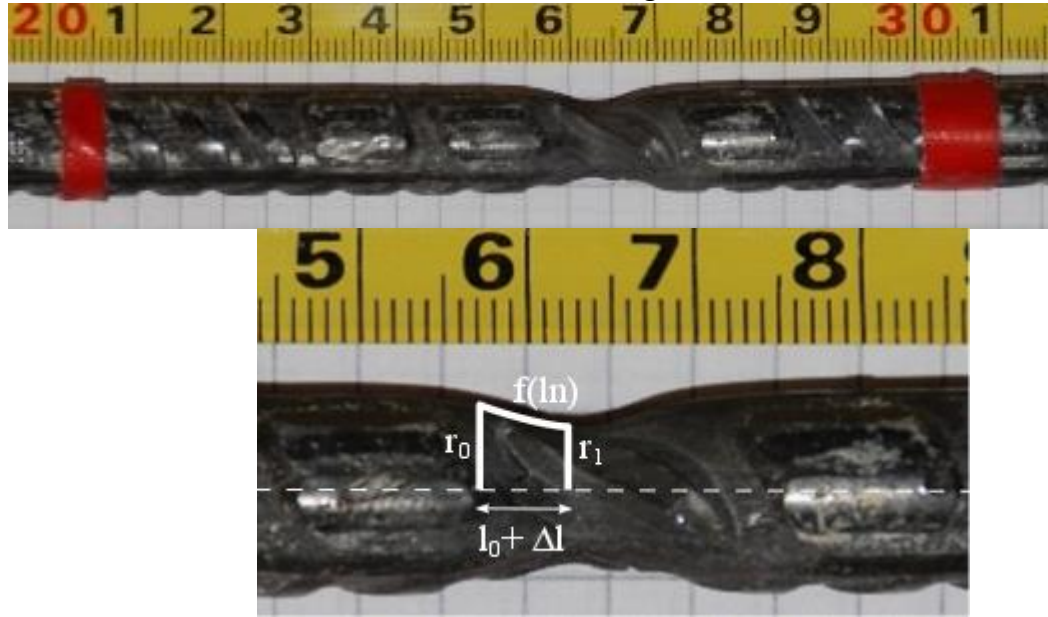


Figure 3.3.2: Tensile Test Specimen 1a, Uni LU 2018

For the numerical simulation also the value of elongation of the bar in relation to the necking zone is required input data. Assuming the reduction of the cross section along the bar follows the function of logarithmic naturalis (ln-Function) and the Volume of the specimen did not change during the test, the average elongation can be calculated with:

$$l_0^* \cdot r_0^2 \cdot \pi \approx (l_0^* + \Delta l^*) \cdot \left(r_1 + \frac{r_0 - r_1}{2}\right)^2 \cdot \pi \quad (3.1)$$

with

r_0 nominal radius before testing

r_1 minimum radius after testing, calculated from measured U_r , Table 3.3

Δl^* calculated elongation of the bar

$l_0^* + \Delta l^*$ length between the points of r_0 and r_1 , calculated from ln-Function

$$l_0^* \cdot r_0^2 \approx (l_0^* + \Delta l^*) \cdot \left(r_1 + \frac{r_0 - r_1}{2}\right)^2 \quad (3.2)$$

$$l_0^* \cdot 6^2 \approx 5.6 \cdot \left(4.12 + \frac{6 - 4.12}{2}\right)^2 \Rightarrow l_0^* = 3.98 \text{ mm}$$

$$(l_0^* + \Delta l^*) - l_0^* = \Delta l^* = 5.6 - 3.98 = 1.62 \text{ mm}$$

And finally, the plastic strain at rupture of the necking zone is calculated:

$$\varepsilon_r^* = \frac{\Delta l^*}{l_0^*} = \frac{1.62}{3.98} = 0.407 \Rightarrow \varepsilon_r^* = 40.7\%$$

4 Evaluation of Push-out Tests

4.1 Test Overview and Results

The test program was defined in such a way, that besides of the non-avoidable variation of the concrete compression strength, only one parameter was varied from one test series to another. Hence, by simple result comparison the influence of the relevant parameter on the load-bearing behaviour could be investigated, Table 4.1.1.

Table 4.1.1: Push-out test Series 2011, investigated parameters

Series	t_w [mm]	\varnothing_o web- opening [mm]	d, diameter dowel bar [mm]	f_{cm}^a [MPa]	Influence of varied parameter by comparison with	
1a	15.5	40	12	26.7	f_{cm} t_w \varnothing_o d	1a – 1b 1a – 2-1a 1a – 2-2a 1a – 2-2b
1b	15.5	40	12	55.1	f_{cm} t_w \varnothing_o d	1b – 1a 1b – 2-1b 1b – 2-2a 1b – 2-2b
2-1a	7.5	40	12	29.5	f_{cm} t_w	2-1a – 2-1b 2-1a – 1a
2-1b	7.5	40	12	58.2	f_{cm} t_w	2-1b – 2-1a 2-1b – 1b
2-2a	15.5	25	12	32.7	\varnothing_o	2-2a – 1a, 2-2a – 1b
2-2b	15.5	40	25	40.0	d	2-2b – 1a, (2-2b – 1b)
2-3 ^b	15.5	25	12	38.3	Influence of concrete in the web-opening	

a) Average value for the Series of three push-out tests

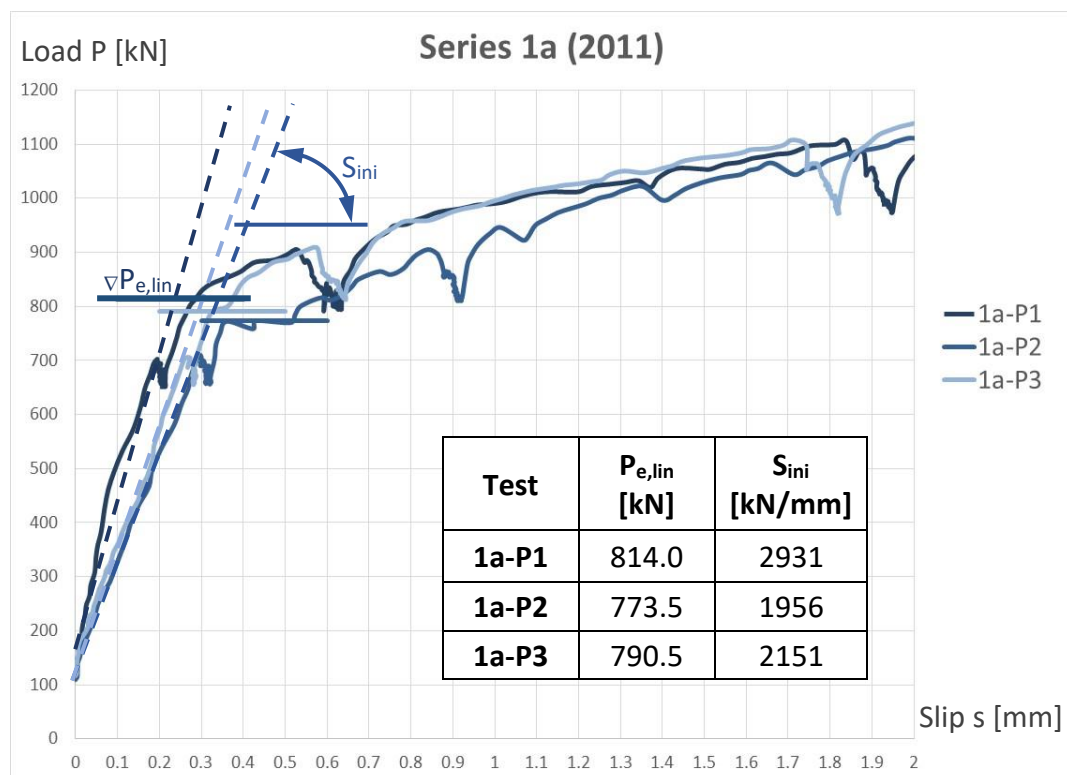
b) Series 2-3: concrete infill in the web-opening

The maximum load obtained in the experiments, $P_{e,max}$, and the initial stiffness S_{ini} , which is defined as a load versus slip ratio, is given as average value for each series in Table 4.1.2. In addition, a load corresponding to the maximum load level in the linear range was defined, $P_{e,lin}$. Up to displacements corresponding to $P_{e,lin}$ the stiffness remains constant at the value S_{ini} . For load levels higher than $P_{e,lin}$ a significant stiffness decrease was observed for all performed push-out tests. The determination of S_{ini} and $P_{e,lin}$ for test Series 1a is shown in Figure 4.1.1. The definition of S_{ini} and $P_{e,lin}$ for test Series 1b, 2-1a, 2-1b, 2-2a and 2-2b is given in Annex B2. A detailed explanation for this significant decrease of the initial stiffness is presented in Section 4.2 and Chapter 6.

Table 4.1.2: Results push-out test Series 2011

Series	f_{cm}^a [MPa]	Initial Stiffness ^a [kN/mm]	$P_{e,lin}^a$ [kN]	$P_{e,max}^a$ [kN]	$P_{e,static}^a$ [kN]
1a	26.7	2346	793	1964	1808
1b	55.1	2950	979	1655	1505
2-1a	29.5	2346	682	1728	1547
2-1b	58.2	2638	911 ^c	1591	1443
2-2a	32.7	2500	766	2030	1890
2-2b	40.0	3359	965	3978 ^d	3540 ^d
2-3^b	38.3	-	-	1417	1233

- a) Average value for the Series of three push-out tests
b) Series 2-3: concrete infill in the web-opening
c) Test 2-1b-P3 not considered
d) Failure of the concrete at the support and not of the dowel reinforcement


Figure 4.1.1: Push-out test Series 1a, definition of S_{ini} and $P_{e,lin}$

The influence of various parameters, namely f_{cm} , t_w , d and \varnothing_o , on the load-bearing behaviour is shown in the subsequent Figures. The reader might bear in mind, that a small variation of f_{cm} for all tests was not avoidable due to the character of the material.

Influence of f_{cm} : Comparison of test Series 1a with 1b and 2-1a with 2-1b

A significant influence on the load-bearing behaviour has the concrete compression class. When comparing results of Series 1a with 1b not only an influence on the maximum load could be observed, but also on the overall load-bearing behaviour, Figure 4.1.2. A higher value of f_{cm} is leading to an increase of $P_{e,lin}$ and an accentuated reduction of stiffness at a higher load level, leading to a horizontal plateau of the load-slip curve. No further load increase is possible, which might be due the absence of friction. The load-slip curves of Series 1a show a reduction of stiffness already at a lower load level, but further load increase is still possible before a plateau is reached at a higher slip. It is remarkable that lower values of f_{cm} led to higher maximum load and higher ductility. This observation could be confirmed by comparison of Series 2-1a with 2-1b, where steel profiles with a smaller web-thickness were tested, Figure 4.1.3.

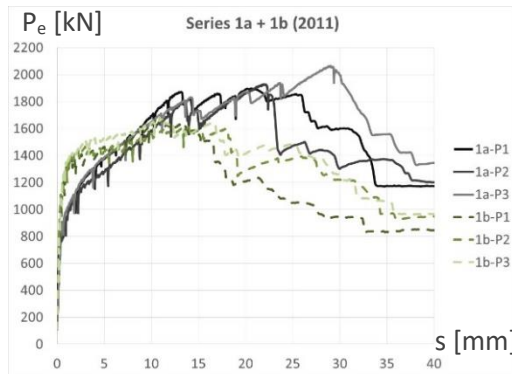


Figure 4.1.2: Series 1a and 1b

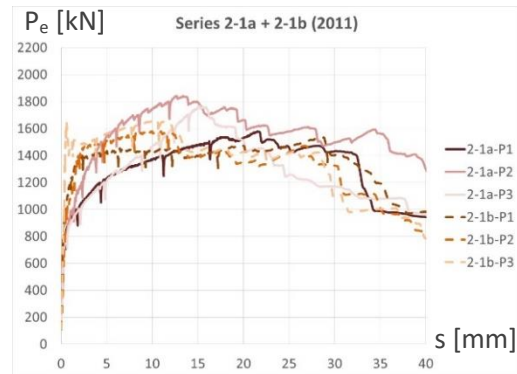


Figure 4.1.3: Series 2-1a and 2-1b

Influence of t_w : Comparison of test Series 1a with 2-1a and 1b with 2-1b

No significant influence of the varied web thickness t_w on the maximum load $P_{e,max}$ could be found, Figures 4.1.4 and 4.1.5. However, a slight tendency of smaller web thickness towards a reduction of the maximum load and towards an earlier failure of the dowel reinforcement could be observed. This influence of t_w is further considered in Section 4.2, where an analytical formulation of P_{lin} is derived.

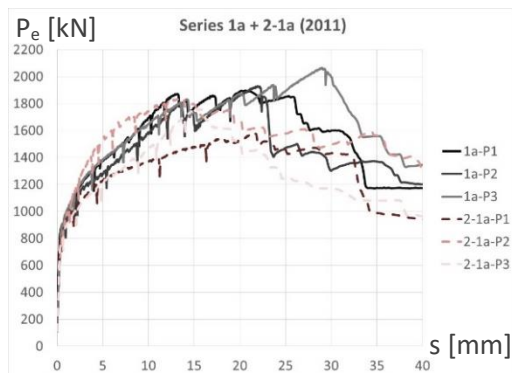


Figure 4.1.4: Series 1a and 2-1a

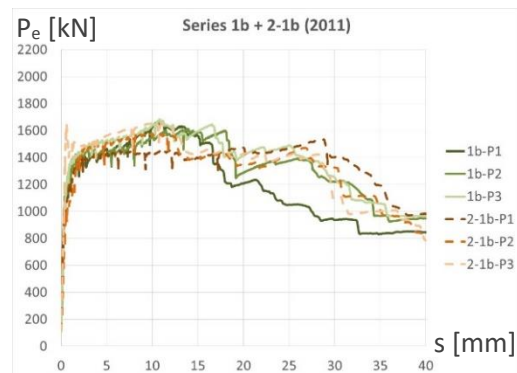


Figure 4.1.5: Series 1b and 2-1b

Influence of d: Comparison of test Series 1a with 2-2b and 1b with 2-2b

An increase of the diameter of the transversal dowel reinforcement d from 12mm to 25mm had a significant influence on the maximum load, Figures 4.1.6 and 4.1.7. In series 2-2b, no failure of the dowel reinforcement was obtained. Instead, the concrete next to the support failed. Therefore, the maximum load measured does not give information about the possible dowel resistance and could not be used to formulate an analytical equation for $d = 25\text{mm}$. Nevertheless, $P_{e,\text{lin}}$ was observed and included into the analytical formulation of $P_{t,\text{lin}}$, see Section 4.2.

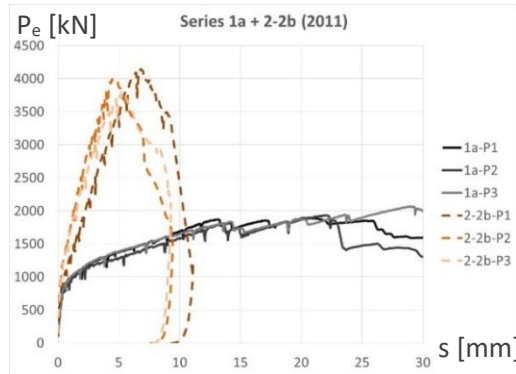


Figure 4.1.6: Series 1a and 2-2b

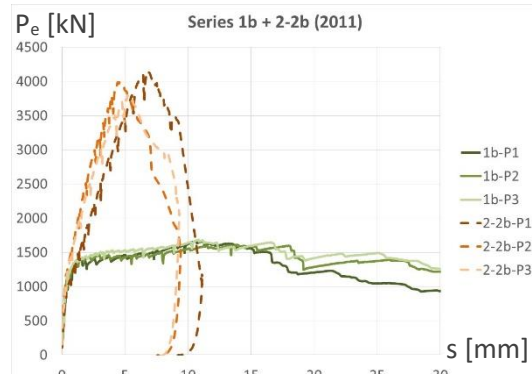


Figure 4.1.7: Series 1b and 2-2b

Influence of \varnothing_o : Comparison of test Series 1a with 2-2a and 1b with 2-2a

No influence of a reduction of the web-opening \varnothing_o from 40mm to 25mm on the value of the maximum load was observed. However, the maximum load was reached at smaller displacements for $\varnothing_o = 25\text{mm}$. In addition, failure of the dowel reinforcement occurred at smaller slip, the dowel behaved less ductile compared to $\varnothing_o = 40\text{mm}$, Figure 4.1.8.

A comparison of series 1b with 2-2a is presented in Figure 4.1.9. The load-bearing behaviour is mainly determined by f_{cm} and less by the variation of \varnothing_o , which confirms the above described influence of f_{cm} .

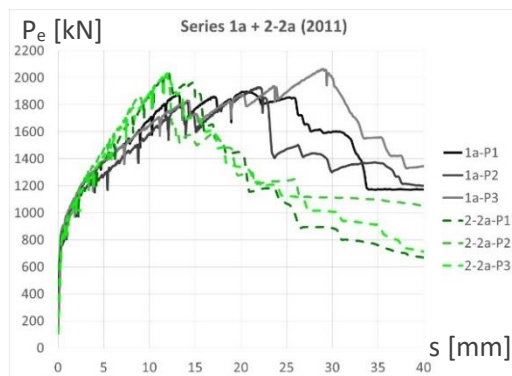


Figure 4.1.8: Series 1a and 2-2a

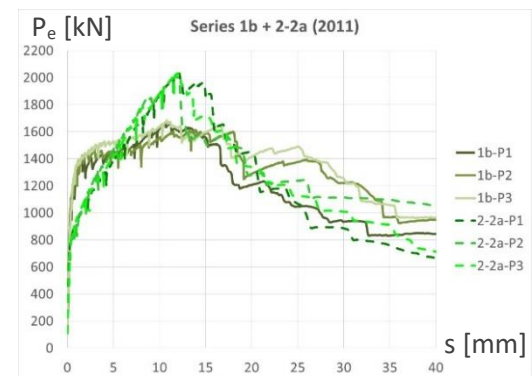


Figure 4.1.9: Series 1b and 2-2a

4.2 Test Analysis

In order to develop an analytical formulation of the load bearing capacity of CoSFB-Dowels, possible correlations of the test results were investigated. The most important results are presented hereafter. In the previous Section, the influence of f_{cm} on the behaviour of load bearing has been shown. It is expected that the concrete compression strength have a significant influence on the maximum experimental load, $P_{e,max}$. In Figure 4.2.1a a plot of $P_{e,max}$ versus the concrete compression strength f_{cm} is shown. No unambiguous relationship between f_{cm} and $P_{e,max}$ is observed. In fact, the maximum load is even inverse proportional to f_{cm} .

Elastic limit, $P_{e,lin}$ – Concrete Component

Hence, a relationship between f_{cm} and the limit of the linear range, $P_{e,lin}$, has been investigated, Figure 4.2.1b. A slight increase of the load with increasing concrete strength can be observed. The reader might remember, that test Series 2-2b failed due to concrete failure at the abutment of the push-out test and not, as for the other test series, due to failure of the dowel reinforcement.

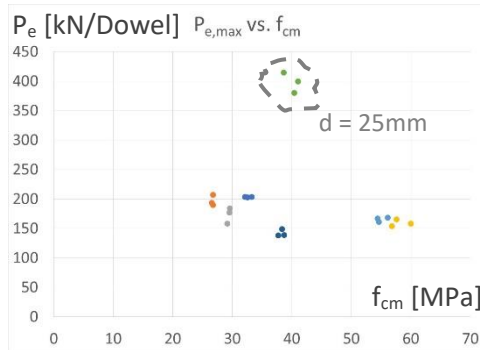


Figure 4.2.1a: $P_{e,max}$ versus f_{cm}

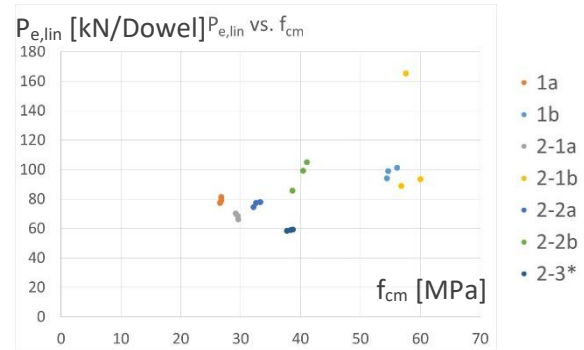


Figure 4.2.1b: $P_{e,lin}$ versus f_{cm}

As shown in Section 4.1, other parameters apart from f_{cm} had influence on the load. Different possible interactions have been investigated. Excellent correlation was found for $P_{e,lin}$ versus $f_{cm} \cdot t_w \cdot \varnothing_O$ with $\eta = P_{e,lin} / f_{cm} \cdot t_w \cdot \varnothing_O$, Figure 4.2.2.

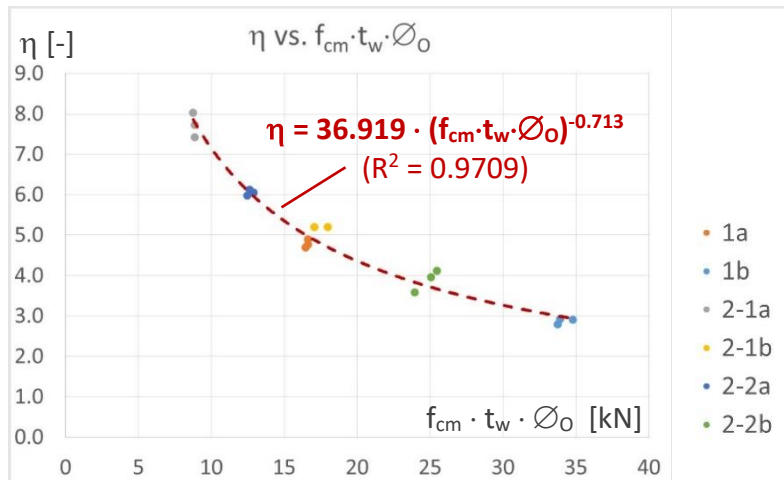


Figure 4.2.2: η versus $f_{cm} \cdot t_w \cdot \varnothing_O$

In the analytical formulation of η the test Series 2-3 was not taken into account. Also the result of test 2-1a-P3 was not considered, because this result is not representative for the given configuration, see Figure B2.4 of Annex B2. Comparing the results of test Series 1a with Series 2-2b no influence of the dowel reinforcement on $P_{e,lin}$ could be found. But, due to the limited amount of available test results, this might be subject of further investigations. The above described process is leading to the following theoretical formulation of the linear load, $P_{t,lin}$:

$$P_{t,lin} = \eta \cdot f_{cm} \cdot t_w \cdot \phi_O \quad (4.1)$$

with

$$\eta = 36.919 \cdot (f_{cm} \cdot t_w \cdot \phi_O)^{-0.713} \text{ [kN]}.$$

The factor η can be interpreted as a confinement factor for the uniaxial concrete compression strength f_{cm} , which is related to the triaxial stress state in the concrete in the web-opening. Previous investigations on the resistance of concrete bearing strength under local pressure found smaller confinement factors [Sou1987], [Li1989], [Ko2011]. The relatively high confinement of the concrete in CoSFB-Dowels is caused by the restrain of the concrete in the circular opening and by the concrete in the chamber of the steel profile. In accordance with previous findings about concrete confinement [Ri1928], [Ri1929], [Md1988] and others, the concrete confinement factor η is inversely proportional to the concrete compression strength, f_{cm} , and to the volume of confined concrete, $t_w \cdot \phi_O$. The load $P_{t,lin}$ as defined by the above given Equation 4.1 represents the maximum load transferable by the concrete component, limited by a local concrete compression strength. This finding corresponds to findings of previous researchers as e.g. given by Leonhart, Wurzer, Zapfe and others.

After P_{lin} is reached, the activation of the dowel reinforcement is initiated, which is confirmed by the measurement of strain gauges, Figures 4.2.3 and 4.2.4. As shown in Figure 4.2.3, the dowel reinforcement in level 1 (the nearest to the load introduction) is activated first, consecutively the other dowel bars are activated.

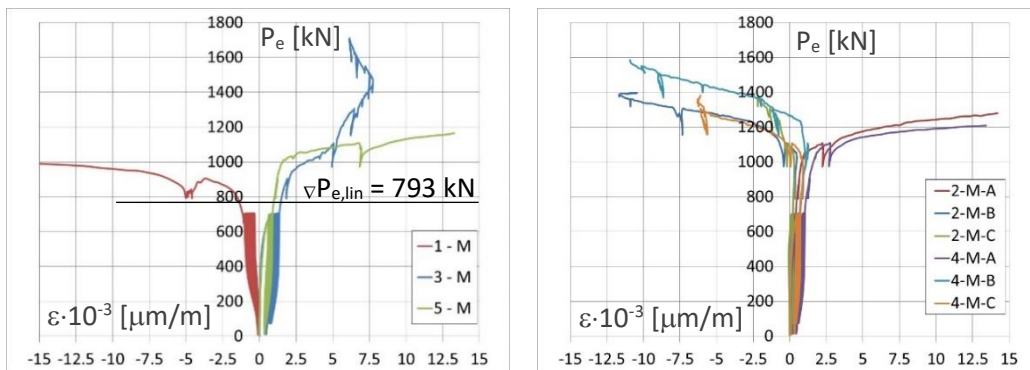


Figure 4.2.3: Test 1a – P1

As explained in Chapter 3, the strain gauge was fixed on the upper edge of the dowel reinforcement of level 1. Three strain gauges were fixed on the reinforcement bars at level 2 and 4, Figure 3.2.2.2. Their positive and negative values allow for the conclusion, that the bar is subjected to bending. With the assumption, that all dowel bars are activated in the same way, the negative strain

measured on level 1 compared to the positive values of level 3 and 5 (the strain gauges was fixed at the lower edge of the bar), also indicates bending of the reinforcement. Only very small strains could be measured below $P_{e,lin}$. These observations are confirmed by all test results, see Figures in Annex B3. The activation of the dowel action exceeding $P_{e,lin}$ could be confirmed by numerical simulation, Chapter 5. With increasing deformation of the dowel axis friction forces are activated.

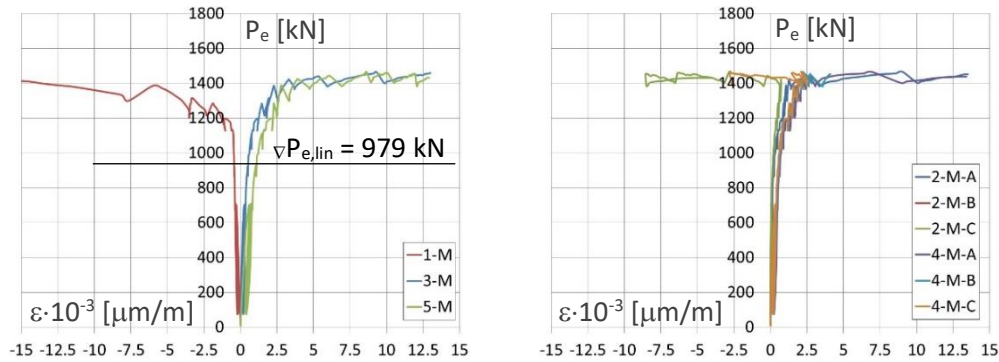


Figure 4.2.4: Test 1b – P2

Initial Stiffness, S_{ini}

In the linear phase of the load-slip curves the increase of the load by several hundred kN is corresponding to a slip value of only 0.1mm, which results in values larger than 2000kN/mm for the initials stiffness, S_{ini} . Hence, a high sensitivity of the calculated values for S_{ini} in relation to the measured slip values was found. Further, the measurement of slip values below 0.1mm are within the tolerances of the testing devices. Therefore, the obtained S_{ini} -values are scattered and the author decided not to derive an analytical formulation for the initial slip. Nevertheless, based on the average slip S_{ini} for each test series, some general tendencies could be identified:

- Comparing the initial stiffness of test Series 1a with Series 1b and of Series 2-1a with 2-1b, a slight proportionality of the stiffness to the concrete compression strength could be observed, Figure 4.2.5 and Table 4.1.2.
- No significant influence of the web thickness t_w (comparison of Series 1a with 2-1a and 1b with 2-1b) could be found.
- No influence of the diameter of web-opening \varnothing_o could be found.
- Compared to test Series 1a and 1b, Series 2-2b shows a higher value of the initial stiffness S_{ini} . This may lead to the conclusion, that the diameter of the dowel reinforcement d has a certain influence on S_{ini} . However, more tests to validate this assumption and to derive a formulation for S_{ini} are needed.

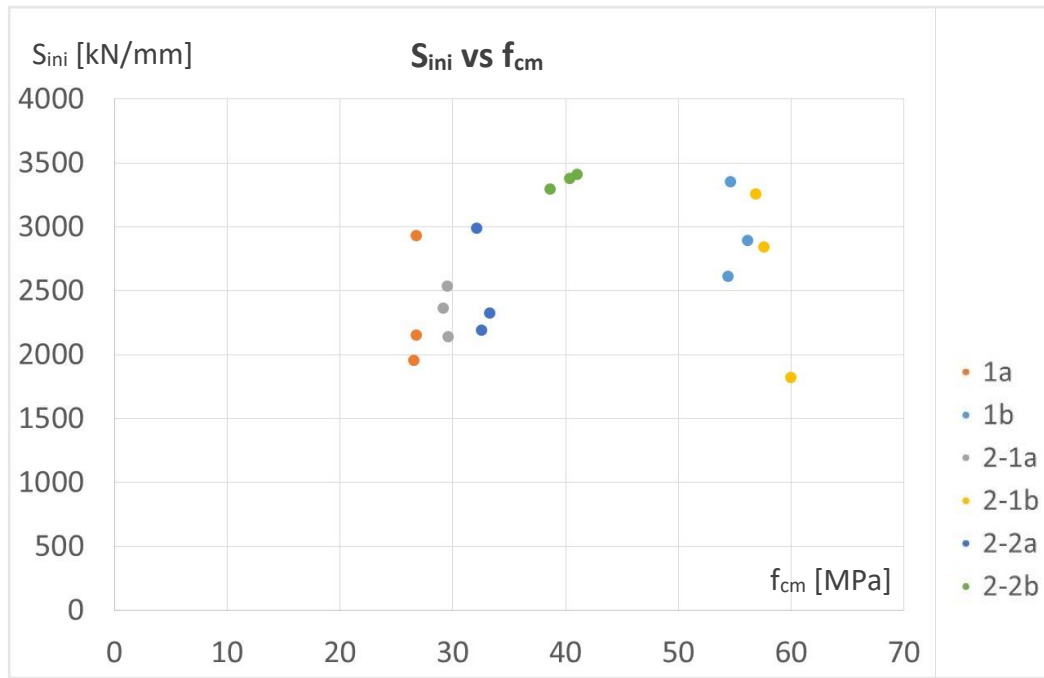


Figure 4.2.5: S_{ini} versus f_{cm}

Dowel action, ΔP

The difference between the maximum load obtained by testing $P_{e,max}$ and the linear load $P_{e,lin}$ for all push-out tests is given in Table 4.2. The load corresponding to dowel action was defined as $\Delta P_e = P_{e,max} - P_{e,lin}$. No direct correlation for ΔP_e to the web-opening or to the web-thickness could be found for the performed push-out tests, Figure 4.2.6. However, it was found that ΔP_e is inversely proportional to f_{cm} , Figure 4.2.7.

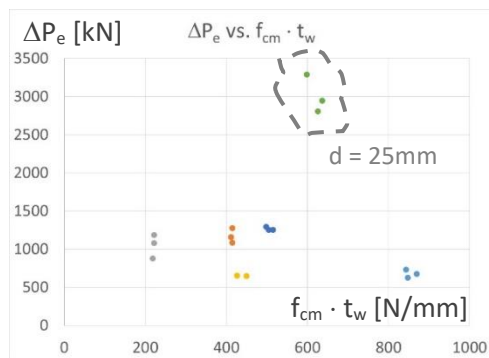


Figure 4.2.6: ΔP_e versus $f_{cm} \cdot t_w$

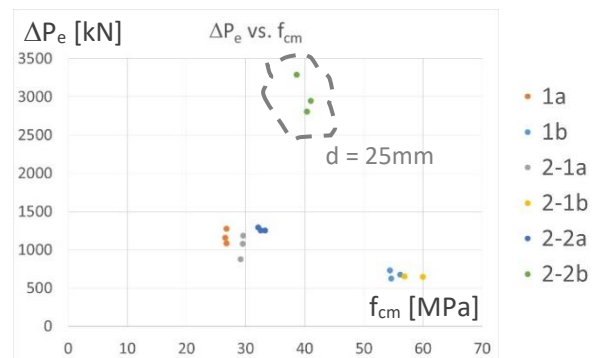


Figure 4.2.7: ΔP_e versus f_{cm}

The diameter of the dowel reinforcement was 12mm, only varied for test Series 2-2b with $d = 25\text{mm}$. Despite a certain influence on ΔP_e is shown in Figures 4.2.6 and 4.2.7, the available amount of test data is not sufficient to perform scientific investigations of the influence of the bar diameter. Nevertheless, the influence of d is considered in the proposed analytical formulation for ΔP_e , Chapter 6.

Table 4.2: Results push-out test Series 2011, ΔP_e

Series	f_{cm} [MPa]	$P_{e,lin}$ [kN]	$P_{e,max}$ [kN]	$\Delta P_e = P_{e,max} - P_{e,lin}$ [kN]
1a-P1	26.8	814.0	1895.5	1081.5
1a-P2	26.6	773.5	1930.5	1157.0
1a-P3	26.8	790.5	2065.0	1274.5
1b-P1	54.4	940.0	1668.0	728.0
1b-P2	54.7	987.0	1612.5	625.5
1b-P3	56.1	1010.5	1684.0	673.5
2-1a-P1	29.2	701.5	1579.5	878.0
2-1a-P2	29.6	659.5	1841.0	1181.5
2-1a-P3	29.6	685.0	1764.5	1079.5
2-1b-P1	56.9	887.0	1536.0	649.0
2-1b-P2	60.0	935.0	1582.5	647.5
2-1b-P3	57.6	1652.5	1655.5	-
2-2a-P1	32.2	744.5	2033.0	1288.5
2-2a-P2	32.6	772.0	2022.0	1250.0
2-2a-P3	33.3	780.0	2034.0	1254.0
2-2b-P1	38.6	856.0	4143.0	3287.0
2-2b-P2	41.1	1047.5	3993.0	2945.5
2-2b-P3	40.4	991.5	3798.5	2807.0

Figure 4.2.8 presents ΔP_e per dowel for test Series with $d = 12\text{mm}$ and concrete in the web-opening (Series 2-2b and 2-3 are not shown) versus f_{cm} . In addition, the theoretical plastic shear resistance $V_{t,pl}$ and tension resistance $N_{t,pl}$ for the dowel reinforcement is marked. The resistance values are calculated as follows:

$$V_{t,pl} = \pi \cdot \frac{d^2}{4} \cdot \frac{f_y}{\sqrt{3}} = \pi \cdot 6^2 \cdot \frac{530.6}{\sqrt{3}} = 34.6\text{kN} \quad (4.2)$$

$$N_{t,pl} = \pi \cdot \frac{d^2}{4} \cdot f_y = \pi \cdot 6^2 \cdot 530.6 = 60.0\text{kN} \quad (4.3)$$

The theoretical plastic shear resistance of the dowel reinforcement $V_{t,pl}$, defines a lower limit of the load bearing capacity of the dowel action using a higher concrete compression strength (Series 1b and 2-1b). Shear is the dominating action on the dowel reinforcement and consequently the failure is dominated by a shear failure of the reinforcement, Figure 4.2.8 Series 1b, 2-1b. The results of tests performed with a lower concrete compression strength (Series 1a, 2-1a, 2-2a) showed a tension dominated failure of the dowel reinforcement, which could be confirmed by analysing the after testing extracted reinforcement bars, Figure 4.2.8 Series 1a, 2-1a, 2-2a.

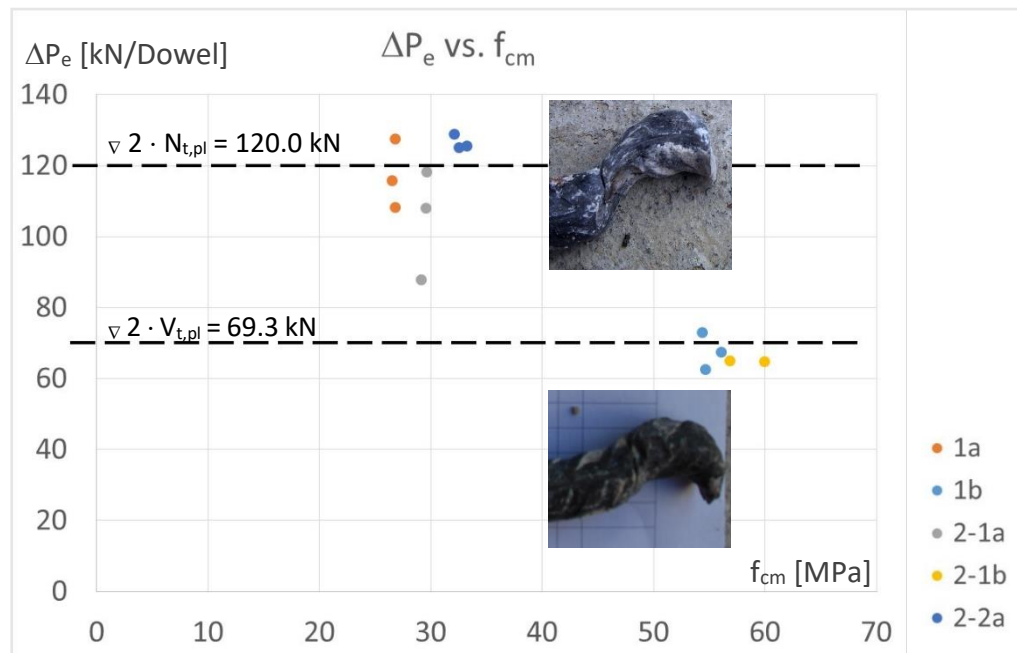


Figure 4.2.8: ΔP_e per dowel versus f_{cm} – Tension and Shear dominated Failure

The load ΔP_e for Series 1a, 2-1a and 2-2a is close to the value of the theoretical plastic tensile strength N_{t,pl}. But, because the dowel bar is subjected to tension, bending and shear, possible interaction of these forces has to be considered and the full plastic tensile strength may not be reached. Additional effects as e.g friction may also contribute to the load transfer. The influence of friction is investigated by numerical simulation, Chapter 5.

The load-slip curves for push-out Series 2-3 are given in Figure 4.2.9. All three tests were performed without concrete infill of the web-openings. Due to the absence of this concrete infill, possible load transfer by the “concrete component” as above described was eliminated. The maximum load obtained is higher than the theoretical plastic tensile strength of the reinforcement, which indicates the activation of friction forces.

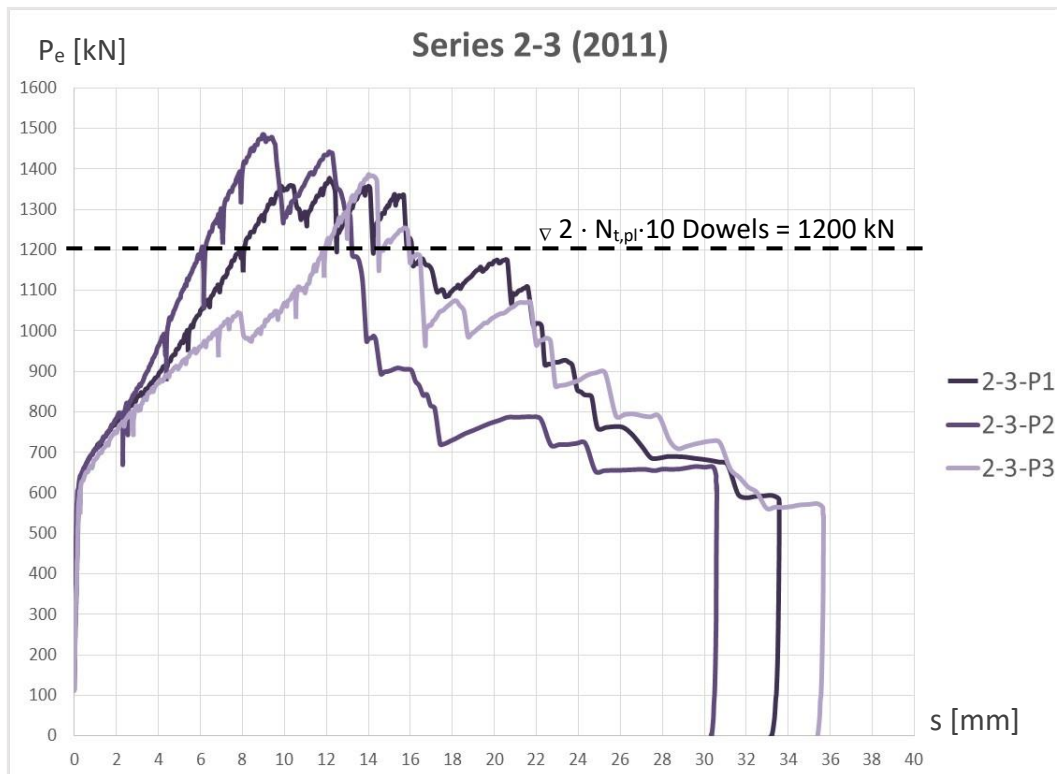


Figure 4.2.9: Load-slip curves Series 2-3

Finally some of the irregularities found by opening of the specimens are presented. This might give possible explanations of the result of test 2-1b-P3. Unfortunately only one push-out specimen per series was opened, no pictures are available for Series 2-1b-P3.



Figure 4.2.10: Test 2-1b-P1, Friction



Figure 4.2.11: Hooked bar, test 2-2a-P3



In Figure 4.2.10 a scratch path of the dowel reinforcement bar on the web of the steel section after cracking is shown. Figure 4.2.11 presents a dowel reinforcement bar, which did not detach from the web-opening after cracking. It was hooked at the edge of the web, which certainly had influenced the measured load-slip values

4.3 Conclusions from Test Analysis

The test observations and the analysis of test results lead to the following explanations of the load bearing behaviour.

- S_{ini}:** As main influencing parameters on the initial stiffness S_{ini} the concrete compression strength f_{cm} could be determined. Also small influence of the diameter of the web-opening was found. Further tests seem to be necessary to allow for final conclusions, especially about a possible influence of the diameter of the dowel reinforcement.
- P_{lin}:** The load level defined as P_{lin} , is influenced by the concrete compression strength f_{cm} and the size of the web-opening, expressed as the product $t_w \cdot \varnothing_O$. In addition, an increase of the uniaxial concrete compression strength due to the increased strength of concrete on small bearing area [Li1989] and the triaxial stress state in the web-opening is influencing P_{lin} .
- P_{max}, ΔP :** The maximum load P_{max} is composed of a concrete component P_{lin} and the activation of the dowel reinforcement, “dowel action”, ΔP . The activation of the dowel reinforcement depends on the strength of the bar on shear and tension and to its ability to crush the concrete underneath. Therefore, P_{max} depends on the strength of the bar in relation to the local bearing strength of the concrete. This relationship is decisive for a possible activation of catenary action of the dowel reinforcement.

Finally, the load-bearing behaviour of CoSFB-Dowels can be described:

An elastic behaviour of the specimen was observed up to the limit of P_{lin} . Reaching the load level of P_{lin} damage of the concrete in the web-opening starts and is quickly progressing. Damage corresponds to a reduction of the local stiffness and consequently, no additional load can be transferred by this load path anymore.

In the presence of transversal reinforcement bars through the web-opening, further load increase beyond P_{lin} is possible. This second load path (= dowel action), is determined by the diameter of the dowel reinforcement, its ultimate strength and its strain at failure, the rupture strain. The dowel reinforcement is subjected to shear forces and, at larger deformations of the dowel axis, to tension. By keeping the diameter and the strength of the dowel reinforcement constant and varying only the concrete strength, the following behaviour was observed:

- At high concrete strength, the dowel bar is subjected mainly to shear forces. The bar is not able to damage the concrete underneath, the axis of the bar cannot deform. The bar is subjected to shear forces only, failure of the dowel reinforcement will occur due to shear.
- At lower concrete strength, the dowel bar is able to crush, to damage the concrete underneath and creates a space, allowing its axis to deform. The dowel bar is subjected to shear and in relation to the increase of the deformation of its axis, to tension. This effect was described by Paulay [Pau1974] as “kinking”.

5 Numerical Simulation of Push-Out Tests

5.1 Introduction

The Series of experimental push-out tests performed in 2011 at the University of Stuttgart has been simulated using FE software Abaqus [Abaqus]. The aim of the simulations was to investigate the internal flow of strain, stresses and forces and further, to identify the contribution of each component (dowel reinforcement, concrete, friction) to the overall load-bearing behaviour. First results of the numerical simulation of CoSFB-Dowels have been already published by the autor [NS2015], [SC2015], [ES2017].

A 3D solid model of the push-out tests has been developed using non-linear material laws to analyse the influence of the concrete compression class, the web thickness and the diameter of the web-opening on the load-bearing behaviour. More than 500 simulations have been performed. The model has been validated by comparison to the results of the push-out tests. Further, a sensitivity study has been performed.

The numerical simulation of the given problem presents a highly non-linear problem with material and contact nonlinearities and large displacements. The simulation has been performed using quasi-static analysis in ABAQUS EXPLICIT, which allows better convergence than ABAQUS STANDARD in the presence of multiple contact definition. Following the recommendations of other researchers modelling push-out tests of composite members [Qur2011], the speed of simulation was set at 0.25mm/sec. This speed has proven to be adequate considering the energy balance verification [Qur2010]. The computation time was optimized by using the standard approach of mass scaling. The influence of different mass scale factors was analysed. For all in this document presented simulations the mass is artificially increased by a factor of 1000.

5.2 Numerical Model

5.2.1 Geometry, Boundary Conditions

One axis of symmetry of the push-out test specimen has been used to reduce the size of the model and consequently the overall computing time. The model is composed of a concrete slab, a hot rolled section HE220M or HE240A, dowel reinforcement and a reinforcement mesh in the concrete slab above the upper flange of the hot rolled steel section. Further, a steel plate has been modelled to represent the floor, on which the specimen has been placed. The displacement of this steel plate was blocked in all three global directions, when at the axis of symmetry only the displacement in y-direction was blocked, Figure 5.2.1.

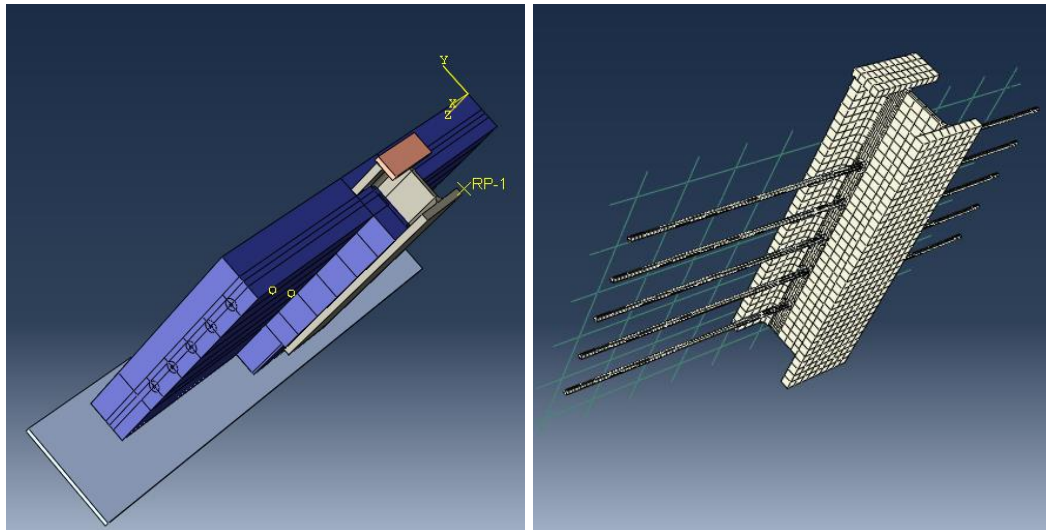


Figure 5.2.1: Geometry of numerical model

5.2.2 Finite Element Mesh

A type of solid element, which is most suitable to deal with non-linear materials and contacts at the same time was used, a C3D8R element: an 8-node linear brick, reduced integration with hourglass control. This element type has been applied to all the hexahedral mesh elements. The reinforcement mesh above the upper flange of the steel section is modelled as a wire, not solid element, and therefore beam elements, type T3D2 were applied. Each part of the model has been partitioned separately, which enabled to create the mesh as a structural mesh, using solid hexahedral elements. The mesh around the dowel reinforcement bars has been made locally finer, as larger deformations and stresses will appear in this area, Figure 5.2.2.

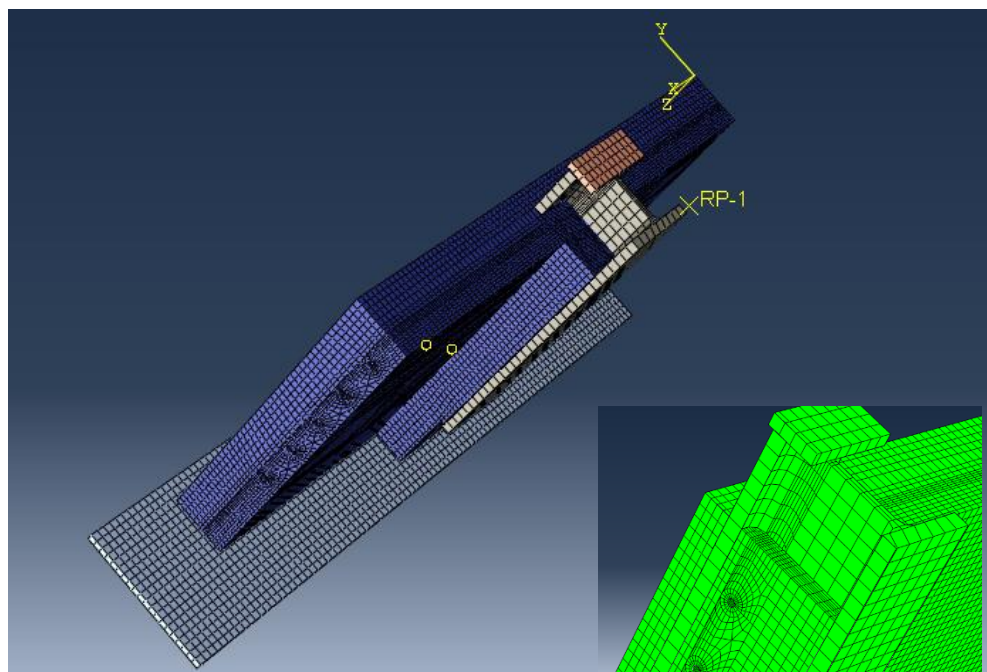


Figure 5.2.2: Finite element mesh

5.2.3 Load

A load introduction plate has been connected to a part of the hot rolled section. The plate has been coupled with a reference point, which was placed on the axis of symmetry. To simulate a displacement controlled testing, a displacement has been applied to this reference point. The reference point allows easily record the load-displacement curve, Point RP-1 in Figure 5.2.2.

5.2.4 Interactions, Contact Definition

The chosen modelling allowed for the definition of different interactions between the individual parts. If not otherwise indicated, hard contact as normal and as tangential behaviour different friction coefficients were applied. Also between the foundation steel plate and the concrete slab, the influence of different values of friction coefficients in tangential direction was analysed. The contact between the dowel reinforcement and the concrete was split into two principal areas: one for the part of the dowel bar in the slab and another one for the dowel bar in the chamber of the hot-rolled steel section, Figure 5.2.4. For the part of the bar in the slab, a tie constraint at the contact surface between the bar and the concrete was chosen. The slab was set as master and the dowel bar as slave surface. For the part of the dowel bar in the chamber various types of contact were analysed, cf. Section 5.4.

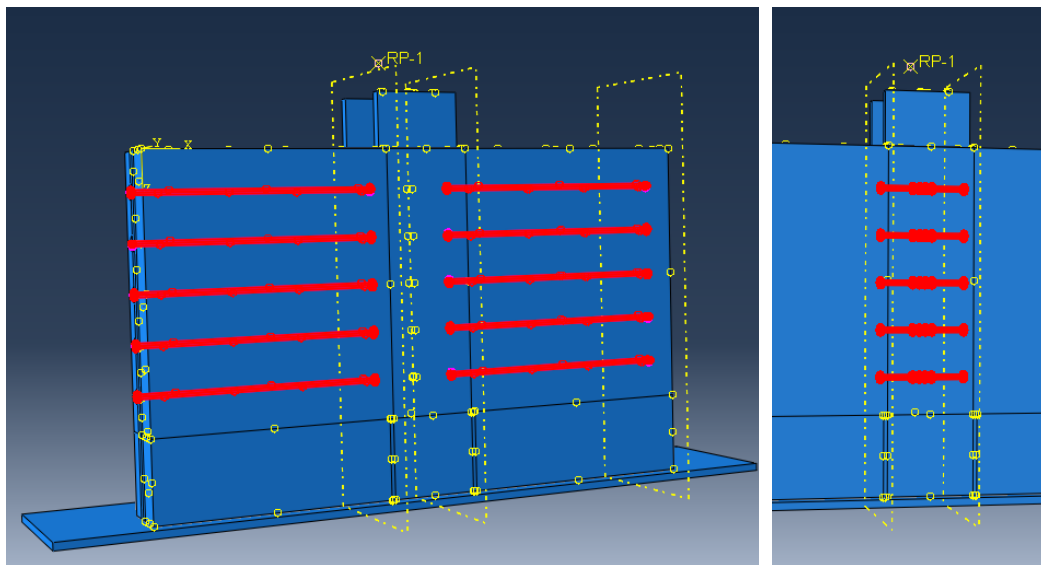


Figure 5.2.4: Areas for contact definition of the dowel reinforcement

5.3 Material Models

5.3.1 Introduction

Various constitutive laws are available in Abaqus, which allow very accurately simulate behaviour of the material in specific load conditions. These models often enable compensating interactions between elements of the system either to simplify the numerical analysis or because the interaction cannot be defined. To allow for the simulation of the failure of the dowel reinforcement as obtained in the tests, material models with ductile and shear damage have been applied for the dowel reinforcement. When it was possible to use simplified material models for structural steel and reinforcement mesh, because no damage has been observed in these parts. The concrete material has been modelled using Concrete Damage Plasticity. Influence of various parameters has been analysed and are presented in this Thesis.

5.3.2 Structural Steel

The structural steel has been modelled as a simple bilinear elasto-plastic material and applied to the hot-rolled steel section. The characteristic parameters of the material have been defined based on the results of tensile tests for specimens taken from the flange and the web as follows, Table 3.2.3.3:

$f_y = 375$ MPa, $f_u = 506$ MPa, $\epsilon_u = 0.15$, Young modulus 210 GPa, Poisson ratio 0.3

5.3.3 Reinforcement Mesh, Q257

Similarly to the structural steel, the material of reinforcement mesh (Q 257) has been also modelled as a simple bilinear elasto-plastic material. The following parameters were used:

Q 257: $f_y = 530.7$ MPa, $f_u = 582.7$ MPa, $\epsilon_u = 0.05$, Young modulus 200 GPa, Poisson ratio 0.3

5.3.4 Dowel Reinforcement

The failure observed in the push-out tests was determined by the dowel reinforcement reaching its rupture strain, cf. Chapter 3. Therefore, the material model used for the dowel reinforcement shall allow for an adequate simulation of the failure mode. Abaqus [Abaqus] gives the possibility for modelling progressive damage and failure in ductile metals, in conjunction with the Mises plasticity model. In general, an undamaged elastic-plastic response in form of true stress-strain relations, a damage initiation criterion (onset of failure/damage) and the evolution of damage has to be defined as input. By using this approach the failure modes observed in the push-out tests of the dowel reinforcement can be simulated adequately. A material model based on damage is consequently applied as explained in the subsequent paragraphs, see also [Pav2013]. The following parts are citations from [Abaqus].

Damage and failure for ductile metals [Abaqus]

Material failure refers to the complete loss of load-carrying capacity as a result of progressive degradation of the material stiffness. The stiffness degradation process is modeled using damage mechanics. As illustrated in Figure 5.3.4.1, the stress-strain behaviour of the material shows distinct phases. The initial material response is linear elastic up to point b, followed by plastic yielding with strain hardening from point b to c. Beyond point c there is a marked reduction of load-carrying capacity until rupture, c – d. The deformation during this last phase is localized in a neck region of a specimen used in tensile test. Point c identifies the material state at the onset of damage, which is referred to as the damage initiation criterion. Beyond this point, the stress-strain response c – d is governed by the evolution of the degradation of the stiffness in the region of strain localization. In the context of damage mechanics c – d can be viewed as the degraded response of the curve c – d' that the material would have followed in the absence of damage.

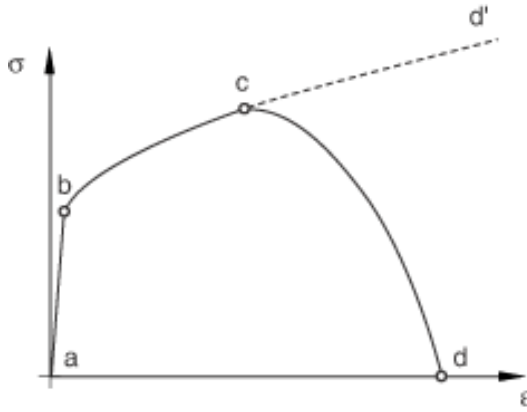


Figure 5.3.4.1: Typical stress-strain behaviour [Abaqus]

Thus, the specification of a failure mechanism consists of the following parts: - the definition of the effective (or undamaged) material response; - a damage initiation criterion; - a damage evolution law. The material data for materials with ductile behaviour should be given as “true” stress σ_{true} and logarithmic strain ϵ_{ln} . They can be derived from test data (engineering stress) using the following equations:

$$\sigma_{true} = \sigma_{test} \cdot (1 + \epsilon_{test}) \quad (5.1)$$

$$\epsilon_{ln} = \ln(1 + \epsilon_{test}) \quad (5.2)$$

The logarithmic plastic strain can be calculated with

$$\epsilon_{ln}^{pl} = \epsilon_{ln} - \epsilon_{el} = \ln(1 + \epsilon_{test}) - \frac{\sigma_{true}}{E} \quad (5.3)$$

where E is the Young modulus of the base material.

The *undamaged elastic-plastic* response is simply modelled by using classical metal plasticity assuming that yielding of the metal is independent of the equivalent pressure stress (Mises yield surface): this observation is confirmed experimentally for most metals. The Mises yield surface is used to define isotropic yielding, it is defined by giving the value of the uniaxial yield stress as a function of uniaxial equivalent plastic strain.

As *damage initiation criterion*, which represents the onset of damage/failure, two main mechanisms causing the fracture of a ductile metal are considered: ductile fracture due to the nucleation, growth, and coalescence of voids; and shear fracture due to shear band localization. Based on phenomenological observations, these two mechanisms call for different forms of the criteria for the onset of damage [Hoo2004]. By specifying multiple damage initiation criteria for the same material, they are treated independently. Once a particular initiation criterion is satisfied, the material stiffness is degraded according to the specified damage evolution law for that criterion.

The *ductile criterion* assumes that the equivalent plastic strain at the onset of damage $\bar{\epsilon}_D^{pl}$ is a function of stress triaxiality and strain rate: $\bar{\epsilon}_D^{pl}(\eta, \dot{\epsilon}^{pl})$, where $\eta = -p/q$ is the stress triaxiality, p is the pressure stress, q is the equivalent Mises stress and $\dot{\epsilon}^{pl}$ is the equivalent plastic strain rate. The stress triaxiality is given by:

$$\eta = \frac{-p}{q} = \frac{(\sigma_1 + \sigma_2 + \sigma_3)/3}{1/\sqrt{2} \cdot \sqrt{(\sigma_1 - \sigma_2)^2 + (\sigma_2 - \sigma_3)^2 + (\sigma_3 - \sigma_1)^2}} \quad (5.4)$$

with the principal stresses σ_1 , σ_2 and σ_3 .

The criterion for damage initiation is met when the following condition is satisfied:

$$\varpi_D = \int \frac{d\bar{\epsilon}_D^{pl}}{\bar{\epsilon}_D^{pl}(\eta, \dot{\epsilon}^{pl})} = 1 \quad (5.5)$$

where ϖ_D is a state variable that increases monotonically with plastic deformation. At each increment during the analysis the incremental increase in

$$\varpi_D \text{ is computed as } \Delta\varpi_D = \frac{\Delta\bar{\epsilon}_D^{pl}}{\bar{\epsilon}_D^{pl}(\eta, \dot{\epsilon}^{pl})} \geq 0. \quad (5.6)$$

The *shear criterion* is a phenomenological model for predicting the onset of damage due to shear band localization. The model assumes that the equivalent plastic strain at the onset of damage $\bar{\epsilon}_S^{pl}$ is a function of the shear stress ratio and strain rate: $\bar{\epsilon}_S^{pl}(\theta_S, \dot{\epsilon}^{pl})$. Here $\theta_S = (q + k_S \cdot p)/\tau_{max}$ is the shear stress ratio τ_{max} is the maximum shear stress, and k_S is a material parameter. The criterion for damage initiation is met when the following condition is satisfied:

$$\varpi_S = \int \frac{d\bar{\epsilon}_S^{pl}}{\bar{\epsilon}_S^{pl}(\theta_S, \dot{\epsilon}^{pl})} = 1 \quad (5.7)$$

where ϖ_S is a state variable that increases monotonically with plastic deformation proportional to the incremental change in equivalent plastic strain. At each increment during the analysis the incremental increase in ϖ_D is computed as

$$\Delta\varpi_S = \frac{\Delta\bar{\epsilon}_S^{pl}}{\bar{\epsilon}_S^{pl}(\theta_S, \dot{\epsilon}^{pl})} \geq 0. \quad (5.8)$$

The *evolution of damage* is defined by a description of the rate of degradation of the material stiffness once the corresponding damage initiation criterion has been reached. At any given time during the analysis the stress tensor in the material is given by the scalar damage equation $\sigma = (1 - D) \cdot \bar{\sigma}$, where D is the overall damage variable and $\bar{\sigma}$ is the effective, undamaged stress tensor computed in the current increment. $\bar{\sigma}$ are the stresses that would exist in the material in the absence of damage. The material has lost its load-carrying capacity when $D = 1$.

The characteristic stress-strain behaviour of a material undergoing damage is illustrated in Figure 5.3.4.2. In the context of an elastic-plastic material with isotropic hardening, the damage manifests itself in two forms: softening of the yield stress and degradation of the elasticity. The solid curve in the Figure represents the damaged stress-strain response, while the dashed curve is the response in the absence of damage. The damaged response depends on the element dimensions to minimize the mesh dependency on the results.

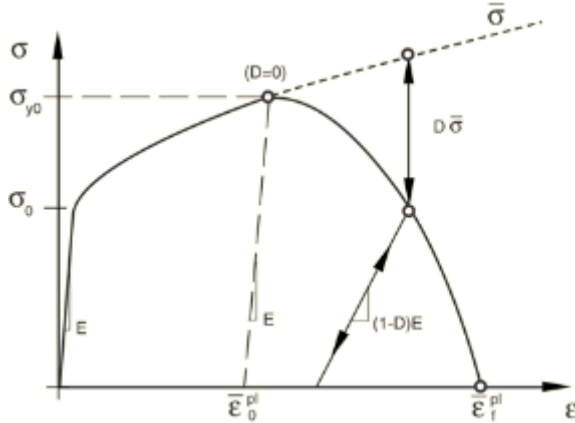


Figure 5.3.4.2: Progressive damage degradation [Abaqus]

In the Figure σ_{y0} and $\bar{\epsilon}_0^{pl}$ are the yield stress and equivalent plastic strain at the onset of damage, and $\bar{\epsilon}_f^{pl}$ is the equivalent plastic strain at failure; that is, when the overall damage variable reaches the value $D = 1$. The overall damage variable, D , captures the combined effect of all active damage mechanisms and is computed in terms of the individual damage variables, d_i .

The value of the equivalent plastic strain at failure, $\bar{\epsilon}_f^{pl}$, depends on the characteristic length of the element and cannot be used as a material parameter for the specification of the damage evolution law. When material damage occurs, the stress-strain relationship no longer accurately represents the material's behaviour. Continuing to use the stress-strain relation introduces a strong mesh dependency based on strain localization, such that the energy dissipated decreases as the mesh is refined. A different approach is required to follow the strain-softening branch of the stress-strain response curve. Instead, the damage evolution law is specified in terms of equivalent plastic displacement, \bar{u}^{pl} , or in terms of fracture energy dissipation, G_f . Hillerborg's (Hil1976) fracture energy proposal is used to reduce mesh dependency by creating a stress-displacement response after damage is initiated. Using brittle fracture concepts, Hillerborg defines the energy required to open a unit area of crack, G_f , as a material parameter. With this approach, the softening response after damage initiation is characterized by a stress-displacement response rather than a stress-strain response.

The implementation of this stress-displacement concept in a finite element model requires the definition of a characteristic length, L , associated with an integration point. The fracture energy is then given as

$$G_f = \int_{\bar{\epsilon}_0^{pl}}^{\bar{\epsilon}_f^{pl}} L \cdot \sigma_y d\bar{\epsilon}^{pl} = \int_0^{\bar{u}_f^{pl}} \sigma_y d\bar{u}^{pl}. \quad (5.9)$$

This expression introduces the definition of the equivalent plastic displacement, \bar{u}^{pl} , as the fracture work conjugate of the yield stress after the onset of damage (work per unit area of the crack). Before damage initiation $\dot{\bar{u}}^{pl} = 0$; after damage initiation $\dot{\bar{u}}^{pl} = L \cdot \dot{\bar{\epsilon}}^{pl}$.

The definition of the characteristic length depends on the element geometry and formulation: it is a typical length of a line across an element for a first-order element; it is half of the same typical length for a second-order element. This definition of the characteristic length is used because the direction in which fracture occurs is not known in advance. Therefore, elements with large aspect ratios will have rather different behaviour depending on the direction in which they crack: some mesh sensitivity remains because of this effect, and elements that have aspect ratios close to unity are recommended.

Each damage initiation criterion may have an associated damage evolution law. The damage evolution law can be specified in terms of equivalent plastic displacement, \bar{u}^{pl} , or in terms of fracture energy dissipation, G_f . Both of these options take into account the characteristic length of the element to alleviate mesh dependency of the results.

The overall damage variable, D , captures the combined effect of all active mechanisms and is computed in terms of individual damage variables, d_i , for each mechanism.

Once the damage initiation criterion has been reached, the effective plastic displacement, \bar{u}^{pl} , is defined with the evolution equation $\dot{\bar{u}}^{pl} = L \cdot \dot{\bar{\epsilon}}^{pl}$, where L is the characteristic length of the element. The evolution of the damage variable with the relative plastic displacement is specified in exponential form.

Assuming an exponential evolution of the damage variable with plastic displacement, as shown in Figure 5.3.4.3. The relative plastic displacement at failure, \bar{u}_f^{pl} , and the exponent α can be specified. The damage variable is given as

$$d = \frac{1 - e^{-\alpha(\bar{u}^{pl}/\bar{u}_f^{pl})}}{1 - e^{-\alpha}}. \quad (5.10)$$

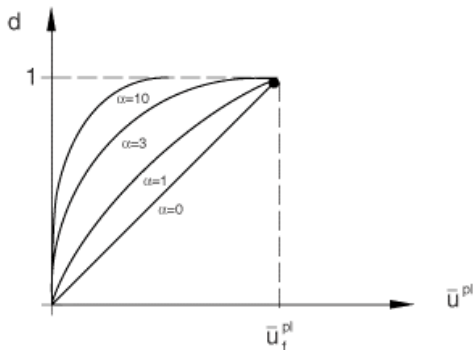


Figure 5.3.4.3: Exponential evolution of damage [Abaqus]

5.3.5 Concrete

5.3.5.1 Introduction

Concrete material shows a quasi-brittle fracture behaviour. After reaching its ultimate strength a fracture connected with decreasing stress develops. To simulate numerically the fracture behaviour of concrete, the cement matrix, aggregates and interfacial transition zones are homogenized within the macroscale material law and a corresponding set of material parameters. Thus, the definitions given in the following are valid only for simulations done in macroscale, size of whole specimens in the order of a scale of meters [Hae2015].

Modeling of reinforced concrete in Abaqus is accomplished by combining standard elements, using this plain concrete cracking model, with “rebar elements”—rods, defined singly or embedded in oriented surfaces, that use a one-dimensional strain theory and that can be used to model the reinforcing itself. The rebar elements are superposed on the mesh of plain concrete elements and are used with standard metal plasticity models that describe the behaviour of the rebar material. This modeling approach allows the concrete behaviour to be considered independently of the rebar, so this section discusses the plain concrete cracking model only. Effects associated with the rebar/concrete interface, such as bond slip and dowel action, cannot be considered in this approach except by modifying some aspects of the plain concrete behaviour to mimic them (such as the use of “tension stiffening” to simulate load transfer across cracks through the rebar). It is generally accepted that concrete exhibits two primary modes of behaviour: a brittle mode in which microcracks coalesce to form discrete macrocracks representing regions of highly localized deformation, and a ductile mode where microcracks develop fairly uniformly throughout the material, leading to nonlocalized deformation. The brittle behaviour is associated with cleavage, shear and mixed mode fracture mechanisms that are observed under tension and tension-compression states of stress. It nearly always involves softening of the material. The ductile behaviour is associated with distributed microcracking mechanisms that are primarily observed under compression states of stress. It is often associated with hardening of the material, although subsequent softening is possible at low confining pressures. The cracking model described here models only the brittle aspects of concrete behaviour.

5.3.5.2 Uniaxial behaviour of concrete in compression

The uniaxial behaviour of concrete is obtained from compression tests and presented in form of stress-strain relationship. Three regions can be distinguished: an elastic, a hardening and a softening region, Figure 5.3.5.2. For the definition of the elastic and the hardening region the non-linear stress-strain relationship according to section 3.1.5 of EN 1992-1-1 [EN1992] is applied. The softening branch is defined by applying a fracture energy approach (“Crushing energy”), which is similar to the softening of concrete in uniaxial tension. This crushing energy method has been first proposed by Feenstra [Fee1996], a description is given in [Krä2004].

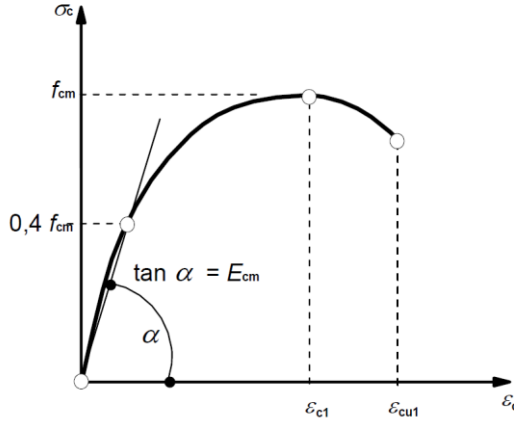


Figure 5.3.5.2: Stress-strain relationship of concrete in uniaxial compression [EN 1992]

This leads to the following definition of the stress-strain relationship of concrete under uniaxial compression.

$$\text{Region 1 – Elastic: } \frac{\sigma_c(\varepsilon_c)}{f_{cm}} = E_{cm} \cdot \frac{\varepsilon_c}{f_{cm}} \quad (5.11a)$$

$$\text{Region 2 – Hardening: } \frac{\sigma_c(\varepsilon_c)}{f_{cm}} = \frac{k \cdot \eta - \eta^2}{1 + (k-2) \cdot \eta} \quad (5.11b)$$

where:

$$\eta = \varepsilon_c / \varepsilon_{c1}$$

ε_{c1} is the strain at peak stress according to Table 3.1 [EN1992]

$$k = 1.05 \cdot E_{cm} \cdot |\varepsilon_{c1}| / f_{cm}, \text{ with } f_{cm} \text{ and } E_{cm} \text{ according to [EN1992]}$$

f_{cm} = determined from tests, see Chapter 3

$$E_{cm} = 22 \cdot (f_{cm}/10)^{0.3} \text{ with } f_{cm} \text{ in [MPa].}$$

$$\text{Region 3 – Softening: } \frac{\sigma_c(\varepsilon_c)}{f_{cm}} = \frac{1/f_{cm}}{\frac{2 + \gamma_c \cdot f_{cm} \cdot \varepsilon_{c1}}{2 \cdot f_{cm}} + \gamma_c \cdot \varepsilon_c + \frac{\gamma_c}{2 \cdot \varepsilon_{c1}} \cdot \varepsilon_{c1}^2} \text{ with } \gamma_c > 0 \quad (5.11c)$$

with

$$\gamma_c = \frac{\pi^2 \cdot f_{cm} \cdot \varepsilon_{c1}}{2 \cdot \left[\frac{G_{cl}}{l_{eq}} - \frac{1}{2} \cdot f_{cm} \cdot \left(\varepsilon_{c1} \cdot (1-b) + b \cdot \frac{f_{cm}}{E_{cm}} \right) \right]^2}$$

where

l_{eq} is the characteristic length of the respective FE integration point. It depends on type, quadrature rule and form of the element [28] and

$$\text{should fulfill the following equation } l_{eq} \geq \frac{G_{cl}}{f_{cm} \cdot \left(\varepsilon_{c1} (1-b) + b \cdot \frac{f_{cm}}{E_{cm}} \right)}.$$

b scalar parameter representing split of inelastic strains into plastic and damaging parts, set to 0.5, [Krä2004].

G_{cl} crushing energy, set to 20 kN/m [Vo1993]

5.3.5.3 Uniaxial behaviour of concrete in tension

In Abaqus [Abaqus] the postfailure behaviour for direct straining across cracks can be specified either by means of a postfailure stress-strain relation or by applying a fracture energy cracking criterion. Because the specification of postfailure behaviour by a stress-strain relation would introduce, in cases of little or no reinforcement, a mesh sensitivity in the results (the finite element predictions do not converge to a unique solution as the mesh is refined because mesh refinement leads to narrower crack bands), the fracture energy criterion as proposed by Hillerborg [Hil1976] for concrete cracking is used in this research. Hillerborg defines the energy required to open a unit area of crack in Mode I G_f^I as a material parameter, using brittle fracture concepts. With this approach, the concrete's brittle behaviour is characterized by a stress-displacement response rather than a stress-strain response. Under tension, a concrete specimen will crack across some section; and its length, after it has been pulled apart sufficiently for most of the stress to be removed (so that the elastic strain is small), will be determined primarily by the opening at the crack, which does not depend on the specimen's length. This fracture energy cracking model is invoked by specifying the postfailure stress as a tabular function of displacement across the crack, as illustrated in Figure 5.3.5.3.

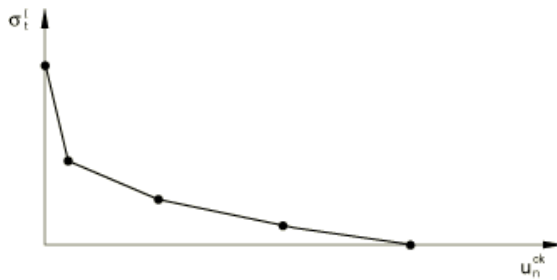


Figure 5.3.5.3: Postfailure stress-displacement curve [Abaqus]

The implementation of the stress-displacement concept in a finite element model requires the definition of a characteristic length associated with a material. The characteristic crack length is based on the element geometry and formulation: it is a typical length of a line across an element for a first-order element; it is half of the same typical length for a second-order element. This definition of the characteristic crack length is used because the direction, in which cracks will occur, is not known in advance. Therefore, elements with large aspect ratios will have rather different behaviour depending on the direction in which they crack: some mesh sensitivity remains because of this effect. Elements that are as close to square as possible are, therefore, recommended.

To define the fracture energy the proposal given in [fib2010] is applied. This approach has successfully been used to simulate similar problems as e.g. the load-bearing behaviour of shear studs in composite slabs [Qur2011]. The fracture energy is defined as the energy required to propagate a tensile crack of unit area, it is dissipated in friction and plastic deformation in the fracture area [fib42].

It depends primarily on the water/cement ratio, the maximum aggregate size and the age of the concrete, in absence of detailed test data it can be estimated as:

$$G_F = 73 \cdot f_{cm}^{0.18} \quad (5.12)$$

with f_{cm} is the mean compressive strength in MPa.

It has been found [Qur2011] that an exponential expression derived by Cornelissen et al [Cor1986] is adequate to define the softening response of concrete using the fracture energy concept. This exponential function can be formulated as:

$$\frac{\sigma_t}{f_t} = f(w) - \frac{w}{w_c} \cdot f(w_c) \quad (5.13)$$

$$f(w) = \left[1 + \left(\frac{c_1 \cdot w}{w_c} \right)^3 \right] \cdot e^{-\left(\frac{c_2 \cdot w}{w_c} \right)} \quad (5.14)$$

where

$c_1 = 3$, $c_2 = 6.93$ [Cor1986]

w is the crack opening displacement

w_c is the crack opening displacement at which stress can no longer be transferred

$w_c = 5.0 \cdot G_f/f_t$ for normal weight concrete [fib2010].

The tensile damage d_t is obtained with $d_t = (f_{ctm} - \sigma_t)/f_{ctm}$, with $f_{ctm} = 0.3 \cdot (f_{cm} - 8)^{2/3}$ according to [EN1992].

5.3.5.4 Multiaxial behaviour - Concrete Damage Plasticity

The Concrete Damage Plasticity (CDP) model is a continuum, plasticity-based, damage model for concrete. It assumes that the main two failure mechanisms are tensile cracking and compressive crushing of the concrete material. The evolution of the yield (or failure) surface is controlled by two hardening variables, $\hat{\varepsilon}_t^{pl}$ and $\hat{\varepsilon}_c^{pl}$, linked to failure mechanisms under tension and compression loading, it is referred to $\hat{\varepsilon}_t^{pl}$ and $\hat{\varepsilon}_c^{pl}$ as tensile and compressive equivalent plastic strains, respectively. The uniaxial tensile and compressive response of concrete is characterized by damaged plasticity, Figure 5.3.5.4.1.

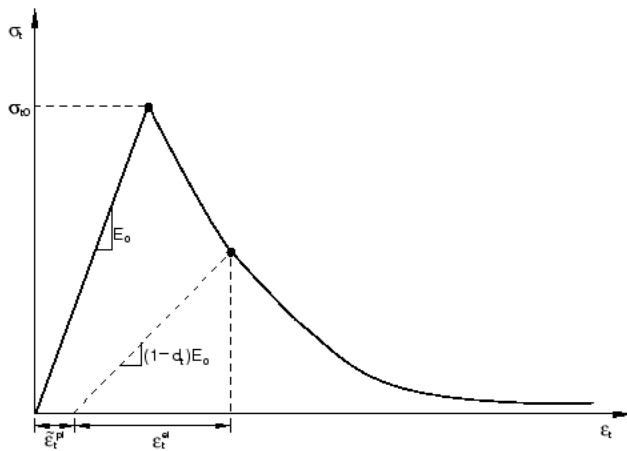


Figure 5.3.5.4.1: Concrete in uniaxial loading in tension [Abaqus]

Under uniaxial tension the stress-strain response follows a linear elastic relationship until the value of the failure stress, σ_{t0} , is reached. The failure stress corresponds to the onset of micro-cracking in the concrete material. Beyond the failure stress the formation of micro-cracks is represented macroscopically with a softening stress-strain response, which induces strain localization in the concrete structure.

Under uniaxial compression the response is linear until the value of initial yield, σ_{c0} . In the plastic regime the response is typically characterized by stress hardening followed by strain softening beyond the ultimate stress, σ_{cu} . This representation, although somewhat simplified, captures the main features of the response of concrete, Figure 5.3.5.4.2.

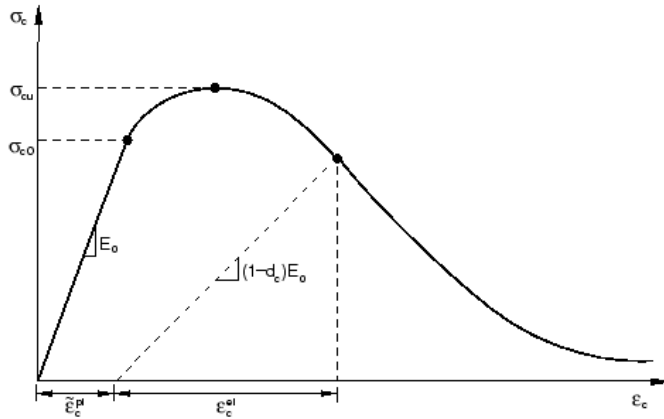


Figure 5.3.5.4.2: Concrete in uniaxial loading in compression [Abaqus]

It is assumed that the uniaxial stress-strain curves can be converted into stress versus plastic-strain curves. (This conversion is performed automatically by Abaqus from the user-provided stress versus “inelastic” strain data, as explained below.) Thus,

$$\begin{aligned}\sigma_t &= \sigma_t(\tilde{\varepsilon}_t^{pl}, \dot{\tilde{\varepsilon}}_t^{pl}, \theta, f_i), \\ \sigma_c &= \sigma_c(\tilde{\varepsilon}_c^{pl}, \dot{\tilde{\varepsilon}}_c^{pl}, \theta, f_i),\end{aligned}$$

where the subscripts t and c refer to tension and compression, respectively; $\tilde{\varepsilon}_t^{pl}$ and $\tilde{\varepsilon}_c^{pl}$ are the equivalent plastic strains, $\dot{\tilde{\varepsilon}}_t^{pl}$ and $\dot{\tilde{\varepsilon}}_c^{pl}$ are the equivalent plastic strain rates, θ is the temperature, and $f_i = (i = 1, 2, \dots)$ are other predefined field variables.

As shown in the Figures here before, when the concrete specimen is unloaded from any point on the strain softening branch of the stress-strain curves, the unloading response is weakened: the elastic stiffness of the material appears to be damaged (or degraded). The degradation of the elastic stiffness is characterized by two damage variables, d_t and d_c , which are assumed to be functions of the plastic strains, temperature, and field variables:

$$\begin{aligned}d_t &= d_t(\tilde{\varepsilon}_t^{pl}, \theta, f_i); 0 \leq d_t \leq 1, \\ d_c &= d_c(\tilde{\varepsilon}_c^{pl}, \theta, f_i); 0 \leq d_c \leq 1.\end{aligned}$$

The damage variables can take values from zero, representing the undamaged material, to one, which represents total loss of strength.

If E_0 is the initial (undamaged) elastic stiffness of the material, the stress-strain relations under uniaxial tension and compression loading are, respectively:

$$\sigma_t = (1 - d_t) \cdot E_0 \cdot (\varepsilon_t - \tilde{\varepsilon}_t^{pl}), \quad (5.15)$$

$$\sigma_c = (1 - d_c) \cdot E_0 \cdot (\varepsilon_c - \tilde{\varepsilon}_c^{pl}). \quad (5.16)$$

The “effective” tensile and compressive cohesion stresses are defined as:

$$\bar{\sigma}_t = \frac{\sigma_t}{(1 - d_t)} = E_0 \cdot (\varepsilon_t - \tilde{\varepsilon}_t^{pl}), \quad (5.17)$$

$$\bar{\sigma}_c = \frac{\sigma_c}{(1 - d_c)} E_0 \cdot (\varepsilon_c - \tilde{\varepsilon}_c^{pl}). \quad (5.18)$$

The effective cohesion stresses determine the size of the yield (or failure) surface.

Defining tension stiffening [Abaqus]

The postfailure behaviour for direct straining is modeled with tension stiffening, which allows to define the strain-softening behaviour for cracked concrete. Tension stiffening is required in the concrete damaged plasticity model. Within this research tension stiffening is specified by applying a fracture energy cracking criterion. Alternatively, the postfailure behaviour could also specified using a stress-strain relationship, but, when there is no reinforcement in significant regions of the model, this approach would introduce unreasonable mesh sensitivity into the results. Means that the finite element predictions do not converge to a unique solution as the mesh is refined, because mesh refinement leads to narrower crack bands. This problem typically occurs if cracking failure occurs only at localized regions in the structure and mesh refinement does not result in the formation of additional cracks.

Therefore, the fracture energy proposal according to Hillerborg (1976) [Hil1976] is used. Which is adequate to allay the concern for many practical purposes. Hillerborg defines the energy required to open a unit area of crack, G_f , as a material parameter, using brittle fracture concepts. With this approach the concrete's brittle behavior is characterized by a stress-displacement response rather than a stress-strain response. Under tension a concrete specimen will crack across some section. After it has been pulled apart sufficiently for most of the stress to be removed (so that the undamaged elastic strain is small), its length will be determined primarily by the opening at the crack. The opening does not depend on the specimen's length. This fracture energy cracking model can be invoked by specifying the postfailure stress as a tabular function of cracking displacement, as already shown in Figure 5.3.5.3.

Defining compressive behaviour [Abaqus]

The stress-strain behaviour of plain concrete in uniaxial compression outside the elastic range can be defined in Abaqus [Abaqus] by providing compressive stress data as a tabular function of inelastic (or crushing) strain, $\tilde{\varepsilon}_c^{in}$. Positive (absolute) values should be given for the compressive stress and strain. The stress-strain curve can be defined beyond the ultimate stress, into the strain-softening regime. Hardening data are given in terms of an inelastic (or crushing) strain, $\tilde{\varepsilon}_c^{in}$, instead of plastic strain, $\tilde{\varepsilon}_c^{pl}$. The compressive inelastic strain is defined as the total strain minus the elastic strain corresponding to the undamaged material, $\tilde{\varepsilon}_c^{in} = \varepsilon_c - \varepsilon_{0c}^{el}$, where $\varepsilon_{0c}^{el} = \sigma_c / E_0$, as illustrated in Figure 5.3.5.4.3.

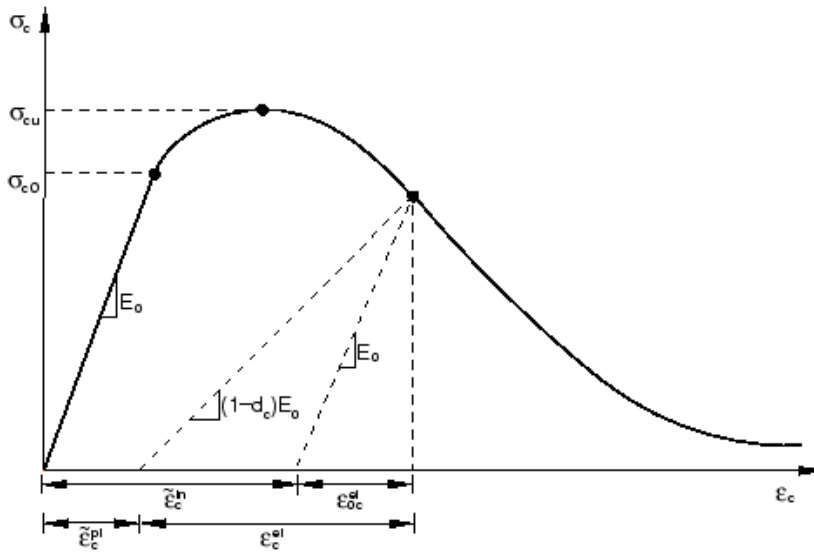


Figure 5.3.5.4.3: Definition of the compressive inelastic strain $\tilde{\varepsilon}_c^{in}$ [Abaqus]

Unloading data are provided to Abaqus in terms of compressive damage curves, $d_c - \tilde{\varepsilon}_c^{in}$, as discussed below. Abaqus automatically converts the inelastic strain values to plastic strain values using the relationship

$$\tilde{\varepsilon}_c^{pl} = \tilde{\varepsilon}_c^{in} - \frac{d_c}{(1-d_c)} \cdot \frac{\sigma_c}{E_0}. \quad (5.19)$$

Yield function [Abaqus]

The model in Abaqus makes use of the yield function of Lubliner et. al. (1989) [Lu1989], with the modifications proposed by Lee and Fenves (1998) [Lee1998] to account for different evolution of strength under tension and compression. The evolution of the yield surface is controlled by the hardening variables, $\tilde{\epsilon}_t^{pl}$ and $\tilde{\epsilon}_c^{pl}$. In terms of effective stresses, the yield function takes the form

$$F = \frac{1}{1-\alpha} \cdot (\bar{q} - 3 \cdot \alpha \cdot \bar{p} + \beta \cdot (\tilde{\epsilon}_t^{pl}) \cdot \langle \hat{\sigma}_{max} \rangle - \gamma \cdot \langle -\hat{\sigma}_{max} \rangle) - \bar{\sigma}_c(\tilde{\epsilon}_c^{pl}) = 0 \quad (5.20)$$

with

$$\begin{aligned} \alpha &= \frac{(\sigma_{b0}/\sigma_{c0})-1}{2 \cdot (\sigma_{b0}/\sigma_{c0})-1}; 0 \leq \alpha \leq 0.5, \\ \beta &= \frac{\bar{\sigma}_c(\tilde{\epsilon}_c^{pl})}{\bar{\sigma}_t(\tilde{\epsilon}_t^{pl})} \cdot (1 - \alpha) - (1 + \alpha), \\ \gamma &= \frac{3 \cdot (1-K_c)}{2 \cdot K_c - 1}. \end{aligned}$$

Here,

- $\hat{\sigma}_{max}$ is the maximum principal effective stress;
- $(\sigma_{b0}/\sigma_{c0})$ is the ratio of initial equibiaxial compressive yield stress to initial uniaxial compressive yield stress (the default value is 1.16);
- K_c is the ratio of the second stress invariant on the tensile meridian, $q(TM)$, to that on the compressive meridian, $q(CM)$, at initial yield for any given value of the pressure invariant p such that the maximum principal stress is negative, $\hat{\sigma}_{max} < 0$ (see Figure 5.3.5.4.4); it must satisfy the condition $0.5 < K_c < 1.0$ (the default value is 2/3);
- $\bar{\sigma}_t(\tilde{\epsilon}_t^{pl})$ is the effective tensile cohesion stress;
- $\bar{\sigma}_c(\tilde{\epsilon}_c^{pl})$ is the effective compressive cohesion stress.

Typical yield surfaces are shown in Figure 5.3.5.4.4 on the deviatoric plane and in Figure 5.3.5.4.5 for plane stress conditions.

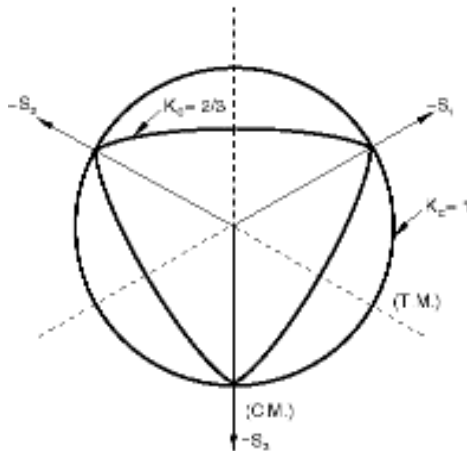


Figure 5.3.5.4.4: Yield surfaces in the deviatoric plane, corresponding to different values of K_c [Abaqus]

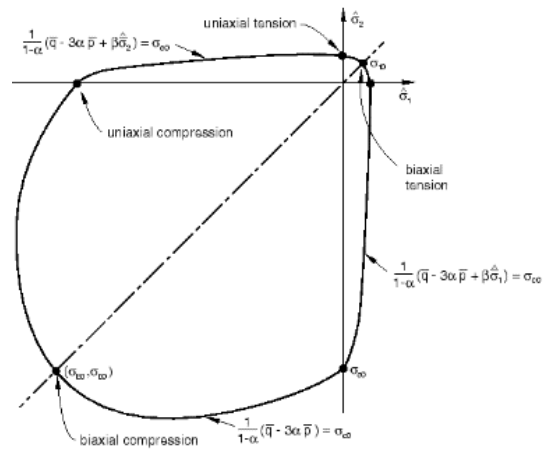


Figure 5.3.5.4.5: Yield surface in plane stress [Abaqus]

5.3.5.5 Concrete confinement

The concrete in the web-opening is restrained by the steel web and by the concrete in the chamber of the steel section. Therefore, this part of the concrete is able to resist a compression much higher than only its uniaxial compression strength. The influence of concrete confinement in the web-opening only and in the whole chamber of the hot-rolled section are analysed in this Thesis, Figure 5.3.5.5.1.

As proposed by Mander [Md1988] the confined concrete compressive strength f_{cc} and the corresponding confined strain ε_{cc} can be determined with:

$$f_{cc} = f_c + k_1 \cdot f_l \quad (5.21)$$

$$\varepsilon_{cc} = \varepsilon_c \cdot \left(1 + k_2 \cdot \frac{f_l}{f_c}\right) \quad (5.22)$$

with the lateral confining pressure f_l , which has to be determined by comparison of the numerical results with test results. The factors k_1 and k_2 are taken as 4.1 and 20.5 as given by Richart et al. [Ri1928].

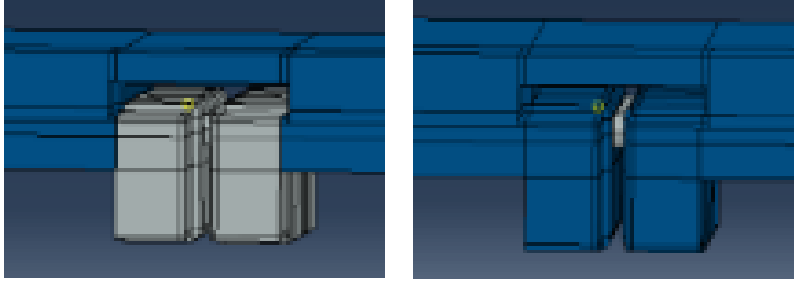


Figure 5.3.5.5.1: Zones of concrete confinement

The uniaxial stress-strain curve for confined concrete can be divided into three parts. An elastic range from zero up to a proportional stress of $0.5 \cdot f_{cc}$ as defined by Hu et al. [Hu, 2003]. The Young's modulus of confined concrete E_{cc} is calculated using the following empirical equation [ACI318M]:

$$E_{cc} = 4700 \cdot \sqrt{f_{cc}} \text{ [MPa]} \quad (5.23)$$

From the proportional stress $0.5 \cdot f_{cc}$ up to the confined concrete strength f_{cc} a non-linear part follows, which can be determined by the stress values f with:

$$f = \frac{E_{cc} \cdot \varepsilon}{1 + (R + R_E - 2) \cdot \left(\frac{\varepsilon}{\varepsilon_{cc}}\right) - (2 \cdot R - 1) \cdot \left(\frac{\varepsilon}{\varepsilon_{cc}}\right)^2 + R \cdot \left(\frac{\varepsilon}{\varepsilon_{cc}}\right)^3} \quad (5.24)$$

where ε represents the strain values between the proportional strain and the confined strain ε_{cc} corresponding to the confined strength f_{cc} , R_E and R are calculated from:

$$R_E = \frac{E_{cc} \cdot \varepsilon_{cc}}{f_{cc}} \quad (5.25)$$

$$R = \frac{R_E \cdot (R_\sigma - 1)}{(R_E - 1)^2} - \frac{1}{R_E} \quad (5.26)$$

As recommended by Hu and Schnobrich [Hu1989] the constants R_σ and R_ε are taken as equal to a value of 4.

The third part of the confined concrete stress-strain curve is a descending part, from the confined concrete strength f_{cc} descending to a value $r \cdot k_3 \cdot f_{cc}$ at a corresponding strain of $11 \cdot \epsilon_{cc}$, Figure 5.3.5.5.2. The factor k_3 is calculated by the method given by [Mir1992] or by [Hu2003]. The factor r takes into account the influence of the concrete compression strength. According to Giakoomelis and Lam [Gia2004] a value of $r = 1.0$ can be used for a concrete cube strength of 30 MPa and for a concrete cube strength equal or greater than 100 MPa a value of 0.5. For the here presented research work a value $r = 1.0$ is used.

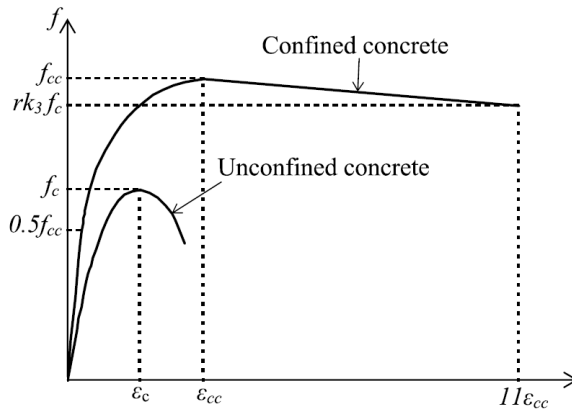


Figure 5.3.5.5.2: Concrete confinement [Elb2011]

5.4 Development of a Numerical Model for Series 1a

5.4.1 Introduction

The development of a numerical model for the simulation of test Series 1a (Table 5.4.1) and the influence of the most important parameters is shown. Unless noted otherwise, the following basic set of parameters has been used, input data is given in Annex C:

- The friction coefficient between steel section and concrete, referred further to as “global” friction was set to 0.1. Frictionless contact was applied for the friction between the steel plate (foundation) and the concrete slab.
- The tensile strength of the concrete was set to the tested value, Table 3.2.3.1. For test series 1a a value of 4.1 MPa was used.
- In accordance to [Qur2011] the fracture energy was increased to a value of $G_F = 6 \cdot 73 \cdot f_{cm}^{0.18}$.
- As standard contact between the part of the dowel reinforcement bar in the chamber of the steel section and the concrete the option “rough” was chosen and for the part of the dowel reinforcement in the concrete slab tie contact was applied, not allowing for any slip between the bar and the concrete.
- Default value of the dilation angle of 36° for concrete damage plasticity was used.
- True stress-strain relationship for the dowel reinforcement was introduced and the maximum elongation for ductile damage was in accordance with the tensile tests, Section 3.4.
- No values for the ultimate deformation of shear damage were available. Therefore, this parameter was developed by comparison of the load-slip curve obtained by testing with the one from numerical simulation, Figure 5.4.2.1.

To analyse possible sensitivity of the results to the size of the finite element mesh, the mesh size of the dowel reinforcement and of the concrete in the chamber of the steel section was varied. Due to the chosen damage approach and the dependency of the ultimate displacement to the mesh size, cf. Section 5.3.4 the characteristic length, consequently the mesh size had an influence on the results, which could not be avoided. As expected, a reduction of the mesh size, while keeping the values for the displacements at failure unchanged, was leading to a less ductile behaviour, no significant influence on the maximum load was observed.

Table 5.4.1: Geometry of push-out Series 1a

Series	t_w [mm]	\varnothing_o web-opening [mm]	d, diameter dowel bar [mm]	f_{cm} [MPa]
1a	15.5	40	12	26.7

5.4.2 Influence of various parameters

Almost 500 simulations were performed to identify influencing parameters and to determine the values. From these simulations with varied input parameters, only the most significant results are given hereafter, describing their influence on the behaviour of CoSFB-Dowel. The following investigation leads to understanding of the behaviour of CoSFB-Dowel, which could not be concluded from the experimental tests only. The findings were used to develop an analytical model.

Shear Damage – Influence of Displacement at Failure

To allow for shear failure of the dowel reinforcement, the option “Shear Damage” in Abaqus [Abaqus] was used. As damage initiation criterion the strain at the onset of necking derived by the displacement controlled tensile tests (cf. Section 3.4) was implemented. For the evolution of damage, the option of an exponential function was chosen. Displacement at failure for shear damage had to be given as an input. Because this value could not be directly derived by testing, it has been determined by comparison of the numerically obtained load-slip curves with the load-slip curves from experimental tests. The full set of input parameters required for shear damage are given in Annex C. Figure 5.4.2.1 shows the numerically obtained load-slip curves for varied values of the displacement at failure. The values for the displacement at failure u_f are given in relation to the strain at the onset of necking ε_n , multiplied by a characteristic length L , which is the length of the finite element ($L = 2\text{mm}$).

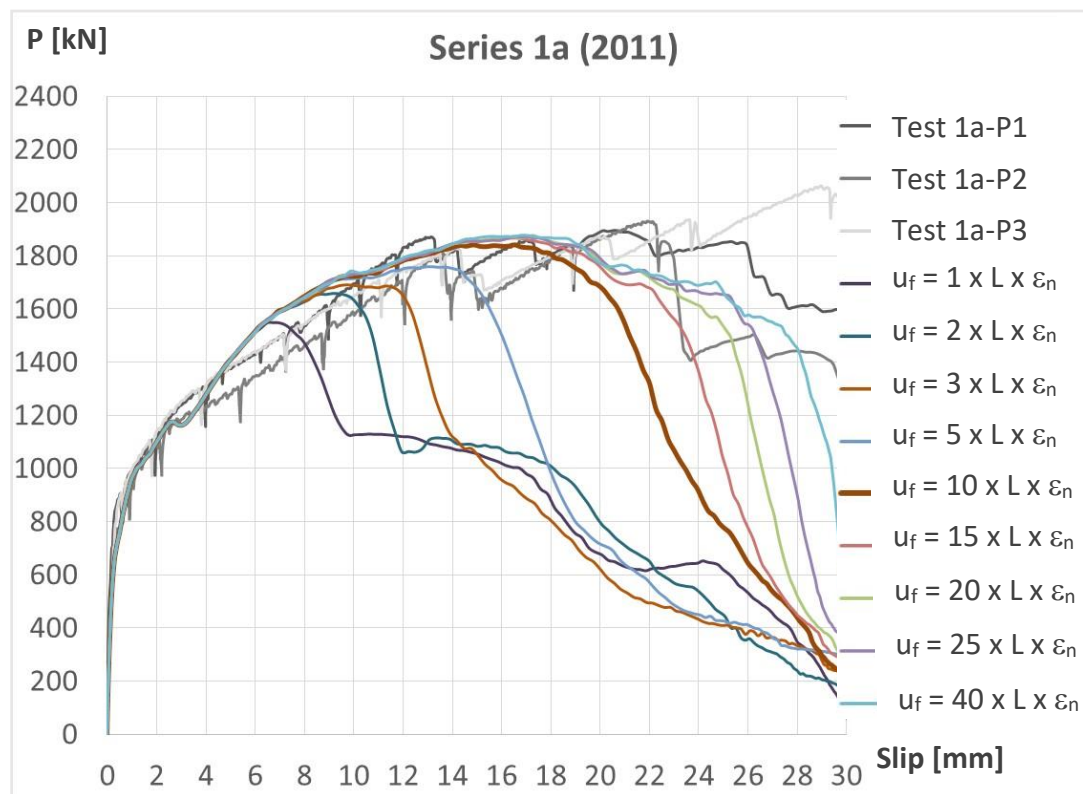


Figure 5.4.2.1: Influence of displacement at failure for shear damage, u_f

An increase of the displacement at failure up to values $10 \times L$ lead to an increase of the maximum load, while further increase is only influencing the ductility. The value $u_f = 10 \times L \times \varepsilon_n$ was chosen to represent the test results in an adequate manner and was set as standard value for further numerical analysis.

Ductile Damage – Influence of Displacement at Failure

For the evolution of ductile damage [Abaqus] the option “Displacement” was chosen to minimize influence of the finite element mesh size on the results. Damage starts at the onset of necking and reaches a value of 1.0 at rupture. The strain at rupture ε_r was determined by tensile tests, (cf. Section 3.4). To obtain the displacement values, the values for plastic strain ε_{pl} have to be multiplied by a characteristic length L , which depends on the size of the finite elements and the type of the used elements. For the used C3D8R elements Pavlovic [Pav2013] determined a factor of $3.1 \times L$ ($L = 2\text{mm}$). Some results for varied displacements values in relation to the plastic strain ε_{pl} are given in Figure 5.4.2.2.

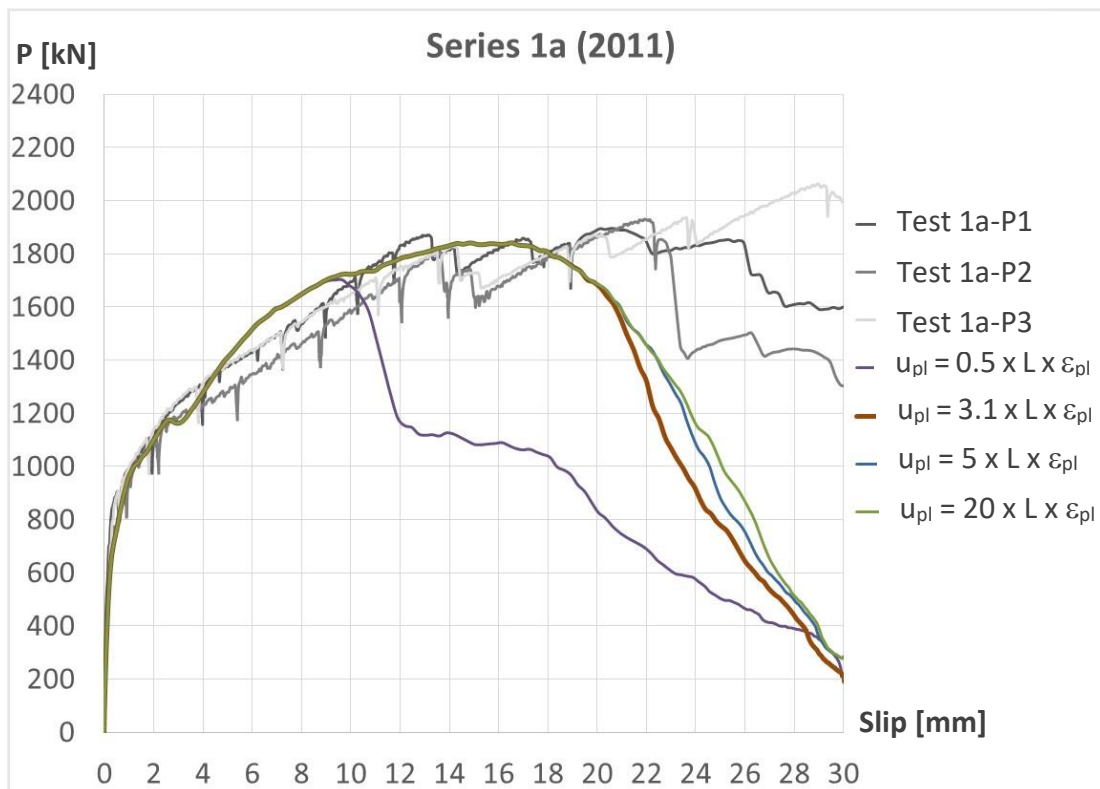


Figure 5.4.2.2: Influence of plastic displacement for ductile damage, u_{pl}

The value $3.1 \times L$ according to Pavlovic seems to represent the test results in an adequate manner. Therefore, this value was used for further analysis.

Influence of concrete tension strength and fracture energy

To analyse the influence of the concrete tensile strength f_{ctm} on the load-slip curve, numerical simulations with different values for the tensile strength are performed. Results are presented in Figure 5.4.2.3.

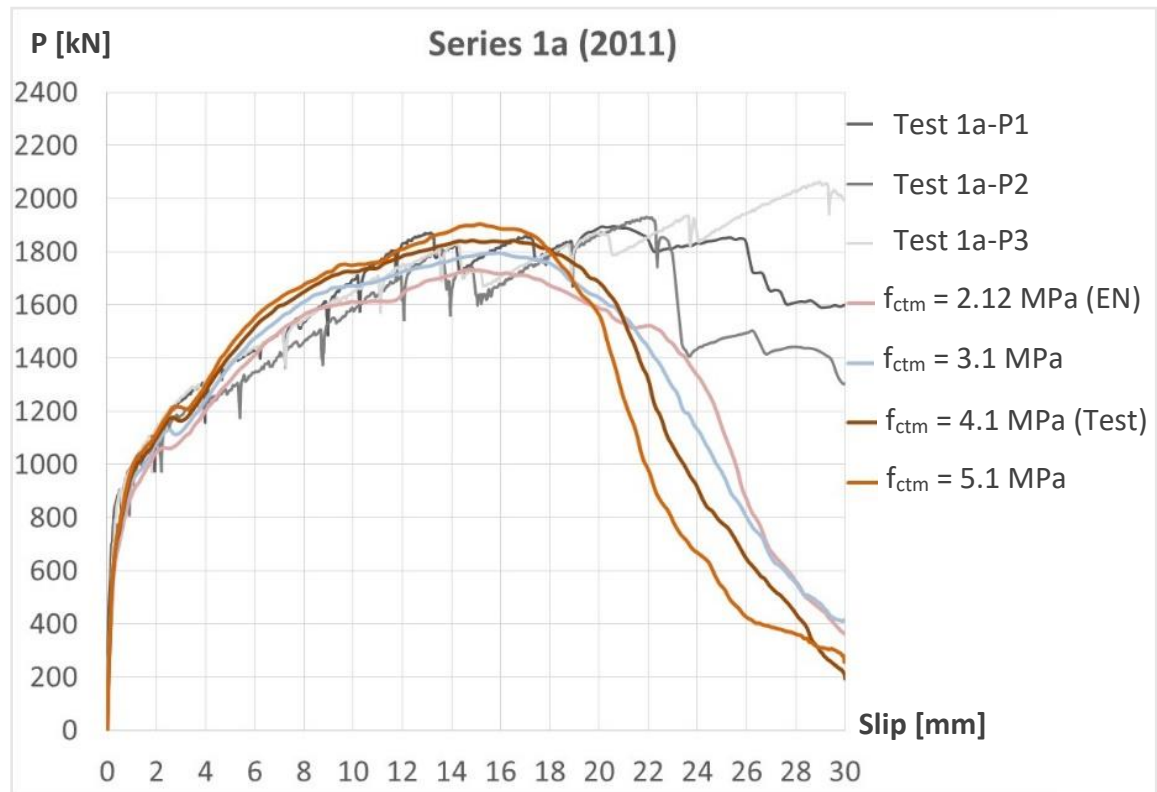
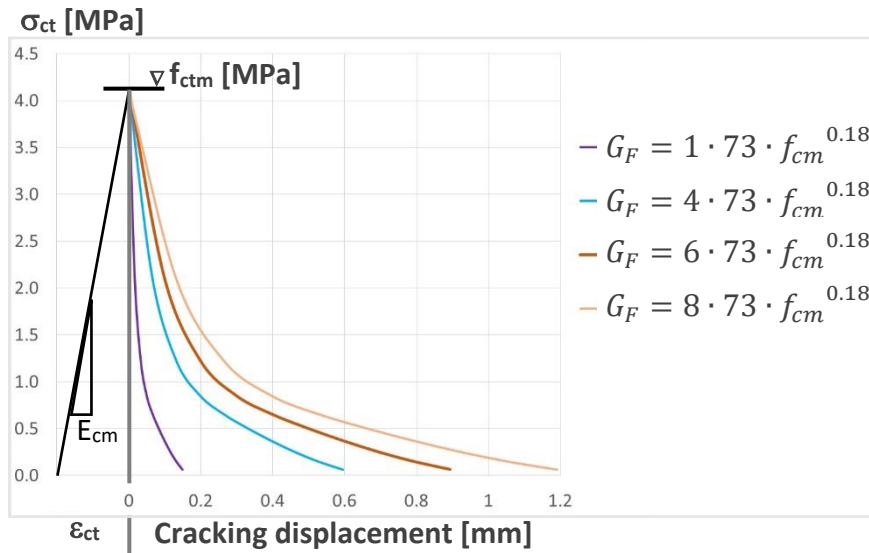
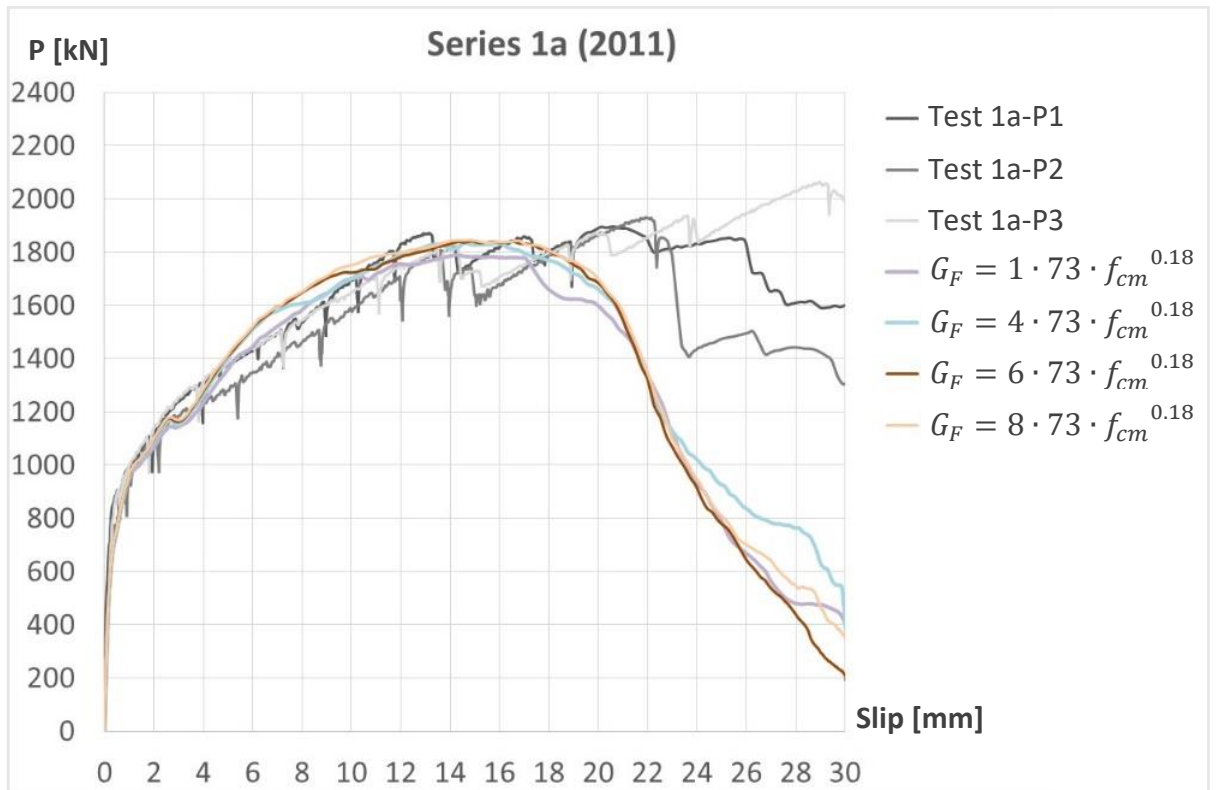


Figure 5.4.2.3: Influence of concrete tension strength, f_{ctm}

An increase of f_{ctm} is leading to small increase of the maximum load, while for smaller values a higher ductility could be observed. The author decided to use for further numerical simulations the by testing obtained value for the tensile strength, with $f_{ctm} = 4.1$ MPa.

According to fib 2010 [fib 2010] the fracture energy G_F can be calculated with $G_F = 73 \cdot f_{cm}^{0.18}$. For the simulation of similar problems, as e.g. the load-bearing behaviour of shear studs, Researchers varied the value of G_F from the above given equation [Qur2011]. The variation of G_F is given in Figure 5.4.2.4, the influence of the fracture energy on the load-slip curve in Figure 5.4.2.5.

Figure 5.4.2.4: Variation of fracture energy, G_F Figure 5.4.2.5: Influence of fracture energy, G_F

The fracture energy G_F has only a minor influence on the load-slip curve. This result confirms that the tensile behaviour of concrete is not decisive for CoSFB-Dowel, which is in line with the observations from the experimental tests.

Influence of friction

Friction defined in the numerical modal was Coulomb-Friction. The friction force F depends on pressure perpendicular to a surface and a friction coefficient. The influence of friction between the specimen and the supporting plate ("Foundation") and the steel section and the concrete ("Global") was analysed by performing numerical simulations with varied friction factors. The results for varied friction factors are presented in Figure 5.4.2.6 and Figure 5.4.2.7.

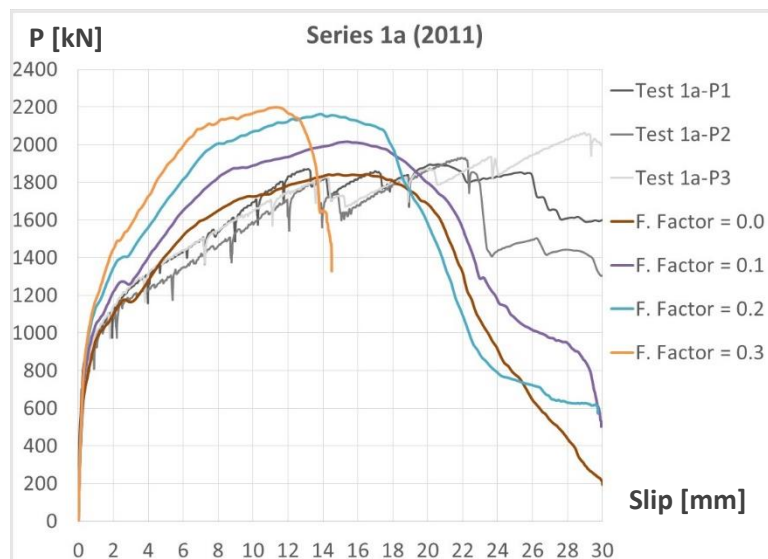


Figure 5.4.2.6: Influence of friction between foundation and specimen

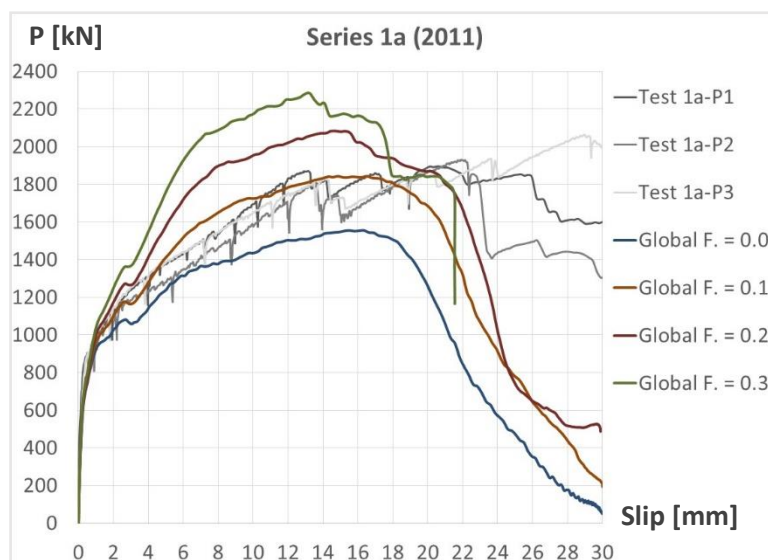


Figure 5.4.2.7: Influence of friction between steel section and concrete

Higher friction factors lead to an increase of the maximum load and to a decrease of the ductility. No influence on the initial stiffness was found. Friction is a parameter, which has often a significant influence on the behaviour, but it is impossible to measure experimentally in the composite structure. Therefore, it is typically derived by comparison of the results with parametrical variation.

Influence of the dilation angle

One of the input parameters of Concrete Damage Plasticity in Abaqus [Abaqus] is the dilation angle. It expresses the angle of inclination of the failure surface towards the hydrostatic axis, measured in the meridional plane. Physically it can be interpreted as a concrete internal friction angle [Kmi2011]. To analyse its influence on the load-slip curve, numerical simulations with varied values for the dilation angle were performed. Results are presented in Figure 5.4.2.8.

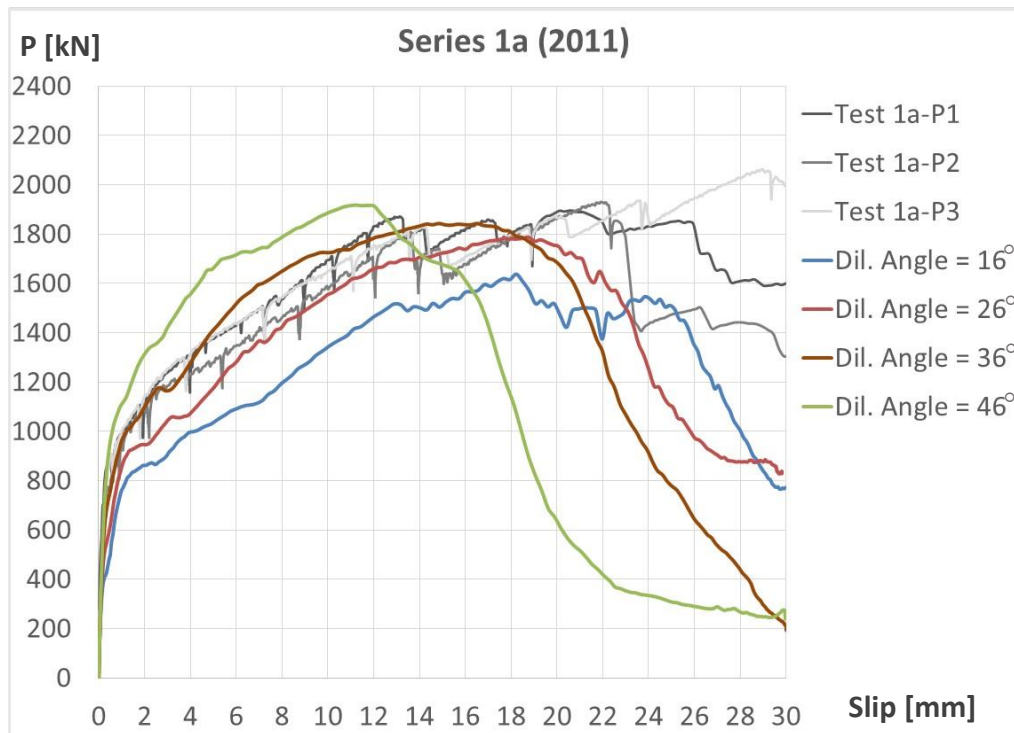


Figure 5.4.2.8: Influence of dilation angle

A dilation angle between 26° and 36° has proven to be adequate to simulate the push-out test Series 1a. The author decided to remain to the standard value of 36° for the simulation of all test series. It is worth mentioning that some researchers work on calibration of CDP model and identification of the most appropriate dilation angle in relation to different structural elements of reinforced concrete structure e.i. beam to column joint [Szc2015].

Influence of reinforcement mesh

In all performed push-out tests a standard reinforcement mesh, a Q257, was placed above the upper flange of the steel section, cf. Figure 5.4.2.9. The possible influence of this reinforcement mesh was analysed by varying the diameter of the reinforcement bars, while keeping the distance between the bars. This way the reinforcement ratio has been differentiated.

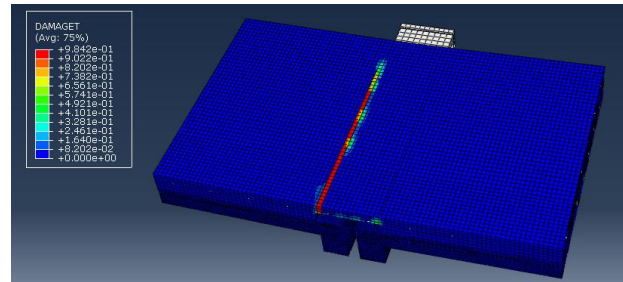
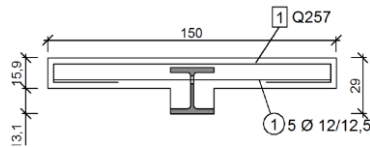


Figure 5.4.2.9: Reinforcement mesh [Stu2011] 5.4.2.10: Concrete tension damage - longitudinal crack

A very small reinforcement mesh (Q 131) is leading to a reduction of the maximum load. Analysing the results of the numerical simulation in detail, the appearance of a longitudinal crack at the edge of the upper flange, progressing with increasing load along the steel section could be identified, Figure 5.4.2.10.

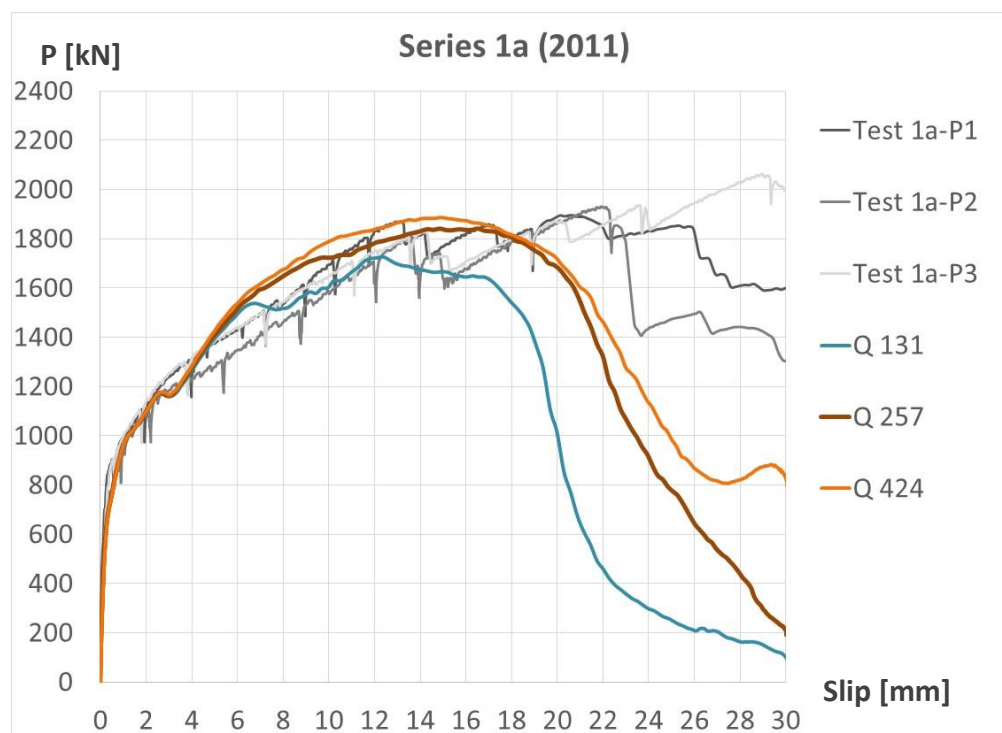


Figure 5.4.2.11: Influence of reinforcement mesh above the upper flange

The Q 424 had only a minor influence on the load-bearing behaviour, Figure 5.4.2.11. This indicates that the certain minimum of reinforcement mesh is necessary and further increase of the ration has no more influence.

Influence of contact definition for the dowel reinforcement

The numerical simulation of the load-bearing behaviour up to failure of the dowel reinforcement requires the development of a numerical model, allowing for an adequate simulation of the local behaviour of the dowel reinforcement in the web-opening and next to it. Therefore, the contact definition between the dowel reinforcement and the surrounding concrete was varied, results are given in Figure 5.4.2.13. For the description of different forms of contact, as “Tie”, “Friction” and “Rough” it is referred to [Abaqus]. Besides different contact definitions for the total length of the dowel reinforcement were analysed, here only the definition of contact in the zone of the chamber of the steel section is given, Figure 5.4.2.12.

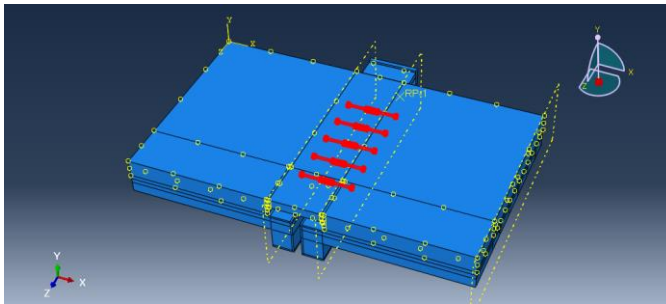


Figure 5.4.2.12: Variation of contact between dowel bar and concrete

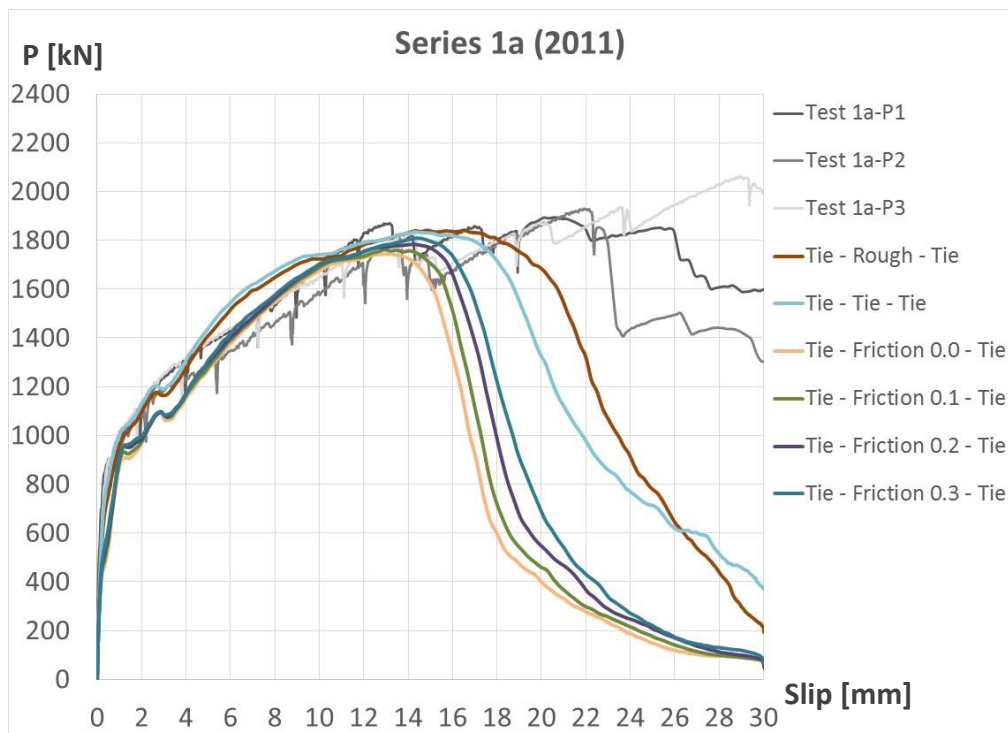


Figure 5.4.2.13: Influence of contact definition for dowel reinforcement

The contact type has an influence not only on the load-slip, but also on the deformation shape, development and position of plastic hinges and development of internal forces. The tie connection outside of the chamber has been justified by the results obtained from the measurement of the strain gauges.

5.5 Simulation of Test Series 1b

The set of input parameters developed based on the numerical simulation of Series 1a, see section 5.4, has been applied to simulate the push-out tests Series 1b. This Series has a higher concrete compression strength, f_{cm} . It has been also expected that the global friction factor might need to be modified. As explained earlier the friction remains test related and different values of friction were used to identify to most appropriate. Figure 5.5.1 shows results for friction factor 0.0 (= frictionless) and 0.1. Geometrical parameters for Series 1b is given in Table 5.5.

Table 5.5: Geometry of push-out Series 1b

Series	t_w [mm]	\varnothing_o web- opening [mm]	d, diameter dowel bar [mm]	f_{cm} [MPa]
1b	15.5	40	12	55.1

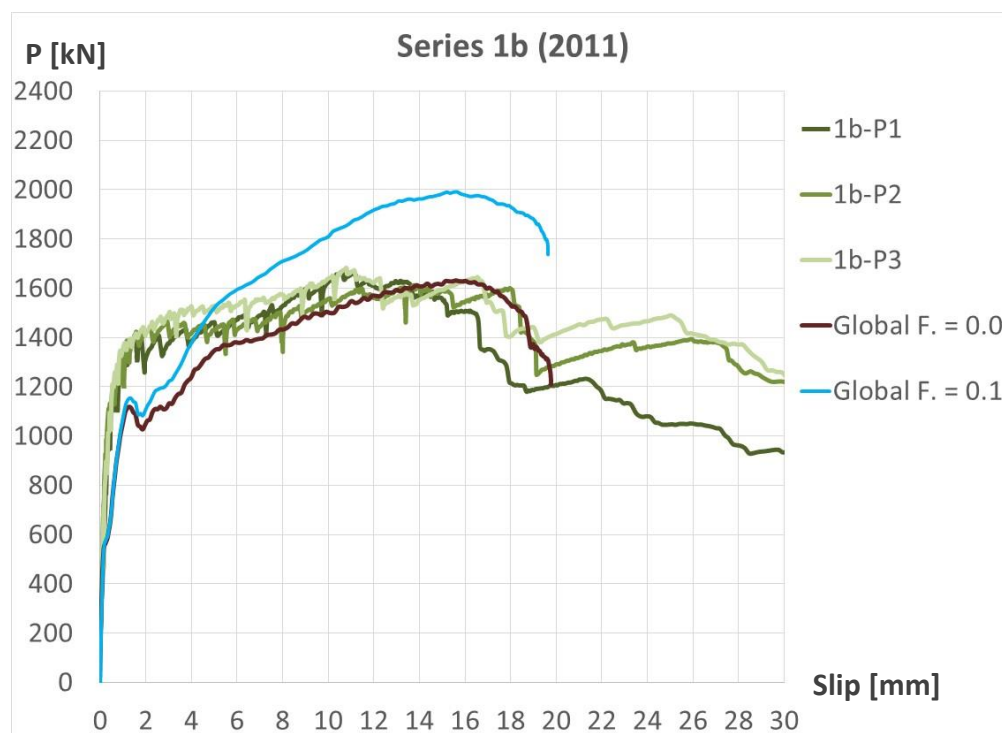


Figure 5.5.1: Simulation of Series 1b, Variation of global friction

Comparing the results obtained by numerical simulation with the test results, the configuration “frictionless” seems to be more adequate to simulate Series 1b. It was also found that the concrete stiffness degrades at a too low load level – at around 1000 kN, the concrete compression damage starts too early.

The concrete in the chamber and especially in the web-opening is restrained by the concrete slab and the steel section. Therefore, concrete confinement approach was applied, Section 5.3.5.5. The definition of a stress-strain relationship of confined concrete depends on various parameters, where the lateral pressure f_l is most representative.

Selected numerical results with different values of lateral pressure, given as the ratio f_l/f_{cm} are presented in Figure 5.5.2. The corresponding load-slip curves are presented in Figure 5.5.3.

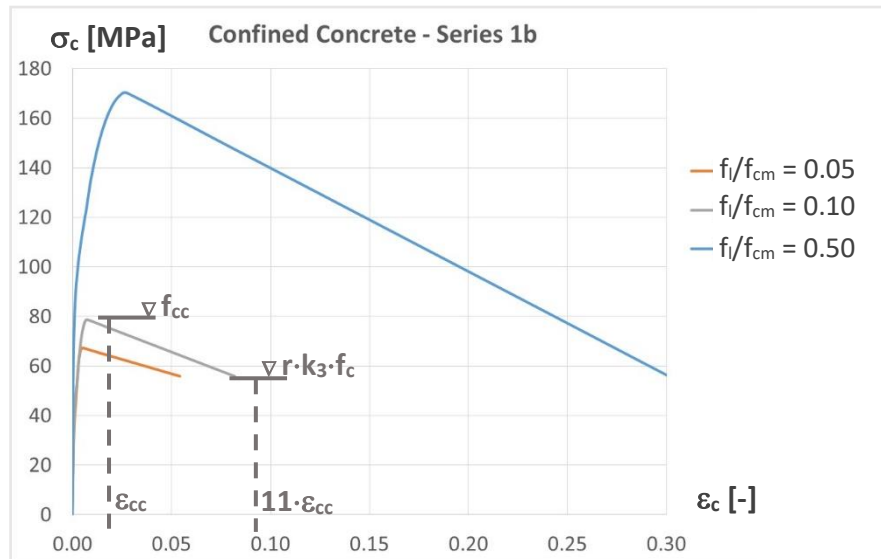


Figure 5.5.2: Stress-strain relationship for concrete confinement

In addition, a zone of confined concrete had to be defined. The author decided to analyse two possible zones of concrete confinement: 1) confinement only in the web-opening, 2) confinement in the whole chamber of the steel section.

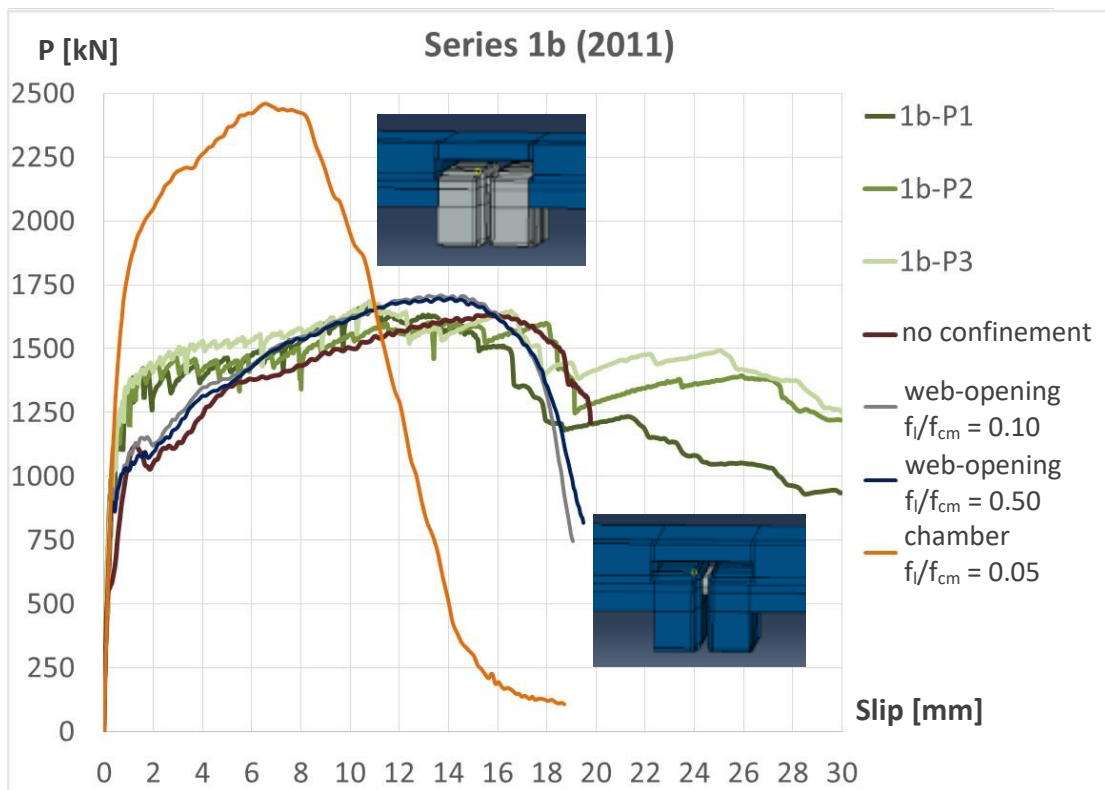


Figure 5.5.3: Influence of concrete confinement, Series 1b

Concrete confinement in the web-opening has little influence on the load-bearing behaviour, which is related to the small volume of concrete in the web-opening. Applying concrete confinement in the whole chamber of the steel section leads to a huge increase of the maximum load even for very small values of lateral pressure. Because of the difficulty to define the zone of confined concrete and the sensitivity of the results to this zone, the author decided not to apply concrete confinement at all in the further analysis and to propose a different approach.

A method, which has been already presented by the author in [ES2017] with an extended “compression-plateau” of the stress-strain relationship of the concrete is applied. The idea behind is the following: concrete subjected to compression stresses is crushed, material is pushed into the pores of the concrete matrix first, before failure of this concrete matrix happens by breaking the connection between the cement and the stones, which is a quasi-ductile behaviour. In relation to the CoSFB-Dowels the concrete slab provides a flexible restrain of the concrete in and next to the web-opening. The expansion of this restrained concrete in a direction perpendicular to the principal direction of the compression stress is fully blocked by the flanges of the steel section and partially by the concrete slab. This partial restrain allows for expansion of the concrete but, compared to the standard uniaxial compression test of concrete, at the same load level the deformation is much smaller. The concrete behaves more ductile than the observed behaviour of a uniaxial compression test. Therefore, numerical simulations are performed by applying an “extended-plateau”. The length of the plateau was simply derived by $\epsilon_{\text{plateau}} = n \times \epsilon_{c1}$. The factor n was varied and the numerically obtained results compared to test results. The applied stress-strain relationships of concrete with extended-plateau are given in Figure 5.5.4, corresponding load-slip curves are given in Figure 5.5.5.

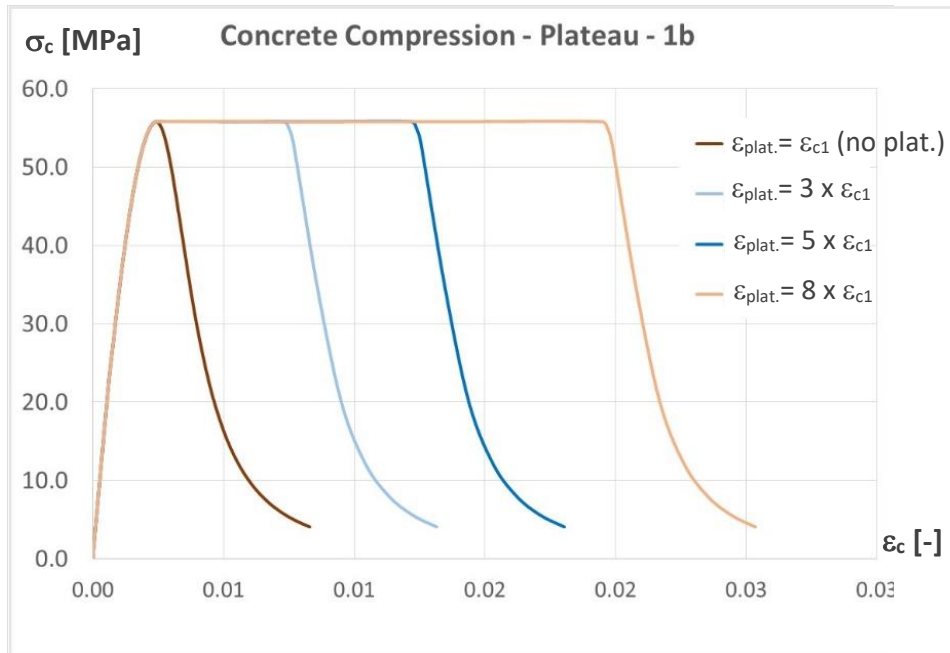


Figure 5.5.4: Concrete compression model with extended-plateau

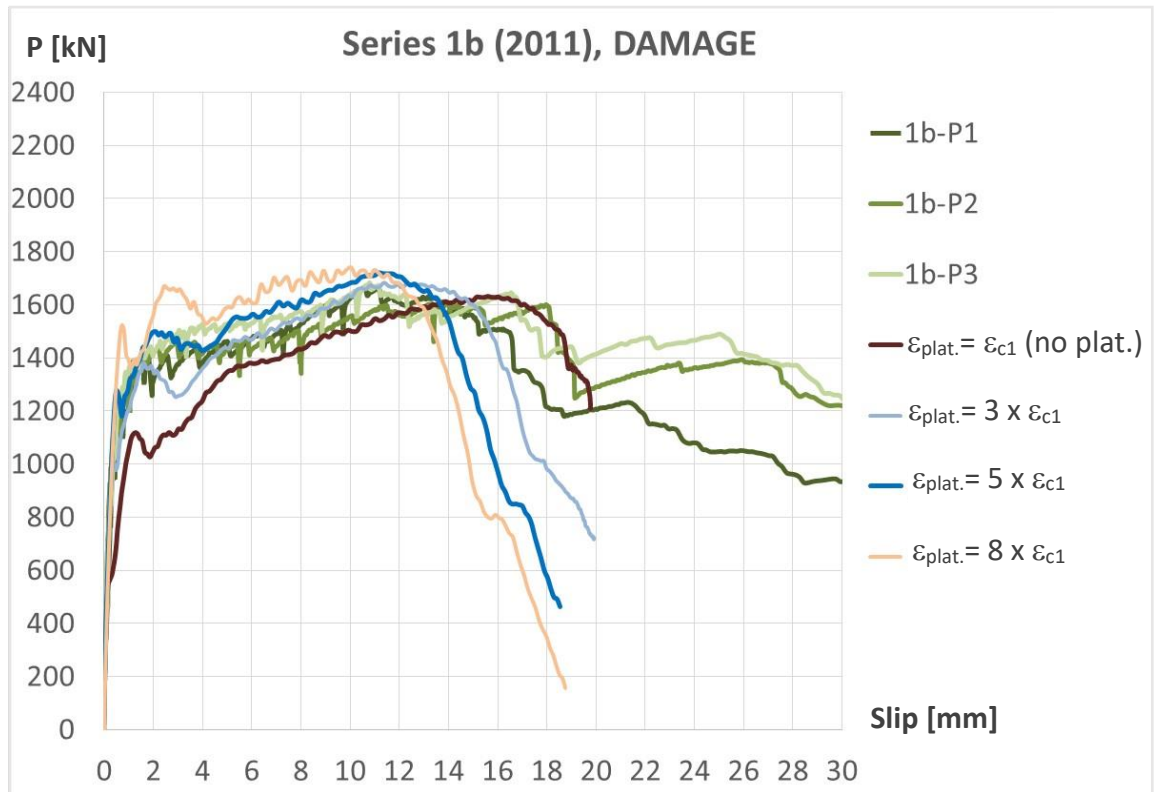


Figure 5.5.5: Influence of extended-plateau, Series 1b

An extension of the concrete compression plateau in the range $3 \times \epsilon_{c1} \leq \epsilon_{\text{plateau}} \leq 5 \times \epsilon_{c1}$ seems to be most adequate to simulate the performed push-out tests. This approach is leading to promising results. However, further validation should be done in relation to the plateau when more test results are available.

5.6 Simulation of Test Series 2-1a and 2-1b

The geometry of Series 2-1a and 2-1b differ from previously analysed Series 1a and 1b by web thickness of the steel section, which is $t_w = 7.5\text{mm}$ while for the other tests it was $t_w = 15.5\text{mm}$, Table 5.6. Results are presented in Figures 5.6.1 and 5.6.2.

Table 5.6: Geometry of push-out Series 2-1a and 2-1b

Series	t_w [mm]	\varnothing_o web-opening [mm]	d, diameter dowel bar [mm]	f_{cm} [MPa]
2-1a	7.5	40	12	29.5
2-1b	7.5	40	12	58.2

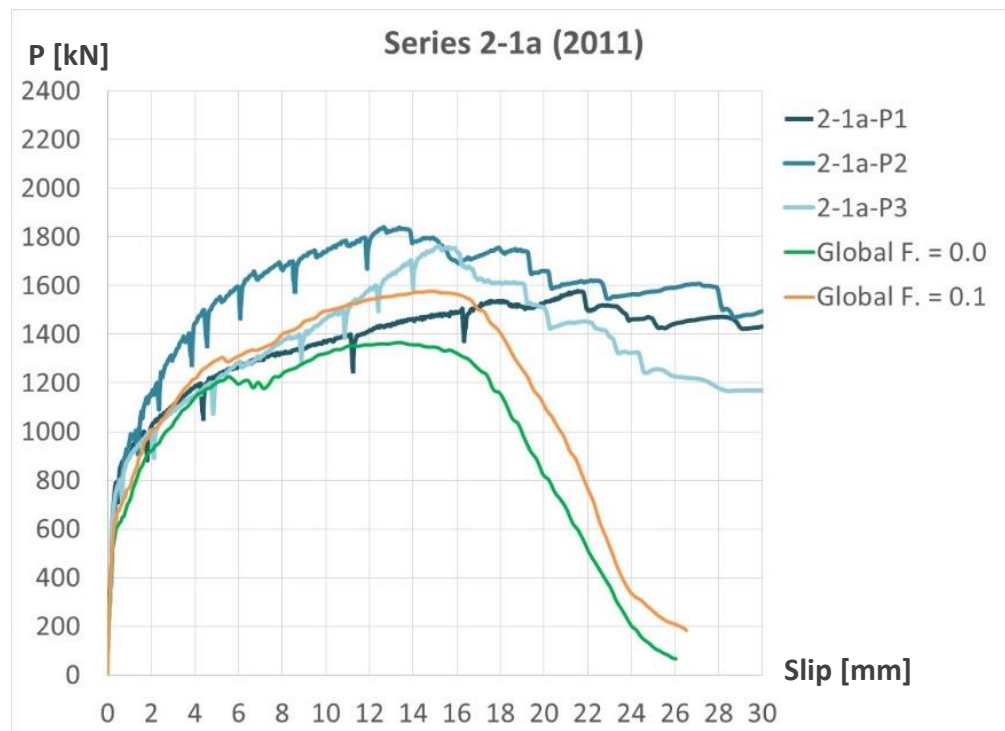


Figure 5.6.1: Simulation of Series 2-1a

As for simulation of Series 1a, also for Series 2-1a a factor 0.1 for global friction is applied to reproduce the test results adequately. It can be observed that the test results for this Series differ for each push-out more than for the previous Series. The results of the simulation fit well within the range obtained from the tests.

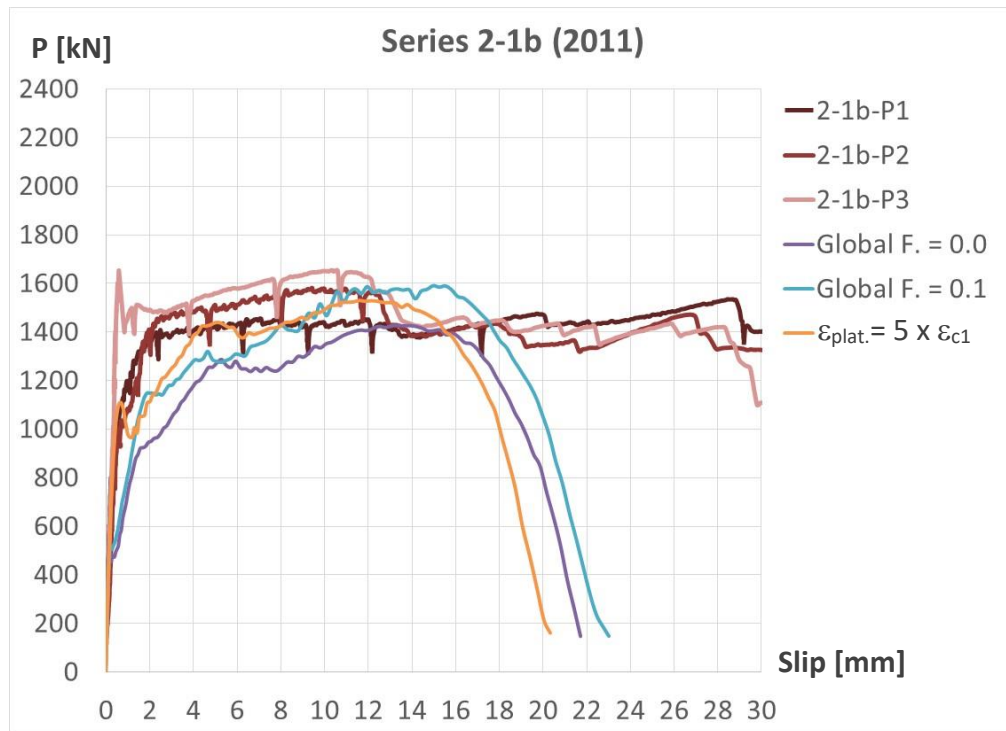


Figure 5.6.2: Simulation of Series 2-1b

Similar as for the simulation of Series 1b, where the concrete compression class was higher, concrete confinement or the extension of the plateau may lead to a better simulation of the test results.

5.7 Simulation of Test Series 2-2a

The push-out test Series 2-2a was performed with a reduced diameter of the web-opening of 25mm instead of 40mm, Table 5.7. Results are given in Figure 5.7.

Table 5.7: Geometry of push-out Series 2-2a

Series	t_w [mm]	\varnothing_o web-opening [mm]	d, diameter dowel bar [mm]	f_{cm} [MPa]
2-2a	15.5	25	12	32.7

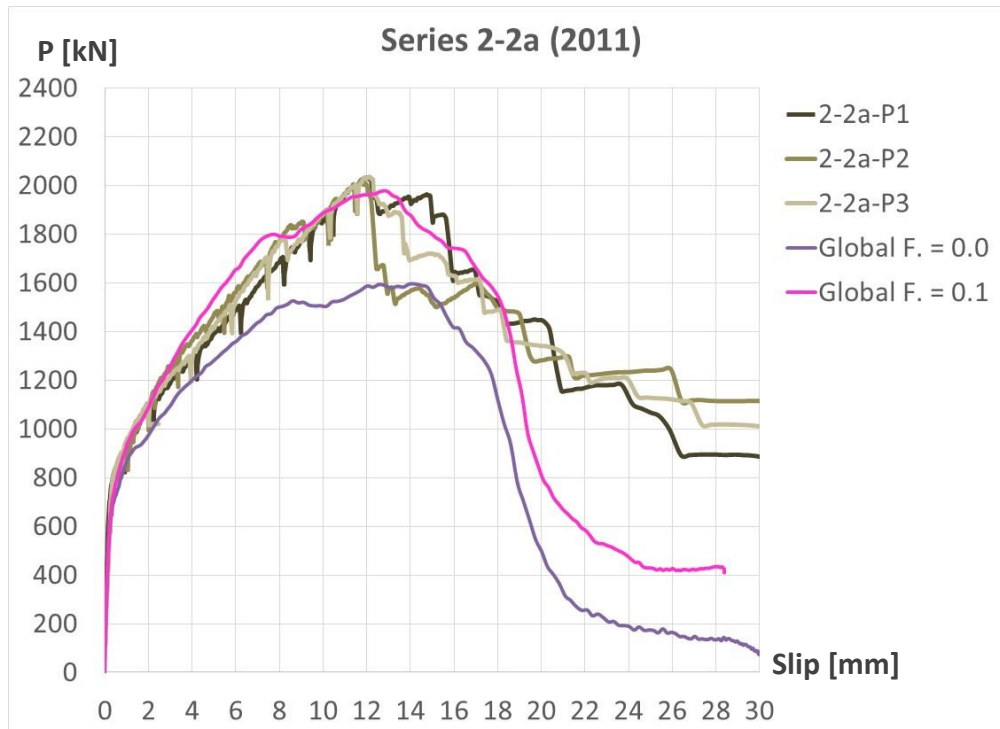


Figure 5.7: Simulation of Series 2-2a

The input parameters derived by detailed analysis of Series 1a are adequate to simulate the test Series 2-2a. As for simulation of Series 1a, the factor for “Global Friction” should be set to a value of 0.1. It should be taken into account, that a larger variation of the web-opening may need adaptation of the numerical model.

5.8 Simulation of Test Series 2-2b

The simulation of the Series 2-2b with a diameter of the dowel reinforcement of 25mm (Table 5.8), for two different friction factors for “Global Friction” between the steel section and the concrete, is presented in Figure 5.8.

Table 5.8: Geometry of push-out Series 2-2b

Series	t_w [mm]	\varnothing_o web-opening [mm]	d, diameter dowel bar [mm]	f_{cm} [MPa]
2-2b	15.5	40	25	40.0

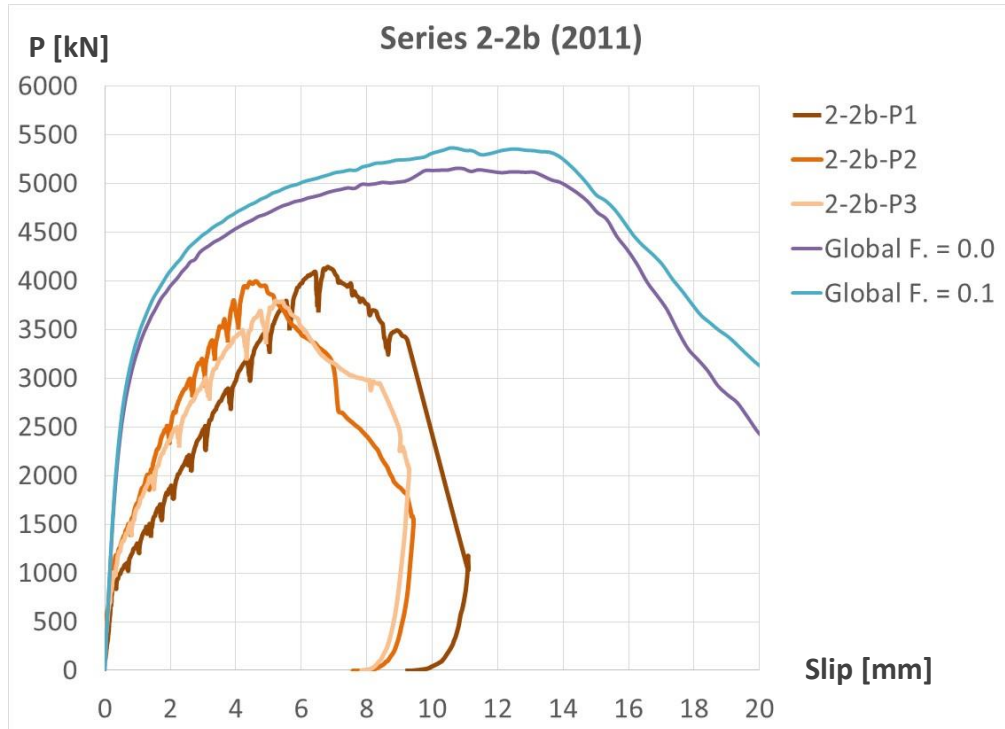


Figure 5.8: Simulation of Series 2-2b

Application of the set of input parameters derived by the analysis presented as defined earlier was not proper to reproduce the load-bearing behaviour and the failure mode of this test. This can be explained by the fact, that no detailed test data was available to define damage models of the rebar diameter 25mm. Instead, a data for the ductile and shear damage obtained from test of bar diameter 12mm was applied. The tests of bar diameter 12mm has been presented in Section 3.4. It is expected that the larger is the diameter of the bar the less ductile it is. Investigation of the damage parameters is necessary to correctly develop a model.

5.9 Simulation of Test Series 2-3

Test Series 2-3 was performed with Silicone infill in the web-openings instead of concrete. In the numerical simulation the Silicone infill was simply simulated by a very soft material, represented by a bi-linear stress-strain relationship with a young modulus of $E_{\text{soft}} = 1000 \text{ MPa}$ and plastic stress $\sigma_{u,\text{soft}} = 10 \text{ MPa}$. The influence of friction between steel profile and concrete (“Global Friction”) was analysed by performing several numerical simulations with varied friction factor. Two results of those simulations are presented in Figure 5.9. Geometry is given in Table 5.9.

Table 5.9: Geometry of push-out Series 2-3

Series	t_w [mm]	\varnothing_o web-opening [mm]	d, diameter dowel bar [mm]	f_{cm} [MPa]
2-3	15.5	25	12	38.3

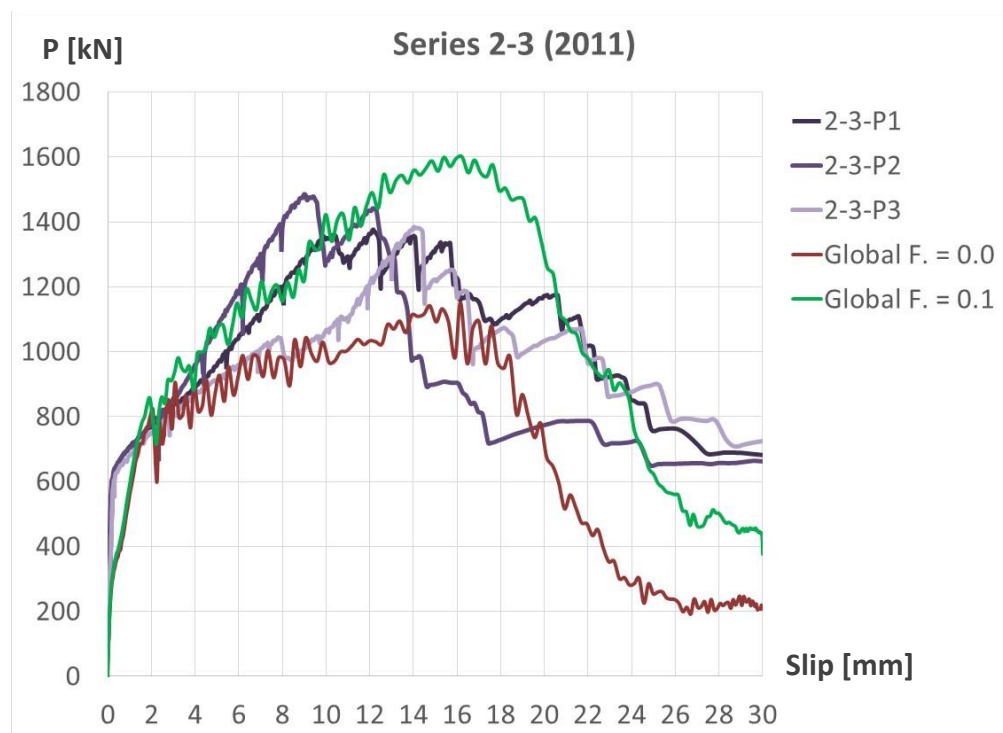


Figure 5.9: Simulation of Series 2-3

5.10 Conclusions from Numerical Simulation

Many different simulations have been performed to analyse an influence of various parameters on the behaviour of CoSFB-Dowel and to gain confidence in the developed model to correctly reproduce the experimental tests. The results of the simulation allow to extract more detailed information related to the development of forces, deformation and failure mechanism. An activation of the dowel reinforcement is of significant interest for this research.

To identify this activation, the shear force V in direction of the acting load P and the corresponding bending moment M are given in Figure 5.10.2. The forces were extracted from the results of the numerical simulation for Series 1a, the simulation was performed with the input parameters presented in Section 5.4. The forces are taken from the integration of principal stress of the cross sectional area of the dowel reinforcement bar (= Slices) at certain positions along the dowel reinforcement. To identify the evolution of these forces, they are printed at different time steps of the simulation, which corresponds to different values of the slip, Figure 5.10.1.

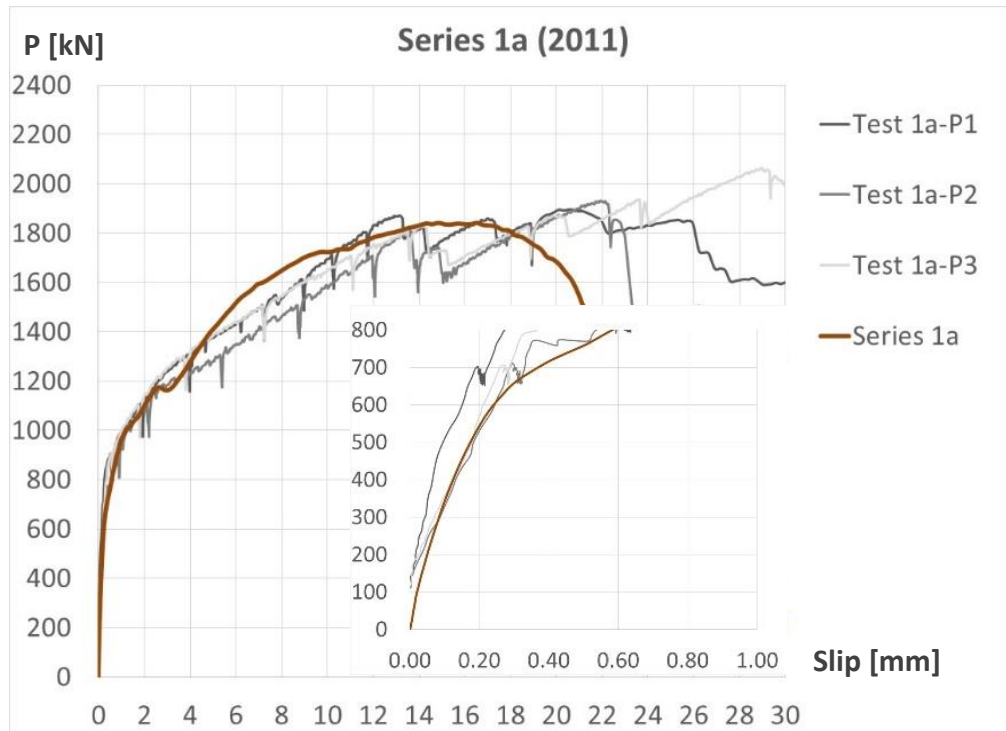


Figure 5.10.1: Simulation of Series 1a, Conclusion

The forces are presented for the dowel bar positioned in the middle of the specimen, level 3, cf. Figure 3.2.2.2.

Dowel reinforcement with Position of Slices:

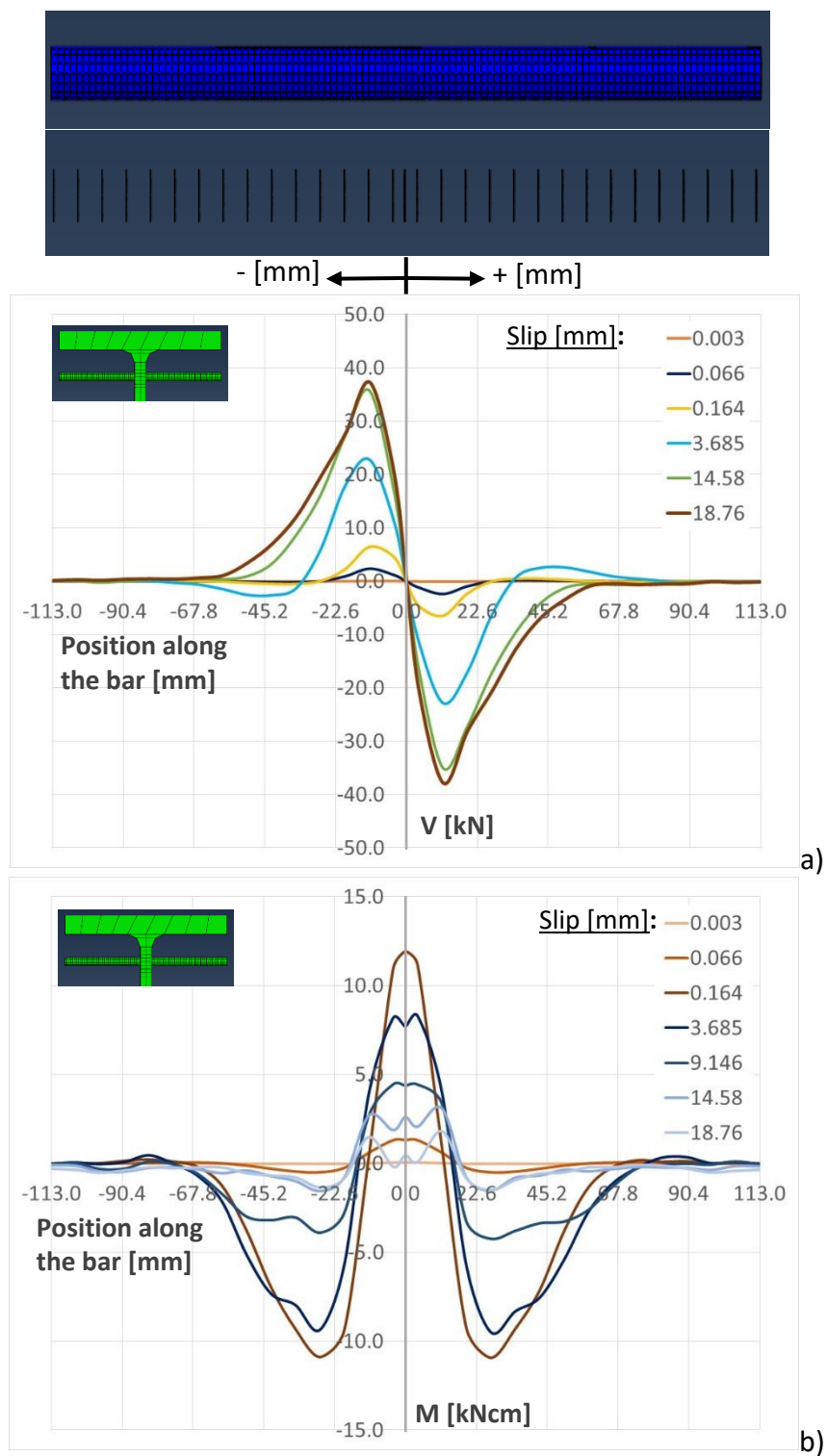


Figure 5.10.2: Forces Dowel Reinforcement: a) Shear Force b) Bending Moment

From the Figure 5.10.2a it can be observed that the shear force in the dowel reinforcement is increasing with increasing slip and corresponding increase of the load P . It is of interest that the position of the maximum shear force along the dowel bar is at the point of zero bending moment and is not varying for increasing load P . Failure of the dowel reinforcement in the simulation corresponds to the slip value, when the maximum shear force in the dowel bar is reached.

In Figure 5.10.2b it is shown, that the bending moment is increasing very quickly and reaches the maximum at small slip values already. At increasing slip, the position of zero bending moment and its maximum is not changing, while, after the maximum moment is reached, the bending moment is reducing progressively. In addition, the development of tension forces along the dowel reinforcement for increasing slip is presented, Figure 5.10.3. With increasing slip, the activation of the dowel bar on tension develops, reaching its maximum when the maximum load P is reached. After failure of the bar the tension force is reducing.

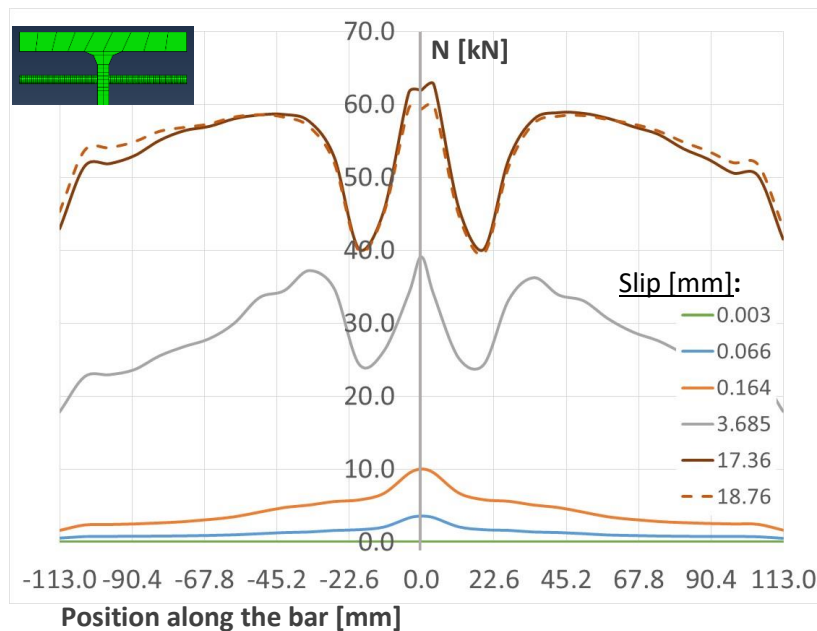


Figure 5.10.3: Tension Forces Dowel Reinforcement

Analysing the tension force it should be noted, that the numerically obtained distribution of this force along the dowel bar depends strongly on the definition of the contact between the bar and the surrounding concrete and the transfer of bond stresses. In the numerical simulation a constant contact was defined as "Rough", while in the performed push-out tests bond stresses might evolve and even reduce with increasing slip.

In Figure 5.10.4 the activation of the dowel reinforcement in respect to shear and bending versus slip is shown. The evolution of shear is presented at a distance of 11.7 mm from the axis of symmetry and the evolution of bending moment at a distance of 0mm (= Position at the axis of symmetry) and at 27.3mm from axis of symmetry, Figure 5.10.2. With increasing slip s , the shear force in the bar is increasing, while the bending moment is initially rapidly increasing at relatively small slip up to its maximum and then decreasing slowly.

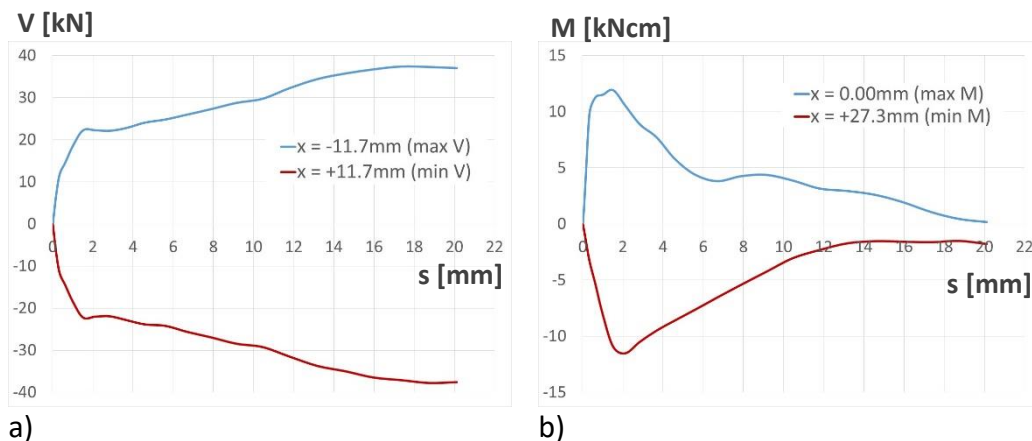


Figure 5.10.4: Evolution of Forces in the dowel bar: a) Shear b) Bending Moment

Finally, the development of the stresses in the dowel reinforcement bar for the bar in middle position of the specimen (Figure 5.10.5) and the development of damage is presented, Table 5.10.1 and Table 5.10.2.

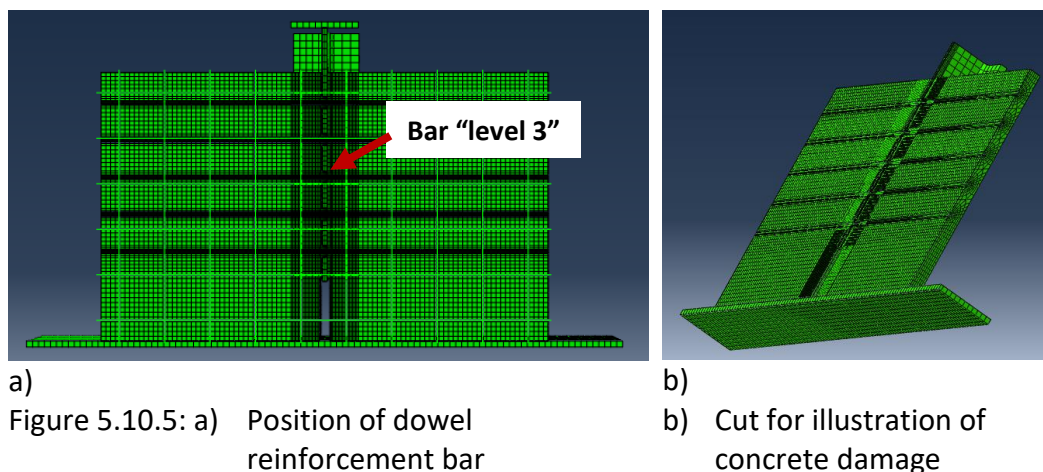
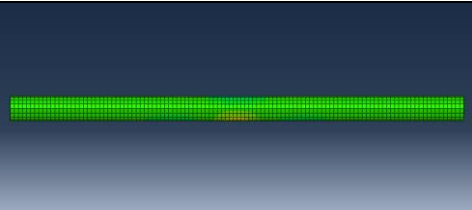
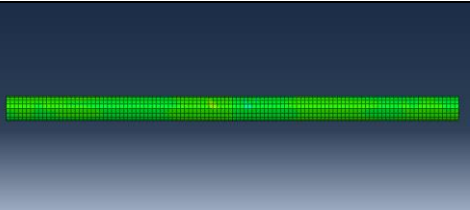
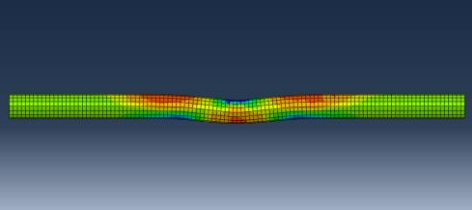
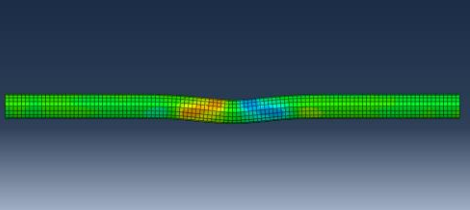
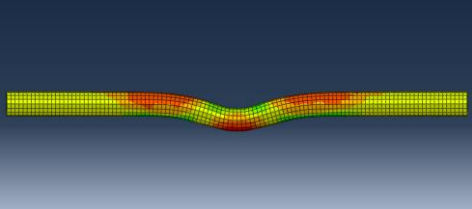
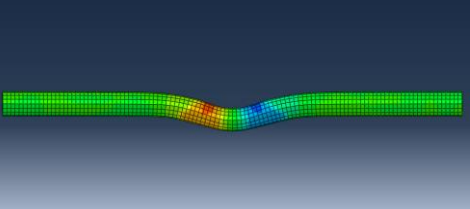
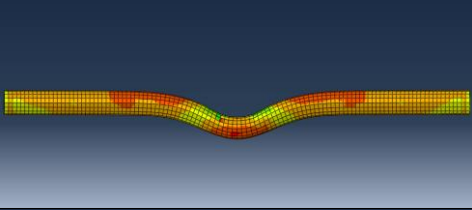
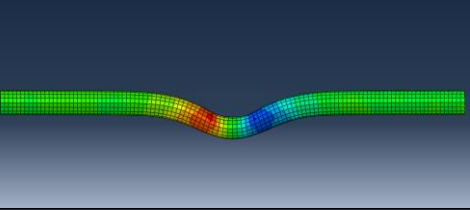
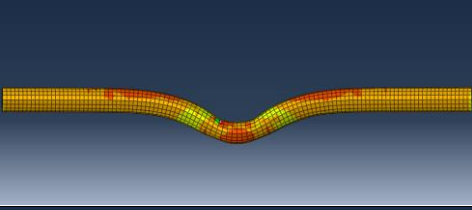
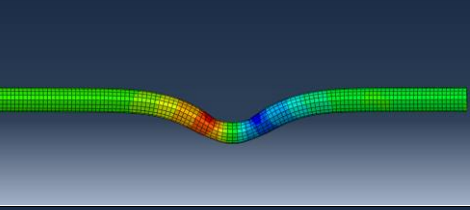
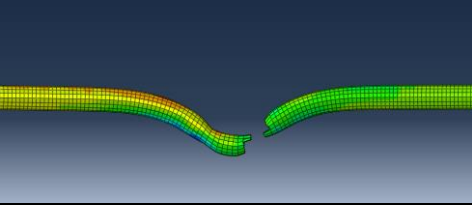
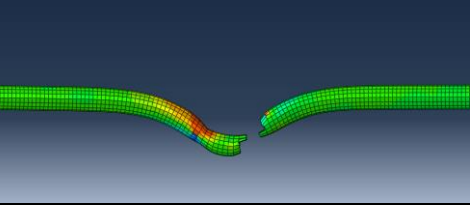


Figure 5.10.5: a) Position of dowel reinforcement bar b) Cut for illustration of concrete damage

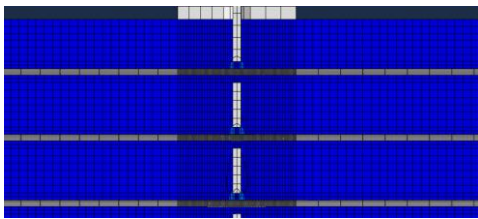
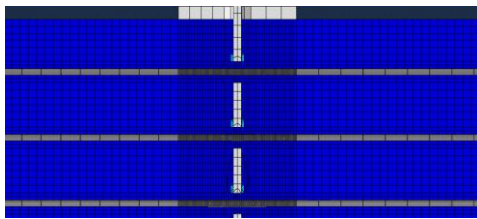
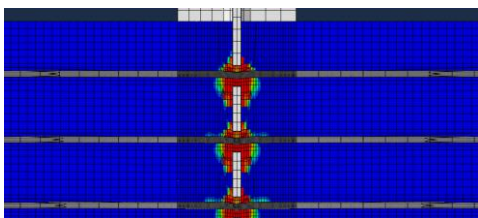
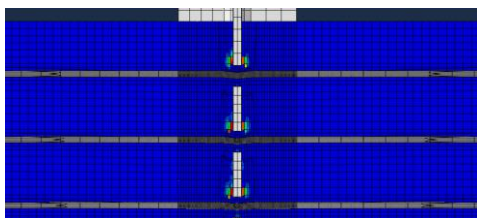
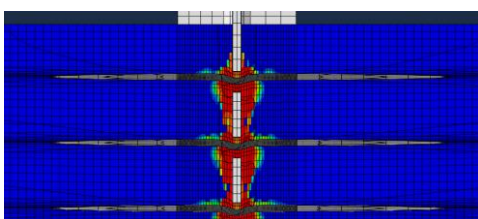
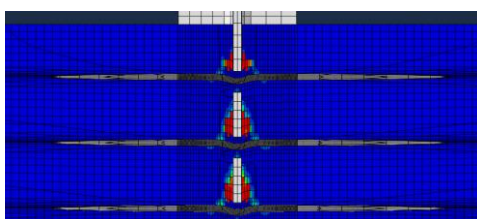
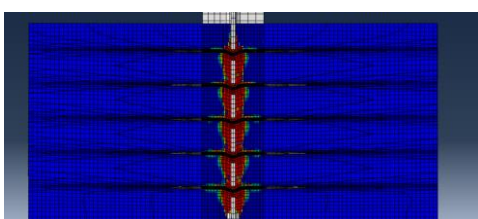
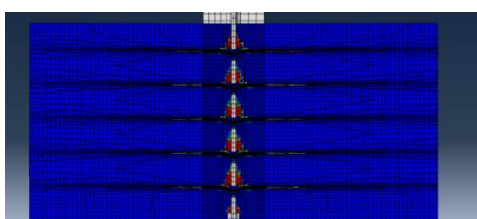
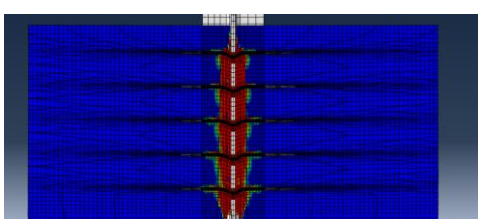
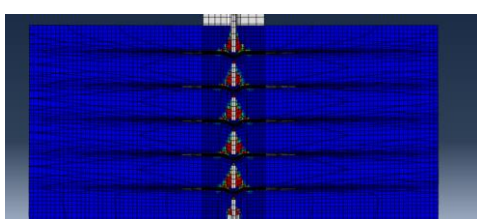
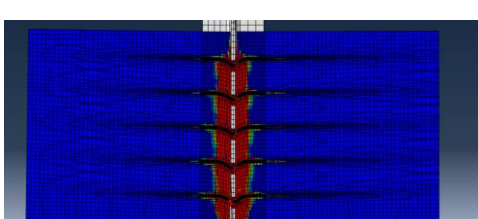
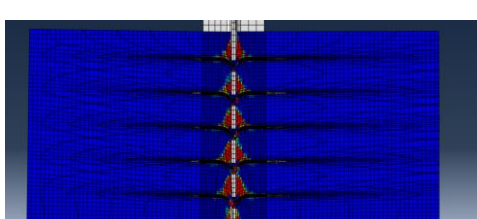
The qualitative development of stresses are given for the part of the dowel reinforcement in the chamber of the steel section. The stresses are given in relation to global coordinates, the deformation of the axis of the dowel reinforcement is considered. Axial stresses σ_{11} and shear stresses σ_{13} are given in Table 5.10.1.

Table 5.10.1: Stress development in dowel reinforcement

Slip [mm]	σ_{11} (in longitudinal bar-direction)	σ_{13} (in the direction of the load P)
0.164		
3.685		
9.146		
14.58		
18.76		
26.02		

The evolution of the concrete damage is presented in Table 5.10.2. The damage is shown at the level of the axis of the dowel reinforcement, cf. Figure 5.10.5.

Table 5.10.2: Evolution of concrete compression and concrete tension damage

Slip [mm]	Compression Damage	Tension Damage
0.164		
3.685		
9.146		
14.58		
18.76		
26.02		

6 Formulation of the Load-Bearing Capacity, P_{max}

6.1 Introduction

In this Chapter the load-bearing capacity of a CoSFB-Dowel is formulated by a simplified analytical approach. It has been identified that the load-bearing capacity, the maximum load P_{max} , is composed by two main components: a concrete component P_{lin} and dowel action P_{Dowel} (= activation of the dowel reinforcement bar). In addition, friction forces P_f may develop and contribute to the maximum load.

The analysis of the push-out tests in combination with the findings obtained by numerical simulation, led to the following explanation of the load-bearing behaviour of CoSFB-Dowels: Up to a value of P_{lin} , the acting load is transferred mainly by the concrete. This is explained by the large volume, strength and stiffness of the concrete in relation to the relatively small stiffness of the dowel reinforcement bar, cf. Chapter 4. At the level of P_{lin} the strength and stiffness of the concrete in the web-opening starts to degrade, which is numerically simulated by damage. Consequently, an activation of the dowel reinforcement starts and increasing the load P further to values above P_{lin} , shear forces in the dowel reinforcement increase. Is the local concrete strength towards the shear capacity of the dowel reinforcement bar relatively small, the bar is able to crush the concrete underneath and is creating a space, which allows the axis of the bar to deform [ES2014]. A mechanism of plastic hinges in the bar develops and the reinforcement bar is activated in tension. This mechanism is related to locally large deformations of the dowel bar and friction forces may develop in addition. Failure occurs when the maximum elongation of the material of the reinforcement bar is exceeded. Is the shear capacity of the dowel reinforcement small in relation to the local concrete compression strength, the above described mechanism cannot develop and the dowel action P_{Dowel} is determined by the shear capacity of the dowel reinforcement only. This behaviour is linked to locally small deformations and no friction is activated.

Based on these findings the load-bearing capacity can be expressed by the following equation:

$$P_{max} = P_{lin} + P_{Dowel}(+P_f) \quad (6.1)$$

The described load-bearing mechanism is determined by 3-dimensional non-linear material behaviour and interactions between concrete and reinforcement bar. This highly non-linear and complex behaviour of CoSFB-Dowels is formulated in the following by a simplified 2-dimensional analytical approach.

6.2 Concrete Component, P_{lin}

As already given in Chapter 4.2, the load level of P_{lin} is mainly determined by the concrete and its compression strength, f_{cm} . Therefore, P_{lin} can be interpreted as a “concrete component” participating on the total load bearing capacity of CoSFB-Dowels. In order to determine an analytical formulation for P_{lin} , the standard method of the statistical measure by the coefficient of determination is applied, Figure 6.2.1.

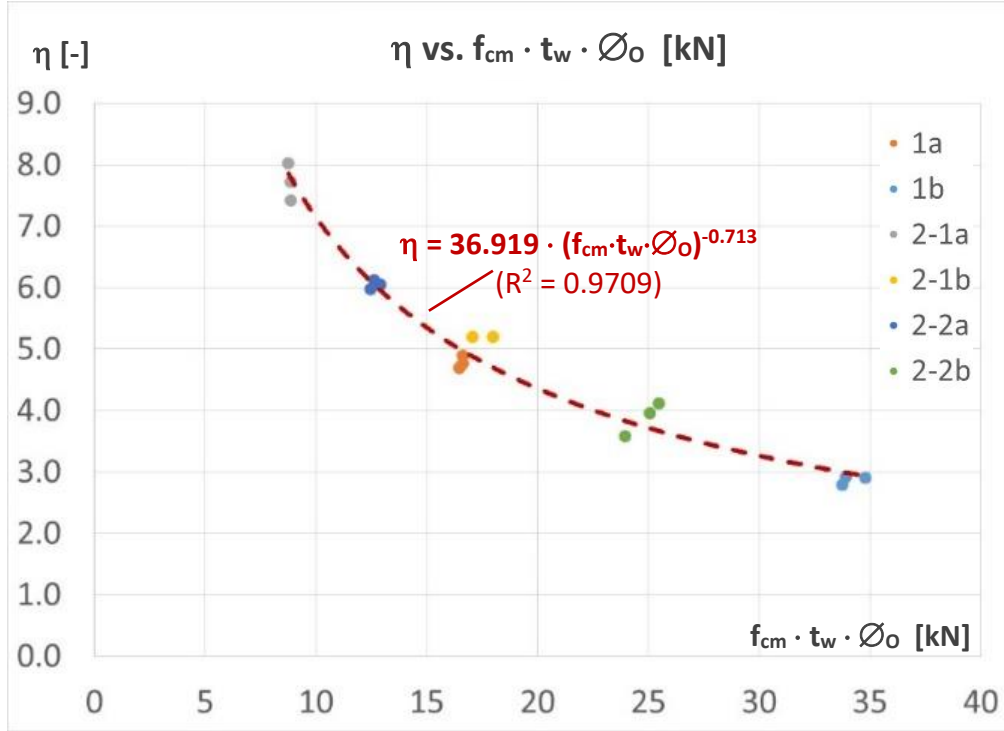


Figure 6.2.1: Correlation of experimental values of $P_{e,lin}$ versus $f_{cm} \cdot t_w \cdot \varnothing_O$

Different possible correlations for P_{lin} were investigated, leading to a semi-empirical Equation for the contribution of the concrete, $P_{t,lin}$:

$$P_{t,lin} = \eta \cdot f_{cm} \cdot t_w \cdot \varnothing_{opening}$$

With $\eta = 36.919 \cdot (f_{cm} \cdot t_w \cdot \varnothing_O)^{-0.713}$, which was derived from the coefficient of determination. The unit of the term $f_{cm} \cdot t_w \cdot \varnothing_O$ has to be in [kN].

Finally the following formulation for $P_{t,linear}$ is obtained:

$$P_{t,lin} = 36.919 \cdot (f_{cm} \cdot t_w \cdot \varnothing_O)^{0.287} \quad (6.2)$$

In the formulation of η , the test Series 2-3 was not taken into account. Further, the result of test 2-1a-P3 was not considered, because this result is not representative for the given configuration, see Figure B2.4 in Annex B2. Comparing the results of test Series 1a with Series 2-2b no influence of the dowel reinforcement on $P_{e,lin}$ could be found. This might be subject of further investigations.

The accuracy of Equation 6.2 in comparison to the test results is given in Figure 6.2.2.

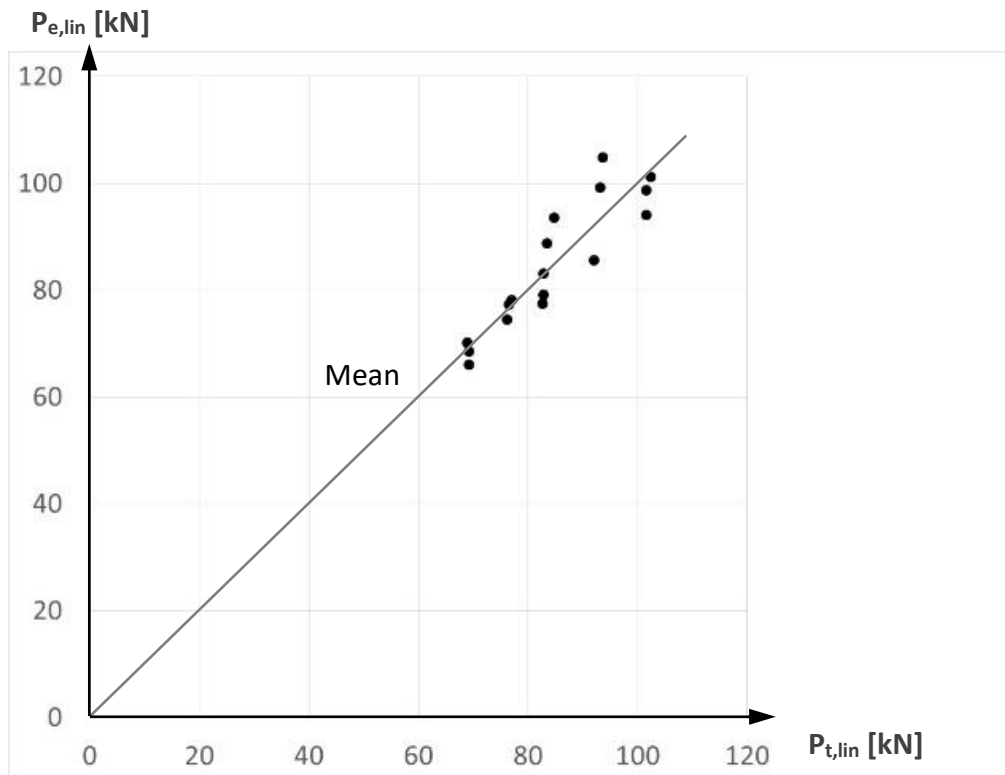


Figure 6.2.2: Comparison of P_e and P_t according to Equation 6.2

6.3 Dowel Action, P_{Dowel}

The load-bearing capacity of the concrete in the web-opening is reached at P_{lin} . Increasing the load further, concrete softening develops and additional load is transferred by the dowel reinforcement. This activation of the dowel reinforcement is further referred to as dowel action. The development of an analytical formulation of the load-bearing capacity of the dowel is based on the assumption that a mechanism of three plastic hinges in the dowel reinforcement develops, Figure 6.3.1.

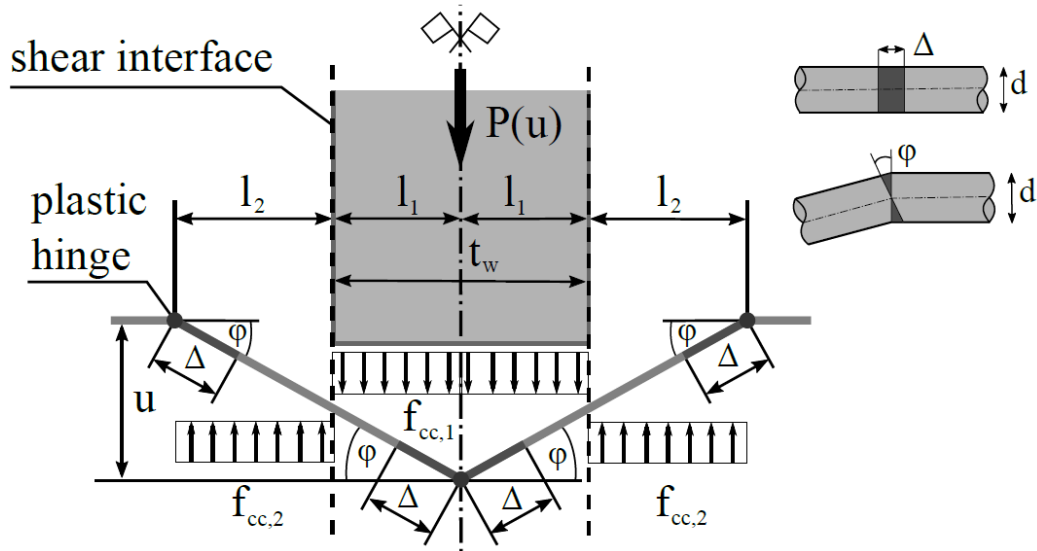


Figure 6.3.1: Development of a mechanism in the dowel reinforcement

Aim of the presented analytical approach is the determination of the limit state, to identify the maximum load the dowel reinforcement can transfer. The limit state is defined either by reaching the deformation capacity of the dowel bar or by reaching the cross-section capacity on shear before the mechanism can develop. As initial stage the dowel bar is still undeformed and is subjected simultaneously to shear and tension, with the maximum shear force at the interface, Figure 6.3.2. It is assumed that the capacity of the bar on bending is reached, the plastic hinges are fully developed ($M = M_{pl}$). The bar is still not subjected to tension ($N = 0$). The concrete bearing strength has reached its maximum under the bar, having a constant, plastic value. To account for the strength increase of the concrete due to triaxial stress state and due to local loading, the uniaxial compression strength is increased by an enhancement factor c , which also allows to distinguish between the concrete in the web-opening and next to it. In case the concrete compression strength under the bar is larger than the shear capacity of the dowel reinforcement the initial shear force, V_{ini} , is larger than the shear capacity of the bar, V_{pl} . The mechanism cannot develop and the bar fails on shear. Thus, the bar is not able to significantly crush the concrete underneath, the dowel axis remains straight and no tension is activated in the bar.

With increasing deformation of the bar and softening of the concrete, the shear force in the bar is reducing, Figure 6.3.3. This happens, when the dowel bar is able to crush the concrete underneath, the dowel axis can deform and a mechanism of three plastic hinges develops, Figure 6.3.1. The deformation of the axis of the dowel bar is enlarging with further increase of the load. Tension force develops in the bar, while the shear force is simultaneously decreasing leading to a higher maximum load.

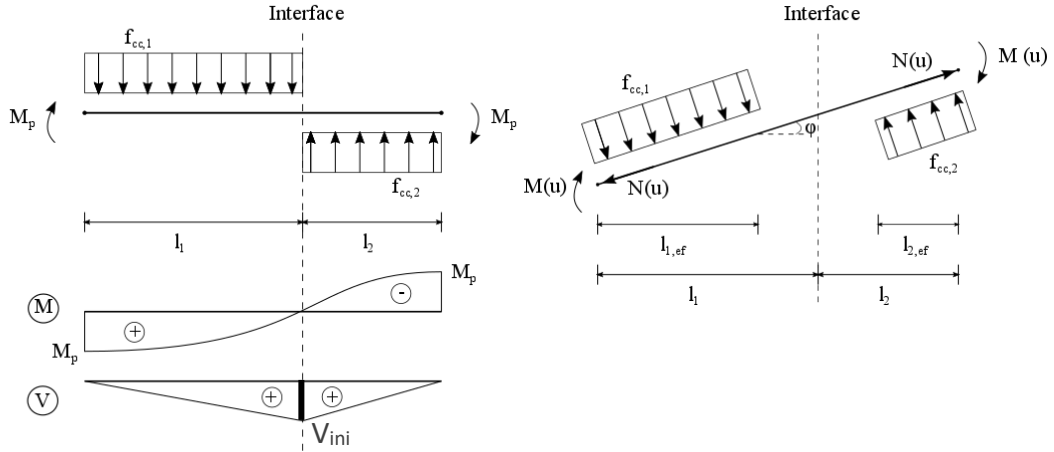


Figure 6.3.2: Undeformed state and distribution of moment and shear Figure 6.3.3: Deformed state with distribution of contact pressure

The limit state is reached, either when the deformation capacity of the dowel bar or the cross-section capacity on shear is reached. To calculate the maximum load P_{Dowel} , the load-displacement response $P(u)$ has to be derived as a function of the displacement u .

Cross-section Capacity for Shear and Tension

The yield condition for a circular cross section subjected to shear and tension forces is given by:

$$f(V, N) = \frac{V}{V_{pl}} + \frac{N}{N_{pl}} - 1 = 0 \quad (6.3)$$

with:

$$V_{pl} = \pi \cdot \frac{d^2}{4} \cdot \frac{f_u}{\sqrt{3}}$$

$$N_{pl} = \pi \cdot \frac{d^2}{4} \cdot f_u$$

f_u = ultimate strength of the dowel reinforcement.

Development of a Mechanism

The load transferred by dowel action P_{Dowel} is formulated as a function of the vertical displacement u . It is based on the assumption of a plastic mechanism with three plastic hinges, cf. Figure 6.3.1. With increasing displacement u , tension forces in the dowel reinforcement gradually develop, until the dowel is subjected to tension only. A state of pure catenary action can be reached, if the dowel material provides sufficient ductility. The non-linear behaviour of the dowel is described by second order plasticity, as formulated by Sorensen for two sided joints, cf. Chapter 2 and [Sor2017].

As described already before, the mechanism can only develop in case the bar provides sufficient shear capacity. Further, at the initial stage the shear capacity of the bar is not reached and the bar is able to crush the concrete underneath to cut its way through.

Rigid-plastic material is assumed for concrete and reinforcement bar, displacements are due to accumulated plastic deformations in the plastic hinges only. Their position depends on the bending capacity of the dowel reinforcement and the concrete compression strength. Assuming the position of the plastic hinges is not changing once they are created, the plastic hinges must undergo also elongations Δ in addition to their rotation φ . The rates of the plastic deformations are determined by establishing the kinematic relationship for the assumed mechanism. By imposing the normality condition of plastic theory and by applying the work Equation for increments of displacements, the load P is formulated as a function of the displacement u .

The hereafter given equations are fully based on the work already published by Sorensen [Sor2017], and adapted to CoSFB-Dowels where necessary.

Mechanism and kinematic relationships [Sor2017]

The relative shear displacement u , is considered as a monotonic function of time, the problem is treated as static displacement controlled and a displacement velocity equal to unity is assumed:

$$u(t) = t \quad (6.4)$$

The relationship between the displacement u and the rotation in the plastic hinges φ is given as:

$$\tan(\varphi) = \frac{u}{l_1 + l_2} \quad (6.5)$$

By assuming the elongation Δ is concentrated in the plastic hinges, the following relationship between u and Δ can be established:

$$\begin{aligned} u^2 + (l_1 + l_2)^2 &= (l_1 + l_2 + 2 \cdot \Delta)^2 \\ u^2 + (l_1 + l_2)^2 &= (l_1 + l_2)^2 + 4 \cdot \Delta \cdot (l_1 + l_2) + 4 \cdot \Delta^2 \\ u^2 &= 4 \cdot \Delta \cdot (l_1 + l_2) + 4 \cdot \Delta^2 \\ \Delta &= -\frac{l_1 + l_2}{2} + \frac{l_1 + l_2}{2} \cdot \sqrt{1 + \left(\frac{u}{l_1 + l_2}\right)^2} \end{aligned} \quad (6.6)$$

Hence, the rates of plastic deformations in the hinges can be as:

$$\dot{\varphi} = \frac{d\varphi}{dt} = \frac{d\varphi}{du} \frac{du}{dt} = \frac{l_1 + l_2}{(l_1 + l_2)^2 + u^2} \quad (6.7)$$

$$\dot{\Delta} = \frac{d\Delta}{dt} = \frac{d\Delta}{du} \frac{du}{dt} = \frac{u}{2 \cdot \sqrt{(l_1 + l_2)^2 + u^2}} \quad (6.8)$$

And the following kinematic condition of the bar can be established:

$$\frac{\dot{\Delta}}{\dot{\varphi}} = \frac{u}{2} \cdot \sqrt{1 + \left(\frac{u}{l_1 + l_2}\right)^2} \quad (6.9)$$

Constitutive relationships and section forces in the plastic hinges [Sor2017]

The capacity of the cross section on tension and shear are:

$$N_{pl} = \pi \cdot \frac{d^2}{4} \cdot f_u \quad (6.10)$$

$$M_{pl} = \frac{1}{6} \cdot d^3 \cdot f_u \quad (6.11)$$

f_u = ultimate strength of the dowel reinforcement.

Plastic deformations may initiate when the yield condition for axial tension and bending of the circular cross section is fulfilled. The yield condition can be formulated as (see Annex D for details):

$$f(M, N) = \frac{N}{N_{pl}} + \frac{2}{\pi} \cdot \left[\arcsin \left(\left(\frac{M}{M_{pl}} \right)^{1/3} \right) - \left(\frac{M}{M_{pl}} \right)^{1/3} \cdot \sqrt{1 - \left(\frac{M}{M_{pl}} \right)^{2/3}} \right] - 1 = 0 \quad (6.12)$$

According to the normality condition of plastic theory the rates of deformations must fulfill the following constitutive relationship:

$$\dot{\varphi} = \lambda \cdot \frac{df}{dM} = \lambda \cdot \frac{8}{\pi \cdot d^3 \cdot f_y} \cdot \frac{1}{\sqrt{1 - \left(\frac{M}{M_{pl}} \right)^{2/3}}} \quad (6.13)$$

$$\dot{\Delta} = \lambda \cdot \frac{df}{dN} = \lambda \cdot \frac{4}{\pi \cdot d^2 \cdot f_y} \quad (6.14)$$

where λ is a positive constant proportional to the displacement velocity. The ratio of the plastic strain rates can be formulated as:

$$\frac{\dot{\Delta}}{\dot{\varphi}} = \frac{d}{2} \cdot \sqrt{1 - \left(\frac{M}{M_{pl}} \right)^{2/3}} \quad (6.15)$$

By combining the kinematic conditions and the state of stresses in the plastic hinges, the bending moment in the plastic hinges $M(u)$ for any given displacement u is formulated:

$$\frac{M(u)}{M_{pl}} = \left[1 - \left(\frac{u}{d} \right)^2 \cdot \left(1 + \left(\frac{u}{l_1 + l_2} \right)^2 \right) \right]^{3/2} \quad (6.16)$$

For increasing displacement u , the bending moment $M(u)$ is progressively reducing. The tension force $N(u)$ may thereafter be determined by imposing $f(M,N) = 0$ in the above given Equation for $M(u)$.

$$\frac{N(u)}{N_{pl}} = 1 - \frac{2}{\pi} \cdot \left[\arcsin \left(\left(\frac{M(u)}{M_{pl}} \right)^{1/3} \right) - \left(\frac{M(u)}{M_{pl}} \right)^{1/3} \cdot \sqrt{1 - \left(\frac{M}{M_{pl}} \right)^{2/3}} \right] \quad (6.17)$$

Effective stress distribution in the concrete [Sor2017]

The assumed displacement field for the rebar implies that it has to cut its way through the concrete and thereby causes local crushing of the concrete. To determine in detail the entire stress distribution within the development of this simplified approach is not possible and might be subject of further investigations. To take into account for the triaxial stress conditions developed in the concrete and for the bearing strength to local pressure, the uniaxial compressive strength is increased by applying an enhancement factor c [Sor2017] see also e.g. [Li1989], [Ra1963].

$$f_{cc} = c \cdot f_c \quad (6.18)$$

where $c > 1$, has to be determined by comparison with the test results. Due to the geometry of the web-opening, separate enhancement factors are used for the concrete in the web-opening and outside of the web-opening.

To determine the position of the plastic hinges an uniformly distributed contact pressure over the lengths l_1 and l_2 of magnitude $f_{cc,1}$ and $f_{cc,2}$ is assumed, Figure 6.3.1. By setting up the vertical force equilibrium and moment equilibrium for the part of the rebar between the plastic hinges and by assuming the moment capacity of the rebar as M_{pl} , it is possible to establish the following equations to calculate l_1 and l_2 :

$$\begin{aligned} \Sigma V = 0: l_2 &= \frac{f_{cc,1}}{f_{cc,2}} \cdot l_1 \\ \Sigma M = 0: M_{pl} - d \cdot f_{cc,1} \cdot (l_1)^2 \cdot \frac{1}{2} &= d \cdot f_{cc,2} \cdot (l_2)^2 \cdot \frac{1}{2} - M_{pl} \\ l_1 &= \sqrt{\frac{2}{3}} \cdot \frac{d}{\sqrt{1 + \frac{f_{cc,1}}{f_{cc,2}}}} \cdot \sqrt{\frac{f_y}{f_{cc,1}}} \leq \frac{t_w}{2} \end{aligned} \quad (6.19)$$

$$l_2 = \sqrt{\frac{2}{3}} \cdot \frac{d}{\sqrt{1 + \frac{f_{cc,2}}{f_{cc,1}}}} \cdot \sqrt{\frac{f_y}{f_{cc,2}}} \quad (6.20)$$

The position of one plastic hinge is at the centreline of the web and therefore known, l_1 is determined by $l_1 = \frac{1}{2} \cdot t_w$. Further, assuming the concrete in the web-opening and in the chamber having originally the same uniaxial concrete compression strength f_{cm} , the ratio of the enhancement factors c_1/c_2 is determined and c_1 can be calculated with:

$$\frac{c_1^2}{c_2} + c_1 = \frac{8}{3} \cdot \frac{f_y}{f_{cm}} \cdot \frac{d^2}{t_w^2} \Rightarrow c_1 = -\frac{c_2}{2} + \sqrt{\frac{c_2^2}{4} + \frac{8}{3} \cdot \frac{f_y}{f_{cm}} \cdot \frac{d^2}{t_w^2}} \cdot c_2 \quad (6.21)$$

When dowel action is accompanied by tension in the rebar (and in the end completely replaced by catenary action) the average contact pressure must decrease due to the assumed material properties and the equilibrium conditions. Since concrete is not a perfect rigid-plastic material, there will be a softening effect which in turn reduces the concrete pressure when the concrete experiences too large compressive strains. Therefore, due to material properties, redistribution of the contact pressure will take place as u increases. In addition to this, the redistribution of stresses must take place in such a way, that equilibrium can be maintained when catenary action starts to develop in the rebar.

By setting up the vertical force equilibrium and moment equilibrium for the part of the rebar between the two plastic hinges for the deformed state (Figure 6.3.3) and by utilizing that the plastic hinges are subjected to $M(u)$ and $N(u)$, the relationship between u and the effective lengths $l_{1,ef}$ and $l_{2,ef}$ can be determined. For further information about the analytical formulation it is referred to Annex D:

$$l_{1,ef} = l_1 \cdot \left[1 - \sqrt{1 - \frac{M(u)}{M_{pl} + \left(\frac{u}{2}\right)^2 \cdot d \cdot \frac{f_{cc,1} \cdot f_{cc,2}}{(f_{cc,1} + f_{cc,2})}}} \right] \quad (6.22)$$

$$l_{2,ef} = l_2 \cdot \left[1 - \sqrt{1 - \frac{M(u)}{M_{pl} + \left(\frac{u}{2}\right)^2 \cdot d \cdot \frac{f_{cc,1} \cdot f_{cc,2}}{(f_{cc,1} + f_{cc,2})}}} \right] \quad (6.23)$$

It appears that the effective length is equal to the initial lengths, when $u = 0$ and reduces to zero when u has reached a value that makes $M(u) = 0$. The latter situation corresponds to a transition to full catenary action where the plastic hinges turn into moment-free hinges. Therefore, the rebar will no longer experience contact pressure between the two hinges, but instead acts as a tie.

Load displacement response [Sor2017]

Using the work Equation it is now possible to determine a load-displacement response. A stationary situation with displacement u and load $P(u)$ is used as a starting point from which an increment of displacement, δu is considered. The external work W_E is then given by:

$$W_E = P(u) \cdot \delta u \quad (6.24)$$

The internal work has contributions from the energy dissipated in the plastic hinges – with the rotation φ and the elongation Δ of plastic hinges outside of the web-opening and $2 \cdot \varphi$ and $2 \cdot \Delta$ in the web-opening, Figure 6.3.1 - as well as the energy absorbed when the concrete crushes under the bar:

$$W_I = 2 \cdot \left(f_{cc,1} \cdot l_{1,ef} \cdot d \cdot \frac{1}{2} \cdot \frac{l_{1,ef}}{l_1} \cdot \delta u_1 + f_{cc,2} \cdot l_{2,ef} \cdot d \cdot \frac{1}{2} \cdot \frac{l_{2,ef}}{l_2} \cdot \delta u_2 + 2 \cdot N(u) \cdot \delta \Delta + 2 \cdot M(u) \cdot \delta \varphi \right) \quad (6.25)$$

The incremental displacement and deformation quantities δu_1 , δu_2 , $\delta \Delta$ and $\delta \varphi$, can be expressed in terms of δu through the following relationships (with $\delta t = \delta u$):

$$\delta \varphi = \dot{\varphi} \delta u \quad (6.26a)$$

$$\delta \Delta = \dot{\Delta} \delta u \quad (6.26b)$$

$$\delta u_1 = \frac{l_1}{l_1 + l_2} \cdot \delta u \quad (6.26c)$$

$$\delta u_2 = \frac{l_2}{l_1 + l_2} \cdot \delta u \quad (6.26d)$$

By inserting the Equations above into the formulation of the internal work and by setting up the work equation $W_E = W_I$, the following solution is obtained for the load-displacement response of a perfectly smooth (frictionless) shear connection:

$$P(u) = P_{Dowel}(u) \quad (6.27)$$

$$P_{Dowel}(u) = f_{cc,1} \cdot d \cdot \frac{l_{1,ef}^2}{l_1 + l_2} + f_{cc,2} \cdot d \cdot \frac{l_{2,ef}^2}{l_1 + l_2} + 4 \cdot N(u) \cdot \dot{\Delta} + 4 \cdot M(u) \cdot \dot{\varphi} \quad (6.28)$$

Here $M(u)$, $N(u)$, $\dot{\Delta}$, $\dot{\varphi}$, l_1 and l_2 can be expressed as explicit functions of the displacement u as shown earlier. The solution is valid as long as u is less than the displacement capacity u_{max} .

Inclusion of friction

With increasing deformation u and increasing tension forces in the dowel bar, friction forces may develop. The friction force P_f might be assumed with:

$$P_f(u) = \mu \cdot N(u) \cdot \cos(\varphi) \quad (6.29)$$

In the absence of detailed research about friction coefficients for CoSFB-Dowels, the author decided to apply a friction factor of $\mu = 0.3$, which is smaller than the friction factor given by section 6.7.4.2 (4) of EN 1994-1-1 [EN1994]. The influence of a possible friction force acting directly in the plastic hinge as described by Puijssers [Pru1988] is not considered.

The above described method and the corresponding equations are fully based on the method developed and presented by Jesper Harald Sorensen [Sor2017], completed by possible shear failure of the dowel reinforcement and adapted to the current problem.

6.4 Limit Condition for a CoSFB-Dowel

Based on the analytical formulations derived before, the limit conditions for a CoSFB-Dowel are determined. A limit state is reached, when the cross-section capacity of the dowel reinforcement on shear is reached before a mechanism can develop. Or, in case the shear capacity is not reached and a mechanism can develop, the limit state is defined by the elongation capacity of the dowel reinforcement, Δ_{max} . This leads to the following limit equations:

Shear Failure

$$\frac{V}{V_{pl}} \leq 1 \quad (6.30)$$

with

$$V = f_{cc,1} \cdot l_{ef,1} \cdot d$$

$$V_{pl} = \pi \cdot \frac{d^2}{4} \cdot \frac{f_u}{\sqrt{3}}$$

f_u = ultimate strength of the dowel reinforcement,

The following limit condition for shear can be derived:

$$\frac{f_{cc,1}}{f_u} \cdot \frac{l_{ef,1}}{d} \cdot \frac{\sqrt{3} \cdot 4}{\pi} \leq 1 \quad (6.31)$$

Deformation Capacity of the Dowel Bar

$$\Delta = -\frac{l_1+l_2}{2} + \frac{l_1+l_2}{2} \cdot \sqrt{1 + \left(\frac{u_{max}}{l_1+l_2}\right)^2} \leq \Delta_{max} \quad (6.32)$$

With

$$l_1 = \sqrt{\frac{2}{3}} \cdot \frac{d}{\sqrt{1 + \frac{f_{cc,1}}{f_{cc,2}}}} \cdot \sqrt{\frac{f_y}{f_{cc,1}}} \leq \frac{t_w}{2}$$

$$l_2 = \sqrt{\frac{2}{3}} \cdot \frac{d}{\sqrt{1 + \frac{f_{cc,2}}{f_{cc,1}}}} \cdot \sqrt{\frac{f_y}{f_{cc,2}}}$$

6.5 Evaluation of the Analytical Method to determine P_{Dowel}

The derived analytical formulation for P_{Dowel} is evaluated by comparison to the push-out test, results are presented in Table 6.5.1. Focus is given to the evaluation of P_{Dowel} , as the accuracy of Equation 6.1 to determine P_{lin} was already shown in Section 6.2, Figure 6.2.2. As already pointed out in the previous sections, the derived Equation to determine the maximum load for dowel action, P_{Dowel} , is based on the assumption that a mechanism of three plastic hinges in the dowel reinforcement develops or the shear capacity of the bar is reached beforehand. The concrete in the web-opening and in the chamber is restrained by the steel profile and by the concrete slab. The developed analytical method is based on the approach already developed by Sorensen [Sor2017]. It enables to quantify the influence of each component on the load-bearing capacity of CoSFB-Dowels, but it is less adequate for a simulation of the non-linear part of the load-slip curve.

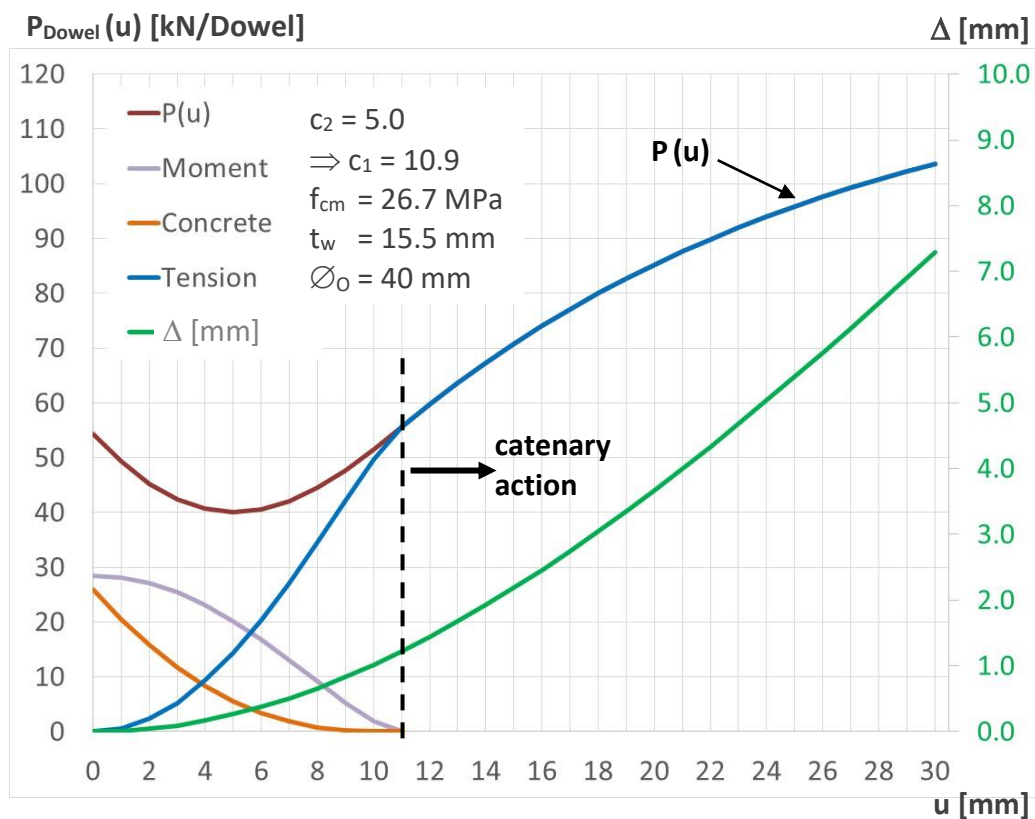


Figure 6.5.1: Evaluation of $P_{Dowel}(u)$

The enhancement factors were empirically determined by comparing values for P_{Dowel} , calculated with Equations (6.28) and (6.29), with the test results. Figure 6.5.1 presents the components contributing to $P_{Dowel}(u)$: crushing of the concrete, bending and tension. In addition, the calculated elongation Δ of the bar is given. The confinement of the concrete strength under the bar was considered by an enhancement factor $c_2 = 5.0$. This value has to be proven to be adequate for CoSFB-Dowels within the given test range. The influence of the enhancement factor is shown in Figure 6.5.3.

With increasing displacement u the load $P(u)$ is first decreasing, which is related to the applied method for concrete softening, then $P(u)$ is quickly increasing. In case $P(u = 0) < 2 \times V_{pl}$, the mechanism can develop and the limit state is defined by the maximum elongation of the bar. The contribution of the bending moment and the concrete are decreasing, when at the same time the contribution of tension is increasing.

The development of tension force and the reduction of shear force in the dowel reinforcement is presented in Figure 6.5.2. Between the plastic hinges the tension force is assumed to be constant, no bond stresses between the bar and the concrete are considered. The shear force is given for the position of its maximum value, at the shear interface. With increasing displacement u , the tension force in the bar is increasing until its capacity on tension is reached. While simultaneously, due to the inclination of the axis of the bar and the softening of the concrete, the shear force is decreasing.

$P_{Dowel}(u)$ [kN/Dowel]

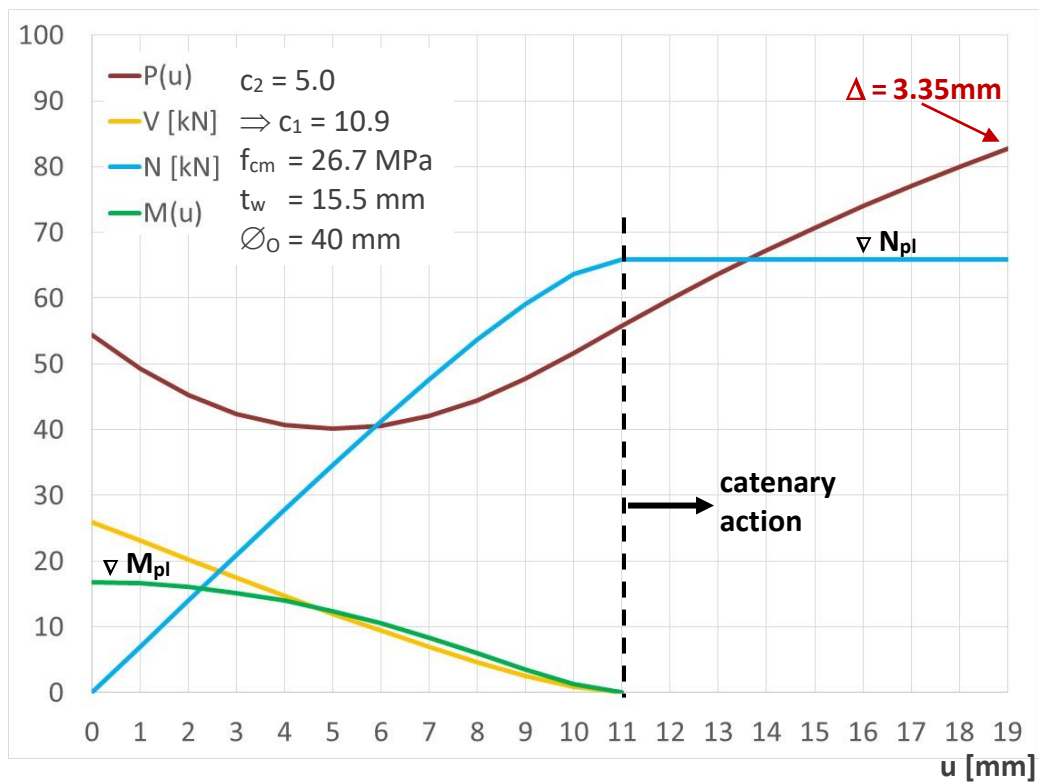


Figure 6.5.2: Development of tension in the dowel reinforcement

The influence of the enhancement factor is presented in Figure 6.5.3. The evolution of the load $P(u)$ is given up to a displacement $u = 30$ mm and the corresponding elongation Δ is indicated. For a lower concrete bearing strength, for smaller enhancement factors, a higher maximum load is reached. Although, to reach this higher load a higher ductility of the dowel bar is required. In practice, the dowel reinforcement has limited ductility and the dowel reinforcement will fail because its maximum elongation is reached.

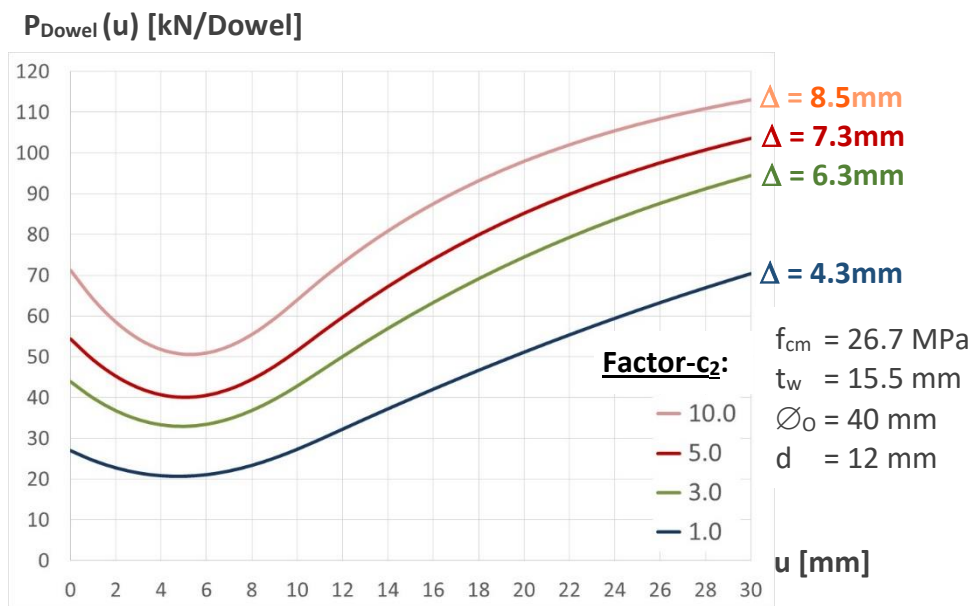


Figure 6.5.3: Influence of enhancement factor

Friction was not considered in the Figures given before. As already pointed out by the author, the derived analytical method is not foreseen to reproduce the non-linear part of the experimentally obtained load-slip curve. It is not possible to reproduce non-linear material behaviour and complex interactions by a simplified analytical method. Nevertheless, to illustrate the influence of different friction factors μ , a comparison to test series 1a is given in Figure 6.5.4.

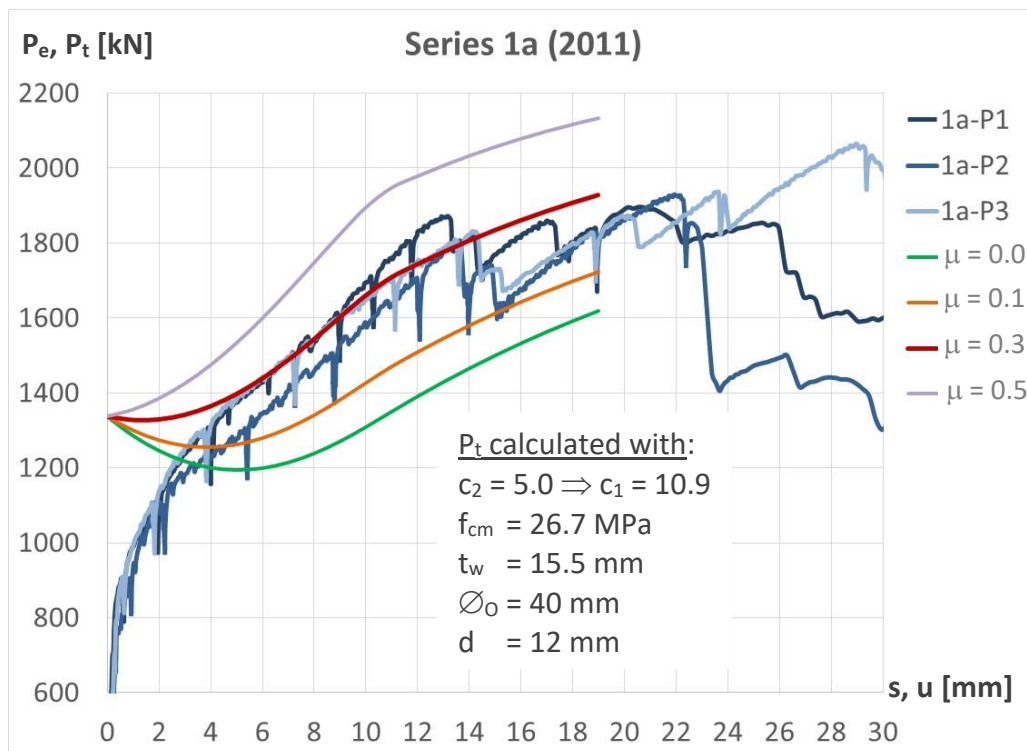


Figure 6.5.4: Influence of friction on $P_{t,Dowel}$ and comparison to Series 1a

Finally, the dowel action, $P_{t,Dowel}$, has been calculated for different values of the concrete compression strength, f_{cm} , and compared with the experimentally obtained values, $P_{e,Dowel}$. In accordance with Chapter 3.4 the estimated maximum elongation of the dowel reinforcement was set to $\Delta_{max} = 3.2\text{mm}$ and a friction factor $\mu = 0.3$ was used. The capacity of the dowel bar on shear and tension was calculated with the ultimate strength, f_u . Results are presented in Table 6.5.1.

Table 6.5.1: Determination of $P_{t,Dowel}$ and comparison with ΔP_e

Test	f_{cm}	c_2	c_1	l_2	u_{max}	$\Delta(u_{max})$	P_t	P_f	$P_{t,Dowel}$	ΔP_e
	[MPa]	[-]	[-]	[mm]			[kN]	[kN]	[kN]	[kN]
1a	26.7	5.0	10.9	16.2	18.5	3.2	81.4	31.1	112.4	117.1
1b	55.1	Shear failure for $c_2 > 6.6$					76.1	-	76.1	67.6
2-1a	29.5	5.0	23.6	16.9	17.4	3.2	85.3	30.1	115.5	104.6
2-1b*	58.2	Shear failure for $c_2 > 4.3$					76.1	-	76.1	64.8
2-2a	32.7	5.0	9.7	14.3	17.9	3.2	83.8	30.5	114.3	126.4
2-2b	40.0	Diameter of dowel reinforcement bar $d = 25\text{mm}$								
2-3	38.3	No concrete in the web-opening								

*Test 2-1b-P3 not considered

With:

u_{max} maximum displacement, corresponding to $\Delta(u_{max})$

$\Delta(u_{max})$ maximum elongation of the dowel reinforcement, with $\Delta(u_{max}) = 3.2\text{mm}$

P_t theoretical load-bearing capacity of the dowel w/o friction

P_f theoretical force transferred by friction, $P_f(u) = \mu \cdot N(u) \cdot \cos(\varphi)$

$P_{t,Dowel}$ theoretical load-bearing capacity of the dowel including friction

ΔP_e experimental load-bearing capacity of the dowel, $\Delta P_e = P_{e,max} - P_{e,lin}$

For a constant diameter of the dowel reinforcement, the development of a mechanism depends on the concrete compression strength. A mechanism developed for Series 1a, 2-1a and 2-2a., when for Series 1b and 2-1b the shear capacity of the bar was reached, before the mechanism could develop. Because no detailed test data for the contribution of the dowel action was available for Series 2-2b and 2-3, no comparison with the analytical method could be done.

Due to the absence of scientific investigations on the enhancement factor for CoSFB-Dowels, more test results are required to investigate possible correlations of the enhancement factor to the concrete compression class, the geometry of the web-opening and to the diameter of the dowel reinforcement. The derived method provides excellent information about the load-bearing behaviour and enables to quantify the maximum load of CoSFB-Dowels. However, due to the limited range of the concrete compression strength used in the tests, more tests are required to validate the method, especially for concrete compression strength in the range $33\text{ MPa} \leq f_{cm} \leq 55\text{ MPa}$.

7 Design Proposal

7.1 Introduction

Based on the findings presented in the previous Chapters, the maximum load is composed by a concrete component, P_{lin} , dowel action, P_{Dowel} , and Friction, P_f , Figure 7.1.

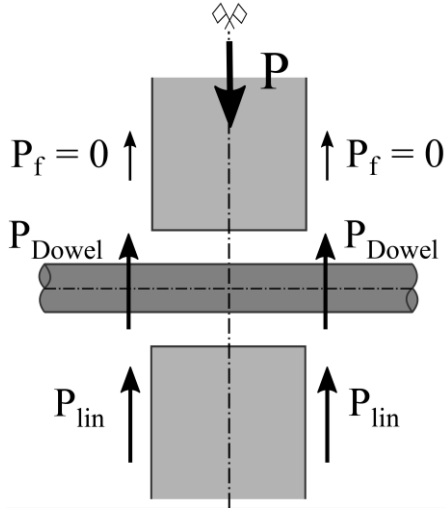


Figure 7.1: Components of a CoSFB-Dowel

In Section 6.2 it is shown, that P_{lin} depends on the concrete compression strength, the web thickness, the diameter of the web-opening and an empirically determined factor η , see Equation (6.2). As shown in Section 6.3, the possible development of a mechanism of three plastic hinges is of significant importance for value of P_{Dowel} . Is the shear capacity of the dowel reinforcement compared to the compression resistance of the confined concrete located next to the web-opening rather small, then no mechanism can develop and the value of P_{Dowel} is determined by the shear capacity of the bar. In case the shear capacity is larger than the local compression strength of the confined concrete, the before described mechanism in the dowel reinforcement can develop, which leads to an increase of the contribution of the dowel bar on the overall load-bearing capacity. However, the available test data was not sufficient to determine the initiation of the mechanism. Therefore, the author decided to limit the value of P_{Dowel} conservatively and safe sided to a lower boundary, the plastic shear resistance of the dowel bar. Consequently, the possible contribution of friction, P_f , is neglected, because the development of friction cannot be assured for in case of a shear failure. Finally, a design Equation for the shear resistance of a CoSFB-Dowel is formulated as the sum of the concrete component, P_{lin} , and the dowel action, P_{Dowel} :

$$P_{Rd} = P_{Rd,CoSFB-Dowel} = P_{Rd,lin} + P_{Rd,Dowel} \quad (7.1)$$

with

$P_{Rd,lin}$ design value of the concrete component

$P_{Rd,Dowel}$ design value of the dowel action

7.2 Design Resistance of the Concrete Component, P_{lin}

The linear range of the load-slip curve is limited by a concrete component, P_{lin} , cf. Section 6.2. A strong correlation of P_{lin} to the web thickness, the diameter of the web-opening and the concrete compression strength was identified, Figure 6.2.1. To determine the theoretical value of this concrete component, $P_{t,lin}$ the following Equation was derived:

$$P_{t,lin} = \eta \cdot f_{cm} \cdot t_w \cdot \phi_{Opening} \quad (7.2)$$

with

η empirical factor derived from the coefficient of determination

$$\eta = 36.919 \cdot (f_{cm} \cdot t_w \cdot \phi_O)^{-0.713}$$

Determination of the design Equation for P_{lin}

To derive the design resistance of the concrete component $P_{Rd,lin}$ a statistical evaluation of Equation 7.2 is done according to Annex D8.2 of EN 1990 [EN1990], see Table 7.2.

Mean value of correction factor:

$$b = \frac{\sum(P_{e,lin} \cdot P_{t,lin})}{\sum(P_{t,lin} \cdot P_{t,lin})} = \frac{123403.4}{123302.8} = 1.0008 \approx 1$$

$$\delta_i = \frac{P_{e,lin}}{b \cdot P_{t,lin}}$$

$$\Delta_i = \ln(\delta_i)$$

$$\bar{\Delta} = \frac{1}{n} \cdot \sum_{i=1}^n \Delta_i = -0.0012$$

$$\sum (\Delta_i - \bar{\Delta})^2 = 0.0523$$

Standard deviation of the error terms:

$$s_{\Delta}^2 = \frac{1}{n-1} \cdot \sum (\Delta_i - \bar{\Delta})^2 = \frac{1}{17-1} \cdot 0.0523 = 0.0033$$

Coefficient of variation of errors:

$$V_{\delta} = \sqrt{\exp(s_{\Delta}^2) - 1} = \sqrt{\exp(0.0033) - 1} = 0.0572 \leq 0.20$$

Standard deviation of the concrete strength “C35” and of the web-thickness according to [Hei2011] and [MC2001]:

$$V_{f_c} = 0.124$$

$$V_{t_w} = 0.100$$

For the diameter of the web-opening no standard deviation was considered, because the holes up to diameter 40mm are typically drilled.

Table 7.2: Statistical evaluation of Equation 7.2

Series	P _{e,lin} [kN]	P _{e,lin} [kN/Dowel]	P _{t,lin} [kN]	P _{e,lin} / P _{t,lin}	δ _i	Δ _i	(Δ _i - Δ̄) ²
1a	814.0	81.4	82.7	0.98	0.983	-0.017	0.0002
	773.5	77.4	82.5	0.94	0.937	-0.065	0.0041
	790.5	79.1	82.7	0.96	0.955	-0.046	0.0020
1b	940.0	94.0	101.4	0.93	0.927	-0.076	0.0056
	987.0	98.7	101.5	0.97	0.972	-0.029	0.0008
	1010.5	101.1	102.3	0.99	0.987	-0.013	0.0001
2-1a	701.5	70.2	68.8	1.02	1.019	0.019	0.0004
	659.5	66.0	69.1	0.95	0.953	-0.048	0.0022
	685.0	68.5	69.1	0.99	0.991	-0.009	0.0001
2-1b	887.0	88.7	83.3	1.06	1.064	0.062	0.0039
	935.0	93.5	84.6	1.10	1.104	0.099	0.0100
	1652.5	-	-	-	-	-	-
2-2a	744.5	74.5	76.2	0.98	0.977	-0.023	0.0005
	772.0	77.2	76.4	1.01	1.009	0.009	0.0001
	780.0	78.0	76.9	1.01	1.013	0.013	0.0002
2-2b	856.0	85.6	91.9	0.93	0.931	-0.071	0.0049
	1047.5	104.8	93.5	1.12	1.120	0.113	0.0130
	991.5	99.2	93.1	1.07	1.065	0.063	0.0041

Coefficient of variation of resistance function V_{rt}:

$$V_{rt}^2 = \frac{1}{g_{rt}^2(X_m)} \cdot \sum_{i=1}^j \left(\frac{\partial g_{rt}}{\partial X_i} \cdot \sigma_i \right)^2 = \sum_{i=1}^j \left(\frac{\partial g_{rt}}{\partial X_i} \cdot \frac{\sigma_i}{g_{rt}(X_m)} \right)^2$$

with σ_i = standard deviation for variable X_i (σ_i² = V_i).

Table 7.3: Partial differentiation of Equation 7.2

Variable	$\frac{\partial g_{rt}}{\partial X_i}$	$\frac{\partial g_{rt}}{\partial X_i} \cdot \frac{1}{g_{rt}(X_m)}$
f _{cm}	$36.919 \cdot 0.287 \cdot (t_w \cdot d_{opening})^{0.287} \cdot f_{cm}^{-0.713}$	$\frac{0.287}{f_{cm}}$
t _w	$36.919 \cdot (f_{cm} \cdot d_{opening})^{0.287} \cdot 0.287 \cdot t_w^{-0.713}$	$\frac{0.287}{t_w}$
d _{Opening}	[-]	[-]

Coefficient of variation of the resistance function is therefore:

$$V_{rt}^2 = \left(\frac{0.287 \cdot \sigma_c}{f_{cm}} \right)^2 + \left(\frac{0.287 \cdot \sigma_{tw}}{t_w} \right)^2 = (0.287 \cdot 0.124)^2 + (0.287 \cdot 0.100)^2 =$$

$$V_{rt}^2 = 0.0021$$

Coefficient of variation:

$$V_r^2 = V_\delta^2 + V_{rt}^2 = 0.0572^2 + 0.0021 = 0.0054$$

Characteristic value of the resistance r_k :

$$r_k = b \cdot g_{rt}(X_m) \cdot \exp(-k_\infty \cdot \alpha_{rt} \cdot Q_{rt} - k_n \cdot \alpha_\delta \cdot Q_\delta - 0.5 \cdot Q^2)$$

$$Q_{rt} = \sigma_{\ln(rt)} = \sqrt{\ln(V_{rt}^2 + 1)} = \sqrt{\ln(0.0021 + 1)} = 0.0457$$

$$Q_\delta = \sigma_{\ln(\delta)} = \sqrt{\ln(V_\delta^2 + 1)} = \sqrt{\ln(0.0572^2 + 1)} = 0.0572$$

$$Q = \sigma_{\ln(r)} = \sqrt{\ln(V_r^2 + 1)} = \sqrt{\ln(0.0054 + 1)} = 0.0731$$

$$\alpha_{rt} = \frac{Q_{rt}}{Q} = \frac{0.0457}{0.0731} = 0.6247$$

$$\alpha_\delta = \frac{Q_\delta}{Q} = \frac{0.0572}{0.0731} = 0.7816$$

The values for the coefficients of variation are taken from [MC2001] and therefore are “known”, consequently the values for k_∞ and k_n are taken from Table D1 of EN 1990 [EN1990] for “ V_x known”, with $k_\infty = 1.64$ and $k_n = k_{20} = 1.68$:

$$r_k = b \cdot g_{rt}(X_m) \cdot \exp(-k_\infty \cdot \alpha_{rt} \cdot Q_{rt} - k_n \cdot \alpha_\delta \cdot Q_\delta - 0.5 \cdot Q^2)$$

$$r_k = 1.0008 \cdot g_{rt}(X_m) \cdot \exp(-k_\infty \cdot 0.6247 \cdot 0.0457 - k_n \cdot 0.7816 \cdot 0.0572 - 0.5 \cdot 0.0731^2)$$

$$r_k = 0.8836 \cdot g_{rt}(X_m)$$

Calculation of the design value of resistance r_d , with Table D2 of EN 1990 [EN1990] for “ V_x known”, with $k_{d,\infty} = 3.04$ and $k_{d,n} = k_{d,20} = 3.16$:

$$r_d = b \cdot g_{rt}(X_m) \cdot \exp(-k_{d,\infty} \cdot \alpha_{rt} \cdot Q_{rt} - k_{d,n} \cdot \alpha_\delta \cdot Q_\delta - 0.5 \cdot Q^2)$$

$$r_d = 1.0008 \cdot g_{rt}(X_m) \cdot \exp(-3.04 \cdot 0.6247 \cdot 0.0457 - 3.16 \cdot 0.7816 \cdot 0.0572 - 0.5 \cdot 0.0731^2)$$

$$r_d = 0.7946 \cdot g_{rt}(X_m)$$

Calculation of the partial safety factor γ_M :

$$\gamma_M = \frac{r_k}{r_d} = \frac{0.8836}{0.7946} = 1.1119$$

Calculation of ratio of nominal resistance to characteristic resistance, k_c :

$$k_c = \frac{r_n}{r_k} = \frac{(f_{ck})^{0.287}}{(f_{cm})^{0.287}} = \frac{(40)^{0.287}}{(48)^{0.287}} = 0.9490$$

with mean values $f_{ck,m} = 40$ MPa and $f_{cm,m} = 48$ MPa for a range of concrete compression classes from C25/30 up to C55/67 [Z-26.4-59].

Calculation of the partial safety factor with respect to the nominal resistance, γ_M^* :

$$\gamma_M^* = \frac{r_n}{r_k} \cdot \frac{r_k}{r_d} = \frac{r_n}{r_d} = \frac{r_n}{r_k} \cdot \gamma_M = k_c \cdot \gamma_M = 0.9490 \cdot 1.1119 = 1.0553$$

Formulation of the design equation for $P_{Rd,lin}$:

$$P_{Rd,lin} = P_{t,lin,n} \cdot \frac{\gamma_v}{\gamma_M^*} \cdot \frac{1}{\gamma_v} = \frac{1.25}{1.0553} \cdot \frac{1}{\gamma_v} \cdot 36.919 \cdot (f_{ck} \cdot t_w \cdot \phi_{Opening})^{0.287}$$

$$P_{Rd,lin} = 43.7 \cdot (f_{ck} \cdot t_w \cdot \phi_{Opening})^{0.287} \cdot \frac{1}{\gamma_v} \quad (7.3)$$

with $\gamma_v = 1.25$.

The mean and characteristic values of $P_{t,lin}$ are given in Figure 7.2.

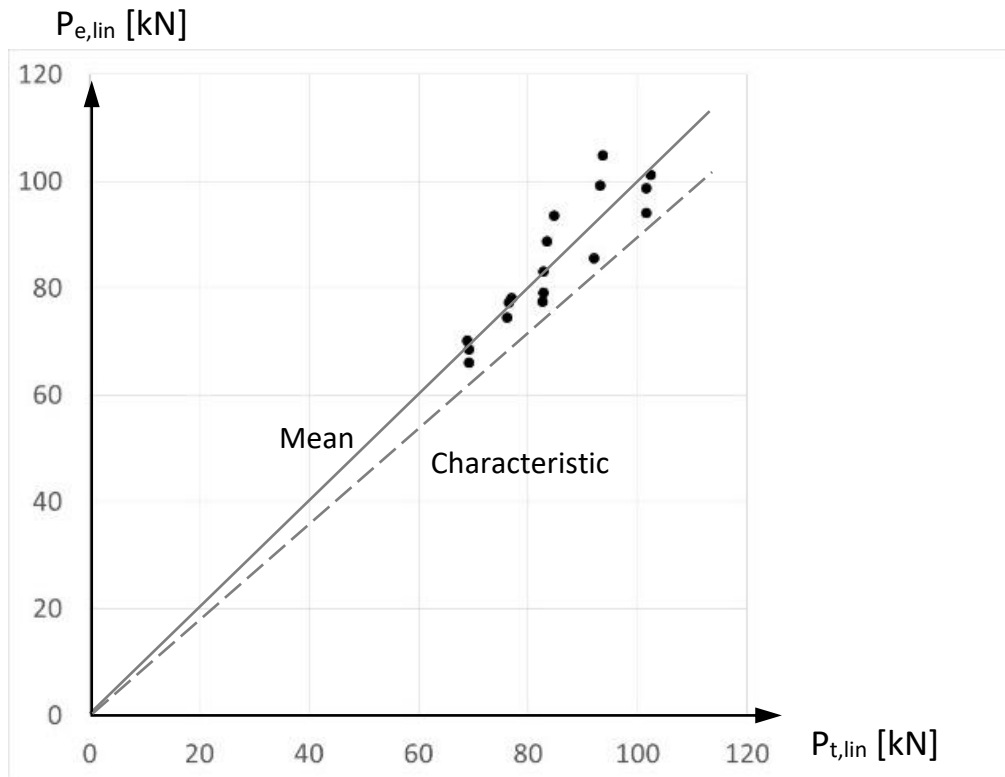


Figure 7.2: Comparison of P_e and P_t according to Equation 7.2 and 7.3

7.3 Design Resistance of the Dowel Action, P_{Dowel}

As already given in Chapter 6 and Section 7.1, the dowel action is limited either by the shear capacity or by the ultimate strain of the dowel bar. The development of a mechanism of plastic hinges depends strongly on the strength of the confined concrete in and next to the web-opening. The available test data was not sufficient to consider both failure modes in a single equation. Especially due to the lack of test data in the range of concrete compression classes $33 \text{ MPa} \leq f_{cm} \leq 55 \text{ MPa}$ it was not possible to determine the multiaxial concrete strength, when the mechanism is not developed anymore and shear failure becomes decisive. Therefore, a design Equation was derived based on the shear capacity of the dowel reinforcement only and the development of a mechanism was not considered. In addition, no friction is taken into account. This approach leads to lower boundary estimation of the load-bearing capacity and consequently to conservative values of the design resistance. Hence, considering two shear interfaces per CoSFB-Dowel the design load, $P_{Rd,Dowel}$, can be determined with:

$$P_{Rd,Dowel} = \frac{2 \cdot V_{pl,bar}}{\gamma_{M2}} \quad (7.4)$$

with

$$\gamma_{M2} = \gamma_v = 1.25$$

$$V_{pl,bar} = \pi \cdot \frac{d^2}{4} \cdot \frac{f_y}{\sqrt{3}}$$

d = diameter of the dowel reinforcement bar

f_y = yield strength of dowel material

7.4 Design Resistance of a CoSFB-Dowel

Concluding, the design resistance of a CoSFB-Dowel, P_{Rd} , can be formulated by using Equation 7.1 and introducing the design Equations for $P_{Rd,lin}$ and $P_{Rd,Dowel}$ from the Sections 7.3 and 7.4.

$$P_{Rd} = P_{Rd,CoSFB-Dowel} = P_{Rd,lin} + P_{Rd,Dowel} \quad (7.1)$$

with

$$P_{Rd,lin} = 43.7 \cdot (f_{ck} \cdot t_w \cdot \phi_{Opening})^{0.287} \cdot \frac{1}{\gamma_v} \quad (7.3)$$

$$P_{Rd,Dowel} = \frac{2 \cdot V_{pl,bar}}{\gamma_{M2}} \quad (7.4)$$

the design Equation for CoSFB-Dowel is formulated as:

$$P_{Rd} = 43.7 \cdot (f_{ck} \cdot t_w \cdot \phi_{Opening})^{0.287} \cdot \frac{1}{\gamma_v} + \frac{2 \cdot V_{pl,bar}}{\gamma_v} \quad (7.5)$$

with

$$\gamma_v = 1.25.$$

Range of Validity

The developed Equation 7.5 is valid for the tested range of parameters only, see Table 7.4:

Table 7.4: Validity range of Equation 7.5

Parameter	Minimum	Maximum
Concrete compression class	C25/30	C55/67
Diameter of dowel reinforcement, d	12mm	
Diameter of web-opening, ϕ_o	25mm	40mm
Web-thickness of the steel section, t_w	7.5mm	15.5mm

Because the contribution of the dowel action was limited to the shear capacity of the dowel reinforcement bar, no verification of the maximum elongation Δ_{max} has to be done.

8 Conclusions

Fundamental investigations of the load-bearing behaviour of CoSFB-Dowels are presented in this Thesis. CoSFB-Dowels connect a steel section to a concrete slab activating a composite action.

The experimental investigations showed different type of failure modes, when the concrete compression strength was identified as the main parameter influencing these modes. Throughout the numerical investigations, it has been identified that the specific geometry of the dowel is allowing for a local concrete confinement, which influences the ability of the reinforcement bar to deform and contributes to the load-bearing capacity of CoSFB-Dowels. Especially for higher concrete compression classes it has been necessary to introduce modification into the concrete constitutive law to account for the strength increase of the concrete due to triaxial stress state and due to local loading. Shear and ductile damage of the metal material was also incorporated to properly define the failure of the bars. All findings were considered in the analytical method derived. The systematic, comprehensive investigation of influential parameters and their interaction, allowed for a detailed formulation of the overall load-bearing behaviour of CoSFB-Dowels. It has been identified that it is determined by a concrete component, dowel action of the dowel reinforcement bar and friction. The contribution of these components is explained with the help of a typical load-slip curve, Figure 8.1.

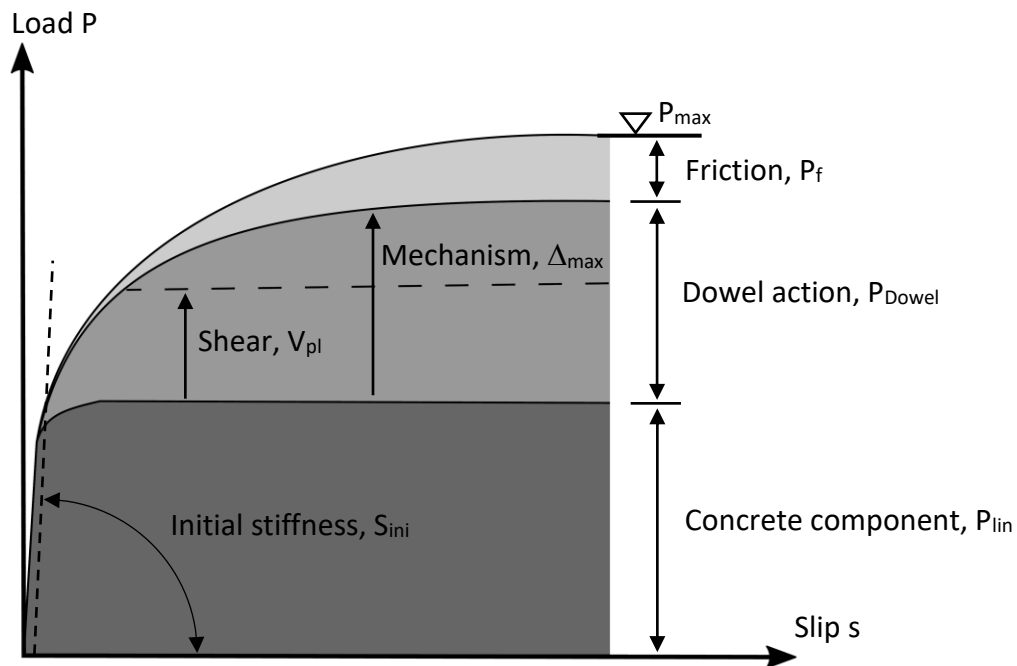


Figure 8.1: Load-bearing behaviour of a CoSFB-Dowel

In the initial, elastic range a linear load-slip relationship is observed. It is mainly characterized by the strength and the stiffness of the concrete. The concrete component, P_{lin} , is limited by the triaxial strength of the concrete in the web-opening, the web-thickness of the steel beam and the diameter of the web-opening.

Reaching its multiaxial compressive strength, stiffness degradation (damage) starts to develop due to concrete crushing. Because the concrete in the web-opening is restrained by the steel section and the concrete slab, the multiaxial compressive strength is much higher than its uniaxial strength. Generally, concrete can be classified as a quasi-brittle material, which fails at larger strains than a brittle material. For details of multiaxial strain-softening of concrete, it is referred to [Mie1986]. Increasing the load P further, the dowel reinforcement is activated. Dowel action starts to develop and non-proportional slip increase is observed. The contribution of the dowel reinforcement bar on the load-bearing capacity of a CoSFB-Dowel (= dowel action), P_{Dowel} , is determined by the plastic bending resistance M_{pl} of the dowel reinforcement, its shear capacity V_{pl} and its elongation capacity (ductility), Δ_{max} . Is the shear capacity of the dowel reinforcement larger than the confined concrete compressive strength, the bar is able to crush the concrete underneath, creating a space and a mechanism of plastic hinges in the dowel reinforcement develops, Figure 8.2. In case the shear capacity is too small, the dowel bar is not able to damage the concrete underneath and the shear capacity of the bar becomes decisive. No mechanism develops in this case.

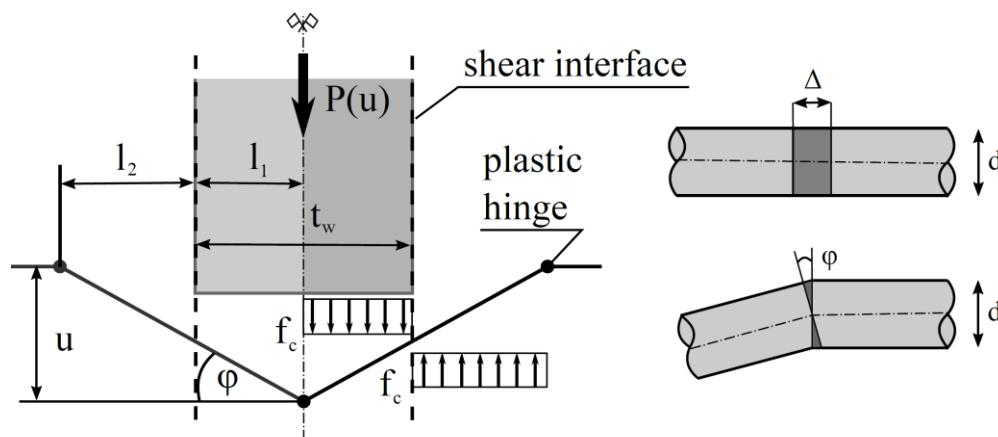


Figure 8.2: Dowel action by a mechanism of plastic hinges

In case the mechanism in the bar developed, additional load P is transferred by the development of tension forces (= catenary action) in the dowel bar. The maximum load, P_{max} , is reached, when the maximum elongation of the reinforcement bar Δ_{max} is reached in the plastic hinges. Therefore, the ultimate load and the ductility of the CoSFB-Dowel depends strongly on the ductility of the material of the dowel reinforcement bar. With increasing tension in the dowel reinforcement, friction between concrete and the steel section develops and contributes to P_{max} .

As general outcome it can be concluded, that, within the tested range of concrete compression classes from C25/30 to C55/67, web-openings drilled in the web of hot-rolled steel sections with a diameter from 25mm to 40mm, dowel reinforcement bars in grade B500B and a diameter of 12mm at least, the applicability of CoSFB-Dowels as shear connector in composite beams subjected to static, monotonic loading has been proven. CoSFB-Dowels show an excellent load-bearing behaviour, a high stiffness in the elastic range and a very ductile behaviour reaching the load bearing capacity.

Outlook

Although the applicability of CoSFB-Dowels has been proven and a conservative design proposal presented, additional tests should be planned and executed to take benefit of the possible development of a mechanism of plastic hinges in the dowel reinforcement bar and the corresponding increase of the load-bearing capacity. Focus should be on the investigation of the concrete strength in and next to the web-opening, especially in the range of $33 \text{ MPa} \leq f_{cm} \leq 55 \text{ MPa}$ in order to determine “enhancement factors” for a wider range of concrete compression classes.

The numerical modelling confirmed the influence of the concrete strength, the web thickness and the diameter of the web-opening on the “elastic limit”, P_{lin} . Additional investigations about a possible contribution of the diameter of the dowel reinforcement bar, especially for bar diameters $> 12\text{mm}$ are of scientific interest.

Further, tests of CoSFB-Dowels with diameters of the dowel reinforcement bar larger than 12mm would allow for a reduction of the quantity of CoSFB-Dowels per beam, allowing for an economical optimisation of composite slim-floor beams. Tests on web-openings with a diameter $> 40\text{mm}$ could lead to the identification of an optimal opening diameter, supporting economical design of composite beams. Possible fields for additional investigations on CoSFB-Dowels are the influence of the horizontal spacing of dowel reinforcement and the position of the web-opening in the cross-section.

Investigations of the behaviour of CoSFB-Dowels under cyclic loading could lead to improved design rules for filler beam bridges.

References

Standards and Technical Approvals

- [ACI318M] American Concrete Institute (ACI): Building Code Requirements for Structural Concrete (ACI 318M-08) and Commentary. ACI, June 2008.
- [DIN1981] DIN, Deutsches Institut für Normung e.V.: Richtlinien für die Bemessung und Ausführung von Stahlverbundträgern. Ausgabe März 1981 und Ergänzende Bestimmungen hierzu, Ausgabe März 1984.
- [DIN10002] DIN EN 10002-1: Metallische Werkstoffe – Zugversuch. Teil 1: Prüfverfahren bei Raumtemperatur. Berlin, Beuth Verlag. Dezember 2001.
- [DIN12390-1] DIN EN 12390-1: Prüfung von Festbeton. Teil 1: Form, Maße und andere Anforderungen für Probekörper und Formen. Berlin, Beuth Verlag. Februar 2001.
- [DIN12390-2] DIN EN 12390-2: Prüfung von Festbeton. Teil 2: Herstellung und Lagerung von Probekörpern für Festigkeitsprüfungen. Berlin, Beuth Verlag. August 2009.
- [DIN12390-3] DIN EN 12390-3: Prüfung von Festbeton. Teil 3: Druckfestigkeit von Probekörpern. Berlin, Beuth Verlag. Juli 2009.
- [DIN12390-4] DIN EN 12390-5: Prüfung von Festbeton. Teil 5: Biegezugfestigkeit von Probekörpern. Berlin, Beuth Verlag. Juli 2009.
- [DIN50125] DIN 50125: Prüfung metallischer Werkstoffe – Zugproben. Berlin, Beuth Verlag. Januar 2004.
- [EN6892] EN ISO 6892-1: Metallic materials – Tensile testing. Part 1: Method of test at room temperature. Berlin, Beuth Verlag. 2009.
- [EN1990] EN 1990, Eurocode 0: Basis of structural design. CEN European Committee for Standardization. Brussels, Belgium 2010.
- [EN1992] EN 1992-1-1, Eurocode 2: Design of concrete structures - Part 1-1: General rules and rules for buildings. CEN European Committee for Standardization. Brussels, Belgium 2012.
- [EN1994] EN 1994-1-1, Eurocode 4: Design of composite steel and concrete structures - Part 1-1: General rules and rules for buildings. CEN European Committee for Standardization. Brussels, Belgium 2010.
- [fib2010] Comite Euro-International du Béton: fib Model Code for Concrete Structures 2010. International Federation for Structural Concrete (fib). Lausanne, Switzerland, 2013.
- [fib42] Comite Euro-International du Béton, Bulletin 42: Constitutive modelling of high strength / high performance concrete. State-of-art report prepared by Taks Group 8.2. International Federation for Structural Concrete (fib). Lausanne, Switzerland, 2008.
- [MC2001] JCSS Probabilistic Model Code – Part 3: Material Properties. Joint Committee on Structural Safety, 2001.
- [Z-26.4-38] German Technical Approval Z-26.4-38: Perfobondleiste. Donges Stahlbau GmbH. DIBt Berlin, Germany, 2007.

References

- [Z-26.4-39] German Technical Approval Z-26.4-39: Kombi - Verdübelung. Kombi Tragwerk GmbH. DIBt, Berlin, Germany, 2000.
- [Z-26.4-56] German Technical Approval Z-26.4-56: Verbunddübelleisten. Stahlinstitut VDEh, Düsseldorf. DIBt, Berlin, Germany, 2013.
- [Z-26.4-59] German Technical Approval Z-26.4-59: CoSFB-Betondübel. ArcelorMittal Belval & Differdange S.A., Luxembourg. DIBt, Berlin, Germany, 2014.

Research Reports

- [Stu2009] Kuhlmann U. et al.: Push-out and girder tests for the determination of the bending capacity and longitudinal shear capacity of Composite Slim-Floor girder with COFRADAL200® deck elements. University of Stuttgart, Germany, 2010. Internal Research Report, ArcelorMittal.
- [Stu2011] Kuhlmann U. et al.: Push-out tests for the determination of the longitudinal shear capacity of Composite Slim-Floor beams. University of Stuttgart, Germany, 2012. Internal Research Report, ArcelorMittal.
- [P621] Feldmann, M., Hegger, J., Hechler, O., Rauscher, S.: Untersuchungen zum Trag- und Verformungsverhalten von Verbundmitteln unter ruhender und nichtruhender Belastung bei Verwendung hochfester Werkstoffe. Forschungsprojekt P621, AiF 13867, Forschungsvereinigung Stahlanwendung (FOSTA), 2007.
- [P804] Feldmann M., Guendel M., Kopp M., Gallwoszus J., Heinemeyer S., Seidl G., Hoyer O.: Neue Systeme fuer Stahlverbundbrücken – Verbundfertigteilträger aus hochfesten Werkstoffen und innovativen Verbundmitteln. Fosta P804. Germany 2009.

Publications

- [Abaqus] Abaqus 6.14. Online Documentation, © Dassault Systèmes, 2011.
- [Ah2010] Ahn J.-H., Lee C.-G., Won J.-H., Kim S.-H.: Shear resistance of the perfobond-rib shear connector depending on concrete strength and rib-arrangement. Journal of Constructional Steel Research 66 (2010), pp. 1295 - 1307. Elsevier Ltd. 2010.
- [An1985] Andrä H.-P.: Neuartige Verbundmittel für den Anschluss von Ortbetonplatten an Stahlträger. Beton-und Stahlbetonbau 12/1985, pp. 325 – 328. Wilhelm Ernst & Sohn Verlag für Architektur und technische Wissenschaften, Berlin, 1985.
- [An1990] Andrä H.-P.: Economical Shear Connectors with High Fatigue Strength. IABSE Conference 1990, Proceedings pp. 167 – 172.
- [Ar2011] Arasaratnam P., Sivakumaran K. S., Tait M. J.: True stress-strain models for structural steel elements. International Scholarly Research Network ISRN Civil Engineering. Vol. 2011, Article ID 656401. 2011

-
- [bfs2015] Braun M., Hechler O., Obiala R., Kuhlmann U.: Innovatives Verbundmittel fuer integrierte Deckentraeger, CoSFB-Betonduebel. Engineering Award from Ingenieurpreis des Deutschen Stahlbaus 2015 (Auszeichnung), Kategorie Buildings. Bauforumstahl (bfs), Germany, 2015.
- [Br1964] Broms Bengt B.: Lateral resistance of piles in cohesive soils. Journal of the Soil Mechanics and Foundation Division, Proceedings of the American Society of Civil Engineers, pp. 27 – 63. March 1964.
- [Br1965] Broms Bengt B.: Design of laterally loaded piles. Journal of the Soil Mechanics and Foundation Division, Proceedings of the American Society of Civil Engineers, pp. 77 – 99. May 1965.
- [Bu2011] Mangerig I., Burger S., Wagner R., Wurzer O., Zapfe C.: Zum Einsatz von Betondübeln im Verbundbau (Teil 1) – Ruhende Beanspruchung. Stahlbau 80 (2011), Issue 12, pp. 885 – 893. Ernst & Sohn Verlag fuer Architektur und technische Wissenschaften. Berlin, Germany 2011.
- [Co200] ArcelorMittal Construction BeNeLux: Arval COFRADAL 200®.
- [Ca2010] Candido-Martins J.P.S., Costa-Neves L.F., P.C.G. da S. Vellasco: Experimental evaluation of the structural response of Perfobond shear connectors. Engineering Structures 32 (2010), pp. 1976 – 1985. Elsevier Ltd. 2010.
- [CC2013] Hechler, O.; Kuhlmann, U.; Eggert, F.; Hauf, G.; Braun, M.; Obiala, R.: CoSFB – Composite slim-floor beam – Experimental test campaign and evaluation. Proceedings of Conference on Composite Construction in Steel and Concrete VII, Australia. 2013.
- [Ch2016] Chung C. H., Lee J., Kim J.S.: Shear strenght of T-Perfobond rib shear connectors. Journal of Civil Enginnering (2016), pp. 1824 – 1834. Springer Verlag 2016.
- [Cl2016] Classen M.: Zum Trag- und Verformungsverhalten von Verbundträgern mit Verbunddübelleisten und großen Stegöffnungen. PhD-Thesis, University of Aachen, Germany 2016.
- [Cor1986] Cornelissen H. A. W., Hordijk D. A., Reinhardt H. W.: Experimental determination of crack softening characteristics of normal weight and lightweight concrete. Heron, 31(20), pp. 45-56, 1986.
- [Dei1992] Dei Poli S., Di Prisco M., Gambarowa P.G.: Shear Response, Deformations, and Subgrade Stiffness of a Dowel Bar Embedded in Concrete. American Concrete Institue (ACI) Journal, November – December 1992, pp. 665 – 675.
- [Du1972] Dulacska H.: Dowel action of reinforcement crossing cracks in concrete. Journal of the American Concrete Institute (ACI), pp. 654 – 757, 1972.
- [ECCS74] Multi-Storey Buildings in Steel. ECCS Documentation No. 74. Brussels, Belgium 1997.
- [ECCS138] Shear Connection in Composite Flexural Members of Steel and Concrete, Matti V. Leskelä – Technical Committee 11, Composite Structures. ECCS Documentation No. 138. Brussels, Belgium 2017.

- [ES2014] Braun M., Obiala R., Odenbreit Chr., Hechler O.: CoSFB – Design and application of a new generation of slim-floor construction. Proceedings of the 7th European Conference on Steel and Composite Structures. Naples, Italy. EUROSTEEL 2014.
- [ES2017] Braun M., Obiala R., Odenbreit Chr.: Numerical simulation of the load bearing behaviour of concrete dowels in slim-floor construction - CoSFB. Proceedings of the 8th European Conference on Steel and Composite Structures. Copenhagen, Denmark. EUROSTEEL 2017.
- [Elb2011] Ellobody E., Young B.: Numerical simulation of concrete encased steel composite columns. Journal of Constructional Steel Research, 67, pp. 211–222, 2011.
- [Fee1996] Feenstra P. H., Borst de R.: A composite plasticity model for concrete. International Journal of Solids and Structures 33. 1996.
- [Fel2007] Feldmann M., Hechler O., Hegger J., Rauscher S.: Neue Untersuchungen zum Ermüdungsverhalten von Verbundträgern aus hochfesten Werkstoffen mit Kopfbolzendübeln und Puzzleleiste. Stahlbau 76 (2007), Issue 11, pp. 826 – 844. Ernst & Sohn Verlag, Berlin, Germany 2007.
- [Fi2007] Fink J., Petraschek T.: Tragmodelle zur Bestimmung der Längsschubtragfähigkeit des Kronendübels als neuartiges Verbindungsmittel im Verbundbau. Stahlbau 76 (2007), No. 10, pp. 761 – 770. Ernst & Sohn Verlag, Berlin, Germany 2007.
- [Fri1938] Friberg B. F.: Design of Dowels in Transverse Joints of Concrete Pavements. American Society of Civil Engineers (ASCE), pp. 1809 – 1828. 1938.
- [Gia2004] Giakoumelis G., Lam, D.: Axial capacity of circular concrete-filled tube columns. Journal of Constructional Steel Research, 60, pp. 1049 – 1068, 2004.
- [Gu2009] Gündel M., Dürr A., Hauke B., Hechler O.: Zur Bemessung von Lochleisten als duktilen Verbundmittel in Verbundträgern aus höherfesten Materialien. Stahlbau 78 (2009), Issue 12, pp. 916 – 924. Ernst & Sohn Verlag, Berlin, Germany 2009.
- [Hae2015] Häussler-Combe U.: Computational Methods for Reinforced Concrete Structures. Ernst & Sohn Verlag, Berlin. Germany 2015.
- [Hau2005] Hauke B.: Shear connectors for composite members of high strength materials. Proceedings of the 4th European Conference on Steel and Composite Structures. Maastricht, The Netherlands. EUROSTEEL 2005.
- [He2016] He S., Fang Z., Fang Y., Liu M., Liu L., Mosallam A.S.: Experimental study on perfobond strip connector in steel-concrete joints of hybrid bridges. Journal of Constructional Steel Research 118 (2016), pp. 169 – 179. Elsevier Ltd. 2016.
- [Hei2011] Heinemeyer S.: Zum Trag- und Verformungsverhalten von Verbundträgern aus ultrahochfestem Beton mit Verbundleisten. PhD-Thesis, University of Aachen, Germany, 2011.
- [Hei2012] Heinemeyer S., Gallwoszus J., Hegger J.: Verbundträger mit Puzzleleiste und hochfesten Werkstoffen. Stahlbau 81 (2012), Issue 8, pp. 595 – 603. Ernst & Sohn Verlag, Berlin, Germany 2012.

- [Hil1976] Hillerborg A, Mod  er M., Petersson P.-E.: Analysis of crack formation and crack growth in concrete by means of fracture mechanics and finite elements. *Cement and Concrete Research*, Vol. 6, pp. 773 – 782. 1976.
- [Hoo2004] Hooputra H., Gese H., Dell H., Werner H.: A Comprehensive Failure Model for Crashworthiness Simulation of Aluminium Extrusions. *International Journal of Crashworthiness*, Vol. 9, No.5, pp. 449–464, 2004.
- [Hu1989] Hu H.-T., Schnobrich W. C.: Constitutive modelling of concrete by using nanoassociated plasticity. American Society of Civil Engineer (ASCE). *Journal of Materials in Civil Engineering*. Vol. 1, No. 4, pp. 199 – 216. November 1989.
- [Hu2003] Hu H.-T., Huang C.-S., Wu M.-H, Wu Y.-M.: Nonlinear analysis of axially loaded concrete-filled tube columns with confinement effect. American Society of Civil Engineer (ASCE). *Journal of Structural Engineering*. Vol. 129, No. 10, pp. 1322 – 1329. October 2003.
- [Je2009] Jeong Y.-J., Kim H.-Y., Koo H.-B.: Longitudinal shear resistance of steel-concrete composite slabs with perfobond shear connectors. *Journal of Constructional Steel Research* 65 (2009), pp. 81 - 88. Elsevier Ltd. 2009.
- [Jo1949] Johansen K. W.: Theory of Timber Connections. *Proceedings of IABSE Conference, Bern*, pp. 249 – 262. 1949.
- [Ki2013] Kim S.-H., Choi K.-T., Park S.-J., Park S.-M., Jung C.-Y.: Experimental shear resistance evaluation of Y-type perfobond rib shear connector. *Journal of Constructional Steel Research* 82 (2013), pp. 1 - 18. Elsevier Ltd. 2013.
- [Kmi2011] Kmiecik P., Kaminski M.: Modelling of reinforced concrete structures and composite structures with concrete strength degradation. *Archives of Civil & Mechanical Engineering*, Volume 11, Issue 3, pp. 623–636, 2011.
- [Kr  2004] Kr  tzig W.B., P  lling R.: An elasto-plastic damage model for reinforced concrete with minimum number of material parameters. *Computers and Structures*, Volume 82, pp. 1201–1215, 2004.
- [Kr1997a] Kraus D., Wurzer O.: Nonlinear finite-element analysis of concrete dowels. *Computers & Structures*, Vol. 64 (1997), No. 4, pp. 1271 – 1279. Elsevier Ltd. 1997.
- [Kr1997b] Kraus D., Wurzer O.: Bearing Capacity of concrete dowels. *IABSE International Conference on Composite Construction, Proceedings* pp. 133 - 138. Innsbruck, Austria 1997.
- [Ko2011] Konrad M.: *Tragverhalten von Kopfbolen in Verbundtr  gern bei senkrecht spannenden Trapezblechprofilen*. University of Stuttgart, Germany 2011.
- [Lee1998] Lee J., Fenves G. L.: Plastic-damage model for cyclic loading of concrete structures. *Journal of Engineering Mechanics*, Vol. 124, No. 8, pp. 892 – 900, 1998.

References

- [Les2005] Leskelä M.V., Peltonen, S.: Behaviour of shallow floor composite beams with solid types of slab. Eurosteel 2005, Maastricht, The Netherlands. Proceedings Volume B, pp. 4.3-9 – 4.3-16, 2005.
- [Les2006] Peltonen, S., Leskelä M.V.: Connection behaviour of a concrete dowel in a circular web hole of a steel beam. Fifth International Conference on Composite Construction in Steel and Concrete, held in Kruger National Park, South Africa, 2004. Conference Proceedings, pp. 544 - 552, 2006.
- [Les2008] Leskelä M.V.: Shear Connection by Transverse Rebars – Shallow Floor Composite Beams. Eurosteel 2008, Graz, Austria. Proceedings Volume A, pp. 273 – 278, 2008.
- [Leo1951] Leonhardt F.: Die Autobahnbrücke über den Rhein bei Köln-Rodenkirchen. Die Bautechnik 28 (1951), Issue 11, pp. 289 – 291. Wilhelm Ernst & Sohn Verlag fuer Architektur und technische Wissenschaften, Berlin, 1951.
- [Leo1987] Leonhardt F., Andrä W., Andrä H.-P., Harre W.: Neues, vorteilhaftes Verbundmittel für Stahlverbund-Tragwerke mit hoher Dauerfestigkeit. Beton- und Stahlbetonbau 12/1987, pp. 325 – 331. Wilhelm Ernst & Sohn Verlag fuer Architektur und technische Wissenschaften, Berlin, 1987.
- [Li1989] Lieberum, K. H.; Reinhardt, K. H.: Strength of concrete on an extremely small bearing area. ACI Structural Journal, Technical Paper, pp. 67 – 76. January – February 1989.
- [Lu1989] Lubliner J., Oliver J., Oller S., Onate E.: A plastic damage model for concrete. Int. J. Solids Structures, Vol. 25, No. 3, pp. 299 – 326. 1989.
- [Ma2014] Manabe Y., Fujiyama C., Kisaku T., Shionaga R.: Influence of coarse aggregate on the shear resistance of perfobond rib shear connector. Science Direct, Procedia Engineering 95 (2014), pp. 454 464. Elsevier Ltd. 2014.
- [Md1988] Mander J. B.; Priestley, M. J. N.; Park, R.: Theoretical stress-strain model for confined concrete. American Society of Civil Engineer (ASCE). Journal of Structural Engineering. Vol. 114, No. 8, pp. 1804 – 1825. August 1988.
- [Mg1997] Mangerig I., Wurzer O.: Zum Tragverhalten von Betondübeln. Tagungsband zur Fachtagung Verbundkonstruktionen, Kaiserslautern, Germany, 1997.
- [Mie1986] Van Mier J. G. M.: Strain-softening of concrete under multiaxial loading conditions. PhD-Thesis, University of Eindhoven, Netherlands. 1984.
- [Mir1992] Mirza, S. A.; Skrabek, B. W.: Statistical analysis of slender composite beam-column strength. American Society of Civil Engineer (ASCE). Journal of Structural Engineering. Vol. 118, No. 5, pp. 1312 – 1332. Mai 1992.

- [NS2015] Braun M., Obiala R., Odenbreit Chr.: Analyses of the load bearing behaviour of deep-embedded concrete dowels, CoSFB. Proceedings of Nordic Steel Conference 2015, Tampere Finland. 2015. Selected by the scientific committee as one of the best contributions and for publishing as article [SC2015].
- [Ogu1997] Oguejiofor E. C., Hosain M. U.: Numerical Analysis of push-out specimens with perfobond rib connectors. *Computers & Structures*, Vol. 62 (1997), No. 4, pp. 617 – 624. Elsevier Ltd. 1997.
- [Pau1974] Paulay T., Park R., Phillips M. H.: Horizontal Construction Joints In Cast-In-Place Reinforced Concrete. American Concrete Institute (ACI), Publication Volume II, pp. 599 – 616, 1974.
- [Pav2013] Pavlovic M.: Resistance of bolted shear connectors in prefabricated composite decks. PhD-Thesis, University of Belgrade, Serbia. 2013.
- [Pe1922] Ilseder Hütte: Handbuch für P-Träger. Peine, Germany 1922.
- [Pel2016] Pelke E., Kurrer K.-E.: Zur Entwicklungsgeschichte des Stahlverbundbaus. *Stahlbau* 85 (2016), Issue 11, pp. 764 – 780. Ernst & Sohn Verlag, Berlin. Germany 2016.
- [Pra1920] Prandtl L.: Ueber die Härte plastischer Körper. *Nachrichten von der königlichen Gesellschaft der Wissenschaften zu Göttingen (Mathematisch physikalische Klasse aus dem Jahre 1920)*, pp. 74 – 85. Berlin 1920.
- [Pru1988] Pruijssers A. F.: Aggregate Interlock and Dowel Action under monotonic and cyclic loading. PhD-Thesis, Delft University Press, 1988.
- [Qur2010] Qureshi J.: Finite element modelling of steel-concrete composite structures. PhD-Thesis, University of Leeds, UK. 2010.
- [Qur2011] Qureshi J., Lam D., Ye J.: Effect of shear connector spacing and layout on the shear connector capacity in composite beams. *Journal of Constructional Steel Research*, No. 67, pp 706-719, 2011.
- [Ra1963] Rasmussen B. H.: Betonindstobte, Tvaerbelastede Boltes og Dornes Baereevne (in Danish), *Bygningsstatistiske Meddelelser*, pp. 39 – 56, 1963. English title: The Carrying Capacity of Transversely Loaded Bolts and Dowels Embedded in Concrete.
- [Re2003] Reitz, D.: Grundlagen zur Bemessung der Perfobondleiste als duktiles Verbundmittel. PhD-Thesis, Darmstadt, Germany. 2003.
- [Ri1928] Richart, F. E.; Brandtzaeg, A.; Brown, R. L.: A study of the failure of concrete under combined compressive stresses. *University of Illinois Bulletin*, No. 185, November 1928, University of Illinois, USA. 1928.
- [Ri1929] Richart, F. E.; Brandtzaeg, A.; Brown, R. L.: The failure of plain and spirally reinforced concrete in compression. *University of Illinois Bulletin*, No. 190, April 1929, University of Illinois, USA. 1929.
- [Ro2011] Rodrigues J. P. C., Laim L.: Behaviour of Perfobond shear connectors at high temperatures. *Engineering Structures* 33 (2011), pp. 2744 – 2753. Elsevier Ltd. 2011.
- [SC2015] Braun M., Obiala R., Odenbreit Chr.: Analyses of the loadbearing behaviour of deep-embedded concrete dowels, CoSFB. *Steel Construction* 8 (2015), Issue 3, pp. 167 – 173. Ernst & Sohn Verlag, Berlin. Germany 2015.

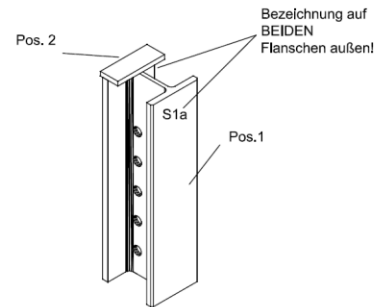
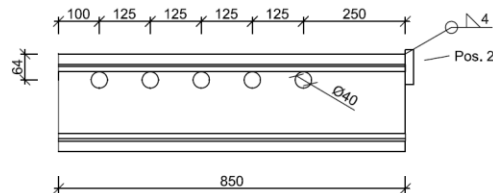
- [Sch2007] Schäfer, M.: Zum Tragverhalten von Flachdecken mit integrierten hohlkastenförmigen Stahlprofilen. PhD-Thesis, University of Wuppertal, Germany. 2007.
- [Se2009] Seidl G.: Behaviour and load bearing capacity of composite dowels in steel-concrete composite girders. PhD-Thesis, Politechnika Wroclawska, Poland, 2009.
- [Sor2016] Sørensen J. H., Hoang L. C., Olesen J. F., Fischer G.: Catenary action in rebars crossing a casting joint loaded in shear. In Proceedings of 11th fib International PhD Symposium in Civil Engineering, pp. 735 – 742. 2016.
- [Sor2017] Sørensen J. H., Hoang L. C., Olesen J. F., Fischer G.: Testing and modeling dowel and catenary action in rebars crossing shear joints in RC. Engineering Structures 145 (2017), pp. 234 – 245, Elsevier Ltd. 2017.
- [Sou1986] Sourashian P., Obaseki K., Rojas M., Sim J.: Analysis of dowel bars acting against concrete core. American Concrete Institute Journal (ACI), pp. 642 – 649, July-August 1986.
- [Sou1987] Sourashian P., Obaseki K., Rojas M.: Bearing strength and stiffness of concrete under reinforcing bars. American Concrete Institute Material Journal (ACI), pp. 179 – 184, May – June 1987.
- [Stb2014a] Braun M., Hechler O., Obiala R.: Untersuchungen zur Verbundwirkung von Betondübeln – Anwendung von tiefliegenden Betondübeln bei Slim-Floor Konstruktionen (CoSFB). Stahlbau 83 (2014), Issue 5, pp. 302 – 308. Ernst & Sohn Verlag, Berlin. Germany 2014.
- [Stb2014b] Braun M., Hechler O., Obiala R., Kuhlmann U., Eggert F., Hauf G., Konrad M.: Experimentelle Untersuchungen von Slim-Floor Trägern in Verbundbauweise – Anwendung von tiefliegenden Betondübeln bei Slim-Floor Konstruktionen (CoSFB). Stahlbau 83 (2014), Issue 10, pp. 741 – 749. Ernst & Sohn Verlag, Berlin. Germany 2014.
- [StK2018] Schäfer M., Braun M., Hauf G.: Flachdecken in Verbundbauweise – Bemessung und Konstruktion von Slim-Floor Trägern. Stahlbau-Kalender 2018, pp. 631 – 741. Ernst & Sohn GmbH & Co. KG. Published 2018, Germany.
- [Su2014] Su Q.-T., Wang W., Luan H.-W., Yang G.-T.: Experimental research on bearing mechanism of perfobond rib shear connectors. Journal of Constructional Steel Research 95 (2014), pp. 22 – 31. Elsevier Ltd. 2014.
- [Szc2015] Szczecina M., Winnicki A.: Calibration of the CDP model parameters in Abaqus. World Congress on Advances in Structural Engineering and Mechanics (ASEM15), 2015. Incheon, Korea, 2015.
- [Ta2011] Tanaka Y., Murakoshi J.: Reexamination of Dowel Behavior of Steel Bars Embedded in Concrete” American Concrete Institute (ACI) Structural Journal, November-December 2011, pp. 659 – 679. 2011.
- [Ti1925] Timoshenko S., Lessels J. M.: Applied elasticity. East Pittsburgh, Pa.: Westinghouse Night School Press 1925, pp. 133 – 141.

- [Val2004] Valente I., Cruz P. J. S.: Experimental analysis of Perfobond shear connection between steel and lightweight concrete. *Journal of Constructional Research* 60 (2004), pp. 465 – 479. Elsevier Ltd. 2004.
- [Val2009] Valente I., Cruz P. J. S.: Experimental analysis of shear connection between steel and lightweight concrete. *Journal of Constructional Research* 65 (2009), pp. 1954 – 1963. Elsevier Ltd. 2009.
- [Via2008] Vianna J. da C., Costa-Neves L. F., Vellasco P. C. G. da S., Andrade S. A. L. de: Structural behaviour of T-Perfobond shear connectors in composite girders: An experimental approach. *Engineering Structures* (2008).
- [Via2009] Vianna J. da C., Costa-Neves L. F., Vellasco P. C. G. da S., Andrade de S. A. L.: Experimental assessment of Perfobond and T-Perfobond shear connectors' structural response. *Journal of Constructional Steel Research* 65 (2009), pp. 408 – 421. Elsevier Ltd. 2009.
- [Via2013] Vianna J. da C., Andrade de S. A. L., Vellasco P. C. G. da S., Costa-Neves L. F.: Experimental study of Perfobond shear connectors in composite construction. *Journal of Constructional Research* 81 (2013), pp. 62 – 75. Elsevier Ltd. 2013.
- [Vin1986] Vintzeleou E. N., Tassios T. P.: Mathematical models for dowel action under monotonic and cyclic conditions. *Magazine of Concrete Research* (London), Vol 38, No. 134, pp. 13 – 22, March 1986.
- [Vin1987] Vintzeleou E. N., Tassios T. P.: Behavior of dowels under cyclic deformations. *American Concrete Institute Structural Journal (ACI)*, pp. 18 – 30, January - February 1987.
- [Vo1993] Vonk R. A.: A micromechanical investigation of softening of concrete loaded in compression. *HERON*, Vol. 38, No. 3. 1993.
- [Wa2011] Wagner R.: Untersuchungen zum Verbundverhalten von Betondübeln in vorwiegend ruhend und nicht ruhend beanspruchten Konstruktionen. *Stahlbau* 80 (2011), , Issue 4, pp. 250 – 255. Ernst & Sohn Verlag fuer Architektur und technische Wissenschaften. Berlin, Germany 2011.
- [Wi2013] Wiese S.: Zum Tragverhalten der neuartigen Verbundmittel "Stahlschare" fuer den filigranen Stahl-Beton-Verbundbau. PhD-Thesis, University of Kaiserslautern, Germany, 2013.
- [Wu1998] Wurzer O.: Zur Tragfähigkeit von Betondübeln. PhD-Thesis, University of the German Armed Forces Munich, Germany, 1998.
- [Za2001] Zapfe C.: Trag- und Verformungsverhalten von Verbundträgern mit Betondübeln zur Uebertragung der Längsschubkräfte. PhD-Thesis, University of the German Armed Forces Munich, Germany, 2001.
- [Za2003] Mangerig I., Zapfe C.: Concrete dowels in composite construction. *Japanese-German Bridge Symposium*, Osaka, Japan 2003.
- [Ze2016] Zheng S., Liu Y., Yoda T., Lin W.: Parametric study on shear capacity of circular-hole and long-hole perfobond shear connector. *Journal of Constructional Research* 117 (2016), pp. 64 – 80. Elsevier Ltd. 2016.

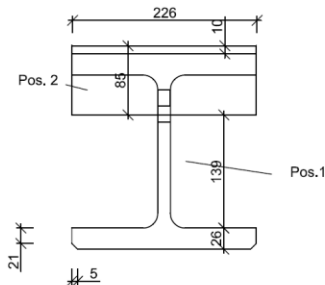
Annex A – Drawings of Push-Out Tests

Push-Out Tests CoSFB (Serie 1a) 6 Stück

Pos.1 HEM220 (l=850mm) S355M inkl. Bohrung M. 1:10



Pos.2 BL 226/85mm (t=20mm) S355 M. 1:5



Alle HEM220-Träger dieses Plans sind auf BEIDEN Oberseiten der Flansche mit S1a zu kennzeichnen. Der untere Flansch ist mit 5mm anzufasen!

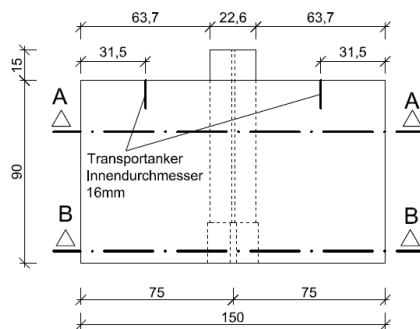
Maße in mm

Summe Stahl				
Pos.	Bez.	Stk.	Material	Gewicht
1	HEM220 l=850mm	6	S355M	599kg
2	Blech 226/85/20	6	S355	18kg
			Summe	617kg

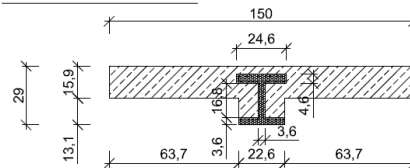
Universität Stuttgart Institut für Konstruktion und Entwurf Pfaffenwaldring 7, 70569 Stuttgart Tel. 0711 - 685- 66243 Fax. 0711 - 685- 66236			
Projekt: CoSFB Zula			
Plan titel: CoSFB POST Serie 1a Stahlplan			
Maßstab: var	gez.: Eg	Plan-Nr. 1a/1	Datum: 17.02.2011
	gepr.:		

Schalplan Push-Out Tests mit HEM220 (Serie 1a) 6 Stück

Seitenansicht M. 1:20



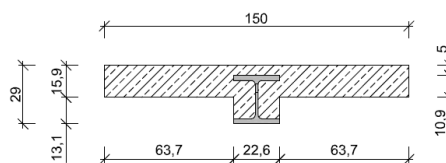
Schnitt B-B M. 1:20



- Beton C20/25
- Stahlprofil HEM 220
- Styropor

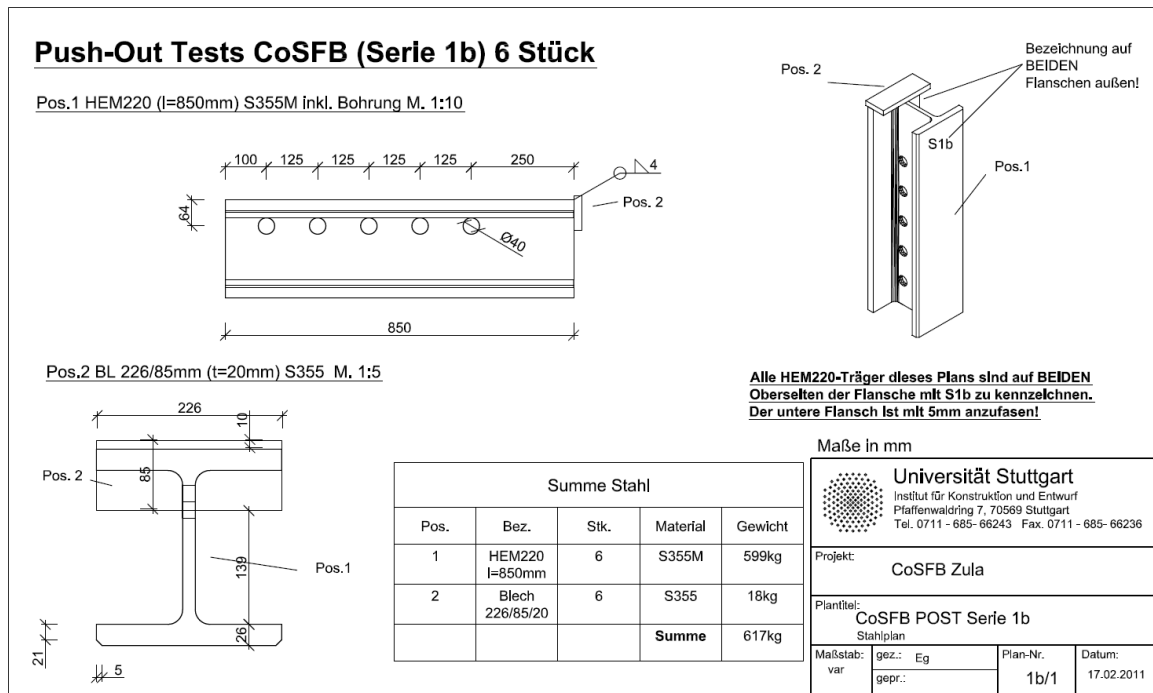
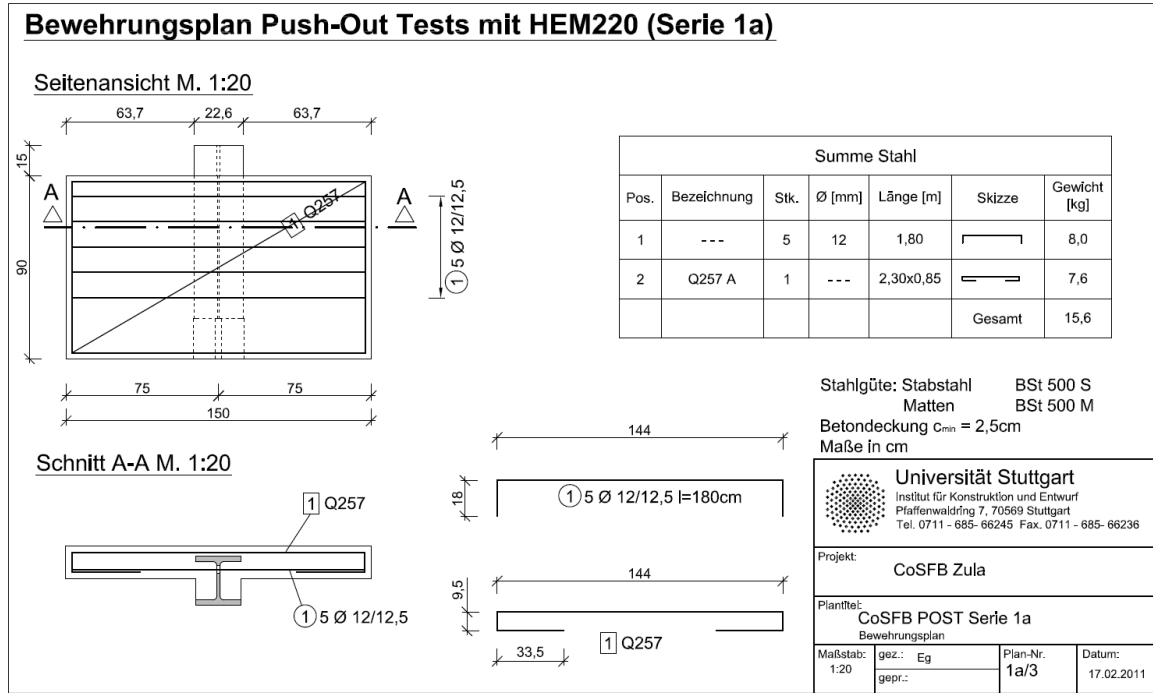
Maße in cm, Betonfestigkeit f_{ck} in N/mm²

Schnitt A-A M. 1:20



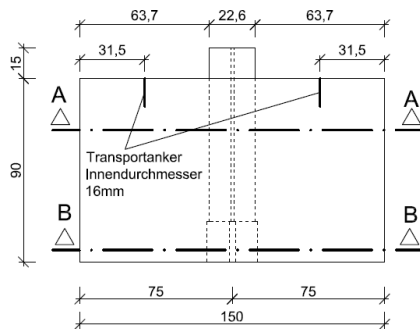
Beton	
Anzahl Prüfkörper	f _{ck} , cube
6	25

Universität Stuttgart Institut für Konstruktion und Entwurf Pfaffenwaldring 7, 70569 Stuttgart Tel. 0711 - 685- 66245 Fax. 0711 - 685- 66236			
Projekt: CoSFB Zula			
Plan titel: CoSFB POST Serie 1a Schalplan			
Maßstab: 1:20	gez.: Eg	Plan-Nr. 1a/2	Datum: 17.02.2011
	gepr.:		

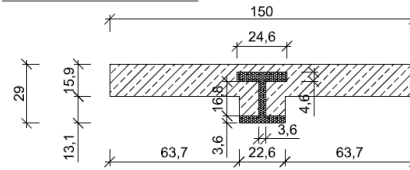


Schalplan Push-Out Tests mit HEM220 (Serie 1b) 6 Stück

Seitenansicht M. 1:20



Schnitt B-B M. 1:20

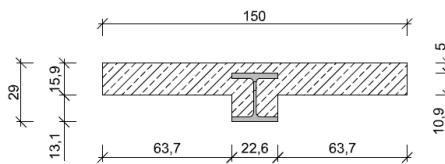


- Beton C50/60
- Stahlprofil HEM 220
- Styropor

Maße in cm, Betonfestigkeit f_{ck} in N/mm²

Universität Stuttgart Institut für Konstruktion und Entwurf Pfaffenwaldring 7, 70569 Stuttgart Tel. 0711 - 685-66245 Fax. 0711 - 685-66236			
Projekt: CoSFB Zula			
Plantheit: CoSFB POST Serie 1b Schalplan			
Maßstab: 1:20	gez.: Eg	Plan-Nr. 1b/2	Datum: 17.02.2011
	gepr.:		

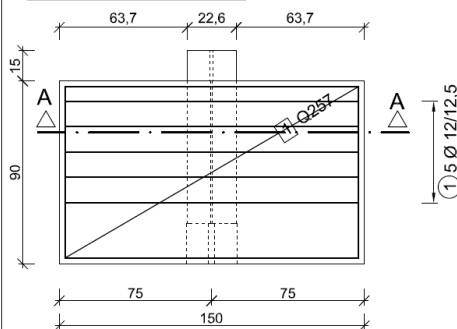
Schnitt A-A M. 1:20



Beton	
Anzahl Prüfkörper	$f_{ck, cube}$
6	60

Bewehrungsplan Push-Out Tests mit HEM220 (Serie 1b)

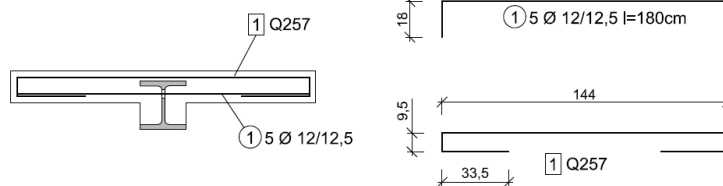
Seitenansicht M. 1:20



Summe Stahl					
Pos.	Bezeichnung	Stk.	Ø [mm]	Länge [m]	Gewicht [kg]
1	---	5	12	1,80	8,0
2	Q257 A	1	---	2,30x0,85	7,6
				Gesamt	15,6

Stahlgüte: Stabstahl BS 500 S
 Matten BS 500 M
 Betondeckung $c_{nom} = 2,5cm$
 Maße in cm

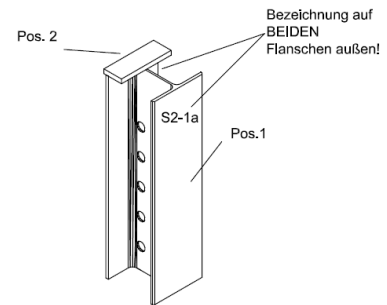
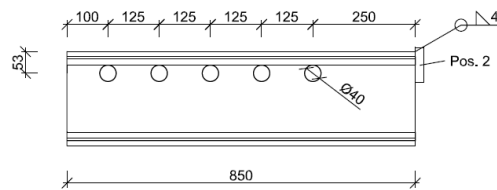
Schnitt A-A M. 1:20



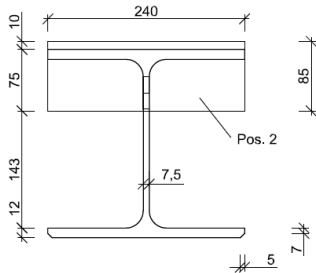
Universität Stuttgart Institut für Konstruktion und Entwurf Pfaffenwaldring 7, 70569 Stuttgart Tel. 0711 - 685-66245 Fax. 0711 - 685-66236			
Projekt: CoSFB Zula			
Plantheit: CoSFB POST Serie 1b Bewehrungsplan			
Maßstab: 1:20	gez.: Eg	Plan-Nr. 1b/3	Datum: 17.02.2011
	gepr.:		

Push-Out Tests CoSFB (Serie 2-1a) 6 Stück

Pos.1 HEA240 (l=850mm) S355M inkl. Bohrung M. 1:10



Pos.2 BL 240/85mm (t=20mm) S355 M. 1:5



Alle HEA240-Träger dieses Plans sind auf BEIDEN Oberseiten der Flansche mit S2-1a zu kennzeichnen. Der untere Flansch ist mit 5mm anzufasen!

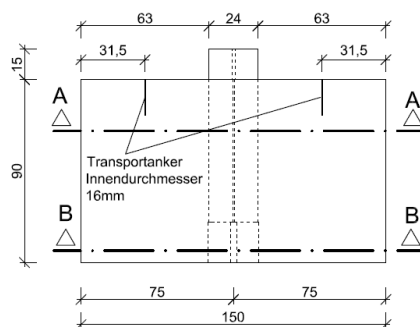
Maße in mm

Summe Stahl				
Pos.	Bez.	Stk.	Material	Gewicht
1	HEA240 l=850mm	6	S355M	308kg
2	Blech 240/85/20	6	S355	20kg
			Summe	328kg

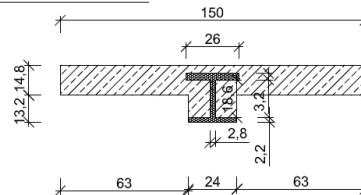
Universität Stuttgart Institut für Konstruktion und Entwurf Pfaffenwaldring 7, 70569 Stuttgart Tel. 0711 - 685-66243 Fax. 0711 - 685-66236			
Projekt:	CoSFB Zula		
Plantitel:	CoSFB POST Serie 2-1a		
Maßstab:	gez.: Eg	Plan-Nr.	Datum:
var	gepr.:	2-1a/1	17.02.2011

Schalplan Push-Out Tests mit HEA240 (Serie 2-1a) 6 Stück

Seitenansicht M. 1:20



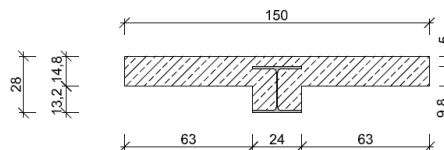
Schnitt B-B M. 1:20



- Beton C30/37
- Stahlprofil HEA 240
- Styropor

Maße in cm, Betonfestigkeit f_{ck} in N/mm²

Schnitt A-A M. 1:20

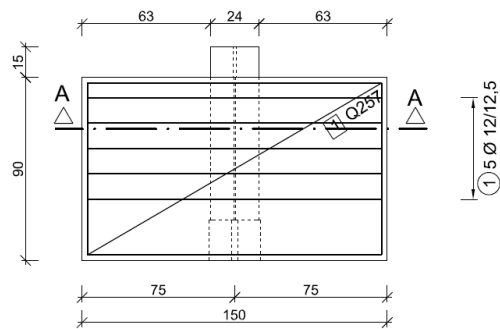


Beton	
Anzahl	$f_{ck, cube}$
6	37

Universität Stuttgart Institut für Konstruktion und Entwurf Pfaffenwaldring 7, 70569 Stuttgart Tel. 0711 - 685-66245 Fax. 0711 - 685-66236			
Projekt:	CoSFB Zula		
Plantitel:	CoSFB POST Serie 2-1a		
Maßstab:	gez.: Eg	Plan-Nr.	Datum:
1:20	gepr.:	2-1a/2	17.02.2011

Bewehrungsplan Push-Out Tests mit HEA240 (Serie 2-1a)

Seitenansicht M. 1:20



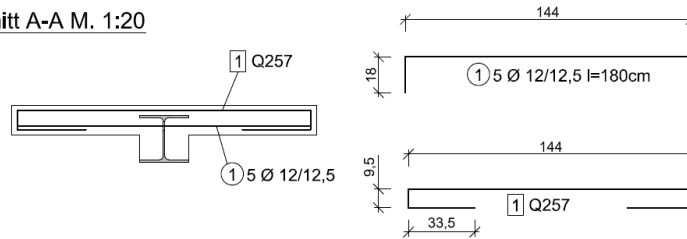
Summe Stahl						
Pos.	Bezeichnung	Stk.	Ø [mm]	Länge [m]	Skizze	Gewicht [kg]
1	---	5	12	1,80		8,0
2	Q257 A	1	---	2,30x0,85		7,6
					Gesamt	15,6

Stahlgüte: Stabstahl BSt 500 S
Matten BSt 500 M

Betondeckung $c_{\text{nom}} = 2,5\text{cm}$

Maße in cm

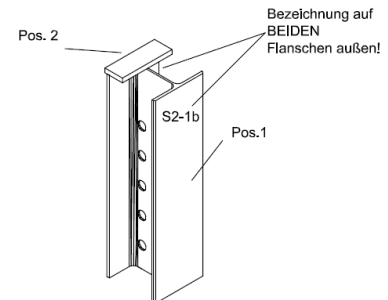
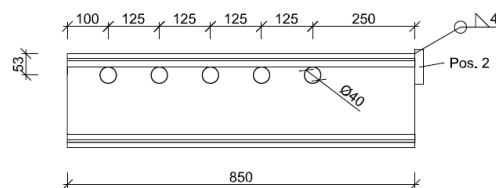
Schnitt A-A M. 1:20



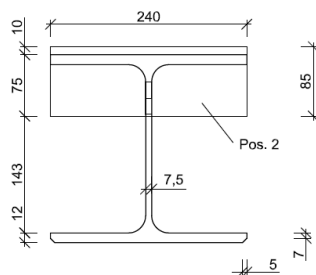
Universität Stuttgart Institut für Konstruktion und Entwurf Pfaffenwaldring 7, 70569 Stuttgart Tel. 0711 - 685-66245 Fax. 0711 - 685-66236			
Projekt: CoSFB Zula			
Planftitel: CoSFB POST Serie 2-1a Bewehrungsplan			
Maßstab: 1:20	gez.: Eg	Plan-Nr. 2-1a/3	Datum: 17.02.2011
	gepr.:		

Push-Out Tests CoSFB (Serie 2-1b) 6 Stück

Pos.1 HEA240 (l=850mm) S355M inkl. Bohrung M. 1:10



Pos.2 BL 240/85mm (t=20mm) S355 M. 1:5

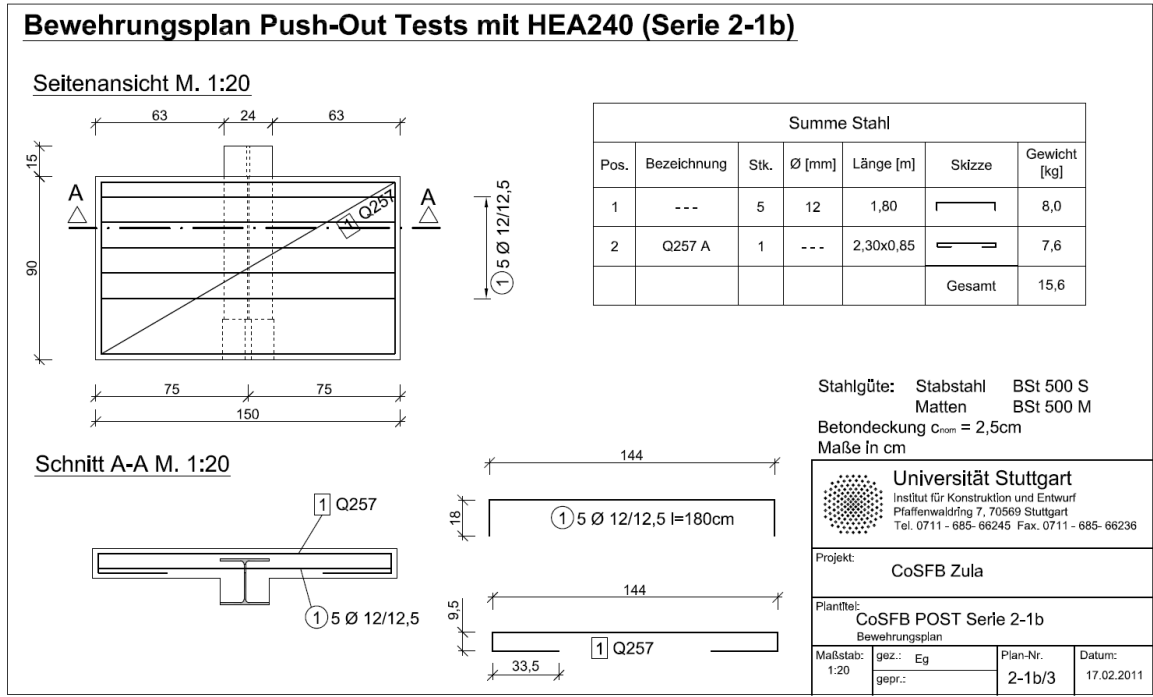
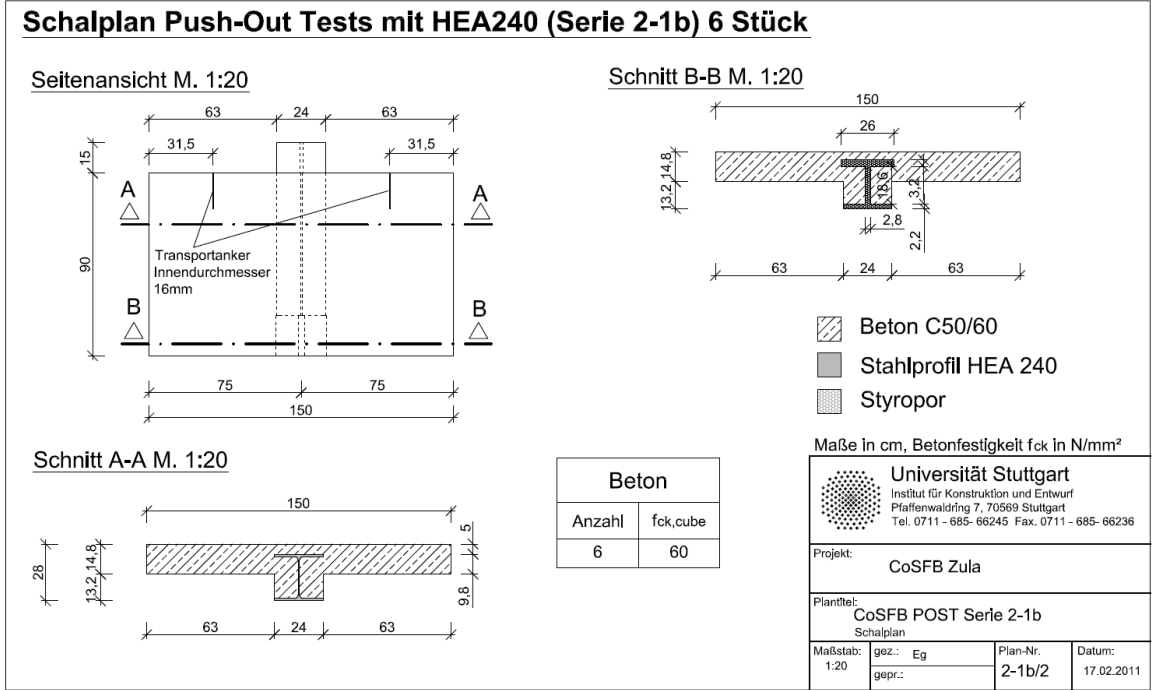


Alle HEA240-Träger dieses Plans sind auf BEIDEN Oberseiten der Flansche mit S2-1b zu kennzeichnen. Der untere Flansch ist mit 5mm anzufasen!

Maße in mm

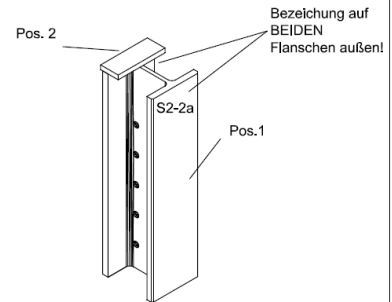
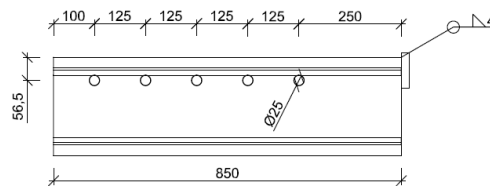
Summe Stahl				
Pos.	Bez.	Stk.	Material	Gewicht
1	HEA240 l=850mm	6	S355M	308kg
2	Blech 240/85/20	6	S355	20kg
			Summe	328kg

Universität Stuttgart Institut für Konstruktion und Entwurf Pfaffenwaldring 7, 70569 Stuttgart Tel. 0711 - 685-66243 Fax. 0711 - 685-66236			
Projekt: CoSFB Zula			
Planftitel: CoSFB POST Serie 2-1b Stahlplan			
Maßstab: var	gez.: Eg	Plan-Nr. 2-1b/1	Datum: 17.02.2011
	gepr.:		

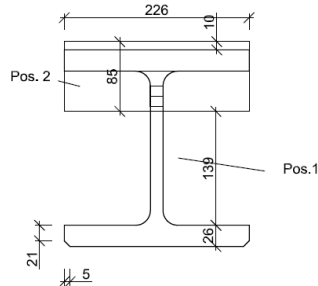


Push-Out Tests CoSFB (Serie 2-2a) 6 Stück

Pos.1 HEM220 (l=850mm) S355M inkl. Bohrung M. 1:10



Pos.2 BL 226/85mm (t=20mm) S355 M. 1:5



Alle HEM220-Träger dieses Plans sind auf BEIDEN Oberseiten der Flansche mit S2-2a zu kennzeichnen. Der untere Flansch ist mit 5mm anzufasen!

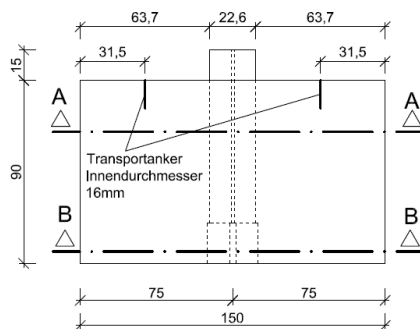
Maße in mm

Summe Stahl				
Pos.	Bez.	Stk.	Material	Gewicht
1	HEM220 l=850mm	6	S355M	599kg
2	Blech 226/85/20	6	S355	18kg
	Summe			617kg

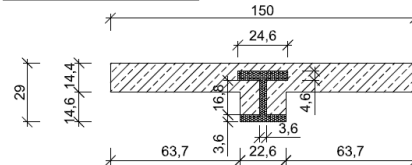
Universität Stuttgart Institut für Konstruktion und Entwurf Pfaffenwaldring 7, 70569 Stuttgart Tel. 0711 - 685-66243 Fax. 0711 - 685-66236			
Projekt: CoSFB Zula			
Planltitel: CoSFB POST Serie 2-2a Stahlplan			
Maßstab: var	gez.: Eg gepr.:	Plan-Nr. 2-2a/1	Datum: 17.02.2011

Schalplan Push-Out Tests mit HEM220 (Serie 2-2a) 6 Stück

Seitenansicht M. 1:20



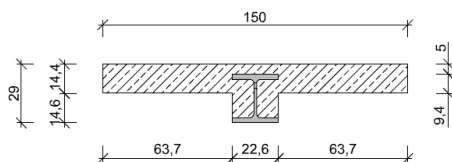
Schnitt B-B M. 1:20



- Beton C30/37
- Stahlprofil HEM 220
- Styropor

Maße in cm, Betonfestigkeit f_c in N/mm²

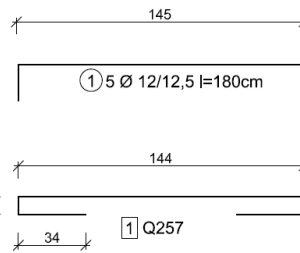
Schnitt A-A M. 1:20



Beton	
Anzahl Prüfkörper	$f_{ck,cube}$
6	37

Universität Stuttgart Institut für Konstruktion und Entwurf Pfaffenwaldring 7, 70569 Stuttgart Tel. 0711 - 685-66245 Fax. 0711 - 685-66236			
Projekt: CoSFB Zula			
Planltitel: CoSFB POST Serie 2-2a Schalplan			
Maßstab: 1:20	gez.: Eg gepr.:	Plan-Nr. 2-2a/2	Datum: 17.02.2011

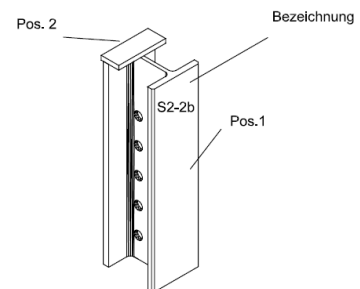
Seitenansicht M. 1:20



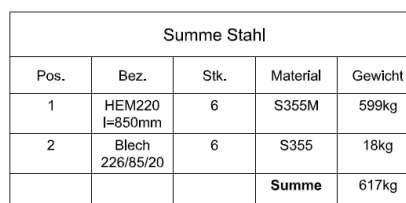
Stahlgüte: Stabstahl BSt 500 S
Matten BSt 500 M
Betondeckung $c_{\text{nom}} = 2,5\text{cm}$
Maße in cm

	Universität Stuttgart Institut für Konstruktion und Entwurf Pfaffenwalderweg 7, 70569 Stuttgart Tel. 0711 - 685- 66245 Fax. 0711 - 685- 66236		
	Projekt: CoSFB Zula		
Plantfest: CoSFB POST Serie 2-2a Bewehrungsplan			
Maßstab: 1:20	gez.: Eg gepr.:	Plan-Nr. 2-2a/3	Datum: 17.02.2011

Pos.1 HEM220 (l=850mm) S355M inkl. Bohrung M. 1:10



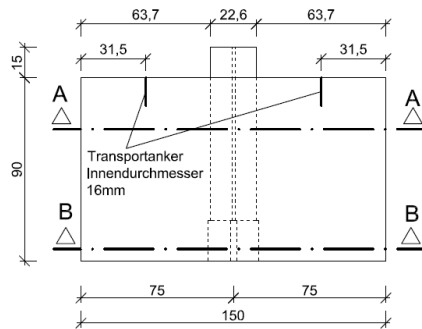
**Alle HEM220-Träger dieses Plans sind auf BEIDEN
Oberselten der Flansche mit S2-2b zu kennzeichnen.
Der untere Flansch ist mit 5mm anzufasen!**



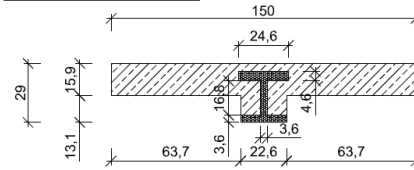
Maße in mm			
 Universität Stuttgart Institut für Konstruktion und Entwurf Pfaffenwaldring 7, 70569 Stuttgart Tel. 0711 - 685- 66243 Fax. 0711 - 685- 66236			
Projekt:		CoSFB Zula	
Plantitel:		CoSFB POST Serie 2-2b Stahlplan	
Maßstab: var	gez.: gepr.: Eg	Plan-Nr. 2-2b/1	Datum: 17.02.2011

Schalplan Push-Out Tests mit HEM220 (Serie 2-2b) 6 Stück

Seitenansicht M. 1:20



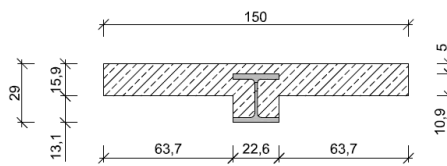
Schnitt B-B M. 1:20



- Beton C30/37
- Stahlprofil HEM 220
- Styropor

Maße in cm, Betonfestigkeit f_{ck} in N/mm²

Schnitt A-A M. 1:20

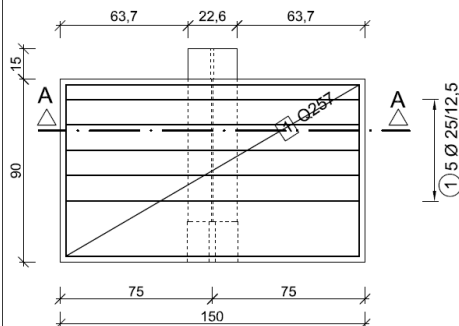


Beton	
Anzahl Prüfkörper	$f_{ck, cube}$
6	37

Universität Stuttgart Institut für Konstruktion und Entwurf Pfaffenwaldring 7, 70569 Stuttgart Tel. 0711 - 685-66245 Fax. 0711 - 685-66236			
Projekt:		CoSFB Zula	
Plantitel:		CoSFB POST Serie 2-2b	
Maßstab:		gez.: Eg	Plan-Nr. 2-2b/2
1:20		gepr.:	Datum: 17.02.2011

Bewehrungsplan Push-Out Tests mit HEM220 (Serie 2-2b)

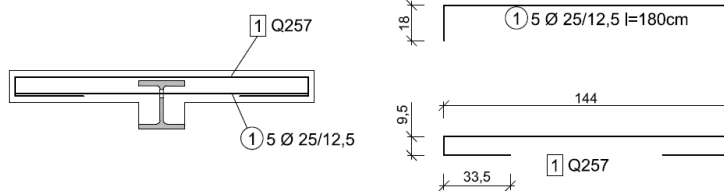
Seitenansicht M. 1:20



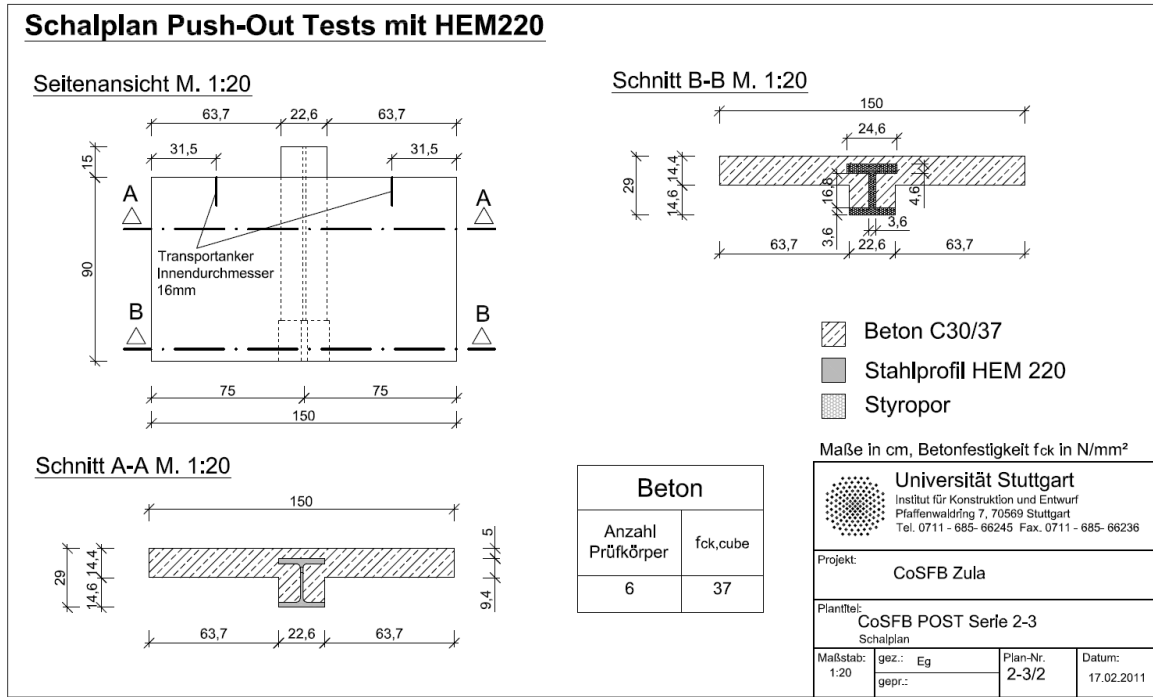
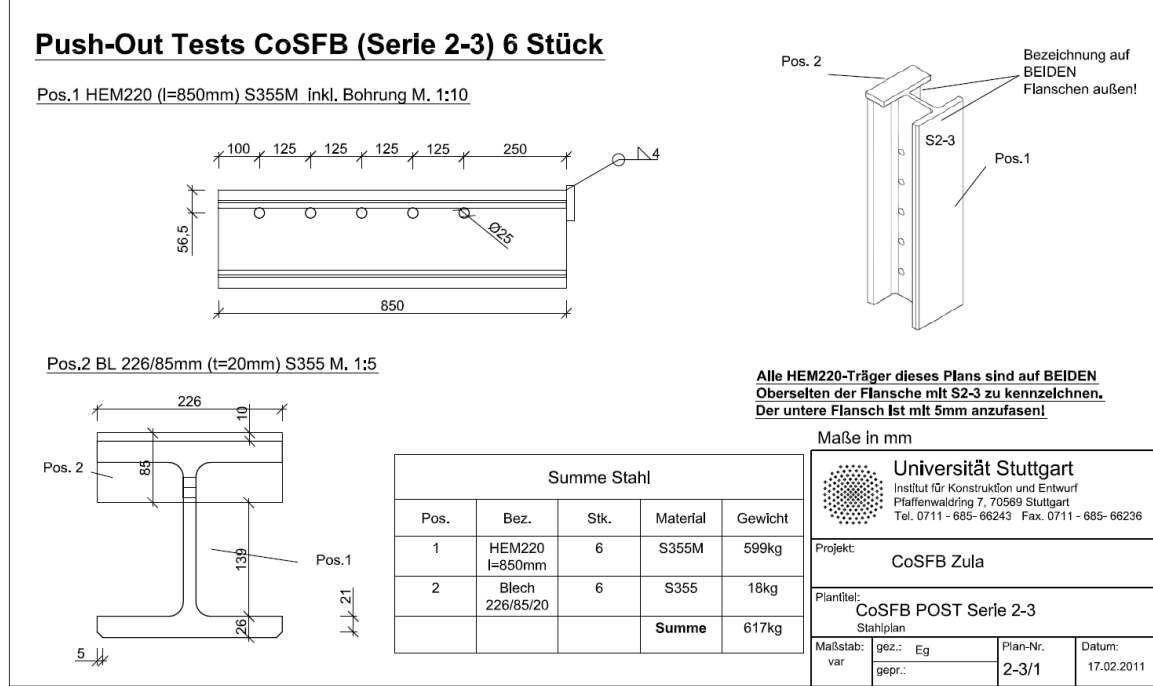
Summe Stahl					
Pos.	Bezeichnung	Stk.	Ø [mm]	Länge [m]	Gewicht [kg]
1	---	5	25	1,80	34,7
2	Q257 A	1	---	2,30x0,85	7,6
				Gesamt	42,3

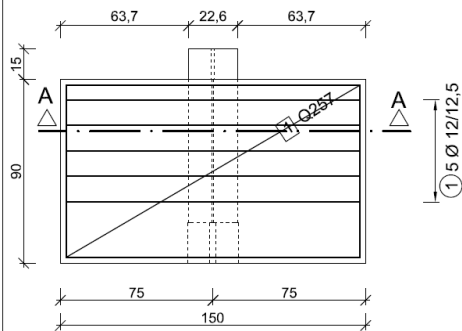
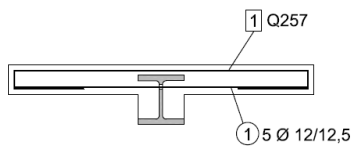
Stahlgüte: Stabstahl BSt 500 S
 Matten BSt 500 M
 Betondeckung $c_{nom} = 2,5\text{cm}$
 Maße in cm

Schnitt A-A M. 1:20



Universität Stuttgart Institut für Konstruktion und Entwurf Pfaffenwaldring 7, 70569 Stuttgart Tel. 0711 - 685-66245 Fax. 0711 - 685-66236			
Projekt:		CoSFB Zula	
Plantitel:		CoSFB POST Serie 2-2b	
Maßstab:		gez.: Eg	Plan-Nr. 2-2b/3
1:20		gepr.:	Datum: 17.02.2011



Bewehrungsplan Push-Out Tests mit HEM220 (Serie 2-3)**Seitenansicht M. 1:20****Schnitt A-A M. 1:20**

Summe Stahl					
Pos.	Bezeichnung	Stk.	Ø [mm]	Länge [m]	Gewicht [kg]
1	---	5	12	1,80	7,9
2	Q257 A	1	---	2,30x0,85	7,6
Gesamt					15,5

Stahlgüte: Stabstahl BS 500 S
Matten BS 500 M
Betondeckung $c_{nom} = 2,5\text{cm}$
Maße in cm

 Universität Stuttgart Institut für Konstruktion und Entwurf Pfaffenwaldring 7, 70569 Stuttgart Tel. 0711 - 685-66245 Fax. 0711 - 685-66236			
Projekt: CoSFB Zula			
Plan titel: CoSFB POST Serie 2-3 Bewehrungsplan			
Maßstab: 1:20	gez.: Eg	Plan-Nr: 2-3/3	Datum: 17.02.2011

Annex B – Test Results

Table 3.2.1: Overview - CoSFB Push-out Tests 2009 + 2011 [Stu2009], [Stu2011]

Year	Series	Test	Section	t_{web} [mm]	web opening [mm]	dowel reinf. [mm]	Concrete Class [MPa]	max. Test Load [kN]
2009	P1	1	HE220M	15.5	40	12	31.8	2141
		2					34.9	2292
		3					35.3	2070
	P2	1	HE220M	15.5	40	12	45.6	2249
		2					36.4	2343
		3					36.3	2254
2011	1a	1	HE220M	15.5	40	12	26.8	1895.5
		2					26.6	1930.5
		3					26.8	2065
	1b	1	HE220M	15.5	40	12	54.4	1668
		2					54.7	1612.5
		3					56.1	1684
	2-1a	1	HE240A	7.5	40	12	29.2	1579.5
		2					29.6	1841
		3					29.6	1764.5
	2-1b	1	HE240A	7.5	40	12	56.9	1536
		2					60.0	1582.5
		3					57.6	1655.5
	2-2a	1	HE220M	15.5	25	12	32.2	2033
		2					32.6	2022
		3					33.3	2034
	2-2b	1	HE220M	15.5	40	25	38.6	4143
		2					41.1	3993
		3					40.4	3798.5
	2-3	1	HE220M	15.5	25	12	37.7	1377.5
		2					38.4	1486
		3					38.7	1386

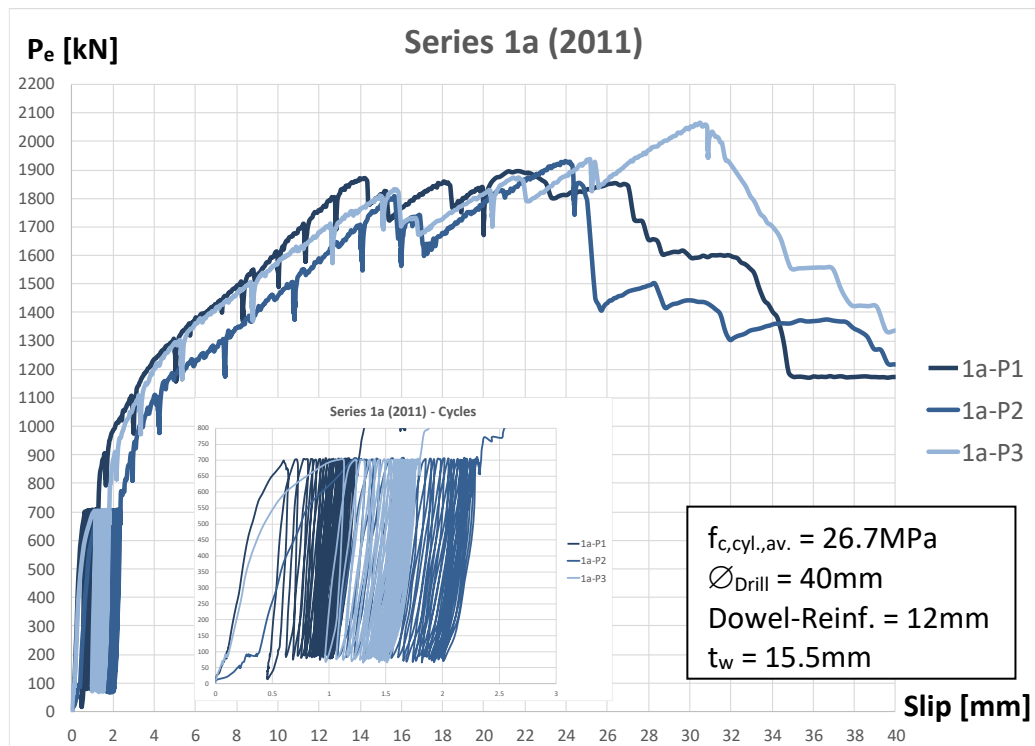
B1 – Load-Slip Curves

Figure B-1a: Load-Slip Curves Series 1a

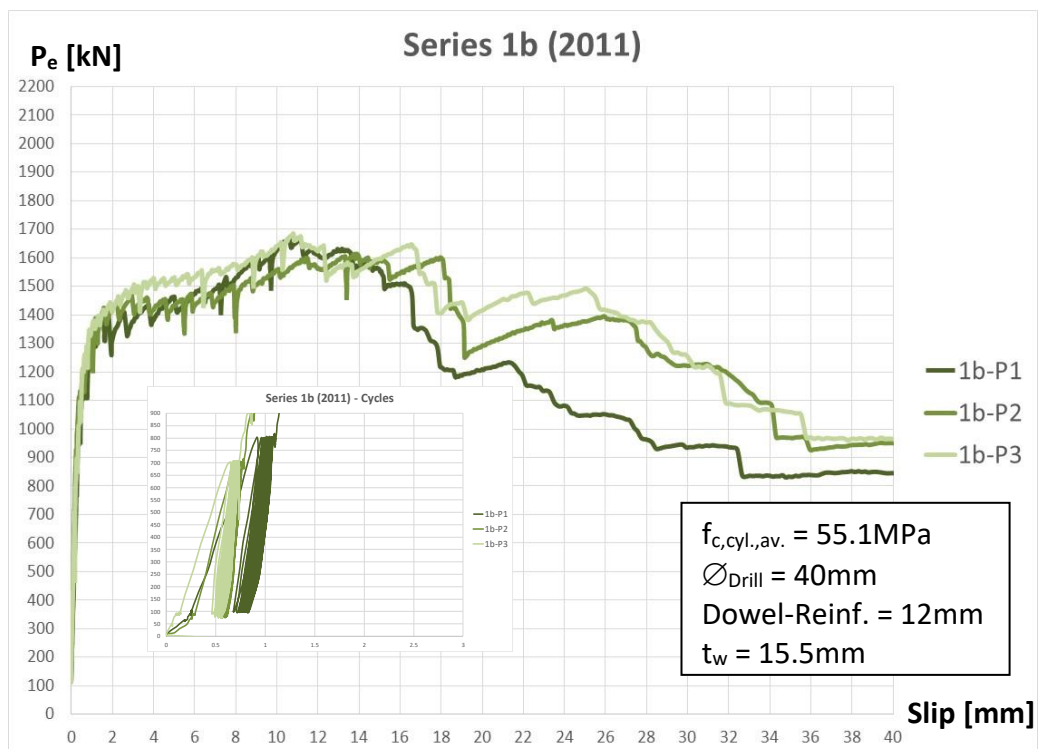


Figure B-1b: Load-Slip Curves Series 1b

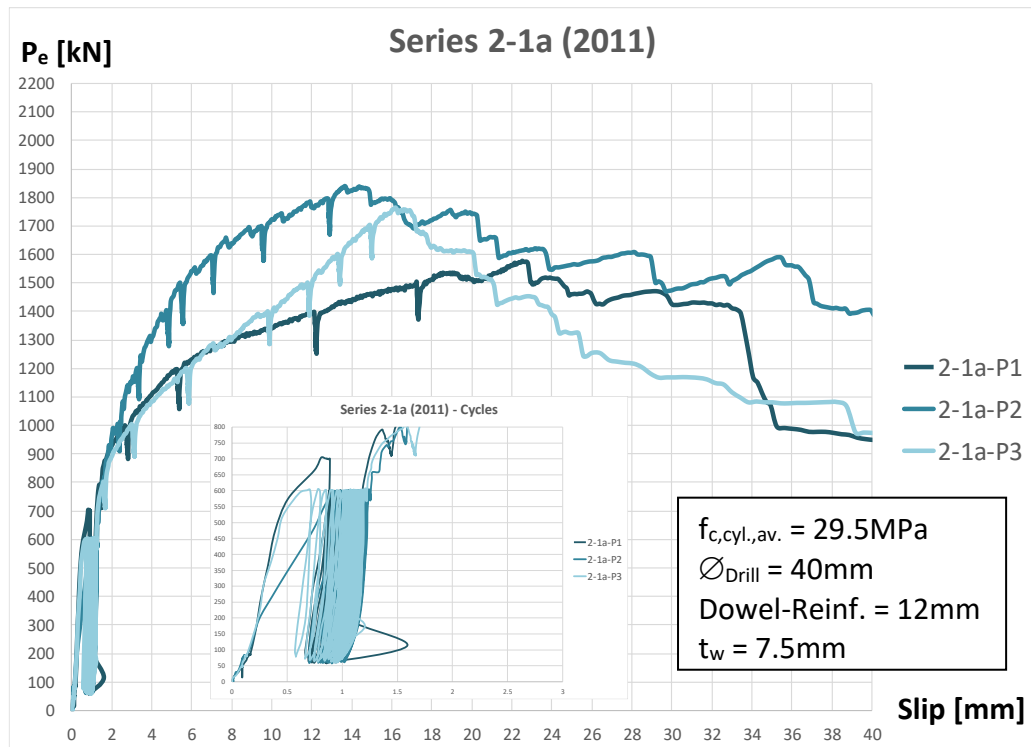


Figure B-2-1a: Load-Slip Curves Series 2-1a

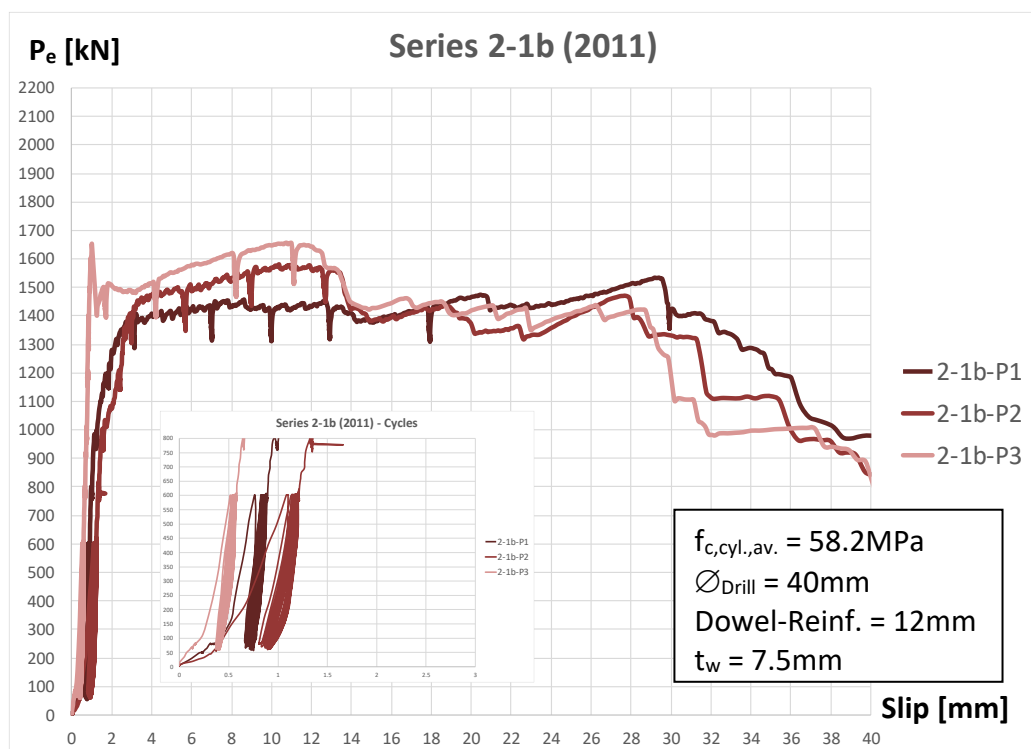


Figure B-2-1b: Load-Slip Curves Series 2-1b

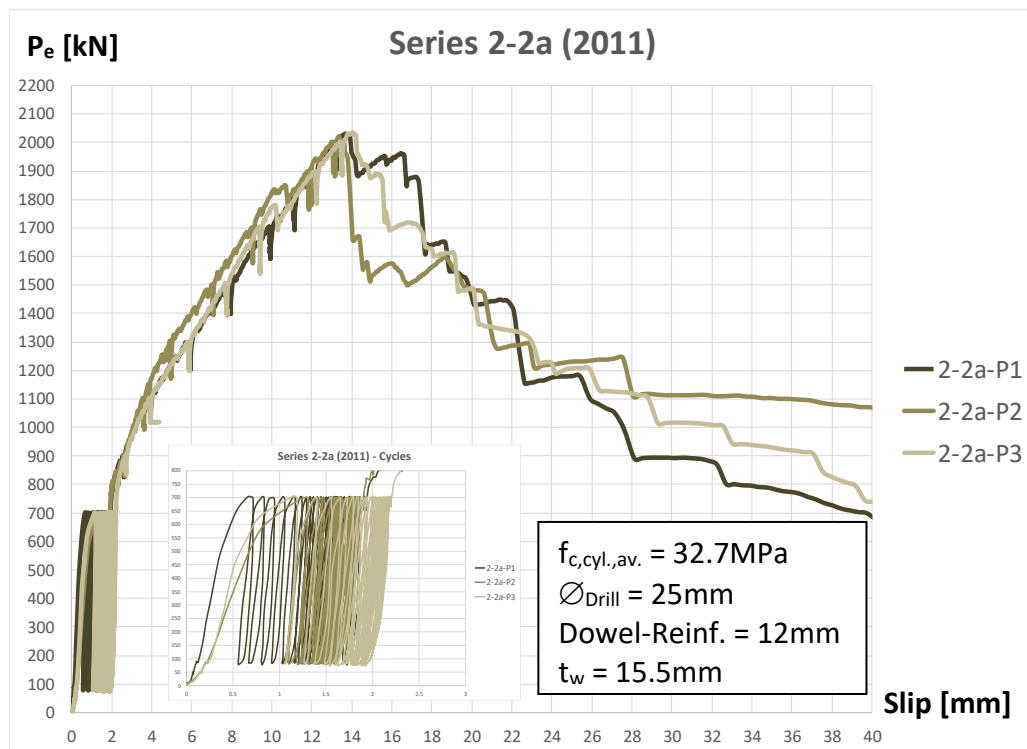


Figure B-2-2a: Load-Slip Curves Series 2-2a

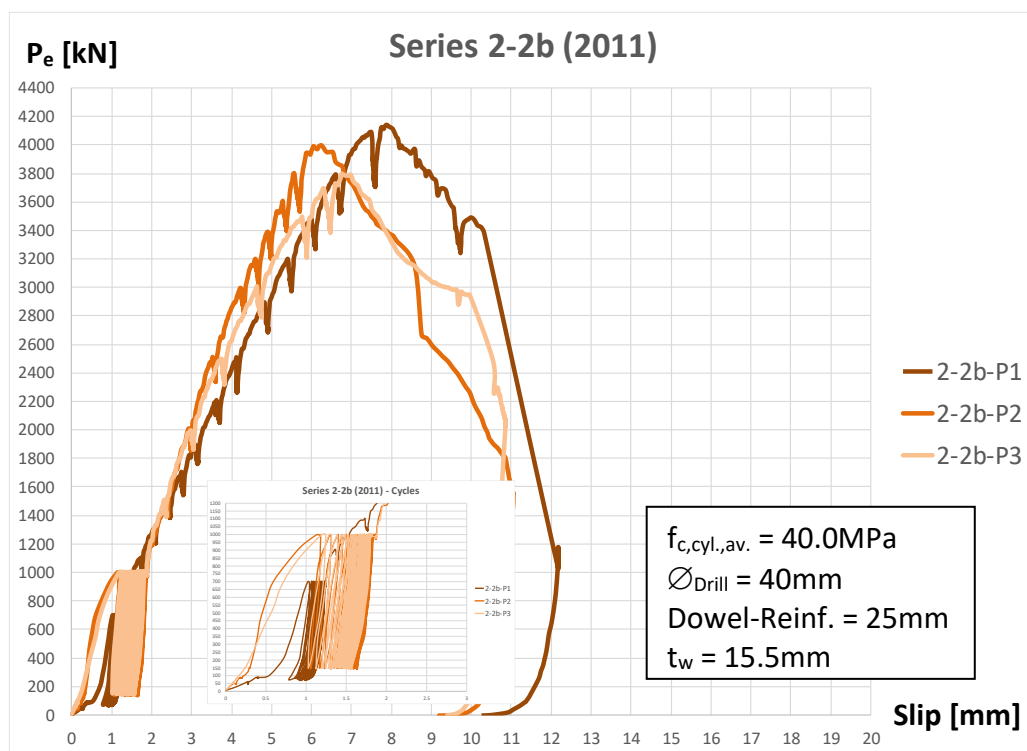


Figure B-2-2b: Load-Slip Curves Series 2-2b

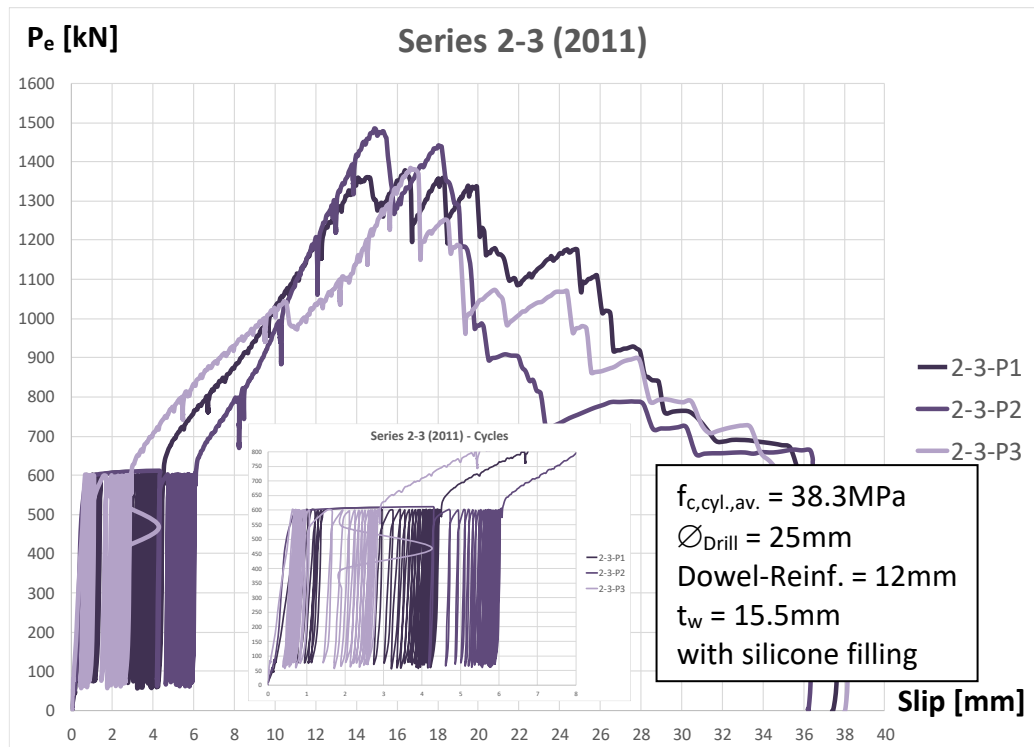


Figure B-2-3: Load-Slip Cuves Series 2-3

B2 – Load-Slip Curves, Initial Stiffness S_{ini} and P_{linear}

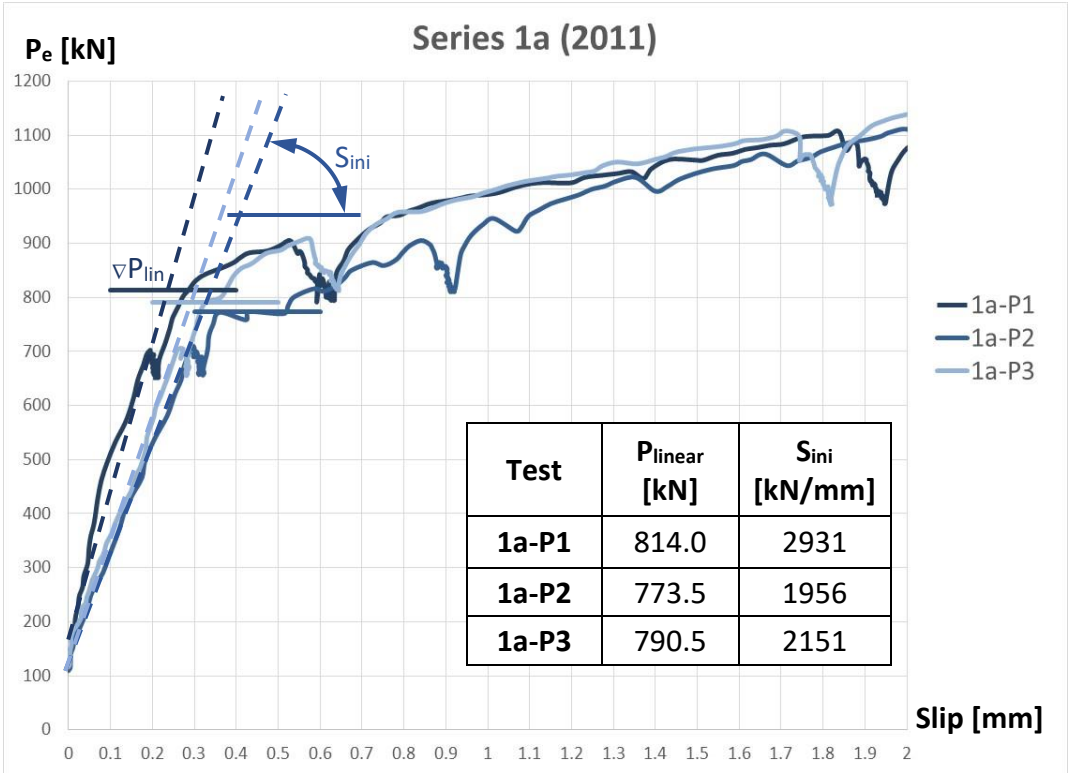


Figure B2.1: Push-out test Series 1a, linear range

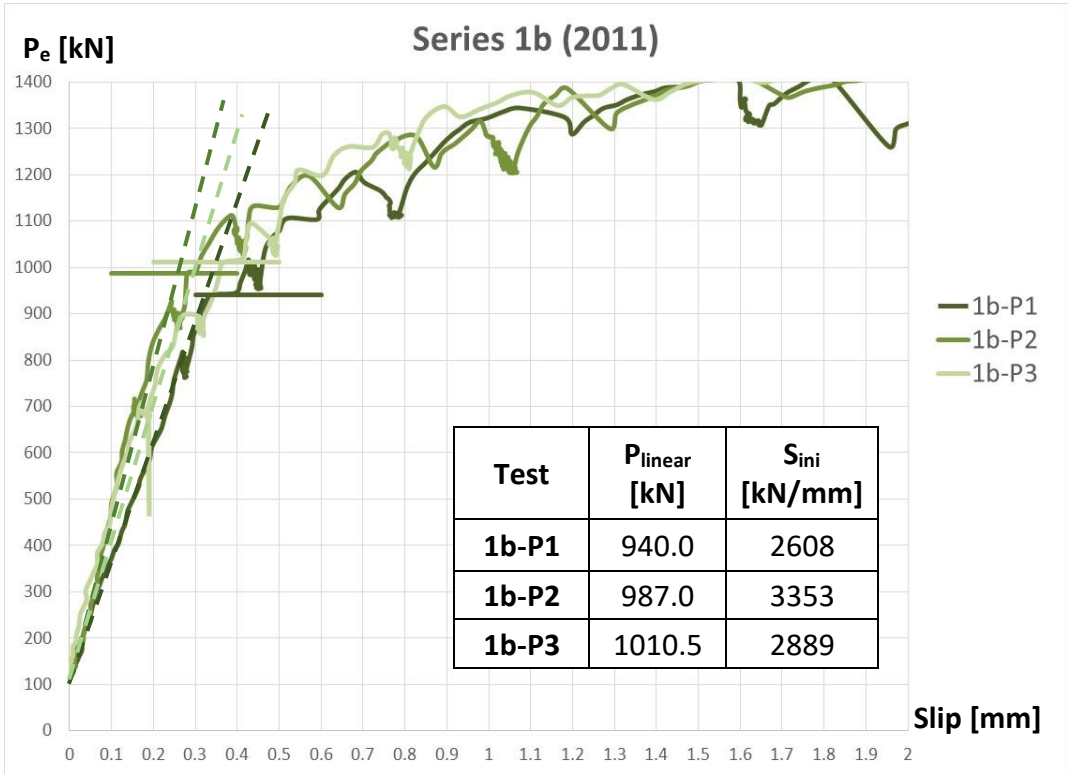


Figure B2.2: Push-out test Series 1b, linear range

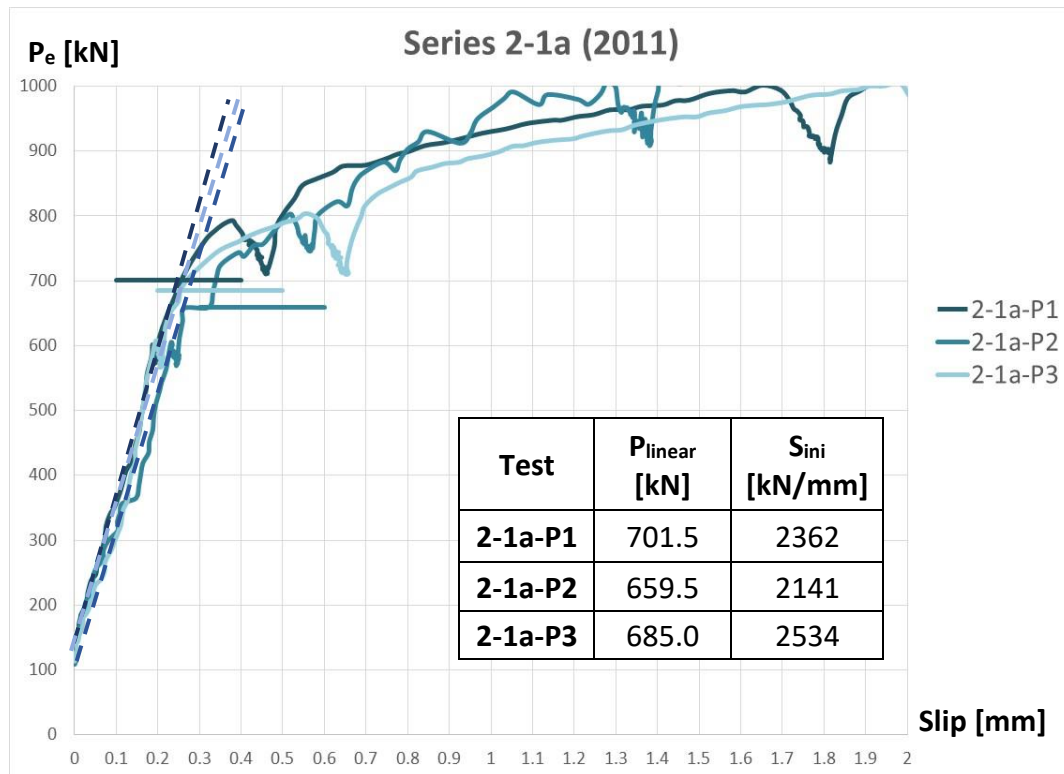


Figure B2.3: Push-out test Series 2-1a, linear range

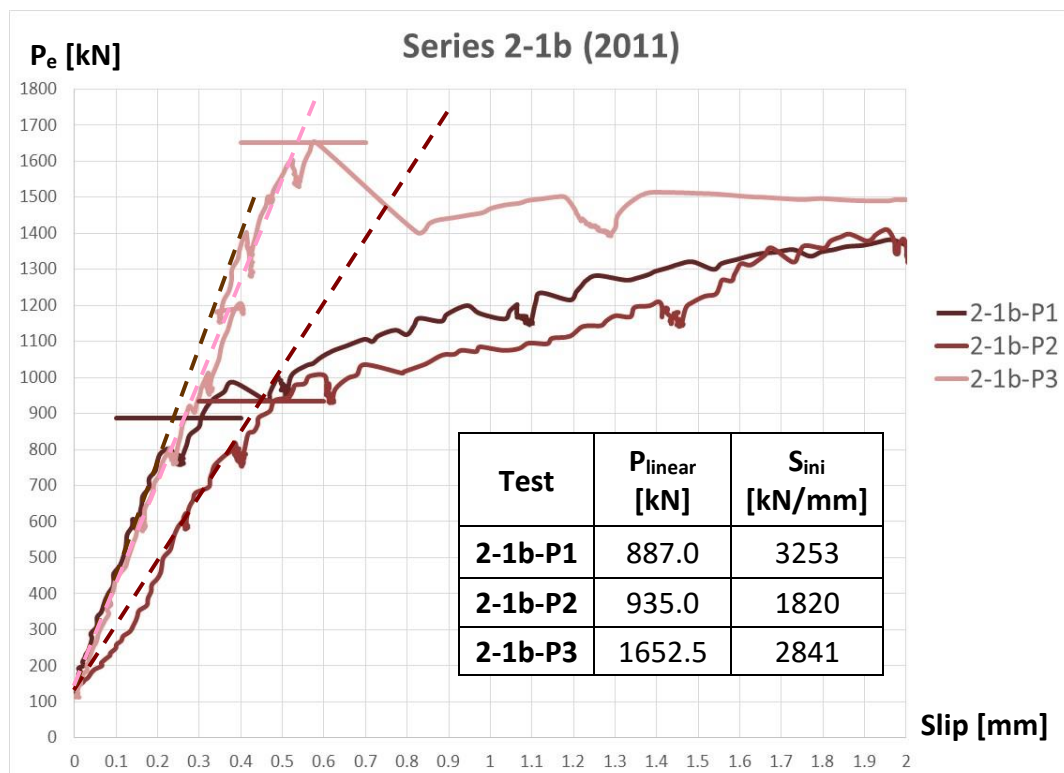


Figure B2.4: Push-out test Series 2-1b, linear range

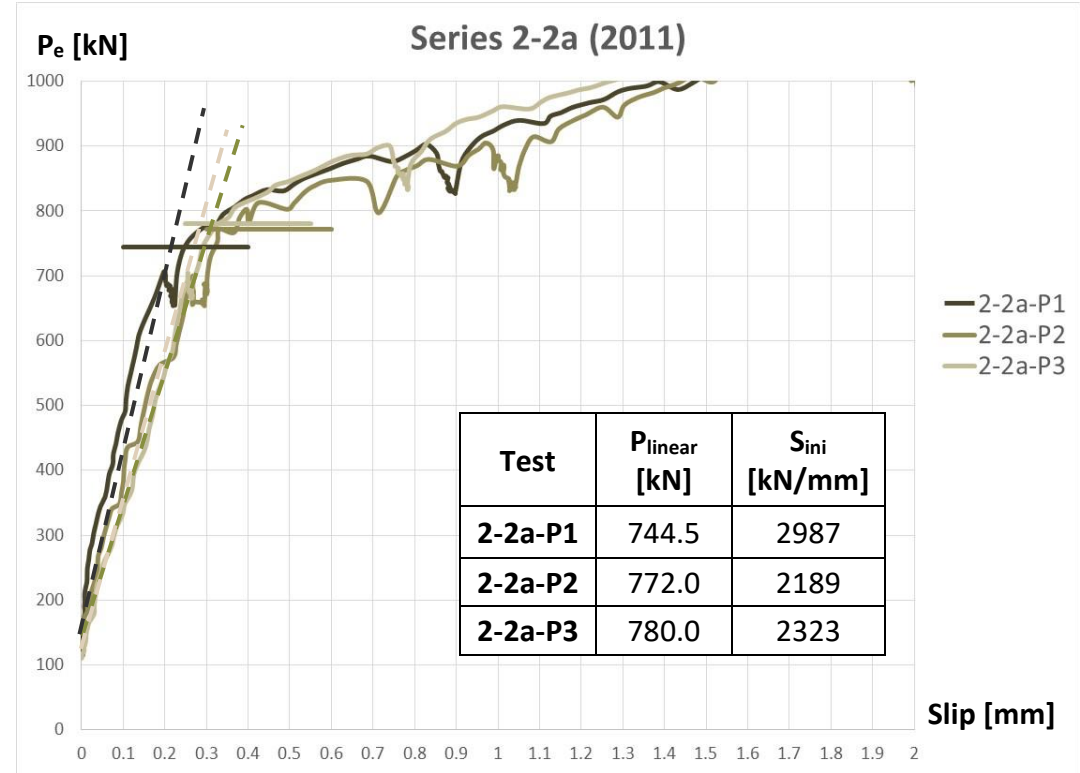


Figure B2.5: Push-out test Series 2-2a, linear range

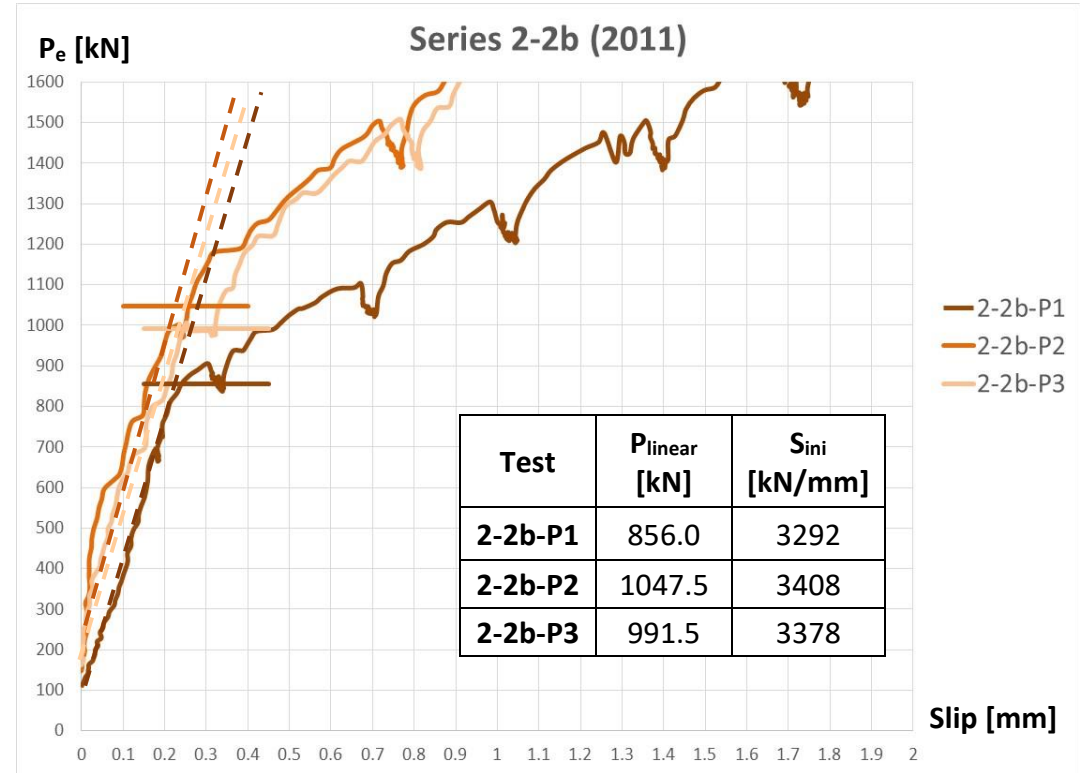


Figure B2.6: Push-out test Series 2-2b, linear range

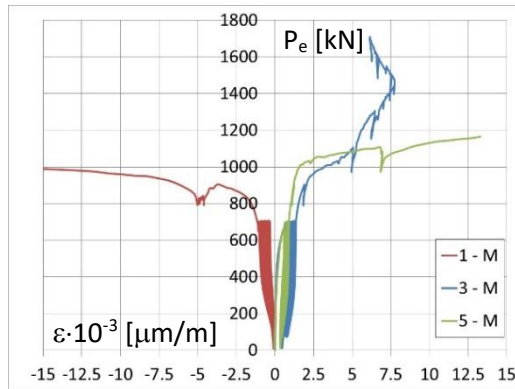


Figure B3-1a1: Test 1a – P1

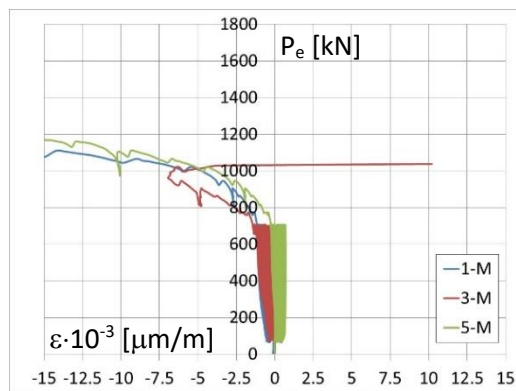
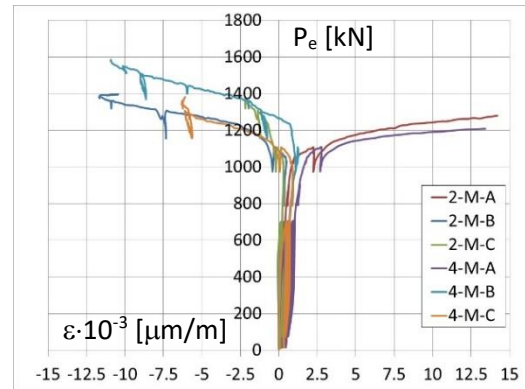


Figure B3-1a2: Test 1a – P2

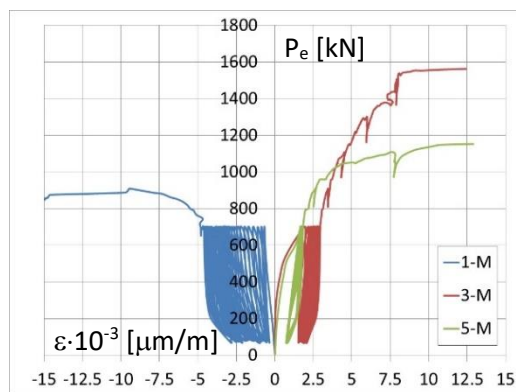
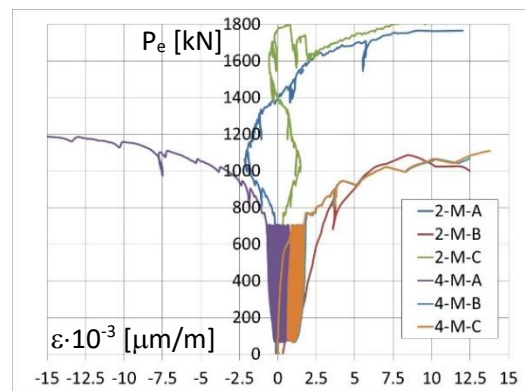
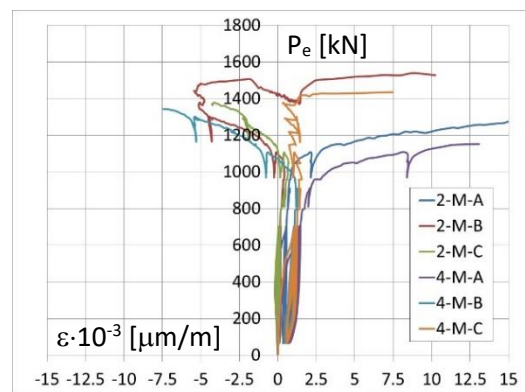
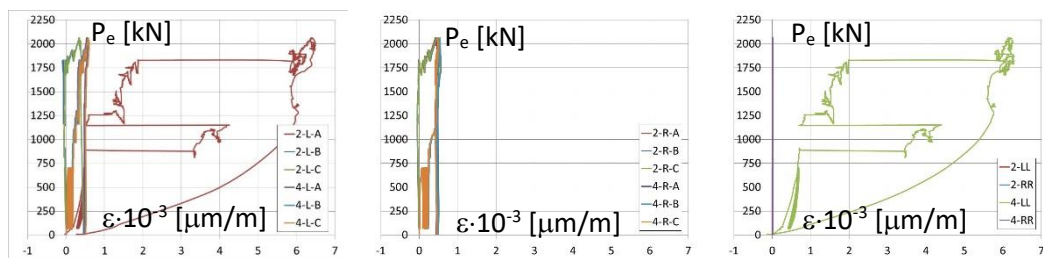
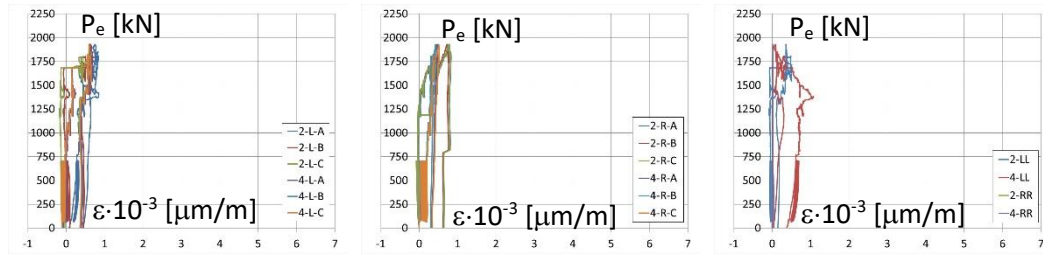
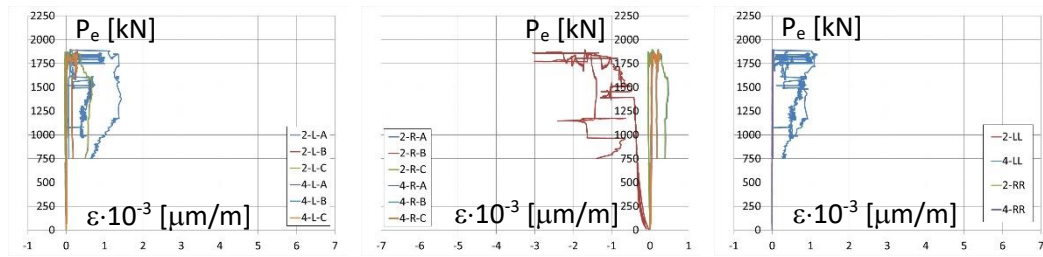


Figure B3-1a3: Test 1a – P3





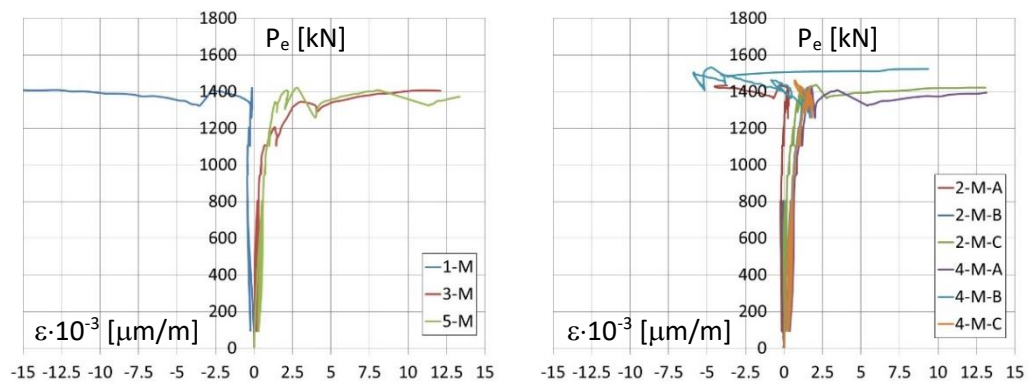


Figure B3-1b1: Test 1b – P1

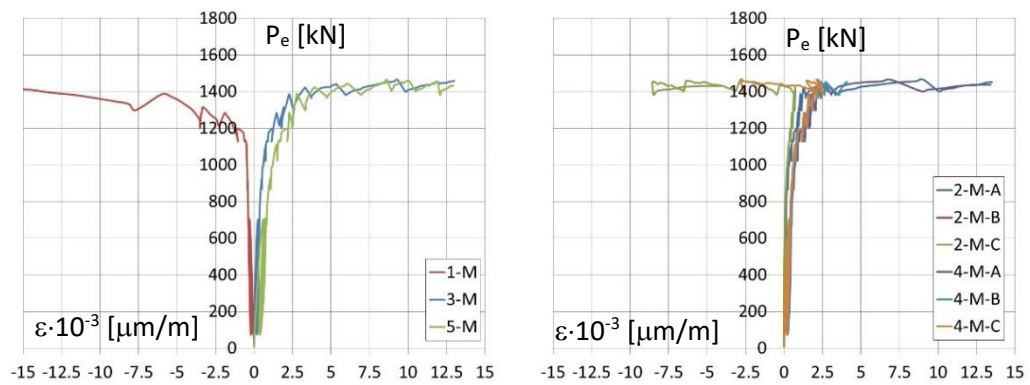


Figure B3-1b2: Test 1b – P2

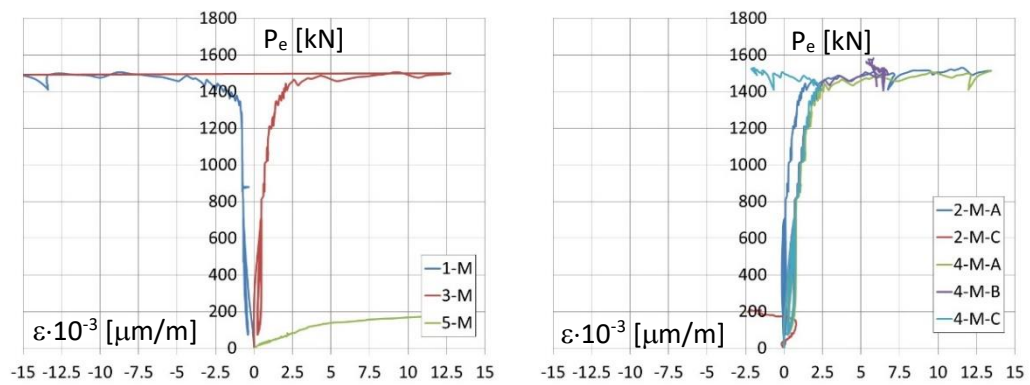


Figure B3-1b3: Test 1b – P3

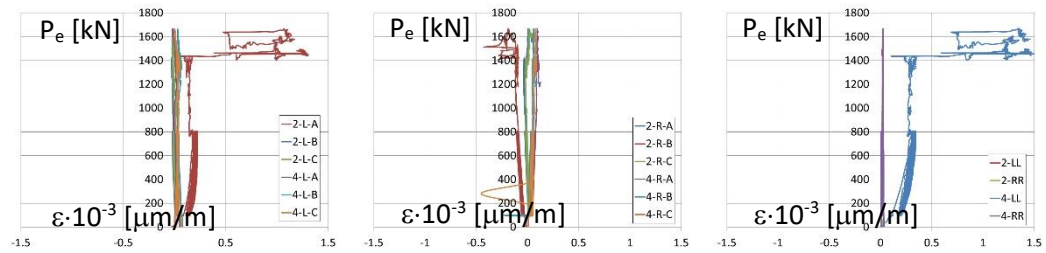


Figure B3-1b1: Test 1b – P1

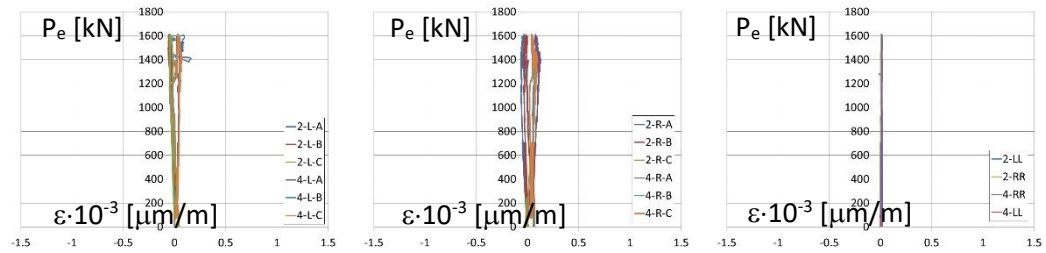


Figure B3-1b2: Test 1b – P2

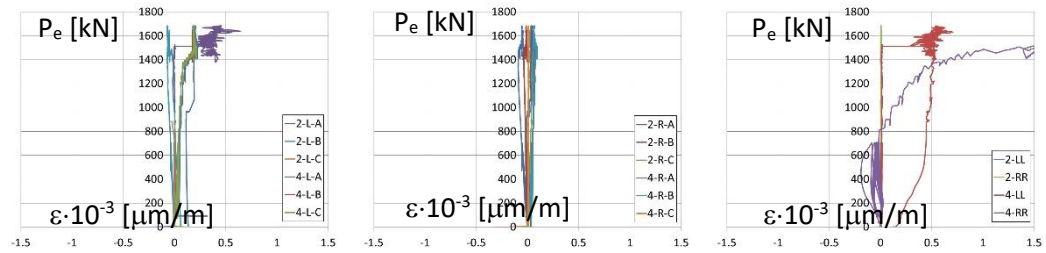


Figure B3-1b3: Test 1b – P3

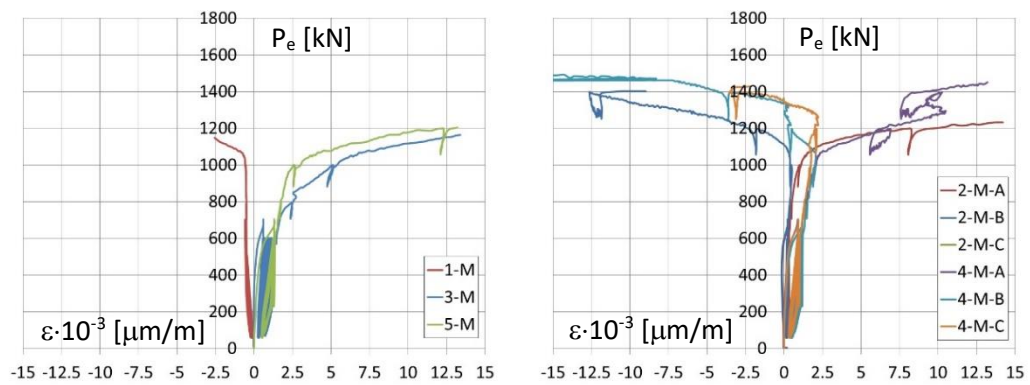


Figure B3-21a1: Test 2-1a – P1

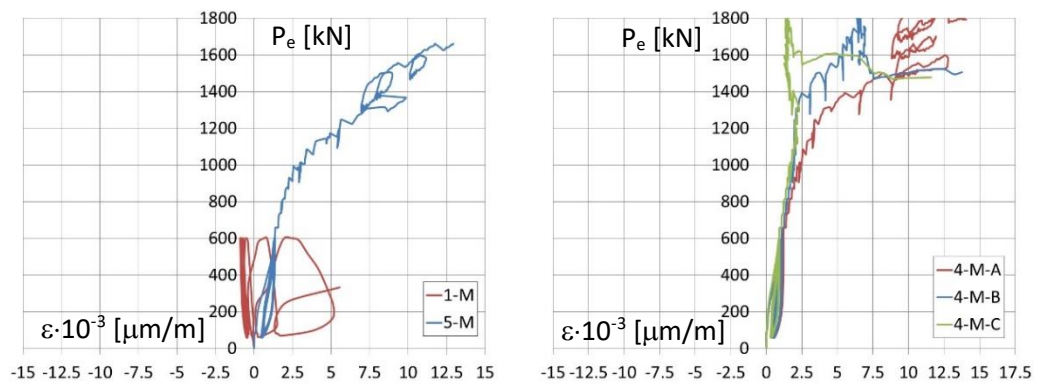


Figure B3-21a2: Test 2-1a – P2

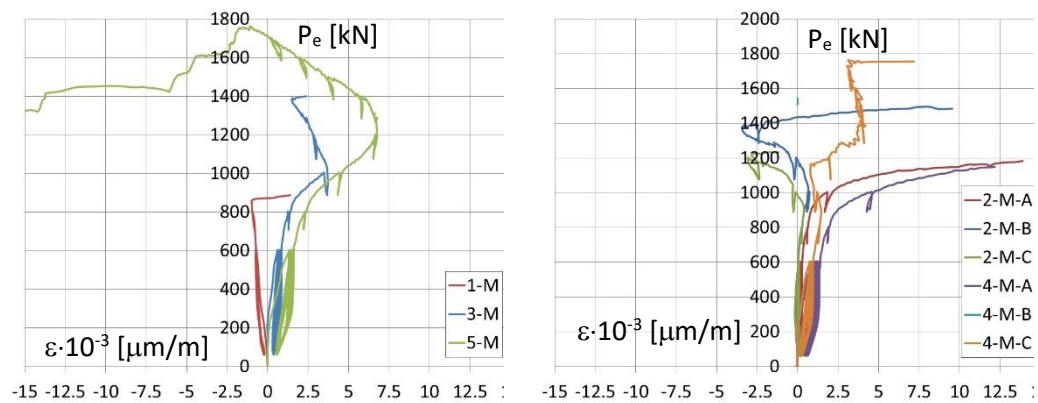
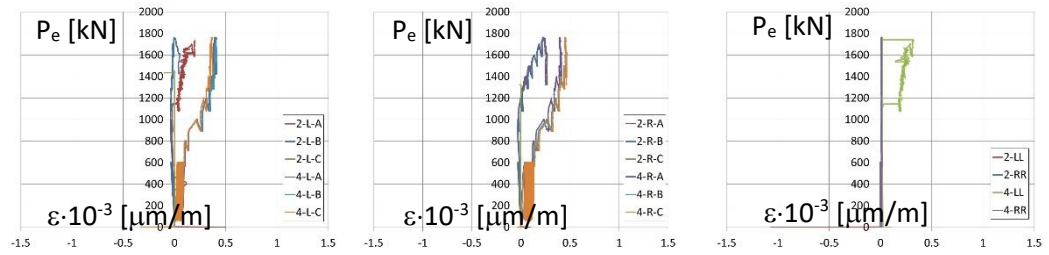
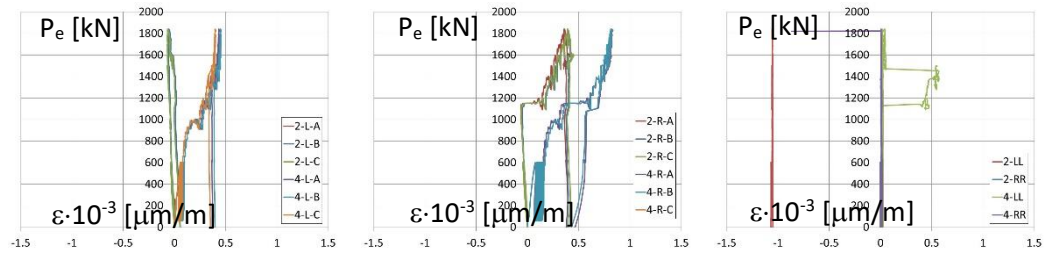
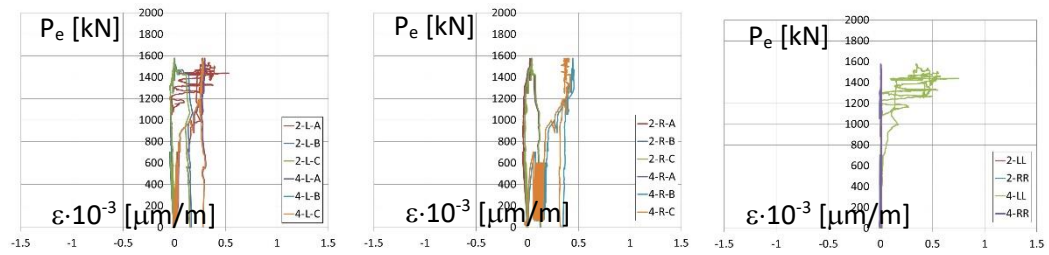


Figure B3-21a3: Test 2-1a – P3



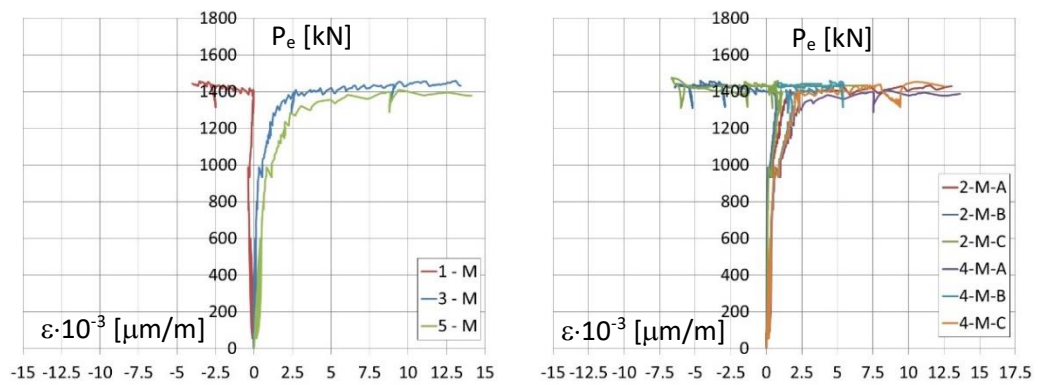


Figure B3-21b1: Test 2-1b – P1

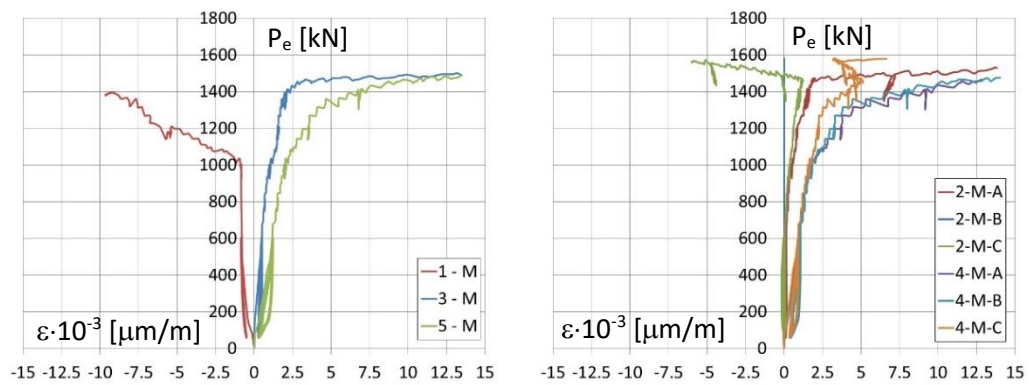


Figure B3-21b2: Test 2-1b – P2

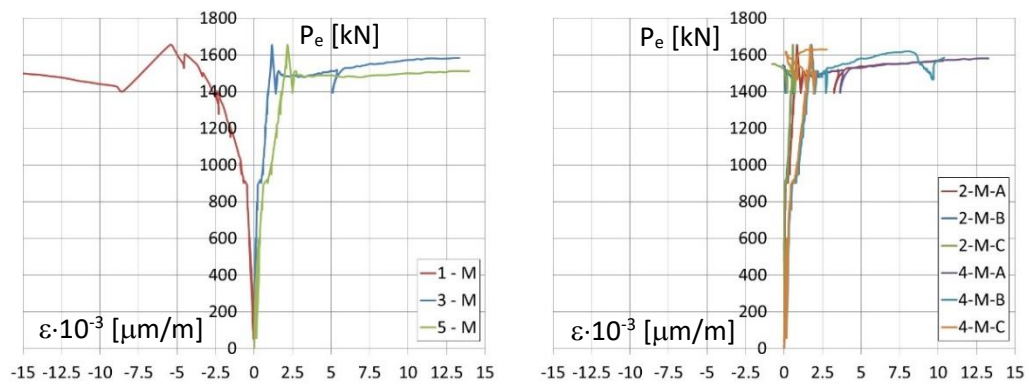
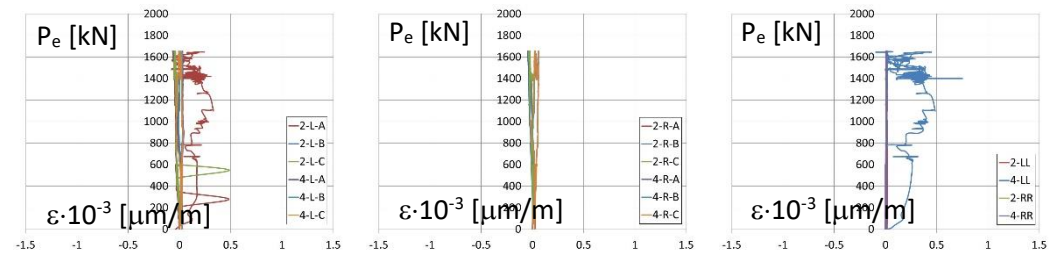
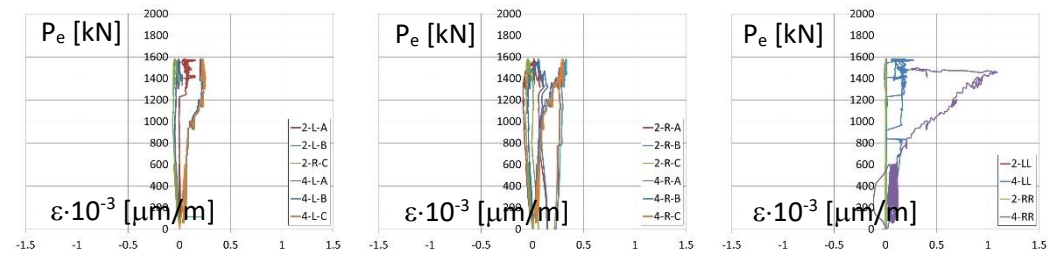
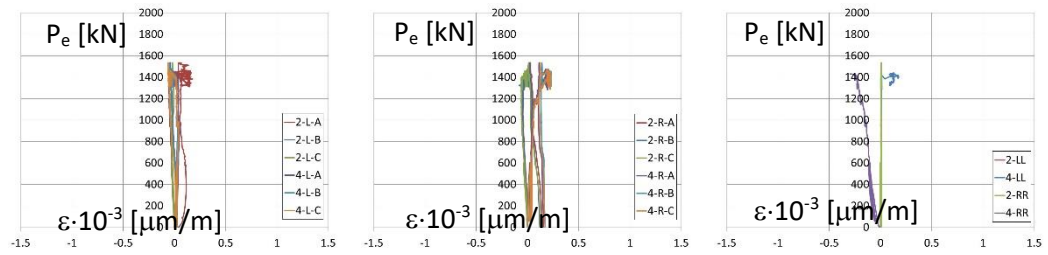


Figure B3-21b3: Test 2-1b – P3



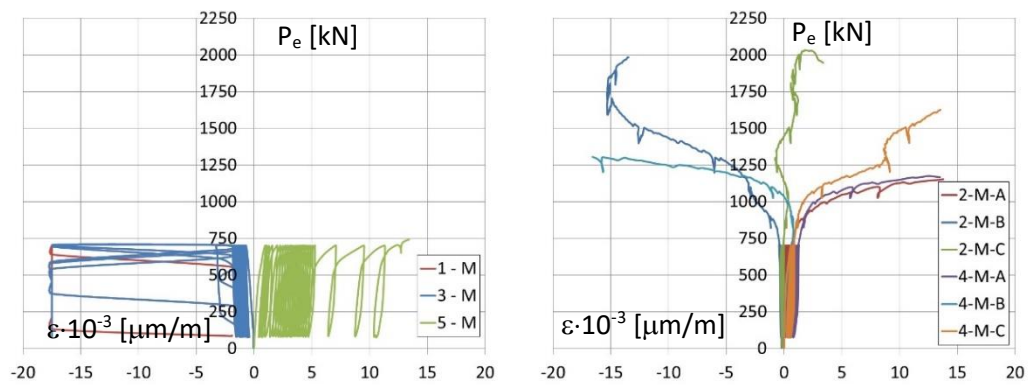


Figure B3-22a1: Test 2-2a – P1

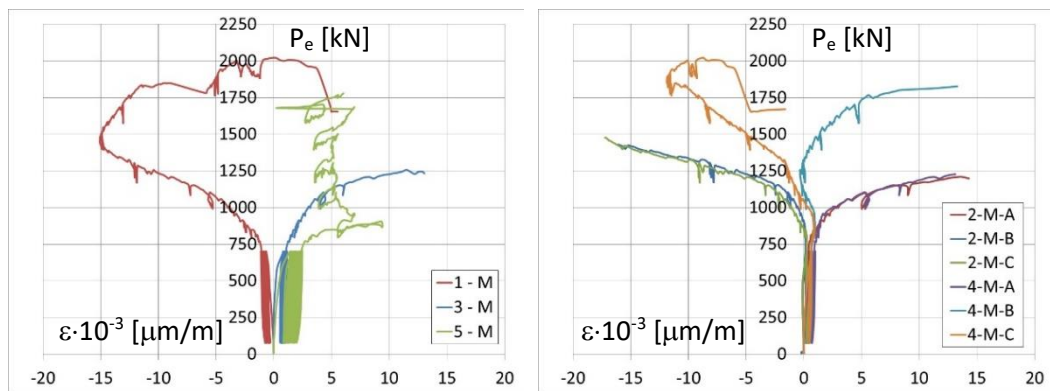


Figure B3-22a2: Test 2-2a – P2

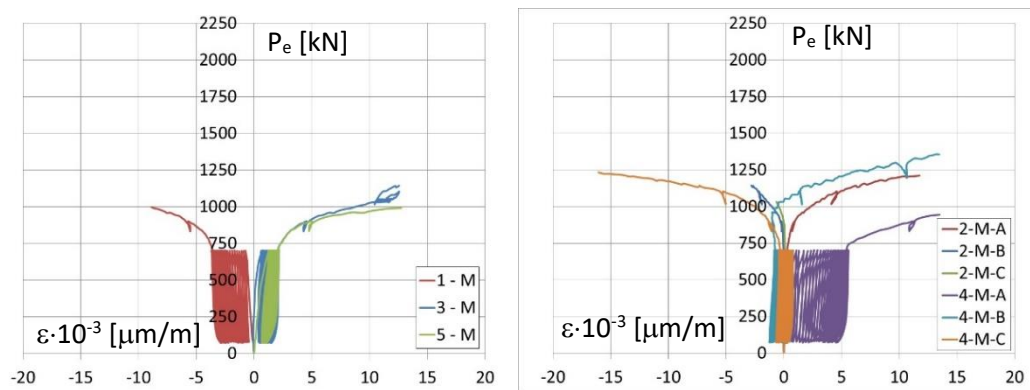


Figure B3-22a3: Test 2-2a – P3

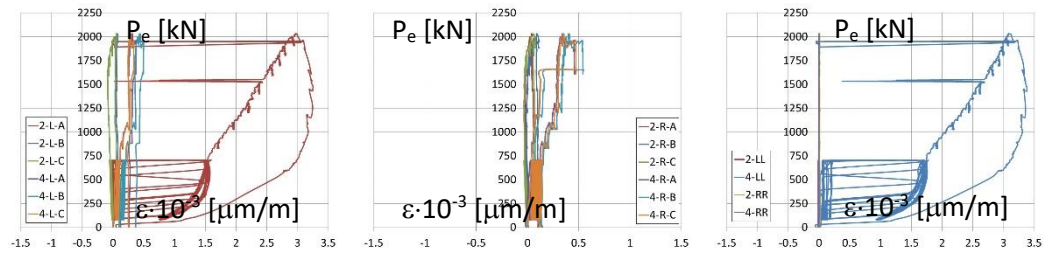


Figure B3-22a1: Test 2-2a – P1

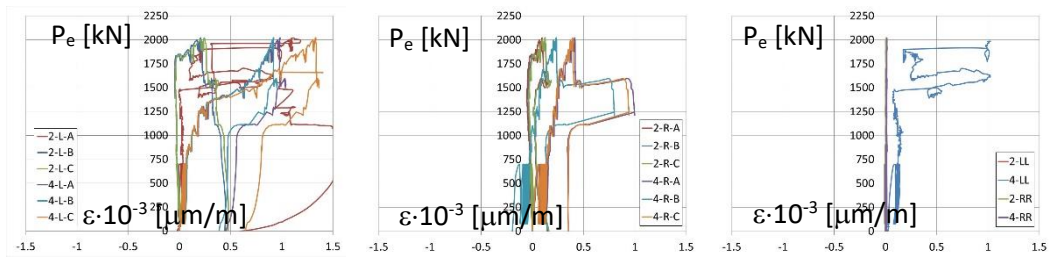


Figure B3-22a2: Test 2-2a – P2

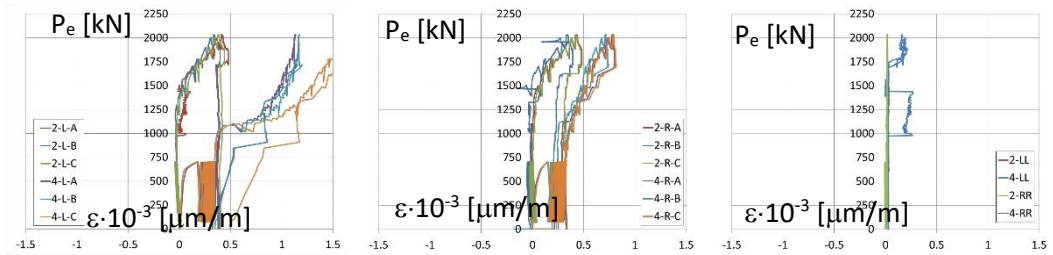


Figure B3-22a3: Test 2-2a – P3

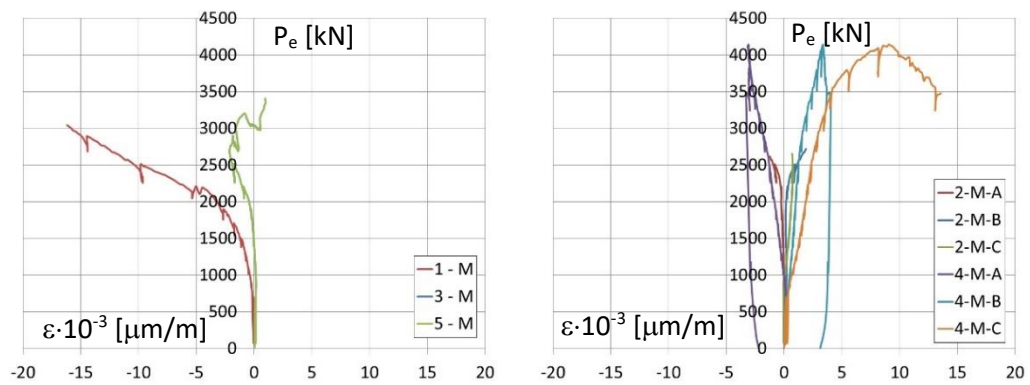


Figure B3-22b1: Test 2-2b – P1

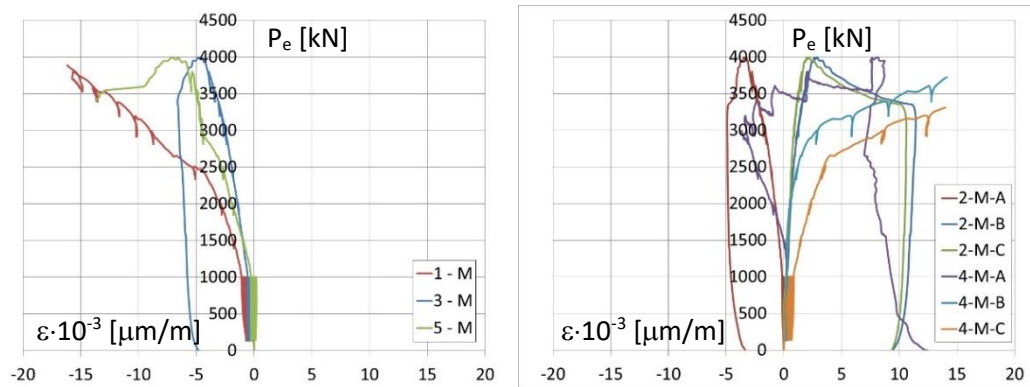


Figure B3-22b2: Test 2-2b – P2

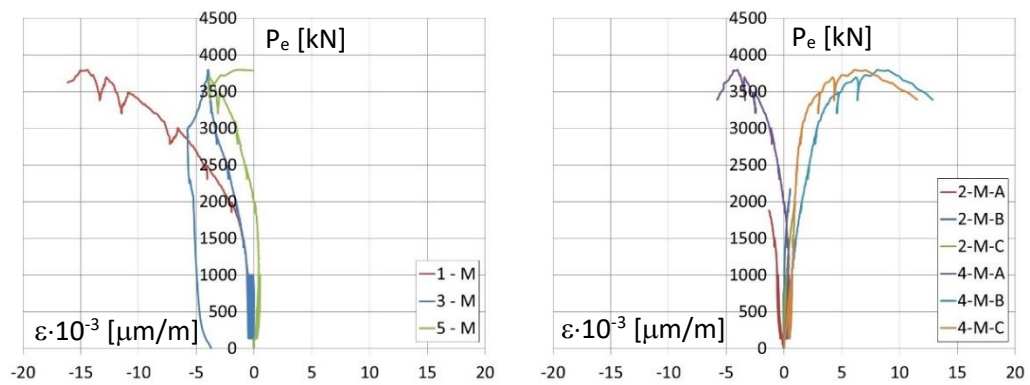


Figure B3-22b3: Test 2-2b – P3

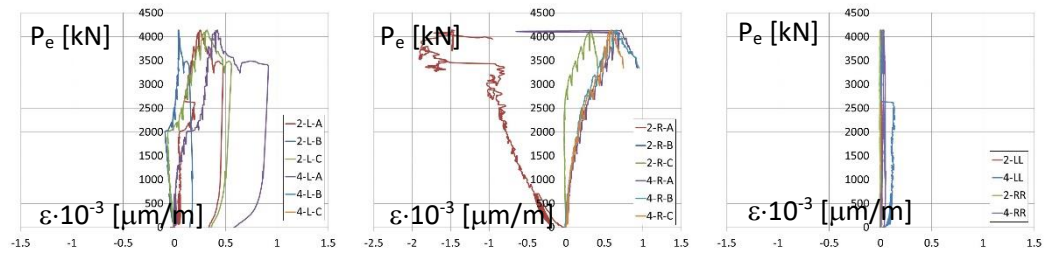


Figure B3-22b1: Test 2-2b – P1

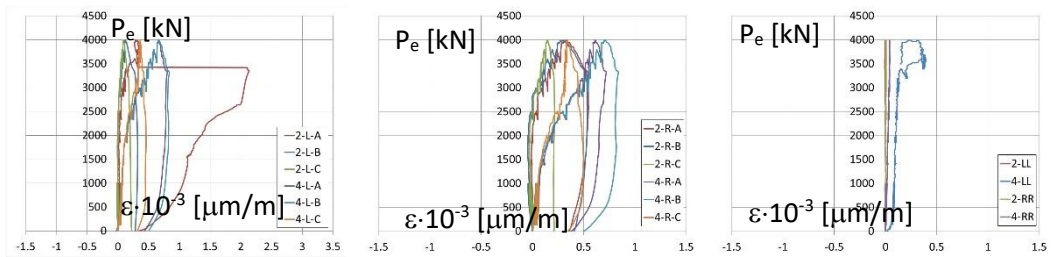


Figure B3-22b2: Test 2-2b – P2

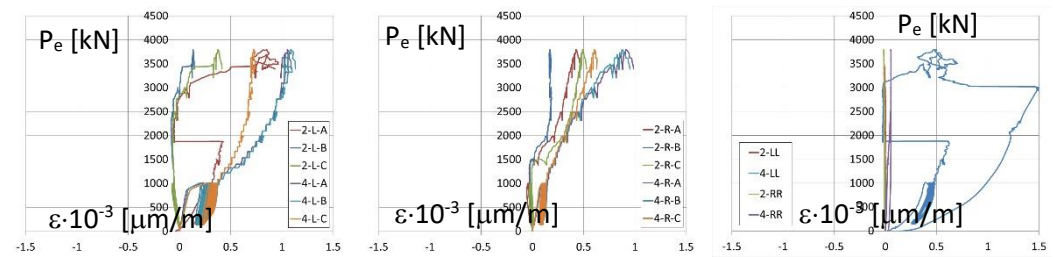


Figure B3-22b3: Test 2-2b – P3

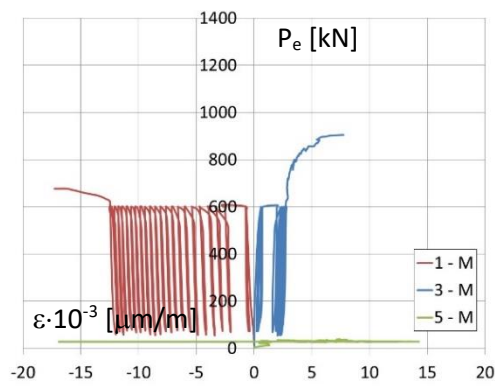


Figure B3-231: Test 2-3 – P1

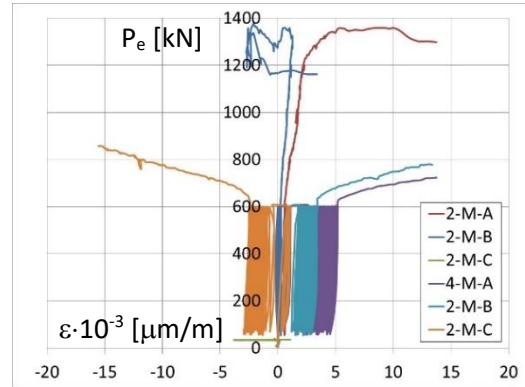


Figure B3-232: Test 2-3 – P2

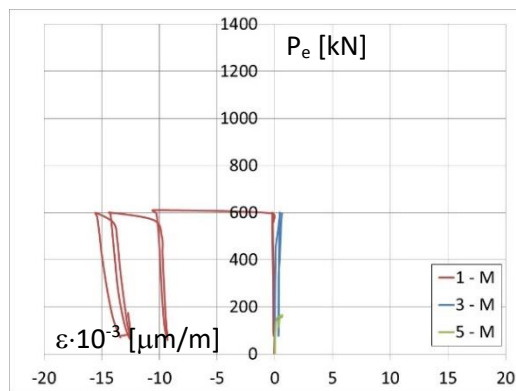
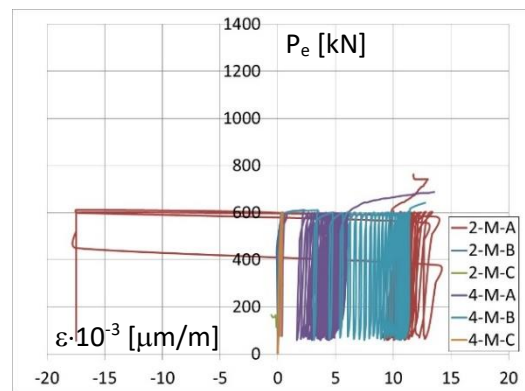


Figure B3-233: Test 2-3 – P3



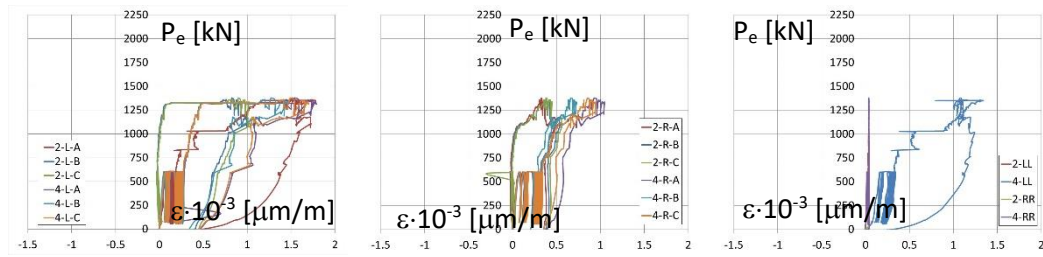


Figure B3-231: Test 2-3 – P1

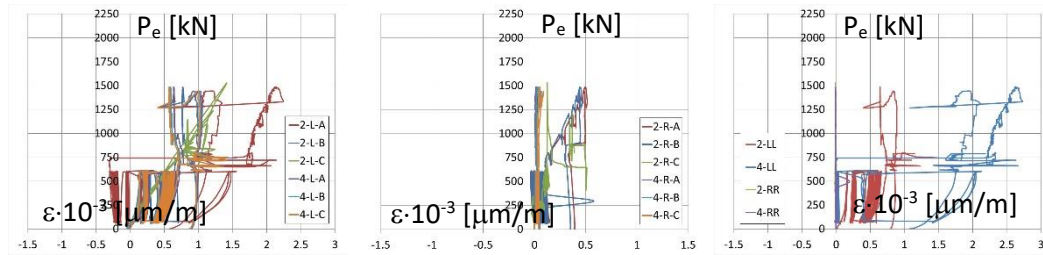


Figure B3-232: Test 2-3 – P2

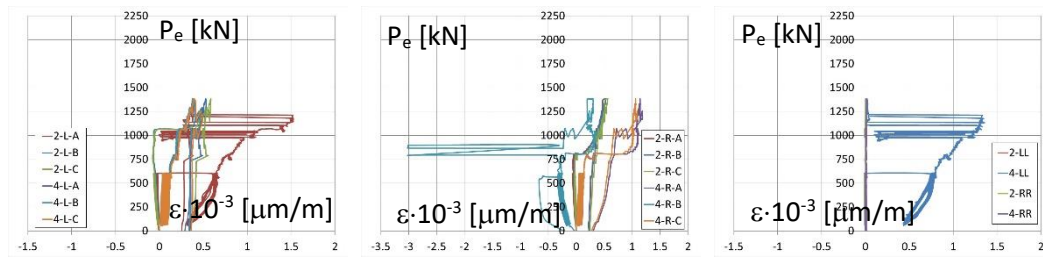


Figure B3-233: Test 2-3 – P3

B4 – Tensile Tests of Dowel Reinforcement Uni LU (2018)

Table 3.3: Tensile Tests Uni LU 2018 – Test Results (Engineering stresses)

Specimen	Length		onset of Necking		Rupture		Circumference after testing
	l_0^a [mm]	l_1^b [mm]	Strain [‰]	Stress [N/mm ²]	Strain [‰]	Stress [N/mm ²]	$2 \times U_r$ [mm]
1a	93	111.9	12.804	596.45	20.147	370.12	51.0
1b – 1	93	111.7	12.642	593.68	19.892	385.96	52.5
2 - 1b – 1	91	110.3	13.824	596.06	21.020	368.24	51.0
2 - 1b – 2	91	110.1	13.226	589.09	20.726	394.31	53.0
2 – 3 – 1	110	128.3	10.366	592.41	16.483	377.46	51.5
Average^c:			13.12	593.8	20.45	379.7	$U_r = 25.9\text{mm}$

^a l_0 = Length between the clamps before testing

^b l_1 = Length between the clamps after testing

^c Test 2-3-1 not considered in calculation of average values



Figure B2-1-a: Tensile Test Specimen 1-a, Uni LU



Figure B2-1-b: Tensile Test Specimen 1-b, Uni LU



Figure B2-2-1b-1: Tensile Test Specimen 2-1b-1, Uni LU



Figure B2-2-1b-2: Tensile Test Specimen 2-1b-2, Uni LU



Figure B2-2-3-1: Tensile Test Specimen 2-3-1, Uni LU

Annex C – Input for Numerical Simulation (Abaqus)

Input Data Abaqus for Simulation of Test Series 1a – Basic Configuration:

Q257

Density 0.00785 (scaled)

Elastic

Ea = 200000, poisson = 0.3

Plastic

Yield stress	Plastic strain
530.7	0
582.7	0.05
10	0.051

S355 Steel section - Load introduction Plate - Foundation Plate

Density 0.00785 (scaled)

Elastic

Ea = 210000, poisson = 0.3

Plastic

Yield stress	Plastic strain
375	0
506	0.15

B500S – Dowel Reinforcement bar, Diameter 12mm

Density 0.00785 (scaled)

Elastic

Ea = 200000, poisson = 0.3

Plastic

True stress	Plastic strain (Logarithmic)
530.7	0
593.8	0.12823
804.5	0.18204
826.14	0.18649

Ductile Damage for metals

Fracture strain	Stress Triaxiality	Strain Rate
0.94750605	-1	0.001
0.34682951	-0.33	0.001
0.21141718	0	0.001
0.18196845	0.1	0.001
0.15662170	0.2	0.001
0.12887376	0.33	0.001
0.09986640	0.5	0.001
0.04717355	1	0.001
0.01052584	2	0.001

Ductile Damage evolution

Type = Displacement

Softening = Tabluar

Degradation = Multiplicative

Damage Variable	Displacement
0.0000	0.7950
0.2640	0.9618
0.5280	1.1287
0.9879	1.1562

SHEAR DAMAGE

Ks = 0.2

Ductile Damage for metals

Fracture strain	Shear Stress Ratio	Strain Rate
0.12823	1.732	0.1

Damage evolution

Type = Displacement

Softening = Exponential

Degradation = Multiplicative

Displacement at Failure	Exponential Law Parameter
2.5646	0.7

Concrete slab

Concrete density = 0.0024 (scaled)

Elastic

 $E_c = 29549$, poisson = 0.2**Concrete Damage Plasticity – CDP**

Dilation Angle	Eccentricity	fb0 / fc0	K	Viscosity Parameter
36	0.1	1.16	0.667	0.00025

Compressive Behaviour

Yield stress	Inelastic strain	Damage Parameter
10.6933	0	0
13.9432	4.8E-005	0
16.9456	0.000104	0
19.4682	0.000176	0
21.5538	0.000263	0
23.2398	0.000364	0
24.56	0.000477	0
25.5441	0.000601	0
26.2188	0.000736	0
26.608	0.00088	0
26.7333	0.001034	0
26.6976	0.001193	0.001336
26.591	0.001354	0.005324
26.4152	0.001518	0.0119
26.173	0.001684	0.020961
25.868	0.001851	0.03237
25.5047	0.002021	0.045959
25.0883	0.002193	0.061534
24.6245	0.002367	0.078884
24.1191	0.002541	0.097789
23.5783	0.002717	0.11802
23.008	0.002894	0.139351
22.4143	0.003072	0.161559
21.8028	0.00325	0.184435
21.1787	0.003429	0.207778
20.5471	0.003608	0.231407
16.8122	0.004681	0.371114
13.5325	0.005738	0.493798
10.8795	0.006773	0.593036
8.8075	0.00779	0.670542
7.2063	0.00879	0.730437
5.9666	0.009778	0.776809
4.9991	0.010757	0.812999
4.236	0.011728	0.841547
3.6269	0.012695	0.86433

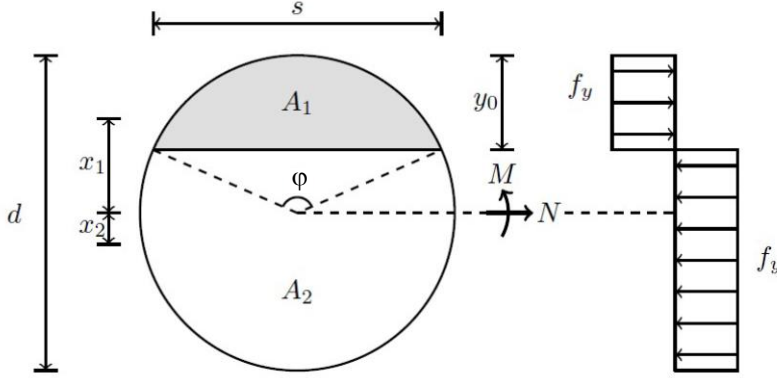
3.1352	0.013658	0.882725
2.7336	0.014617	0.897745
2.4023	0.015575	0.910139
2.1262	0.01653	0.920467

Tensile Behaviour

Yield stress	Displacement	Damage Parameter
4.1	0	0
2.0944	0.0992	0.4892
1.2243	0.1984	0.7014
0.8528	0.2976	0.792
0.6546	0.3968	0.8404
0.5048	0.496	0.8769
0.3707	0.5952	0.9096
0.2504	0.6944	0.9389
0.1479	0.7936	0.9639
0.0648	0.8928	0.9842

Annex D – Analytics

Yield Condition for Circular Cross Section, by J. H. Sorensen [Sor2017]:



Areas:

$$A_{tot} = \pi \cdot \frac{d^2}{4}; A_1 = \frac{d^2}{8} \cdot (\varphi - \sin(\varphi));$$

Secant length: $S_1 = d \cdot \sin\left(\frac{\varphi}{2}\right)$

Distance to geometric centroid: $x_1 = \frac{S_1^3}{12 \cdot A_1}$

Plastic tension capacity: $N_{pl} = \frac{\pi}{4} \cdot d^2 \cdot f_y$

Normal force at full plastic stress distribution:

$$N = (A_{tot} - 2 \cdot A_1) \cdot f_y = \pi \cdot \frac{d^2}{4} - 2 \cdot \frac{d^2}{8} \cdot (\varphi - \sin(\varphi)) \cdot f_y$$

Normalized with N_{pl} : $\frac{N}{N_{pl}} = 1 - \frac{1}{\pi} \cdot (\varphi - \sin(\varphi))$

Plastic bending moment: $M_{pl} = \frac{1}{6} \cdot d^3 \cdot f_y$

Bending moment at full plastic stress distribution:

$$M = A_1 \cdot f_y \cdot X_1 + A_2 \cdot f_y \cdot X_2 = A_1 \cdot f_y \cdot \frac{S_1^3}{12 \cdot A_1} + A_2 \cdot f_y \cdot \frac{S_1^3}{12 \cdot A_2}$$

$$M = 2 \cdot f_y \cdot \frac{S_1^3}{12} = \frac{1}{6} \cdot f_y \cdot d^3 \cdot \sin^3\left(\frac{\varphi}{2}\right)$$

Normalized with M_{pl} : $\frac{M}{M_{pl}} = \sin^3\left(\frac{\varphi}{2}\right) \Rightarrow \varphi = 2 \cdot \arcsin\left(\left(\frac{M}{M_{pl}}\right)^{1/3}\right)$

Substituting θ into equation for N/N_{pl} :

$$\frac{N}{N_{pl}} = 1 - \frac{1}{\pi} \cdot \left(2 \cdot \arcsin\left(\left(\frac{M}{M_{pl}}\right)^{1/3}\right) - \sin\left(2 \cdot \arcsin\left(\left(\frac{M}{M_{pl}}\right)^{1/3}\right)\right) \right)$$

With: $\sin(2 \cdot \arcsin(x)) = 2 \cdot x \cdot \sqrt{1 - x^2}$

Which finally can be expressed as yield condition:

$$f(M, N) = \frac{N}{N_{pl}} + \frac{2}{\pi} \cdot \left[\arcsin\left(\left(\frac{M}{M_{pl}}\right)^{1/3}\right) - \left(\frac{M}{M_{pl}}\right)^{1/3} \cdot \sqrt{1 - \left(\frac{M}{M_{pl}}\right)^{2/3}} \right] - 1 = 0$$

Equations by H. J. Sørensen [Sor2017]:

$$\begin{aligned}
l_{1,ef} &= l_{1,ef,in} \cdot \cos(\varphi); l_{2,ef} = l_{2,ef,in} \cdot \cos(\varphi); \cos(\varphi) = \frac{l_1 + l_2}{\sqrt{(l_1 + l_2)^2 + u^2}} \\
l_1 &= \sqrt{\frac{2}{3}} \cdot \frac{d}{\sqrt{1 + \frac{f_{cc,1}}{f_{cc,2}}}} \cdot \sqrt{\frac{f_y}{f_{cc,1}}}; l_2 = \sqrt{\frac{2}{3}} \cdot \frac{d}{\sqrt{1 + \frac{f_{cc,2}}{f_{cc,1}}}} \cdot \sqrt{\frac{f_y}{f_{cc,2}}} \\
l_1 + l_2 &= \sqrt{\frac{2}{3}} \cdot \frac{d}{\sqrt{1 + \frac{f_{cc,1}}{f_{cc,2}}}} \cdot \sqrt{\frac{f_y}{f_{cc,1}}} + \sqrt{\frac{2}{3}} \cdot \frac{d}{\sqrt{1 + \frac{f_{cc,2}}{f_{cc,1}}}} \cdot \sqrt{\frac{f_y}{f_{cc,2}}} \\
l_1 + l_2 &= \sqrt{\frac{2}{3}} \cdot d \cdot \sqrt{f_y} \cdot \left(\frac{1}{\sqrt{f_{cc,1}}} \cdot \frac{\sqrt{f_{cc,2}}}{\sqrt{f_{cc,1} + f_{cc,2}}} + \frac{1}{\sqrt{f_{cc,2}}} \cdot \frac{\sqrt{f_{cc,1}}}{\sqrt{f_{cc,1} + f_{cc,2}}} \right) \\
l_1 + l_2 &= \sqrt{\frac{2}{3}} \cdot d \cdot \sqrt{f_y} \cdot \frac{1}{\sqrt{f_{cc,1} + f_{cc,2}}} \left(\frac{\sqrt{f_{cc,2}}}{\sqrt{f_{cc,1}}} + \frac{\sqrt{f_{cc,1}}}{\sqrt{f_{cc,2}}} \right) \\
l_1 + l_2 &= \sqrt{\frac{2}{3}} \cdot d \cdot \sqrt{f_y} \cdot \frac{1}{\sqrt{f_{cc,1} + f_{cc,2}}} \left(\frac{f_{cc,2}}{\sqrt{f_{cc,1} \cdot f_{cc,2}}} + \frac{f_{cc,1}}{\sqrt{f_{cc,1} \cdot f_{cc,2}}} \right) \\
l_1 + l_2 &= \sqrt{\frac{2}{3}} \cdot d \cdot \sqrt{f_y} \cdot \frac{\sqrt{f_{cc,1} + f_{cc,2}}}{\sqrt{f_{cc,1} \cdot f_{cc,2}}} \\
(l_1 + l_2)^2 &= \frac{2}{3} \cdot d^2 \cdot f_y \cdot \frac{f_{cc,1} + f_{cc,2}}{f_{cc,1} \cdot f_{cc,2}} \\
l_1 + l_2 &= \sqrt{\frac{2}{3}} \cdot d \cdot \sqrt{f_y} \cdot \frac{1}{\sqrt{f_{cc,1} + f_{cc,2}}} \left(\frac{\sqrt{f_{cc,2}}}{\sqrt{f_{cc,1}}} + \frac{\sqrt{f_{cc,1}}}{\sqrt{f_{cc,2}}} \right) \\
l_1 + l_2 &= \sqrt{\frac{2}{3}} \cdot d \cdot \sqrt{f_y} \cdot \frac{\sqrt{\frac{1}{f_{cc,2}}}}{\sqrt{1 + \frac{f_{cc,1}}{f_{cc,2}}}} \left(\frac{\sqrt{f_{cc,2}}}{\sqrt{f_{cc,1}}} + \frac{\sqrt{f_{cc,1}}}{\sqrt{f_{cc,2}}} \right) \\
l_1 + l_2 &= \sqrt{\frac{2}{3}} \cdot d \cdot \sqrt{f_y} \cdot \frac{1}{\sqrt{1 + \frac{f_{cc,1}}{f_{cc,2}}}} \left(\frac{1}{\sqrt{f_{cc,1}}} + \frac{\sqrt{f_{cc,1}}}{f_{cc,2}} \right) \\
l_1 + l_2 &= \sqrt{\frac{2}{3}} \cdot d \cdot \sqrt{f_y} \cdot \frac{1}{\sqrt{1 + \frac{f_{cc,1}}{f_{cc,2}}}} \frac{1}{\sqrt{f_{cc,1}}} \cdot \left(1 + \frac{f_{cc,1}}{f_{cc,2}} \right) \\
l_1 + l_2 &= l_1 \cdot \left(1 + \frac{f_{cc,1}}{f_{cc,2}} \right)
\end{aligned}$$

Force equilibrium $\Sigma V = 0$:

$$l_{1,ef,in} \cdot d \cdot f_{cc,1} = l_{2,ef,in} \cdot d \cdot f_{cc,2}$$

$$\Rightarrow l_{2,ef,in} = l_{1,ef,in} \cdot \frac{f_{cc,1}}{f_{cc,2}} \Rightarrow l_{2,ef} = l_{1,ef} \cdot \frac{f_{cc,1}}{f_{cc,2}} \Rightarrow l_2 = l_1 \cdot \frac{f_{cc,1}}{f_{cc,2}}$$

Moment equilibrium $\Sigma M = 0$:

$$\frac{1}{2} \cdot l_{1,ef,in}^2 \cdot d \cdot f_{cc,1} - l_{2,ef,in} \cdot d \cdot f_{cc,2} \cdot \left(\frac{l_1 + l_2}{\cos(\varphi)} - \frac{l_{2,ef,in}}{2} \right) + 2 \cdot M(u) = 0$$

$$\frac{d}{2} \cdot \frac{l_{1,ef}^2}{\cos^2(\varphi)} \cdot f_{cc,1} + \frac{d}{2} \cdot \frac{l_{2,ef}^2}{\cos^2(\varphi)} \cdot f_{cc,2} - \frac{l_{2,ef} \cdot (l_1 + l_2)}{\cos^2(\varphi)} \cdot d \cdot f_{cc,2} + 2 \cdot M(u) = 0$$

$$\frac{l_{1,ef}^2}{\cos^2(\varphi)} \cdot f_{cc,1} + \frac{l_{2,ef}^2}{\cos^2(\varphi)} \cdot f_{cc,2} - \frac{l_{2,ef} \cdot (l_1 + l_2)}{\cos^2(\varphi)} \cdot 2 \cdot f_{cc,2} + \frac{4}{d} \cdot M(u) = 0$$

$$l_{1,ef}^2 \cdot \left(1 + \frac{f_{cc,1}}{f_{cc,2}} \right) - l_{1,ef} \cdot (l_1 + l_2) \cdot 2 + \frac{4 \cdot M(u) \cdot (l_1 + l_2)^2}{d \cdot f_{cc,1} \cdot ((l_1 + l_2)^2 + u^2)} = 0$$

Solving for $l_{1,ef}$:

$$l_{1,ef,1,2} = \frac{2 \cdot (l_1 + l_2) \pm \sqrt{4 \cdot (l_1 + l_2)^2 - 4 \cdot \left(1 + \frac{f_{cc,1}}{f_{cc,2}} \right) \cdot \frac{4 \cdot M(u) \cdot (l_1 + l_2)^2}{d \cdot f_{cc,1} \cdot ((l_1 + l_2)^2 + u^2)}}}{2 \cdot \left(1 + \frac{f_{cc,1}}{f_{cc,2}} \right)}$$

$$l_{1,ef} = \frac{(l_1 + l_2) + \sqrt{(l_1 + l_2)^2 - \left(1 + \frac{f_{cc,1}}{f_{cc,2}} \right) \cdot \frac{4 \cdot M(u) \cdot (l_1 + l_2)^2}{d \cdot f_{cc,1} \cdot ((l_1 + l_2)^2 + u^2)}}}{\left(1 + \frac{f_{cc,1}}{f_{cc,2}} \right)}$$

$$l_{1,ef} = \frac{(l_1 + l_2)}{\left(1 + \frac{f_{cc,1}}{f_{cc,2}} \right)} \cdot \left[1 - \sqrt{1 - \left(1 + \frac{f_{cc,1}}{f_{cc,2}} \right) \cdot \frac{4 \cdot M(u)}{d \cdot f_{cc,1} \cdot ((l_1 + l_2)^2 + u^2)}} \right]$$

$$l_{1,ef} = l_1 \cdot \left[1 - \sqrt{1 - \left(1 + \frac{f_{cc,1}}{f_{cc,2}} \right) \cdot \frac{4 \cdot M(u)}{d \cdot f_{cc,1} \cdot \left(l_1^2 \cdot \left(1 + \frac{f_{cc,1}}{f_{cc,2}} \right)^2 + u^2 \right)}} \right]$$

$$l_{1,ef} = l_1 \cdot \left[1 - \sqrt{1 - \frac{4 \cdot M(u)}{d \cdot f_{cc,1} \cdot l_1^2 \cdot \left(1 + \frac{f_{cc,1}}{f_{cc,2}} \right) + \frac{d \cdot f_{cc,1} \cdot u^2}{\left(1 + \frac{f_{cc,1}}{f_{cc,2}} \right)}}} \right]$$

$$l_{1,ef} = l_1 \cdot \left[1 - \sqrt{1 - \frac{4 \cdot M(u)}{d \cdot f_{cc,1} \cdot \left(\sqrt{\frac{2}{3}} \cdot \frac{d}{\sqrt{1 + \frac{f_{cc,1}}{f_{cc,2}}}} \cdot \sqrt{\frac{f_y}{f_{cc,1}}} \right)^2 \cdot \left(1 + \frac{f_{cc,1}}{f_{cc,2}} \right) + \frac{d \cdot f_{cc,1} \cdot u^2}{\left(1 + \frac{f_{cc,1}}{f_{cc,2}} \right)}}} \right]$$

$$l_{1,ef} = l_1 \cdot \left[1 - \sqrt{1 - \frac{4 \cdot M(u)}{\frac{2}{3} \cdot d^3 \cdot f_y + d \cdot u^2 \cdot \frac{f_{cc,1}}{\left(1 + \frac{f_{cc,1}}{f_{cc,2}} \right)}}} \right]$$

$$l_{1,ef} = l_1 \cdot \left[1 - \sqrt{1 - \frac{M(u)}{M_{pl} + \left(\frac{u}{2} \right)^2 \cdot d \cdot \frac{f_{cc,1} \cdot f_{cc,2}}{(f_{cc,1} + f_{cc,2})}}} \right]$$

